Sequence-specific Inhibition of DNA Polymerase by Phenanthrene Quinone Diimine Complexes of Rhodium(III)

Thesis by

Timothy Wilmot Johann

In Partial Fulfillment of the Requirements

for the Degree of

Doctor of Philosophy

California Institute of Technology

Pasadena, California

1997

(Submitted January 30, 1997)

Acknowledgements

I wish to express my thanks to my thesis advisor, Jacqueline K. Barton, for her enthusiasm and her support during my tenure at Caltech.

The work presented in this thesis could not have occurred if not for the help of many others. The NMR experiments presented in Chapter 2 were the result of my work with/for Dr. Sonya Franklin. The initial experiments which greatly facilitated these NMR studies were carried out by Brian Hudson and Brian Jackson. The binding constant studies presented were the result of many discussions with Brian Jackson, Curt Hastings, and Brian Hudson. I thank them all for many insightful debates which helped to determine what was going on in these studies. Dr. Masako Kato also deserves a great deal of thanks for synthesizing metal complex stocks which were used in the NMR and binding constant studies presented here.

Many people have contributed to my education at Caltech. Dr. Inho Lee taught me many of the molecular biology techniques that I would use in my graduate career. The entire Barton group, past and present including Mo Renta, deserves thanks for all their help and discussions over the years. They are a wonderful group of people to work with and learn from.

I would also like to thank Dian Buchness, Steve Gould, Elly Noe, Chris Smith, and the rest of the Caltech staff for their friendly support over the years.

I have been fortunate to have many sources of emotional support while at Caltech. First and foremost, I would like to thank my family for their support before, after, and during graduate school. Their constant love and encouragement has always been a source of great strength in my life. I would also like to thank Ai Ching Lim who has been a very dear and caring friend. She has been instrumental in helping me through many of the trials of the last few years. All the Barton group deserves a great deal of thanks for providing a wonderful working environment. Specifically, Brian Jackson, Brian Hudson, Marilena Fitzsimons, Dan Hall, Cathy Sarisky, Megan Nunez, Kitty Erkkila, Duncan Odom, Mo Renta, and Susanne Lin have all been close friends who have offered much support when needed.

Abstract

The DNA binding characteristics of several phenanthrenequinone diimine (phi) complexes of rhodium (III) as well as their ability to inhibit functionally DNA polymerase have been investigated. Affinity constants have been determined to be $5x10^7$ M^{-1} and $1x10^8$ M^{-1} for Δ and Λ 1-Rh(MGP)$_2$phi^{5+} binding to the DNA sequences 5'-CATCTG-3' and 5'-CATATG-3' respectively. The exchange rate, at 21°C, has been determined to be 16 s^{-1} for the binding of 1-Λ-Rh(MGP)$_2$phi^{5+} to 5'-CATATG-3' through the use of variable temperature ^{1}H-NMR. Similar ^{1}H-NMR experiments were carried out to determine the kinetics of the interaction of 1-Δ-Rh(MGP)$_2$phi^{5+} with a duplex DNA of the sequence 5'-CGCATCTGAC-3'. 1-Λ-Rh(MGP)$_2$phi^{5+}, 1-Δ-Rh(MGP)$_2$phi^{5+}, and Rh(MT)phi^{3+}, which binds to 5'-TGCA-3', were found to be potent sequence-specific inhibitors of DNA polymerase. All of these complexes bind to DNA through intercalation. In experiments where two templates competed for extension by DNA polymerase, these complexes were shown to inhibit the extension of templates containing their binding sequences as compared to control templates. Furthermore, in direct competition experiments containing two templates, where each contained a binding sequence for a different metal complex, the relative activity of DNA polymerase on each template was "tuned" by the addition of metal complex specific for that template. Δ-Rh(DPB)$_2$phi^{3+} was also found to be a potent inhibitor of DNA polymerase, but not in a template-specific manner. The relative potency of sequence-specific inhibition shown by 1-Λ-Rh(MGP)$_2$phi^{5+}, 1-Δ-Rh(MGP)$_2$phi^{5+}, and Rh(MT)phi^{3+} was compared to the binding kinetics, complex size, complex charge, binding affinity and binding induced DNA distortion for these

complexes. Greater DNA distortion was found to correlate with greater inhibition. These studies have shown that these molecules not only bind to DNA in a sequence-specific manner, but can functionally inhibit enzymatic reactions in a sequence-specific manner as well.

Table of Contents

List of Figures

Page

Chapter 1.

Chapter 2.

List of Tables

Chapter 2:

Chapter 3:

Chapter 1: Recognition of DNA by Octahedral Coordination Complexes*

1.1 Introduction

DNA is the blueprint for the great diversity of cells in each of us. Exactly 46 molecules of DNA contain all the information necessary to make a human being, and the same 46 molecules, thus the same information, are present in each cell of that human being. The differences between cells that become brain and cells that become muscle do not arise from differences in the information contained in the DNA of these cells, but from differences in how that information is read or accessed. In undifferentiated cancerous cells, seemingly insignificant changes in the DNA library cascade into large differences in which sequences in the library are read, and uncontrollable cell growth results.

How this DNA information is accessed is determined in large measure by ensembles of non-covalent binding interactions between DNA sites and proteins, which regulate and control gene expression.[1] Repressor proteins bind selectively to 8-12 base pair sequences of DNA and block the transcription of certain genes. Transcriptional amplifiers, in contrast, in binding to their specific targets, can enhance the expression of selected genes by more than 1000-fold. Each of these events constitutes an example of molecular recognition. How do these DNA-binding proteins selectively identify one site on the DNA duplex rather than another?

---

* This chapter was adapted from Johann, T. W.; Barton, J. K.; *Phil. Trans. R. Soc. Lond. A*, **1996**, 354, 299.

† Abbreviations used in this chapter are as follows: HET: 2-hydroxyethanethiolate; phen: phenanthroline; TMP: 3,4,7,8-tetramethyl-1,10,-phenanthroline; Me_2trien: (2R,9R)-diamino-4,7-diazadecane; pyr: pyrimidine; pur: purine; [12]aneS_4: 1,4,7,10-tetrathiacyclododecane; en: ethylenediamine; phi: 9,10-phenanthrolinequinonediimine; terpy: 2,2',2''-terpyridine; bpy: 2,2'-bipyridyl; TBP: TATA box binding protein; DPB: 4,4'-diphenyl-2,2'-bipyridyl; DMB: 5,5'-dimethyl-2,2'-bipyridyl; MGP: 4-guanidylmethyl-1,10-phenanthroline; phen: 1,10-phenanthroline; dppz: dipyridophenazine; EDTA: ethylenediaminetetraacetic acid; DIP: 4,7-diphenylphenanthroline.

A major focus of our laboratory has been in the design of small coordination complexes as mimics of these large DNA-binding proteins.[2,3] What are the chemical principles that govern site-selective recognition of nucleic acids, and can we construct small synthetic metal complexes rationally which selectively discriminate among sites utilizing these principles? From a practical standpoint, the construction of these small synthetic complexes lays the foundation for the rational design of new chemotherapeutics targeted to nucleic acids. Fundamentally, in constructing and applying generations of complexes to DNA recognition, we hope to elucidate some of the principles which govern these remarkably selective non-covalent interactions with macromolecules.

1.1.1 DNA Structure and Modes of Recognition

As shown in Figure 1.1, DNA is a polymer of nucleotide units consisting of a ribose sugar, a phosphate, and a heterocyclic aromatic base.[4] The information in the DNA polymer is contained in the ordering or sequence of the four different bases: guanine, adenine, cytosine, and thymine. Two of these polymers associate into a double helix via hydrogen bonds between the bases. Adenines associate with thymines and cytosines with guanines in an arrangement referred to as a base pair. As can also be seen in Figure 1.1, this pairing presents two different faces, two unique sets of possible hydrogen bonds and van der Waals contacts available for non-covalent interaction with proteins or small molecules which associate with the DNA polymer. When base pairs are viewed in the context of the DNA double helix, as is also illustrated, the faces of the base pairs combine to form the major and minor grooves of DNA. These grooves differ from each other in width and depth as well as in the number and variety of possible hydrogen bonds and van der Waals contacts.

Figure 1.1 (left) The building blocks of a DNA polymer. (center) The major and minor groove sides of adenine:thymine and guanine:cytosine base pairs. (right) Space filling model of the major and minor grooves in a DNA polymer. The ribbons trace the phosphate backbone.

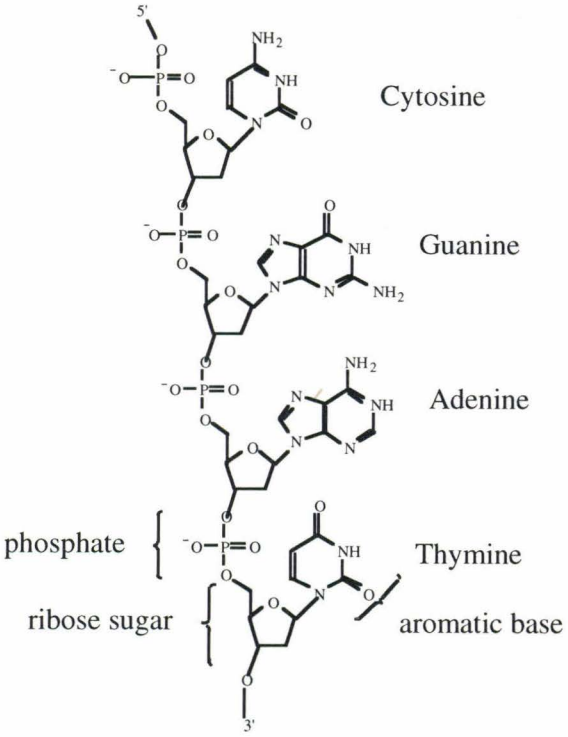

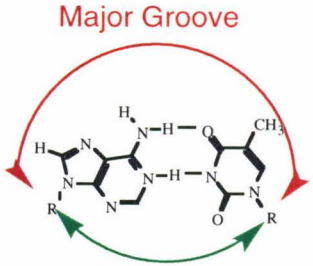

Adenine:Thymine

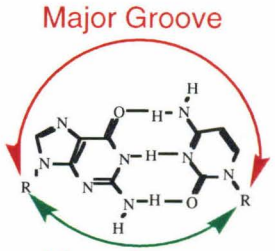

Guanine:Cytosine

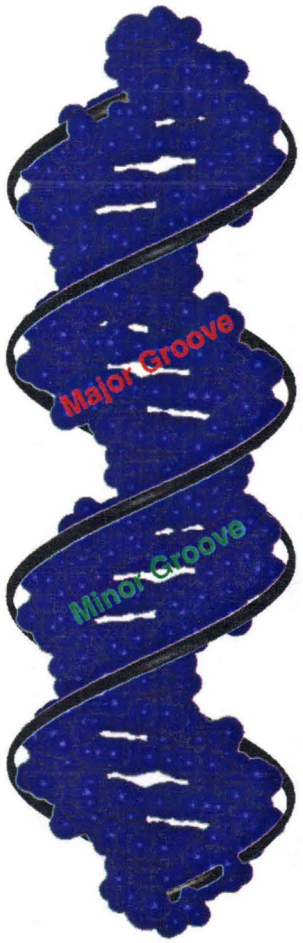

Historically, it was thought that proteins might recognize specific DNA substrates by matching particular amino acid hydrogen bonds and van der Waals functionalities with those of the individual DNA bases.[5] This type of recognition was termed direct readout and was supported by the fact that most proteins bind primarily in the major groove of DNA, which has a greater number and variety of functionalities to specify sequence. Over the past decade, a range of studies have made it increasingly clear that the act of recognition is much more complex.[6] Despite a growing body of structural data, no general rules for the recognition of DNA by amino acid side chains have emerged.[7] Specific amino acids have been shown to recognize more than one base and, inversely, each base has been shown to be recognized by a number of different amino acids. The recognition properties of individual amino acids are largely dependent on their three-dimensional orientation relative to the DNA. These orientations are in turn determined by the local and global structure of the protein. Furthermore, the three-dimensional characteristics of double stranded DNA are just as complex.[4] The sequence of a particular DNA determines its characteristics such as groove width and depth as well as the positions and orientations of the bases, sugars, and phosphates relative to each other in space. The DNA double helix is not simply a uniformly spiraling staircase of linear base pair sequence. Instead, the three-dimensional structure of DNA is polymorphic and in a way which depends upon the sequence.[8] Recognition which depends upon these local variations in the three-dimensional structure of the double helix has been termed shape selection or indirect readout, and this binding mode plays at least as important a role as direct readout in the recognition of DNA.[9,10]

1.1.2 The Ensemble of Non-covalent Interactions

DNA binding proteins tend to have affinities for DNA of at least 10^6 M^{-1} which corresponds to contacts with the double helix worth 8 kcal more than the contacts they make with the solvent. Hydrogen bonds and methyl-methyl van der Waals contacts are worth approximately 0.25-2 kcals for DNA binding versus water.[11,12,13] The task of designing a small synthetic molecule which would make enough specific contacts with the complex three dimensional structure of DNA to achieve high affinity is indeed daunting. Instead, both DNA-binding proteins and their small molecular mimics in achieving high affinity binding to DNA take advantage of a range of non-specific interactions, as well as those which specify site contacts. Indeed, as a result of these non-specific contacts, achieving high affinity is not difficult. The challenge lies in obtaining specificity, or in other words a high ratio in affinity constant for specific versus non-specific sites.

An important means to generate non-specific interaction of molecules with DNA is based upon electrostatics. DNA is a polyanion with a -2 charge for each base pair unit. Positively charged molecules will therefore associate with DNA non-specifically on the basis of electrostatic interactions alone. Thus, many DNA-binding proteins tend to be basic, and small molecule mimics are similarly positively charged.

We take advantage of intercalation as a sequence-neutral non-covalent interaction of our coordination complexes with DNA. As first proposed by Lerman, intercalation occurs when a planar aromatic heterocycle inserts itself between the base pairs of the double helix.[14] Figure 1.2 illustrates the structurally characterized intercalation of $Pt(terpy)HET^+$ into the dinucleotide $(dCpG)_2$.[15] Note that the base step is expanded from the normal 3.4 Å distance to 6.8 Å and unwound by 23° to make room for the intercalator. A binding energy of 5-8 kcals

is gained by the interaction of delocalized π-orbitals of intercalating molecules with the π-orbitals of the heterocyclic aromatic base stack.[16] In the 1970's, Lippard and coworkers carried out a series of studies demonstrating that square planar platinum(II) complexes containing aromatic heterocyclic ligands could intercalate into duplex DNA in a fashion reminiscent of classical organic natural product intercalators.[17,18] Our studies have been based upon intercalation by octahedral complexes. This expansion of the coordination number converts a two-dimensional interaction to three dimensions.

The intercalation by aromatic heterocycles into dinucleotides has actually been crystallographically characterized in many instances.[16] Most of these natural products insert into the base stack from the minor groove. An exception is the platinum complex which inserts into the duplex via the major groove. This major groove orientation may very well be a general feature of metallointercalation. Many ^{1}H-NMR and biophysical studies have consistently demonstrated a similar major groove orientation for the octahedral metallointercalators.[19-23] In addition to expanding to three dimensions, this major groove intercalation by the octahedral complex has the advantage of delivering functional groups on the coordination complex with stereochemical control to sites in the major groove, where DNA sequence-specifying functional groups are most abundant.

1.1.3 Coordination Complexes in Probing Recognition

Transition metal chemistry offers tremendous utility in defining interactions with DNA. This utility and chemical diversity are illustrated by the many natural and more recent unnatural metal complex-DNA interactions explored in our laboratory and elsewhere.

Figure 1.2 Space filling illustration of Pt(terpy)HET^+ (HET = 2-hydroxyethanethiolate) intercalated into the dinucleotide $(dCpG)_2$. View is perpendicular to the helix axis.

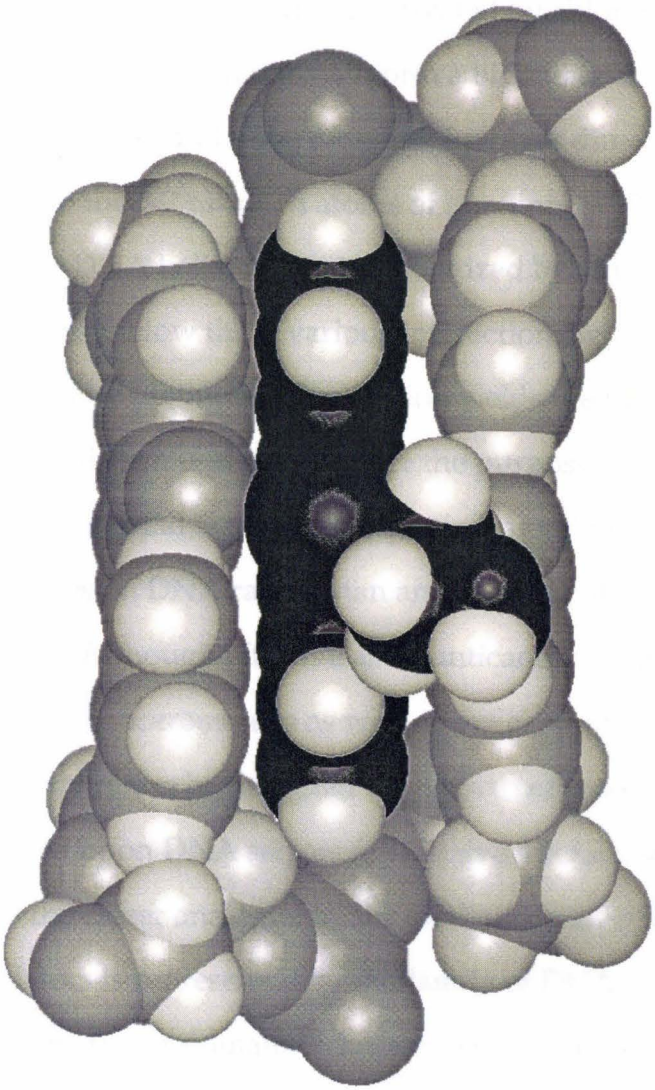

The best example of the application of metal-nucleic acid chemistry to chemotherapy to date rests in the simple coordination complex $(NH_3)_2PtCl_2$, *cis*-platin, which is a remarkably effective antitumor drug.[24] *Cis*-platin is used worldwide as an anticancer agent and is considered a cure for testicular cancer. The mode of action of *cis*-platin represents an area of intensive research. Studies have established that, once *cis*-platin is activated by chloride loss and hydrolysis, the diammineplatinum(II) moiety may form a bidentate crosslink to adjacent guanines on the DNA strand. The crosslink involves direct coordination of the platinum center to the N7 nitrogen atoms of guanines. [25] This crosslink leads to a severe kink in the DNA helix, which is recognized by structure-specific DNA-binding proteins.[26,27] How these various interactions with DNA-binding proteins promoted by platinum coordination yields the preferential toxicity to cancerous cells is still not understood. For the purpose of this discussion, what is important to keep in mind is that the *cis*-platin lesion involves *direct* coordination to nucleophilic sites on DNA rather than an ensemble of sequence-specific non-covalent contacts. Although effective as an anticancer agent, *cis*-platin shows cytotoxicity in non-cancerous cells as well. New generations of transition metal complexes must therefore be designed to achieve cell-specific cytotoxicity, presumably based upon DNA sequence-selective interaction.

Perhaps the closer analogue to our studies of non-covalent binding by metallointercalators is represented by the family of DNA-binding proteins containing the zinc finger domain.[28] It has been discovered that this zinc finger structural motif is ubiquitous to eukaryotic transcriptional activators. In this structural motif, a zinc ion coordinates two cysteines and two histidines within a ~ 30 residue polypeptide so as to fold the peptide into a structurally well-defined and stable domain. Multiple domains then interact sequence-specifically in the major groove of DNA (or RNA). Thus the zinc center defines a structural unit

with the surrounding peptide ligands. This structural unit non-covalently associates with DNA, poising functional groups for an ensemble of specific contacts.

This zinc finger motif therefore illustrates the utility of the metal center in defining the geometry and stereochemistry for the ligand structure which encapsulates it. Using octahedral coordination complexes in synthetic structures targeted to DNA, one may similarly control the structure and stereochemistry of surrounding ligands. Furthermore, ligands may be varied systematically and with synthetic facility to generate a family of structures targeted to DNA. Lastly, the potential for rigidity in these coordination complexes offers an additional element of definition and control in the design of DNA-binding complexes.

Transition metal complexes furthermore serve as powerful handles to probe DNA recognition. The spectroscopic properties of these complexes afford useful tools for the determination of affinities, modes, and orientations of binding. For example, the octahedral immine complexes of ruthenium(II) have strong visible absorbance and luminescence properties which change upon binding to DNA.[29] Paramagnetic metal complexes allow the use of NMR techniques to determine positions of binding via shifted and broadened DNA peaks.[30] The presence of heavier metals aids in the elucidation of complex crystal structures of large nucleic acids by x-ray crystallography.[31,32]

Importantly, metal complexes also provide reactive probes of DNA. The first chemical DNA footprinting reagent was developed by appending FeEDTA onto methidium, a common sequence-neutral intercalator.[33] In the presence of a reducing agent and hydrogen peroxide, hydroxyl radicals could be generated near the DNA using Fenton chemistry associated with the DNA-bound ferrous center. High concentrations of hydroxyl radicals promote DNA strand scission which may be monitored using high resolution gel electrophoresis techniques.

Tullius and coworkers then developed FeEDTA itself as a means of generating hydroxyl radicals in solution to probe DNA.[34] Dervan and coworkers also applied this oxidative metal chemistry in developing the more general technique of affinity cleaving by appending FeEDTA onto specific, as well as non-specific, DNA-binding molecules.[35] The reactive metal, in promoting DNA strand scission through redox chemistry, could be applied to mark sites of binding by different appended moieties.

In addition, oxidative DNA cleavage as a probe of DNA structure and reactions has been applied in studies using copper phenanthroline complexes, nickel macrocycles, and various metalloporphyrins.[36-39] Perhaps the natural analogue for metal-promoted oxidative chemistry of DNA lies in metallobleomycin, a natural product which chelates a metal and is also used in chemotherapy.[40] Bleomycin coordinates ferrous ion to form a complex which binds DNA in the minor groove with intercalation of the pendant bithiazole moiety.[41,42] A series of elegant mechanistic studies have shown that reaction with dioxygen leads to a ferryl intermediate which abstracts the C4'-H atom of the deoxyribose, promoting DNA strand scission.[43] This metal-promoted DNA cleavage is thought to be a critical element of the efficacy of the antitumor drug.

In our own studies of octahedral metallointercalators, the ability of photooxidation by rhodium(III) complexes to produce photoinduced DNA cleavage has been exploited. In these reactions, photolysis of DNA bound complexes of rhodium(III) likely activates the intercalated ligand, which is positioned in the major groove of duplex DNA. This activation takes the form of a ligand to metal charge transfer which directly abstracts the C3' hydrogen of deoxyribose and results in strand scission. Product analyses have been consistent with this mechanism.[22] This photoinduced DNA cleavage chemistry

may therefore similarly be applied in high resolution gel electrophoresis experiments to mark the sites of binding by the metallointercalator.

1.2 Recognition Based on Shape Selection

Recognition based upon shape-selection has been examined.[44] Complexes have been prepared with shapes and symmetries which match those of sites on DNA.[9] Indeed, these same complexes may be applied in probing the local variations in structure along the DNA helix. In general, what we learned from these initial studies, time and again, was the power of shape-selection in achieving high site-selectivity. Complexes lacking hydrogen bond donors or acceptors may be targeted to sites with specificities rivaling DNA-binding proteins.

1.2.1 Coordination Complex Chirality and the Right-Handed Double Helix

One of the simplest examples of shape selection lies in the chiral interactions of tris(phenanthroline) metal complexes with the right-handed B-DNA helix.[45] Photophysical and ^{1}H-NMR studies indicate that each enantiomer binds to DNA via two modes: one in which the complex partially intercalates between the bases in the major groove, and one in which the complex binds against the surface of the minor groove.[21,30,46] These studies also indicated a preference for the Δ enantiomer upon intercalation into the right-handed helix and a preference for the complementary symmetry of the Λ-isomer in surface-binding to right-handed DNA.

These results can be best explained if one considers the geometry of the ancillary ligands when the complex binds via intercalation. As can be seen from Figure 1.3, the Δ-isomer of the complex fits nicely into the major groove of right-handed DNA with the ancillary ligands extending along the groove, thus minimizing steric clashes with the right-handed phosphate backbone. On the

Figure 1.3 An illustration of both enantiomers of the tris(phenanthroline) metal complexes intercalated into DNA. Note the steric clashes of the phenanthroline ligands of the Λ-enantiomer with the backbone of the right-handed duplex.

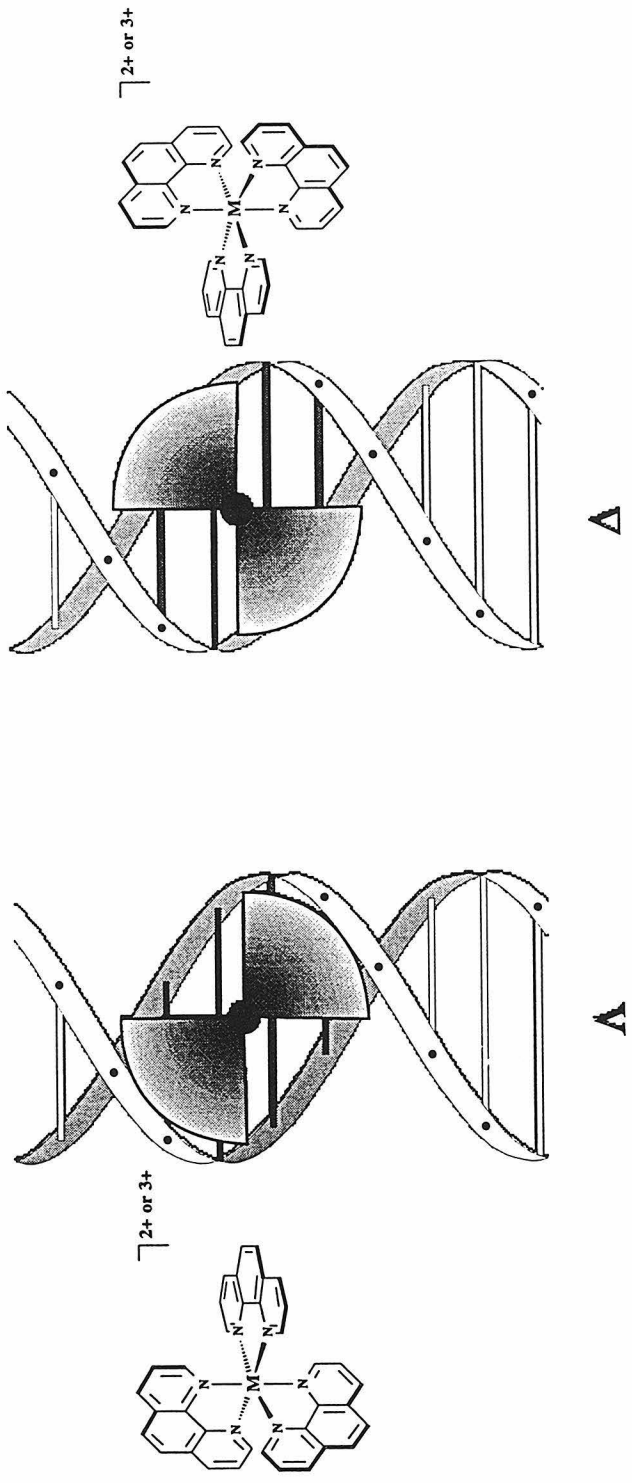
2+ or 3+
M
N
Δ
2+ or 3+
M
N
Λ

other hand, intercalation of the Λ-isomer positions the ancillary ligands against the groove and steric clashes with the phosphate backbone occur so as to destabilize the binding by this mode. A similar effect is seen with isomers of $Rh(phen)_2phi^{3+}$ and $Ru(phen)_2dppz^{2+}$, shown in Figure 1.4, where the presence of the phi and dppz ligands with enhanced surface areas for stacking leads to high affinity intercalation for both enantiomeric forms.[19,20] In these cases, the enantioselective preference for the Δ-isomer is maintained.[47,48] More support for this model is offered by the observation that the size of the ancillary ligands determines the extent of the enantioselective effect. As shown in Figure 1.5, for the family of metal complexes $Rh(bpy)_2phi^{3+}$, $Rh(DMB)_2phi^{3+}$, and $Rh(DPB)_2phi^{3+}$, the enantioselectivity increases from left to right with increasing ancillary ligand size.[49,50] Indeed, Λ-$Rh(DPB)_2phi^{3+}$ shows no detectable binding to B-DNA at 1,000 times the concentration of that where Δ-$Rh(DPB)_2phi^{3+}$ binds specifically.

1.2.2 Size and Shape of the Grooves

The major and minor grooves of a nucleic acid duplex offer different surfaces and shapes for recognition. Groove shapes become more varied still as a function of nucleic acid sequence and local conformation. A simple example of the heterogeneity of groove shape can be seen in the comparison of double stranded DNA, which is primarily in the B-conformation, with double stranded RNA, which adopts the A-conformation. Metal complex probes can be constructed which are sensitive to this variability in groove width and depth.

One such complex is $Ru(TMP)_3^{2+}$.[51] The complex binds nucleic acids via van der Waals contacts and electrostatics in the minor groove. For B-form nucleic acids, the minor groove is deep and narrow with the base stack protected from solution, as shown in Figure 1.6. The bulky TMP ligands on the complex

Figure 1.4 The metal complexes $Rh(phen)_2phi^{3+}$ and $Ru(phen)_2dppz^{2+}$.

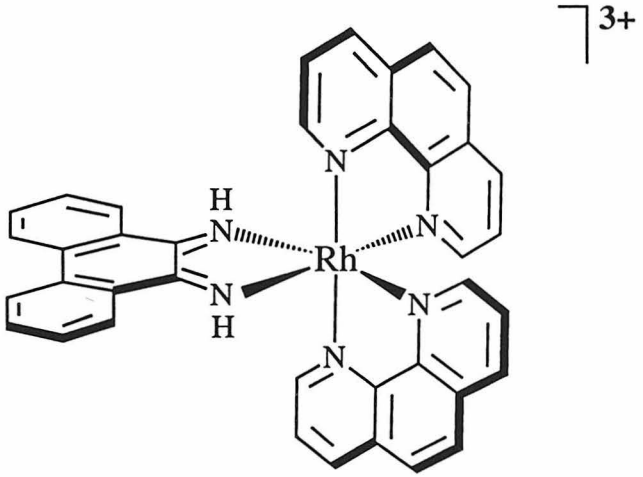

Δ-[Rh(phen)$_2$phi]$^{3+}$

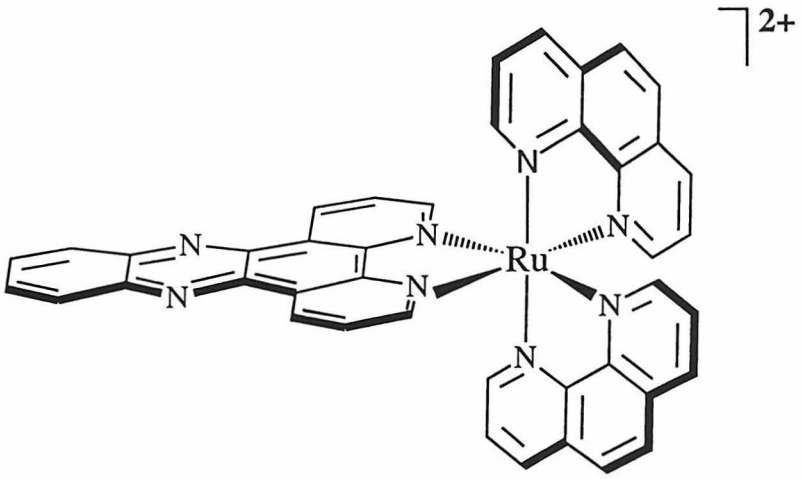

Δ-[Ru(phen)$_2$dppz]$^{2+}$

Figure 1.5 Effect of ancillary ligands on enantioselectivity. Enantioselectivity increases with increasing ligand size from left to right.

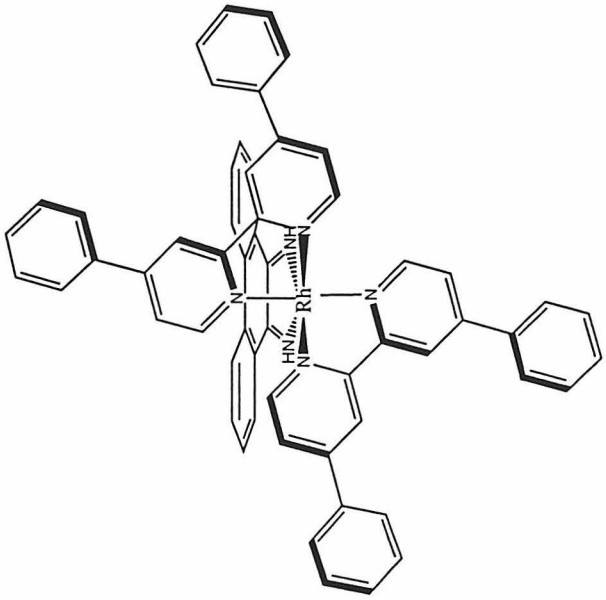

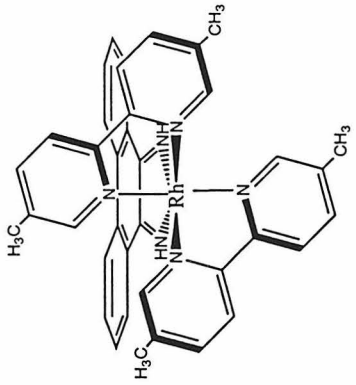

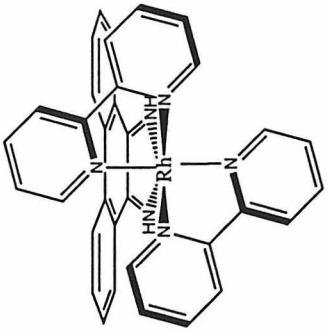

Figure 1.6 Stereoviews illustrating the size and shape complementarity of Λ–Ru(TMP)$_3^{2+}$ (left) and Δ-Rh(phen)$_2$phi^{3+} (right) with the grooves of A-form (top) and B-form (bottom) nucleic acids. Λ–Ru(TMP)$_3^{3+}$ is illustrated bound against the minor groove and Δ-Rh(phen)$_2$phi^{3+} is poised for intercalation in the major groove. In A-form nucleic acids, the shallow minor groove presents an accessible surface for binding by Λ–Ru(TMP)$_3^{2+}$. Meanwhile, the backbone in the major groove has closed down, preventing the intercalation of Δ-Rh(phen)$_2$phi^{3+}. In contrast, the tetramethylphenanthroline ligands of Λ–Ru(TMP)$_3^{2+}$ are too large to contact the base stack in the minor groove of B-form nucleic acids without clashing with the phosphate backbone. In the major groove, Δ-Rh(phen)$_2$phi^{3+} has ample room to intercalate into the base stack.

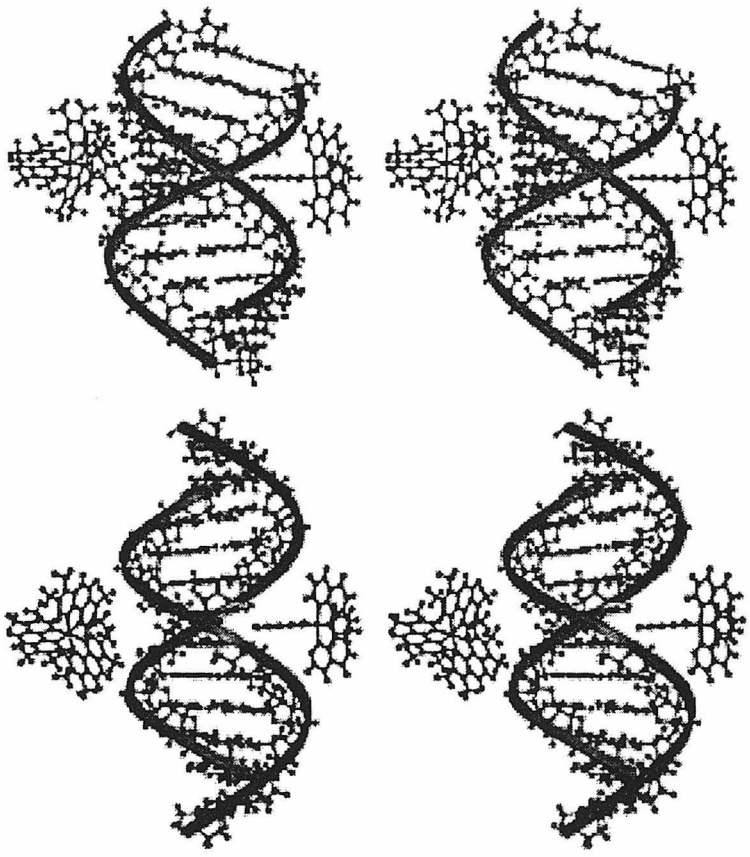

are just too large to get past the phosphate backbone and make van der Waals contacts with the base pairs. The minor groove of A-form nucleic acids adopts a completely different shape. In this case, the groove is shallow and wide, presenting the base stack to solution where the complex can easily interact with it.

A good probe of the shape of the major groove of nucleic acids is the intercalating metal complex Rh(phen)2phi^{3+}. While the complex binds avidly to B-form DNA, it shows low affinity for A-form nucleic acids like duplex RNA. This observation can be explained by the general groove shape of A and B-form nucleic acids. As illustrated in Figure 1.6, A-form nucleic acids possess a very narrow and deep major groove that does not allow enough space for the complex to reach and intercalate into the base stack. B-form nucleic acids, however, have a much shallower and wider major groove so that the complex can reach the base stack to gain the stabilization afforded by intercalative stacking.[52]

The fact that Rh(phen)2phi^{3+} does not bind to A-form nucleic acids makes it an excellent probe of RNA tertiary structure.[53] On yeast tRNA^{phe}, for which extensive crystallographic data exist, photocleavage studies have shown the complex to bind sites of triple base interactions and structured loops, while the complex shows no detectable binding to the A-form double stranded regions. Having characterized the binding properties of the complex to tRNA, binding studies were then carried out on tDNA, which was proposed to have a tertiary structure similar to RNA, although crystallographic data was lacking. As shown in Figure 1.7, the complex targeted the same sites on tDNA as on tRNA.[54] In addition, however, targeting of 5'-pyrimidine-pyrimidine-purine-3' (5'-pyr-pyr-pur-3') sites were observed in putative double helical regions. This specificity indicated that the tDNA was forming globally the same structure as the tRNA, but that its double stranded regions adopted the B-form instead of A-form.

Figure 1.7 Illustration of Rh(phen)2phi^{3+} photocleavage on tRNA^{Phe} and tDNA^{Phe}. Black circles denote positions of cleavage on both tRNA^{Phe} and tDNA^{Phe}, while grey circles denote positions of cleavage on tDNA^{Phe} only. Note that Rh(phen)2phi^{3+} cleaves double helical regions only on tDNA^{Phe}, indicating these regions are B-form only in tDNA^{Phe}. On both folded polymers, sites of tertiary interaction are targeted.

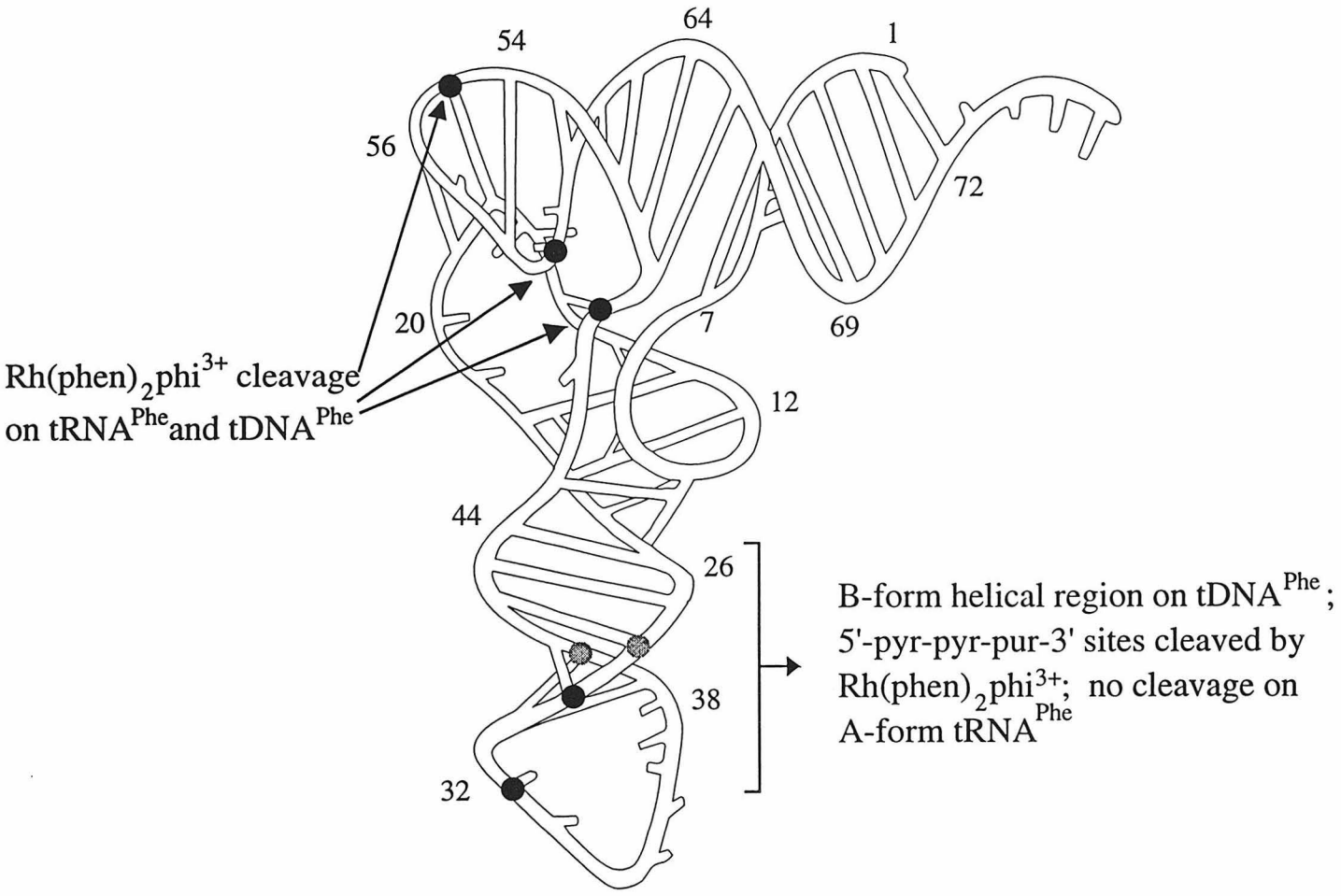
64
54
1
56
72
20
7
69
12
44
26
38
32
Rh(phen)2phi3+ cleavage
on tRNAPhe and tDNAPhe
B-form helical region on tDNAPhe;
5'-pyr-pyr-pur-3' sites cleaved by
Rh(phen)2phi3+; no cleavage on
A-form tRNAPhe

1.2.3 Local Variations in DNA Propeller Twisting

A more subtle example of shape selection is illustrated by the sequence-selective binding of Rh(phen)2phi^{3+} to B-form DNA itself. The rhodium complex contains no hydrogen bonding functionalities, yet DNA photocleavage studies have demonstrated a selective binding to 5'-pyr-pyr-pur-3' sequences with intercalation between the pyr-pur base step.[55] This result can be explained by steric clashes between the ancillary ligands and the DNA. Modeling studies have shown that the 2,9 hydrogens of the phenanthroline ligands may clash with the DNA bases upon intercalation of the phi ligand. Propeller twisting of the DNA bases can open up the intercalation site to allow more room for these hydrogens in a conformation referred to as an open major groove. As can be seen from Figure 1.8, the open major groove creates a chiral site for the complex in addition to that present due to the handedness of the helix. This affords even greater enantioselectivity in binding. This notion is supported by the quantitative correlation of enantioselective cleavage by Rh(phen)2phi^{3+} with propeller twisting at such sites measured through x-ray crystallographic studies of different B-form oligonucleotides.[52] Thus, shape-selective targeting by Rh(phen)2phi^{3+} may be applied as a chemical probe of the "openness" of the major groove.

1.2.4 Site-Specificity Rivaling a DNA Binding Protein

An example of the power of shape selection in determining sequence specificity is seen in the metal complex Rh(DPB)2phi^{3+}, shown in Figure 1.9. The diphenyl-bipyridyl ancillary ligands of this complex contain no potential hydrogen bonding functionalities, yet the specificity of the complex spans 8 base pairs.[49] The complex must be recognizing its target site based on the shape of this recognition sequence, 5'-CTCTAGAG-3'. Molecular modeling of the

Figure 1.8 Schematic illustration of the chiral binding site created by propellor twisting in an open major groove. The enantiomers of $Rh(phen)_2phi^{3+}$, also shown, provide probes of this propeller twisting.

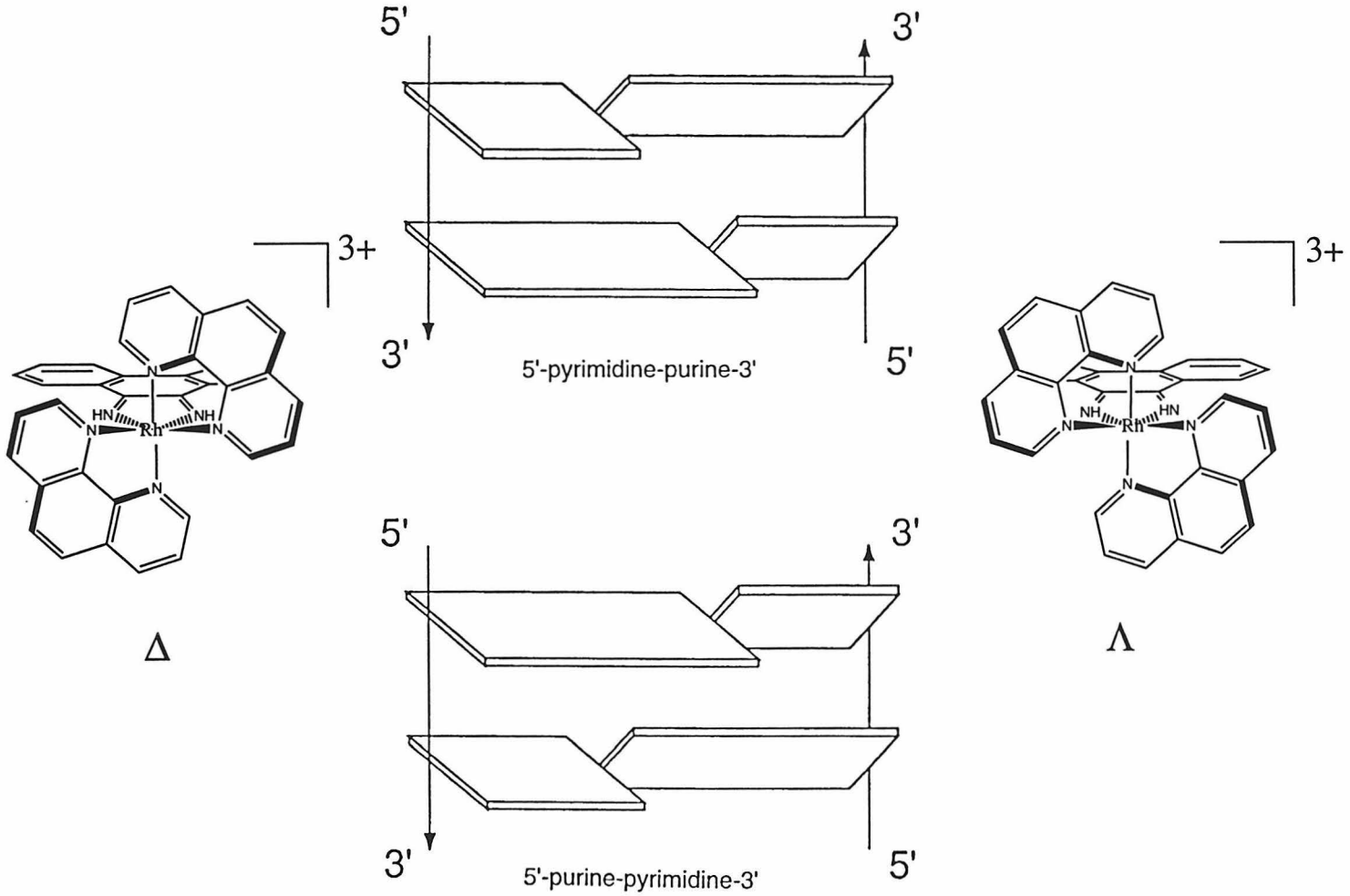
5'
3'
3'
5'
5'-pyrimidine-purine-3'
5'
3'
3'
5'
5'-purine-pyrimidine-3'
3+
3+
Δ
Λ

complex with DNA indicates that it is only large enough to span 6 base pairs, and photocleavage data indicate that the complex intercalates between the highlighted C and T. The cleavage site places the complex in a position such that it cannot reach the two 3' bases of its recognition sequence. This result led to the proposal that two complexes dimerize across the recognition sequence. Photocleavage and DNA footprinting studies were carried out on DNAs containing the 8 base pair full recognition site, as well as a 6 base pair monomeric subsite 5'-CTCTAG-3'. The binding affinity of the complex to the 8 base pair site was found to exceed the binding affinity to the 6 base pair site. These results were consistent with two complexes binding to the 8 base pair site in a cooperative manner with a 2 kcal interaction energy. This non-covalent dimerization in fact reflects a strategy exploited by DNA binding proteins[6] to substantially enhance site-specificity, a strategy which may also be utilized in subsequent generations of metal complexes being designed.

1.3 Direct Readout

Shape selection can provide a powerful influence on the sequence specificity of a molecule binding to DNA. In fact, $Rh(DPB)_2phi^{3+}$ with its 8 base pair recognition sequence is the most specific complex we have created to date. However, binding by shape selection is a tremendously complicated process involving many weak interactions and steric factors. While there is an increasing body of structural data becoming available for oligonucleotides, the rules governing the subtle heterogeneities of the double helix shape based on sequence is still poorly understood. This rudimentary understanding severely limits the use of shape selection in the predictive design of sequence specific DNA binding molecules.

Figure 1.9 Δ-Rh(DPB)2phi^{3+} and its palindromic recognition site.

5'-CTCTAGAG-3'
3'-GAGATCTC-5'

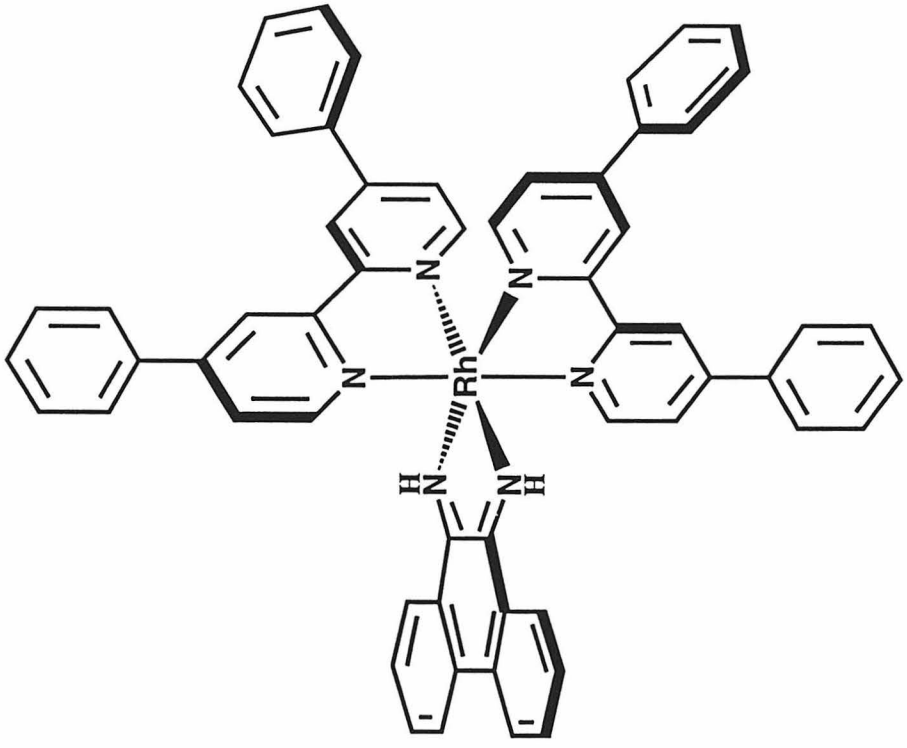

A potentially more predictive approach to the design of sequence-specific molecules is the use of direct hydrogen bonds and van der Waals contacts to functional groups on the DNA base pairs. As mentioned earlier, coordinatively saturated, octahedral, metal complexes make an excellent scaffolding for the placement of functional groups for such contacts. In order to better understand the energetics and constraints involved in the design of molecules which would recognize DNA via these contacts, we can apply coordination chemistry, starting with quite simple complexes, to characterize these interactions.

1.3.1 Hydrogen Bonds

An example of a simple synthetic metal complex which recognizes a sequence based on hydrogen bonding contacts is $Rh(NH_3)_4phi^{3+}$. ^1H NMR and DNA photocleavage studies have shown a preference for the complex to intercalate between 5'-GC-3' steps.[11,56] ^1H NMR data on $Rh(NH_3)_4phi^{3+}$ bound to $d(TGGCCA)_2$ indicate that the complex is deeply intercalated between the central 5'-GC-3' base step, and that the axial ammines of the complex are therefore placed in position to form specific hydrogen bonds with the O6 of the guanines above and below (Figure 1.10). A series of related compounds constructed to test if the amine hydrogen bonding contacts may be generally responsible for the 5'-GC-3' specificity is shown in Figure 1.11. Indeed, all of the $Rh(phi)^{3+}$ complexes containing saturated axial amines also show the preference for 5'-GC-3' recognition. In contrast, $Rh([12]aneS_4)phi^{3+}$, which lacks amines and thus the ability to donate hydrogen bonds to the DNA bases, lacks this 5'-GC-3' specificity.

Figure 1.10 $Rh(NH_3)_4phi^{3+}$ and a schematic of its hydrogen bonding contacts to a DNA 5'-GC-3' step upon intercalation in the major groove.

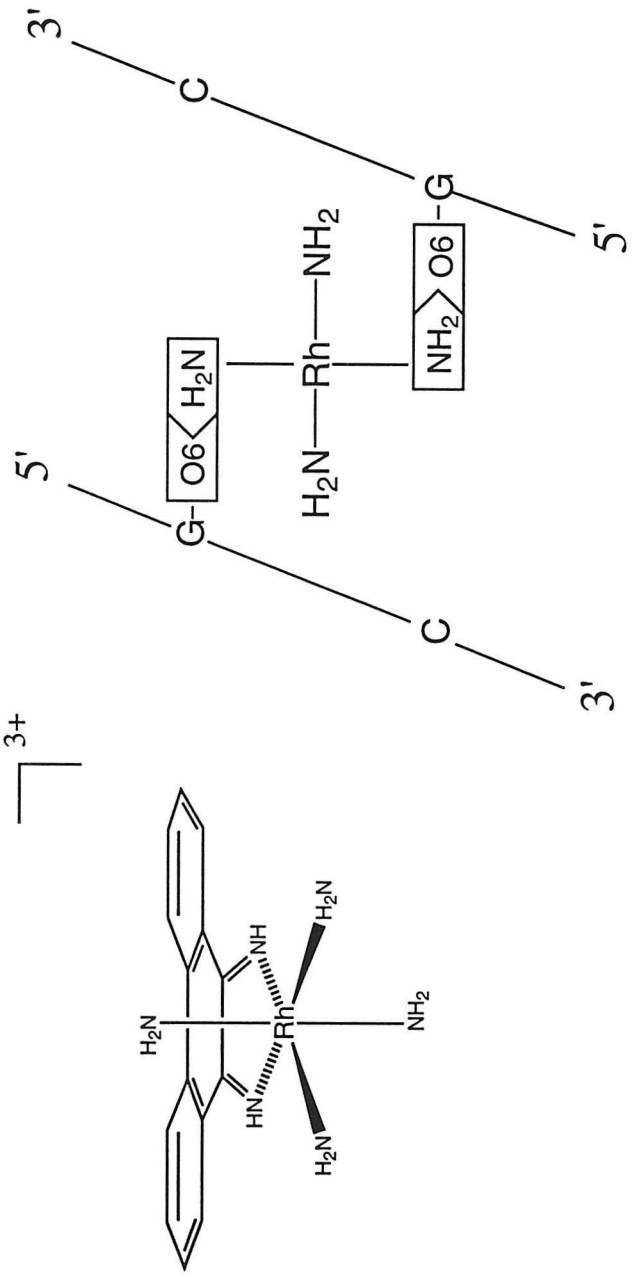
3'
C
5'
G
O6
H2N
Rh
NH2
H2N
NH2
O6
G
5'
C
3'
3+
H2N
NH
H2N
Rh
NH2
HN
H2N

Figure 1.11 Family of rhodium complexes constructed to test the importance of hydrogen bonding for 5'-GC-3' specificity. All complexes are found to target 5'-GC-3' steps except Rh(S_4-cyclen)phi^{3+}, which lacks hydrogen bonding functionalities.

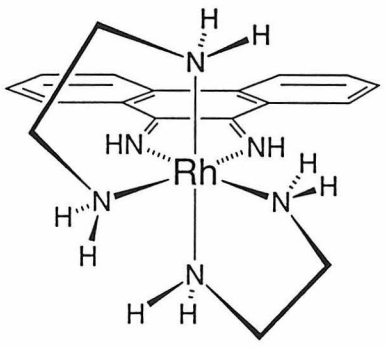

Λ-[Rh(en)$_2$phi]$^{3+}$

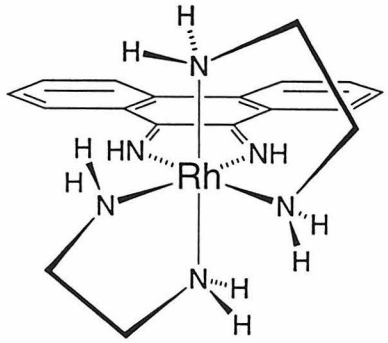

Δ-[Rh(en)$_2$phi]$^{3+}$

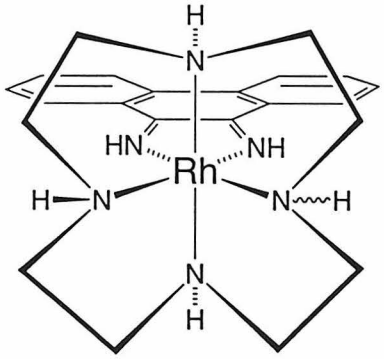

[Rh(cyclen)phi]$^{3+}$

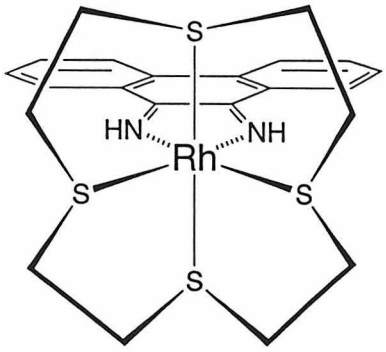

[Rh(S$_4$-cyclen)phi]$^{3+}$

1.3.2 van der Waals Interactions

DNA binding studies with enantiomers of $Rh(en)_2phi^{3+}$, both of which contain axial amines for hydrogen bonding, but which differ in disposition of the en ligands, showed differing specificities. While both enantiomers did indeed display a strong affinity for 5'-GC-3' base steps, Λ-$Rh(en)_2phi^{3+}$ showed also significant binding to 5'-TX-3' base steps; this site recognition is absent for the Δ-enantiomer. This result cannot be explained based on differences in hydrogen bonding, as both complexes contain axial amines which are similarly disposed. Shape selection due to steric clashes of the ancillary ethylene diamine ligands with the phosphate backbone is also not responsible, as these ligands are too small to account sterically for this interaction. Molecular modeling, however, indicates that the methylene groups of the ancillary en ligands are positioned in the Λ-enantiomer and not in the Δ-enantiomer for specific van der Waals contacts with the methyl group of 5'-thymines in the DNA major groove, as illustrated in Figure 1.12. To test the importance of this contact, uracil, which is identical to thymine except it lacks the methyl group, was substituted for thymine in synthetic oligonucleotides used to test recognition. DNA photocleavage studies were conducted on the synthetic oligonucleotides containing both uracil and thymine, and the results were compared. Oligonucleotides containing uracil showed no significant enantioselectivity in cleavage by $Rh(en)_2phi^{3+}$ enantiomers as compared to oligonucleotides containing thymine. This result indicates the essentiality of the methyl group of thymine for the binding by the Λ-enantiomer. This non-covalent contact was found to provide ~ 1 kcal stability. Importantly, the result supported directly the notion that these metallointercalators access the DNA from the major groove.

Figure 1.12 Schematic of methyl-methylene van der Waals interactions between the enantiomers of $Rh(en)_2phi^{3+}$ and 5'-TA-3'.

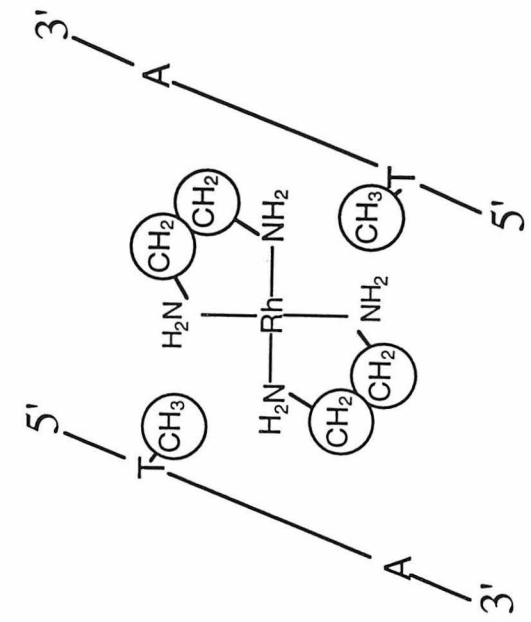
3'
A
5'
T
CH3
CH2
CH2
H2N
NH2
Rh
NH2
H2N
CH2
CH2
NH2
CH3
T
5'
A
3'

Δ

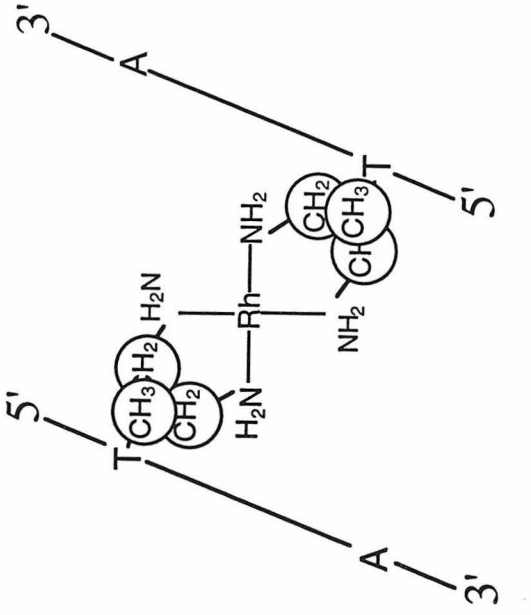
3'
A
5'
T
CH3
CH2
H2N
H2N
Rh
NH2
NH2
CH2
CH
CH3
T
5'
A
3'

Λ

1.3.3 Assembling Non-covalent Contacts for Predictable Specificity

With the information gained from the studies of hydrogen bonding and van der Waals contacts described above, the complex Δ-α-[Rh[(R,R)-Me_2trien]phi^{3+} was designed.[23] The complex is a derivative of Δ-$Rh(en)_2phi^{3+}$ which combines hydrogen bonding functionalities and van der Waals contacts to afford predictable 4 base pair specificity. This complex was designed specifically to target the sequence 5'-TGCA-3'. Modeling studies indicated that the axial amines of the complex are well-positioned for hydrogen bonding to the O6 of guanines, while the pendant methyl groups are disposed appropriately for van der Waals contacts with the methyl groups of the thymines 2 bases to the 5'-side, as shown in Figure 1.13.

As a demonstration of the flexibility of coordination chemistry for new design, the differences in recognition by the various structural isomers of Rh(Me_2trien)phi^{3+} were examined (see Figure 1.14). All 12 isomers were isolated, structurally characterized, and stereochemistry determined.[57] Each isomer contains the axial amines in position to hydrogen bond with the O6 of guanine. However, these isomers offer eight unique placements of the two methyl groups in three dimensional space. Modeling indicated that only Δ-α-[Rh[(R,R)-Me_2trien]phi^{3+} contains the correct geometry for stereospecific van der Waals contacts between both its methyl groups and the methyl groups of the thymines of the sequence 5'-TGCA-3'.

Importantly, photocleavage studies show that only this Δ-α isomer binds to 5'-TGCA-3'.[23] Titration studies of the complex with DNA indicated the preference of binding to sites of 5'-TGCA-3'>5'-GCA-3'>5'-GC-3'. The affinity of the complex for each of these sites decreases by approximately 1 kcal from left to right consistent with the loss of a methyl-methyl van der Waals contact.

Figure 1.13 Schematic of Δ-α-[Rh[(R,R)-Me2trien]phi^{3+} bound to its recognition sequence.

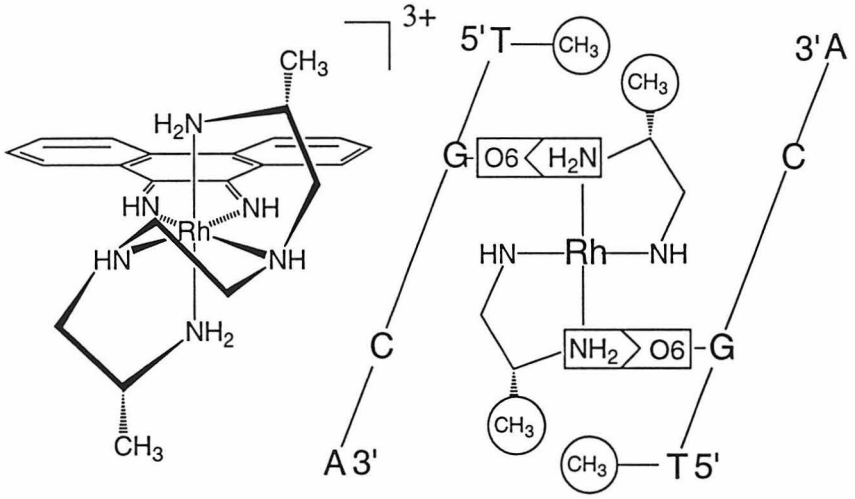
3+
CH3
H2N
HN
Rh
NH
HN
NH
NH2
CH3
5'T
CH3
CH3
G
O6
H2N
C
HN
Rh
NH
C
NH2
O6
G
CH3
A 3'
CH3
T 5'
3'A

Figure 1.14 Structural isomers of [Rh[(R,R)-Me$_2$trien]phi^{3+} (the enantiomers are not shown).

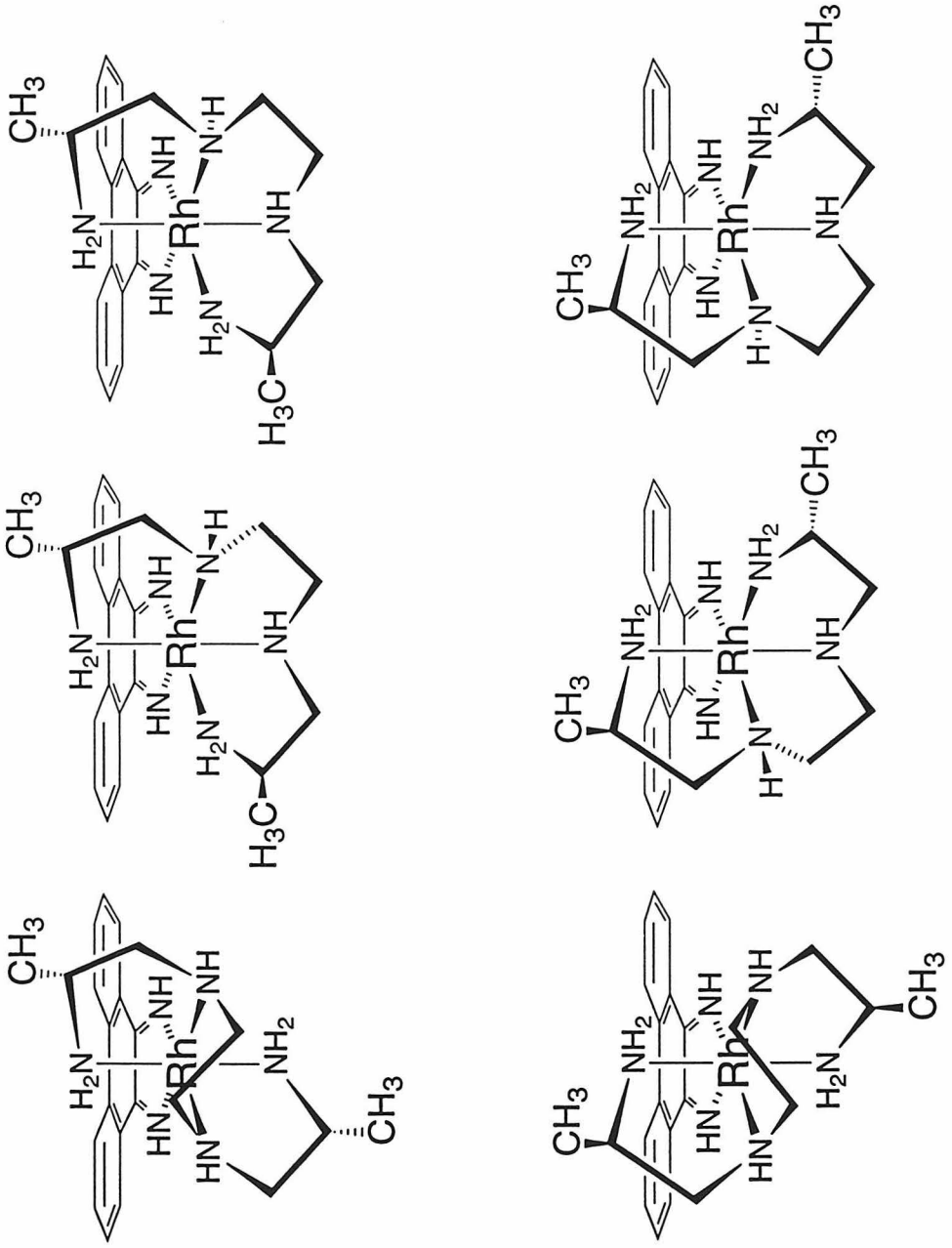

Figure 1.15 NMR structural model of Δ-α-[Rh[(R,R)-Me_2trien]phi^{3+} bound to the decamer d(GAGTGCACTC)$_2$.

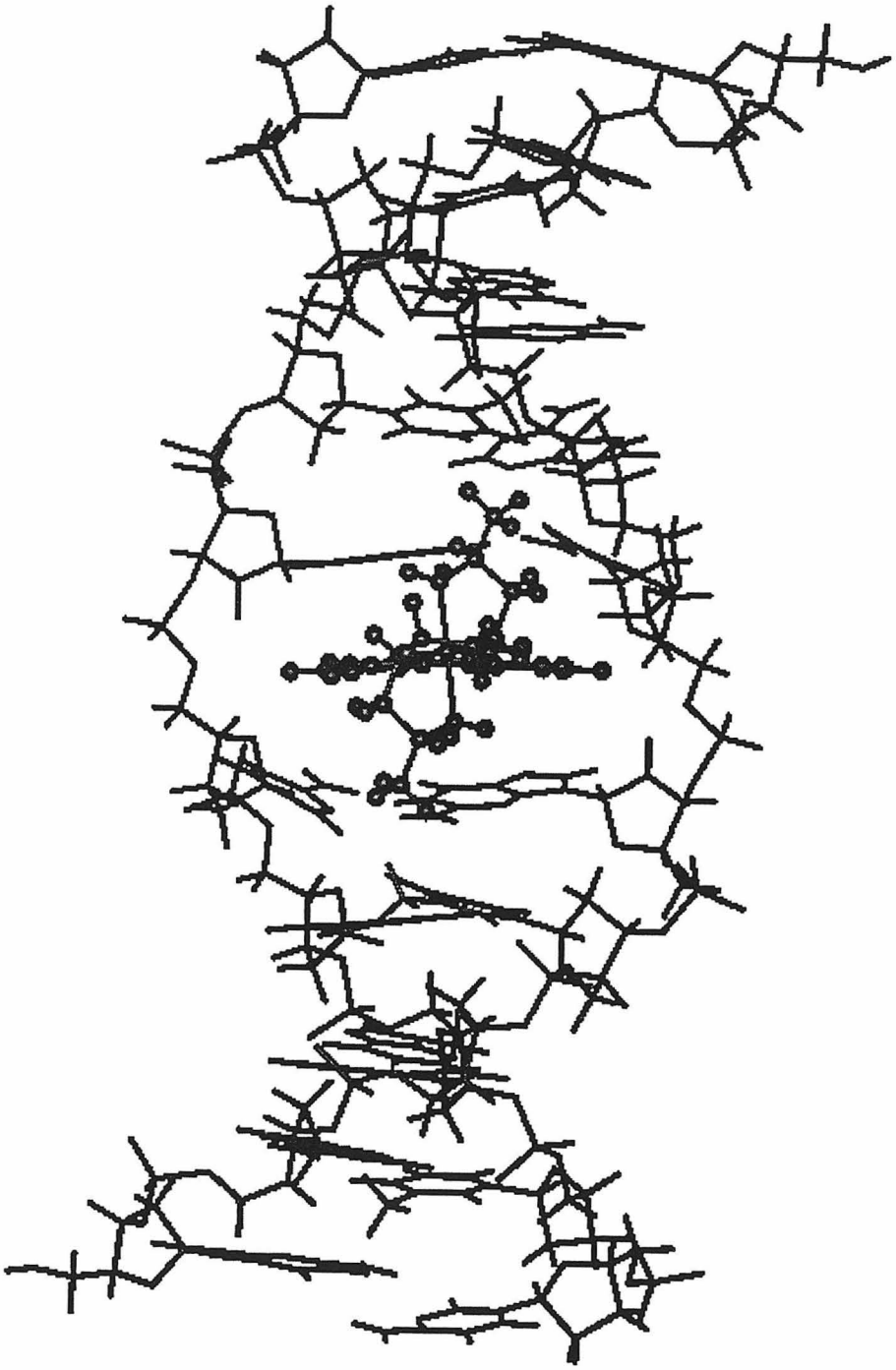

Recently, a high resolution ^{1}H-NMR structure of the complex bound to the DNA decamer d(GAGTGCACTC)$_2$, illustrated in Figure 1.15, has demonstrated that the complex intercalates between the central 5'-GC-3' step of the decamer, and that the designed van der Waals interaction is present between the complex methyl groups and the methyl groups of thymine.[58] This NMR structure represents that of the smallest site-specific molecule bound to the largest DNA yet characterized using high resolution NMR spectroscopy. The site-specificity demonstrates the utility of a minimalist approach. This large duplex oligonucleotide containing a single intercalator bound at one specific site furthermore provides an excellent system for examining the long range effects of intercalation. The ^{1}H-NMR data indicate that little distortion occurs to the DNA outside the site of intercalation; no bending of the duplex is observed. Instead, unwinding is evident at the central 5'-GC-step to accommodate the intercalator with preferential stacking of the phi ligand between with guanine bases on opposing strands. This intercalation poises the ancillary Me2trien ligand in the major groove for direct hydrogen bonding contacts with the guanines and direct methyl-methyl contacts with thymines two bases above and below. This structure represents the first example of a rationally designed synthetic metal complex interacting site-specifically with duplex DNA. Predictable site-specificity may be achieved by building up an ensemble of contacts in the major groove using metallointercalation as a platform.

1.4 Combining Direct Readout and Shape Selection: Recognition Based on Sequence-Dependent DNA Twistability

Λ-1-Rh(MGP)$_2$phi^{5+}, shown in Figure 1.16, represents an example of a metallointercalator which combines both shape-selection and direct readout and which binds DNA with high affinity and specificity. This complex targets the 6

Figure 1.16 (top) Two of the C_2-symmetric isomers of $Rh(MGP)_2phi^{3+}$. (bottom) Hydrogen bonding contacts between the guanidinium group of arginine and a guanine cytosine base pair.

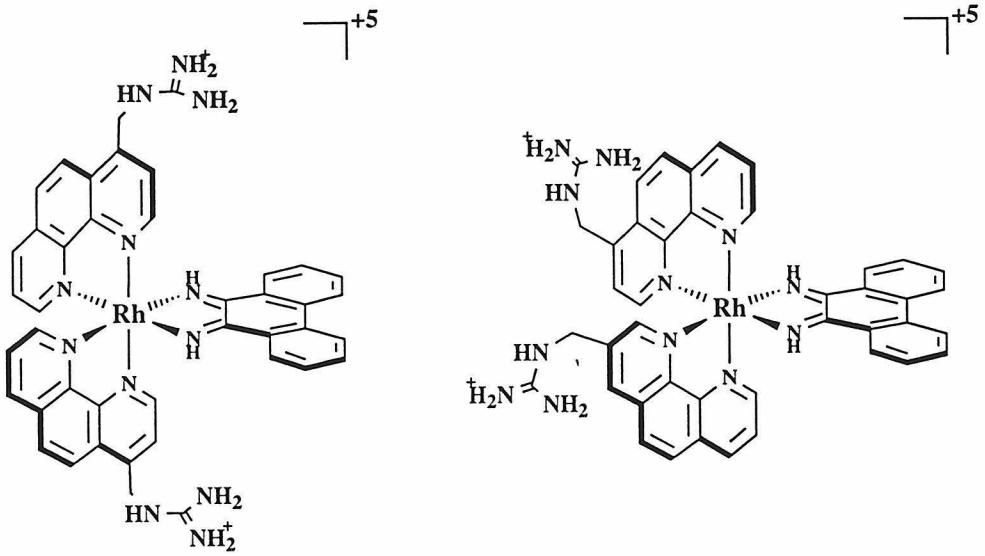
+5
+5
Rh
Rh

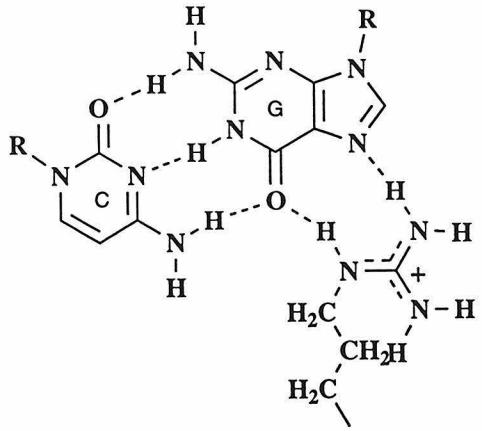
G
C

base pair site 5'-CATATG-3' with specificity and at subnanomolar concentrations.[59]

Isomers of Rh(MGP)2phi^{5+} were actually first prepared as a second generation analogue of Rh(phen)2phi^{3+} containing pendant guanidinium groups. While the absence of a general amino acid/DNA recognition code is clear, one frequent peptide recognition element observed in crystal structures, notably of zinc finger proteins, has involved targeting of guanine by the guanidinium side chain of arginine.[7] Also as illustrated in Figure 1.16, a guanidinium group can donate hydrogen bonds to both the guanine O6 and N7 atoms. The intention was to prepare a derivative of Rh(phen)2phi^{3+} in which the central element of the recognition site would be a 5'-pyr-pyr-pur-3' site, governed by the shape-selective interaction of Δ-Rh(phen)2phi^{3+}, and the periphery of the recognition site would be G-C base pairs, targeted by direct readout by the pendant guanidinium groups. The isomer with guanidinium group disposed away from the phi ligand, also shown in Figure 1.16, would offer a useful control for the electrostatic gain presented by introducing two positively charged functionalities onto the metal complex.

The recognition characteristics of the resultant complexes observed were quite remarkable. Although Δ-1-Rh(MGP)2phi^{3+} showed site-specificities which may reflect the design criterion, extremely high specificity and affinity were observed using the Λ-isomer for a site containing a central 5'-ATAT-3', which is not preferentially targeted by Λ-Rh(phen)2phi^{3+}. Photocleavage studies on a series of sequences indicated the essentiality of the central TA base step for recognition at any concentration, and oligonucleotide substitution studies using 7-deazaguanine confirmed the direct contact of the guanidinium groups of Λ-1-Rh(MGP)2phi^{5+} with the N7 nitrogen atoms of guanines in the 1 and 6 positions of the 6 base pair site.

The highly specific recognition was found to depend upon a sequence-specific twistability of DNA. This sequence-dependent twistability was determined in a DNA unwinding assay we developed, schematically illustrated in Figure 1.17, and based upon earlier elegant assays for DNA bending designed by Crothers and coworkers.[60] Earlier studies had shown that six adenines in a row, an A tract, cause the DNA helix to bend roughly 20°. If a series of these A tracts are placed in proper phase with the helical repeat of DNA, the bend becomes additive, and large curves in the DNA polymer are produced. Two sets of five additive A tracts, producing a 100° bend, were therefore ligated together with a variable sized central oligonucleotide containing the specific recognition sequence for Λ-1-Rh(MGP)$_2$phi^{5+}.[59] When the length of the linker oligonucleotide was a multiple of 10.5 base pairs, which corresponds to a 360° twist of the helix, the A tracks are in phase with each other and produce a 200° overall curvature in the DNA. This bent oligomer is well positioned for intramolecular cyclization by the enzyme ligase. If the metal complex specifically binds to the central region so as to unwind the DNA, altering the relative phasing of the two bent segments to an "S"-shaped structure, then intramolecular cyclization by ligase is inhibited. Perhaps the better demonstration of sequence-specific unwinding, however, is apparent in comparing intramolecular cyclization for the oligonucleotide phased in the "S"-shape without metal complex in the absence and presence of metal. Here, addition of metal complex, also illustrated in Figure 1.17, would serve to unwind the central segment so as to position the two bent segments for facile cyclization; in this case ligation by the enzyme is accelerated by the metal complex.

Using this assay, it was determined that in the presence of Λ-1-Rh(MGP)$_2$phi^{3+}, the site is unwound by 70° ± 10°, a substantial unwinding of the duplex. It has not yet determined if this sequence is particularly twistable in

Figure 1.17 Assay used to determine the extent of DNA unwinding upon binding by 1-Λ-Rh(MGP)2phi^{3+}. As illustrated, the metal complex, in sequence-specifically unwinding the DNA, macroscopically alters the structure of a bent DNA. A bent structure is converted to S-shaped or an S-shaped structure to a bent one. These structural alterations can be detected in solution through measurements of the intramolecular cyclization by these DNA substrates.

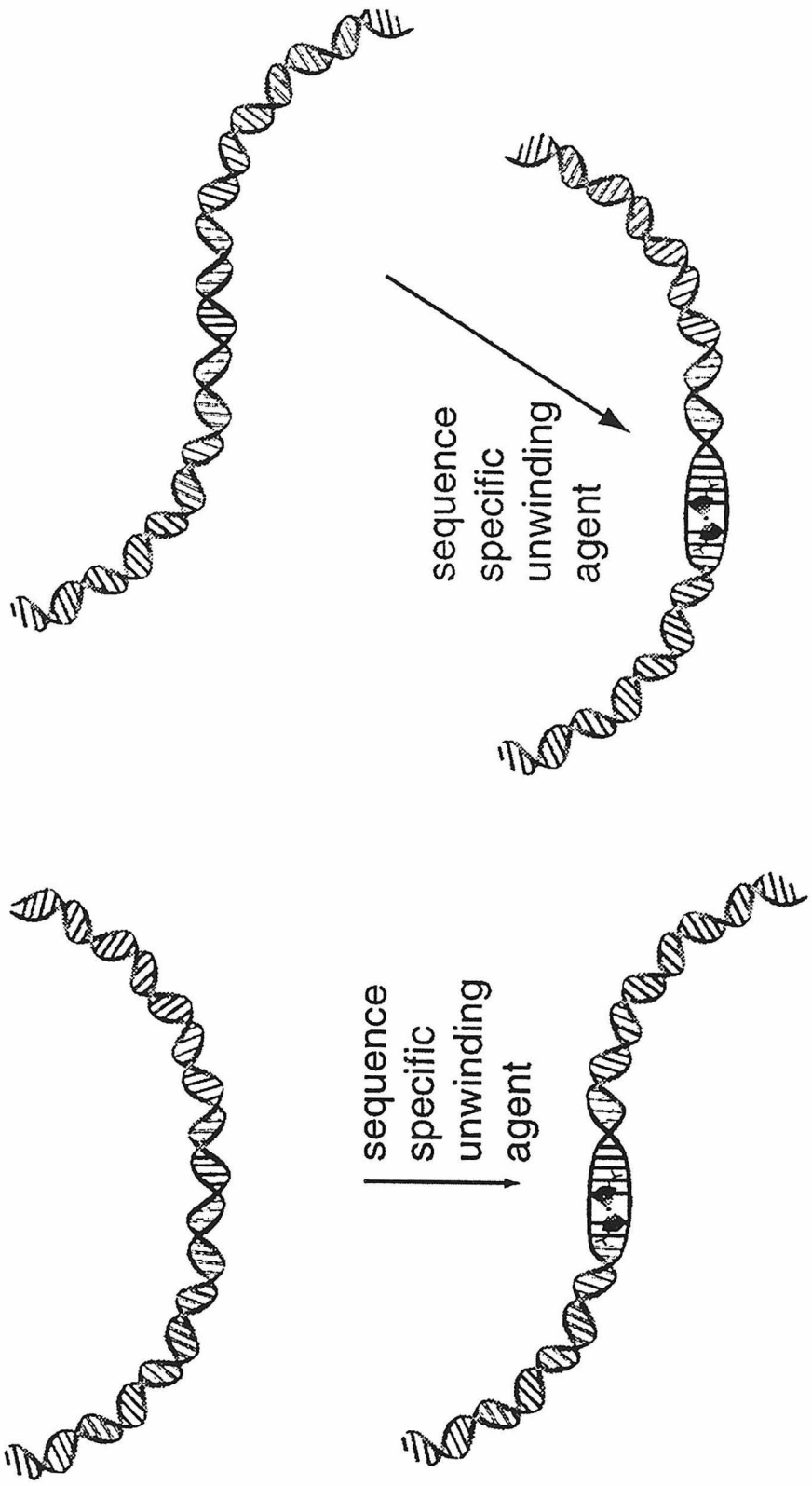
sequence
specific
unwinding
agent
sequence
specific
unwinding
agent

the absence of metal and binding by the rhodium complex, with its pendant guanidinium groups properly disposed, traps the unwound site, or whether the metal complex promotes the sequence-specific duplex unwinding. It is important to note in this context, however, that an essential transcriptional activator, the TATA-box binding protein (TBP), recognizes the sequence 5'-TATATAAA-3'. This site is similar to that recognized by the rhodium complex and is substantially bent and also unwound by more than 80°.[61,62] Studies with the rhodium complex therefore offer remarkable analogies to critical protein-DNA interactions. Moreover, these studies indicate quite clearly how the coupling of direct readout strategies to some conformational switch, or sequence-dependent twisting, can offer a remarkably high level of specificity in DNA site-recognition.

1.5 Metal- Peptide Chimeras

In nature, the recognition domains of proteins can often be broken down into discrete units. Often, the functionalities of a protein which make specific contacts with the DNA are localized to an α-helix which lies in the DNA major groove, while substantial non-specific DNA binding affinity is gained from a variety of electrostatic interactions with the phosphate backbone.[6] Frequently, site-specific affinities of DNA binding proteins are found to be 10^9-10^{10} M^{-1}, while affinities for non-specific DNA range from 10^4-10^7 M^{-1}. The site-specific recognition helices, however, cannot be separated from their parent proteins and used as sequence-specific DNA binding molecules because, without the remainder of non-specific contacts, they lack sufficient affinity for detectable binding. Furthermore, in the context of their natural proteins, these recognition units are specifically directed to the major groove in the correct orientation and conformation for binding.

Once again, transition metal chemistry is a valuable tool for the construction of sequence-specific DNA-binding molecules using peptides to achieve selectivity. To overcome the aforementioned problems, we have attached a series of recognition helices to the sequence-neutral metallointercalator $Rh(phi)_2phen^{3+}$.[63] In this chimera (Figure 1.18), the metal complex provides the non-specific binding energy necessary to bring the peptide into contact with the DNA in the major groove while the peptide provides the sequence specificity.

A family of metal peptide chimeras was prepared to investigate the binding properties of a peptide recognition helix. Attachment of this small recognition peptide to the metal complex resulted in a chimera which was remarkably specific for the sequence 5'-CCA-3'. No cleavage at these sites was found by the metal complex lacking the appended peptide. Hence, site-specific recognition depended upon interactions by the peptide. Systematic substitutions of amino acids in the appended peptide were made to determine which amino acids were responsible for the conformation and the sequence-specificity of the "recognition helix." Specific recognition of the chimera was found to depend sensitively upon the glutamic acid at position 10. Any mutation at this position resulted in a loss of specificity for DNA as well as a loss in α-helicity. Even conservative mutations such as replacing the glutamate with an aspartate, glutamate methyl ester, or glutamine disrupted binding. Importantly, alanine substitution at this position preserved α-helicity but site-selectivity was nonetheless lost. Hence, the glutamate appeared essential both to form an α-helix and for a specific contact in the DNA major groove. We have proposed the model shown in Figure 1.19 for this site-specific interaction, in which the metal complex is intercalated into the DNA with the α-helical peptide directed along the major groove to achieve a direct contact between the essential glutamate and

Figure 1.18 A metal-peptide intercalating chimera.

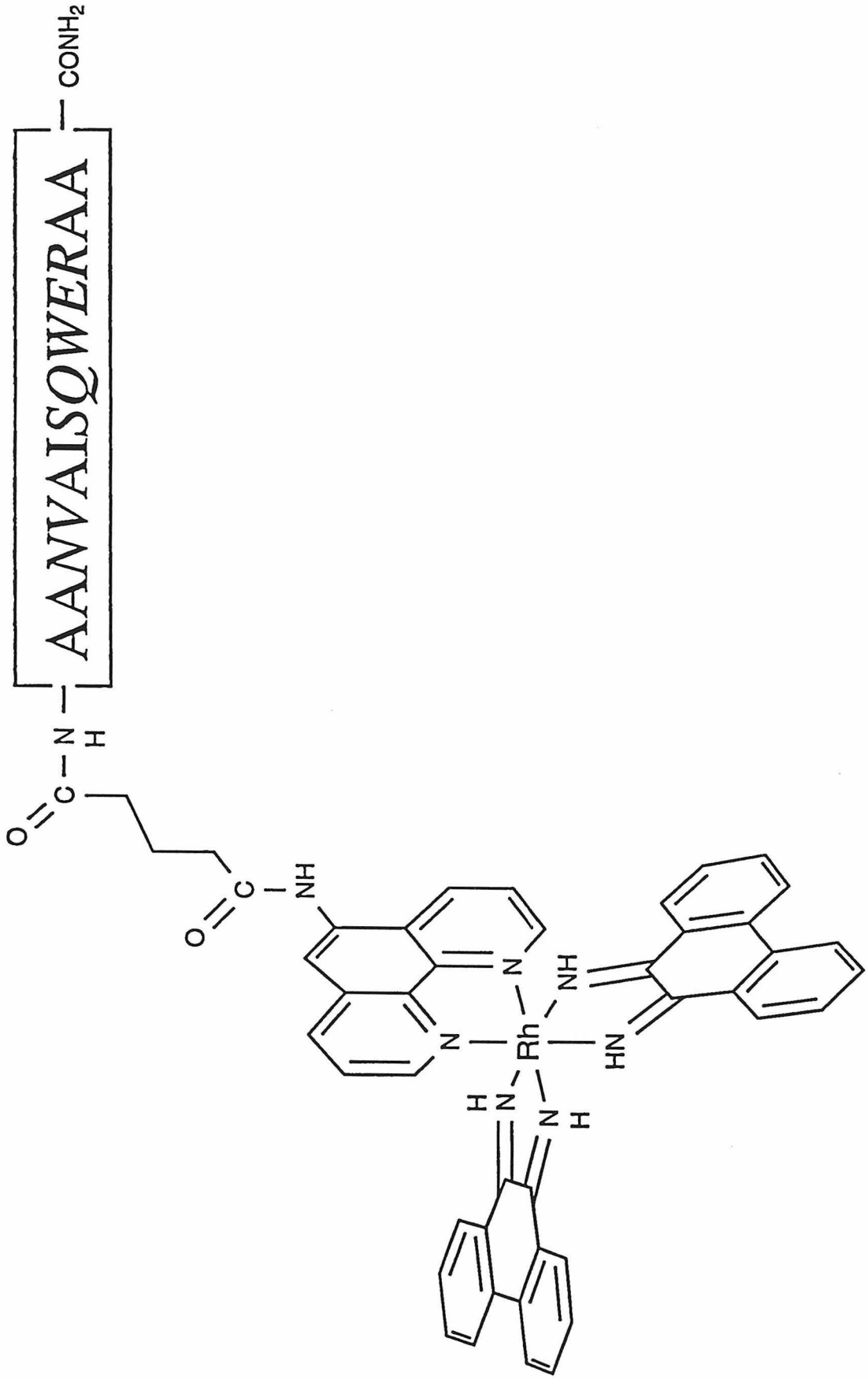
AANVAISQWERAA
CONH2
O
C
N
H
O
C
NH
N
Rh
N
NH
HN
H
N
N
H

Figure 1.19 A model of the metal-peptide chimera shown in Figure 1.18 bound to its recognition sequence. Note the α-helical conformation of the appended peptide with the glutamate side chain disposed for a specific contact with cytosine.

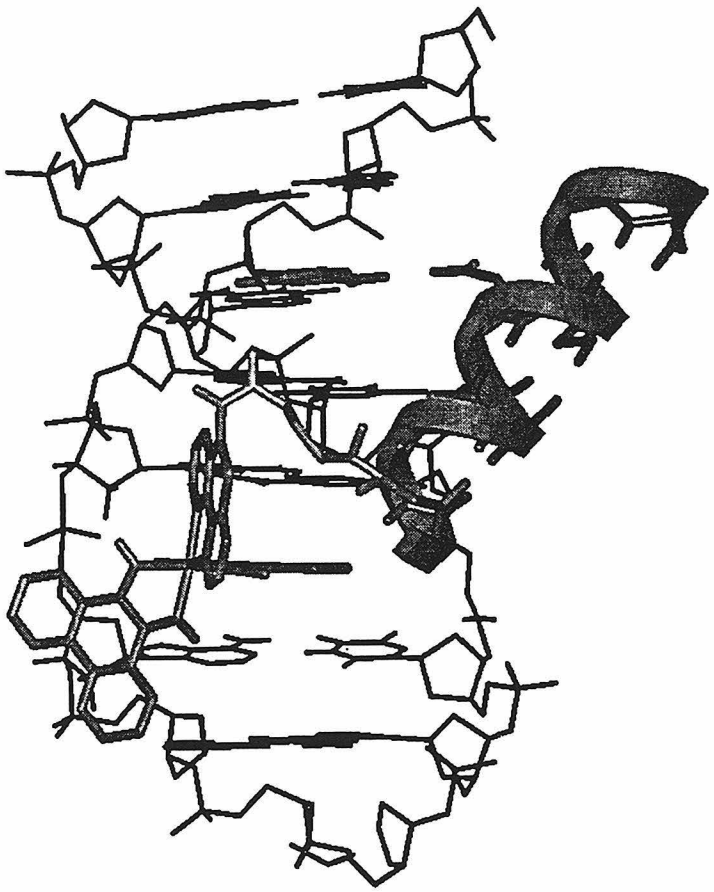

the amine group of cytosine. We propose 5'-CA-3' recognition to depend on the shape-selective opening of the major groove at the CA step. Importantly, as we saw in recognition by Rh(MGP)$_2$phi^{3+}, here too, a high level of specificity is derived from a sequence (peptide)-dependent conformational switch. For the peptide positioned in the α-helix to achieve contacts with the DNA major groove, a high level of specificity results.

1.6 Conclusion

Studies designing coordination complexes which bind DNA have provided valuable insights on the principles of site-specific recognition. Specificity has been designed through a combination of shape selection and direct readout. Like DNA-binding proteins, complexes may be prepared using the metal center as a scaffold from which to append a range of functionalities for sequence-specific contacts in the major groove. Metallointercalation provides a versatile platform for these interactions. Appending peptides to metallointercalators has resulted in a whole new array of sequence-specific DNA-binding complexes. Additionally, from the studies of binding by 1-Λ-Rh(MGP)$_2$phi^{5+}, notions concerning DNA sequence-dependent twistability and conformational switches have emerged. By coupling an ensemble of sequence-specific contacts to a conformational switch, a remarkable level of specificity can be achieved.

Chapter 2 of this thesis describes further investigations into the DNA recognition and binding properties of the enantiomers of 1-Rh(MGP)$_2$phi^{5+}. Quantitative affinity constants for Δ and Λ -1-Rh(MGP)$_2$phi^{5+} binding to their recognition sequences, 5'-CATCTG-3' and 5'-CATATG-3' respectively, are described. Rate constants of association and dissociation of 1-Λ -Rh(MGP)$_2$phi^{5+}

from 5'-CATATG-3' are also described in Chapter 2. These data contribute the greater understanding of how these complexes interact with DNA.

The ultimate goal in designing metal complexes which target specific DNA sequences is their application as therapeutics in the treatment of molecular diseases. In this regard, the most sequence-specific molecule is useless if it fails to show an effect on biological function. Early studies on $Co(DIP)_3^{3+}$ have shown that despite the high positive charge on this complex, it is avidly concentrated in the nuclei of mammalian cells.[63] To date, molecules of high specificity which have been constructed include Δ-$Rh(DPB)_2phi^{3+}$, 1-Λ-$Rh(MGP)_2phi^{5+}$, 1-Δ-$Rh(MGP)_2phi^{5+}$, and $Rh(MT)_2phi^{3+}$ which target 8, 6, and 4 base pair sites respectively. These compounds differ in chemical properties such as solubility, charge, and size. Chapter 3 of this thesis describes investigations into the ability of these complexes to inhibit the interactions of proteins with DNA in a template-directed manner. The relative potency of each complex is then compared to its chemical properties and its DNA binding characteristics. The results of this comparison yield important insights for the design of future therapeutics for the treatment of molecular disease.

1.7 References

1. Watson, J. D.; Hopkins, N. H.; Roberts, J. W.; Steitz, J. A.; Weiner, A. M.; Molecular Biology of the Gene 4th ed. **1987,** The Benjamin/Cummings Publishing Company, Inc.
2. Dupureur, C. M.; Barton, J. K.; In *Comprehensive Supramolecular Chemistry* , **1995** Ed. J.-M. Lehn, Pergamon Press, in press.
3. Sitlani, A. & Barton, J. K. 1995 Recognition of nucleic acids by transition metal complexes. In *Handbook on Metal-Ligand Interactions in Biological Fluids*, Marcel Dekker, in press.
4. Saenger, W.; Principles of Nucleic Acid Structure, **1984**, Springer-Verlag.
5. Seeman, N. C.; Rosenberg, J. M.; Rich, A.; *Proc. Natl. Acad. Sci. U. S. A..*, **1976**, 73, 804.
6. Steitz, T. A.; *Quart. Rev. Biophys.* , **1990**, 23, 205.
7. Pabo, C. O.; Sauer, R. T.; *Ann. Rev. Biochem.*, **1992**, 61, 1053.
8. Rich, A.; *Gene* , **1993**, 135, 99.
9. Chow, C. S.; Barton, J. K.; *Meth. Enzym.* , **1992**, 212, 219.
10. Otwinowski, Z.; Schevitz, R. W.; Zhang, R.-G.; Lawson, C. L.; Joachimiak, A.; Marmorstein, R. Q.; Luisi, B. F.; Sigler, P. B.;*Nature* , **1988**, 335, 321.
11. Krotz, A. H.; Kuo, L. Y.; Shields, T. P.; Barton, J. K.; *J. Am. Chem. Soc.* , **1993**, 115, 3877.
12. Donner, J.; Caruthers, M. H.; Gill, S. J.; *J. Biol. Chem.* , **1982**, 257, 4826.
13. Singleton, S. F.; Dervan, P. B.; *J. Am. Chem. Soc.* , **1992**, 114, 6957.
14. Lerman, L. S., *J. Mol. Biol.* , **1961**, 3, 18.
15. Wang, A. H. -J.; Nathans, J.; van der Marel, G.; van Boom, J. H.; Rich, A.; *Nature* , **1978**, 276, 471.
16. Berman, H. M.; Young, P. R.; *Ann. Rev. Biophys. Bioeng.* , **1981**, 10, 87.

17. Jennette, K. W.; Lippard, S. J.; Vassiliades, G. A.; Bauer, W. R.; *Proc. Natl. Acad. Sci., U.S.A.* , **1974**, 71, 3839.

18. Bond, P. J.; Langridge, R.; Jennette, K. W.; Lippard, S. J.; *Proc. Natl. Acad. Sci., U.S.A.* , **1975**, 72, 4825.

19. David, S. S.; Barton, J. K.; *J. Am. Chem. Soc.* , **1993**, 115, 2984.

20. Dupureur, C. M.; Barton, J. K.; *J. Am. Chem. Soc.*, **1994**, 116, 10286.

21. Rehmann, J. P.; Barton, J. K.; *Biochemistry*, **1990**, 29, 1701.

22. Sitlani, A.; Long, E. C.; Pyle, A. M.; Barton, J. K.; *J. Am. Chem. Soc.*, **1992**, 114, 2303.

23. Krotz, A. H.; Hudson, B. P.; Barton, J. K.; *J. Am. Chem. Soc.*, **1993**, 115, 12577.

24. Sundquist, W. I.; Lippard, S. J.; *Coord. Chem. Rev.*, **1990**, 100, 293.

25. Sherman, S. E.; Gibson, D.; Wang, A. H. J.; Lippard, S. J.; *Science* , **1985**, 230, 412.

26. Takahara, P. M.; Rozenzweig, A. C.; Frederick, C. A.; Lippard, S. J.; *Nature*, **1995**, 377, 649.

27. Chow, C. S.; Barnes, C. M.; Lippard, S. J.; *Biochemistry* , **1995**, 34, 2956.

28. Berg, J. M.; *Current Opinion in Structural Biology* , **1993**, 3, 11.

29. Murphy, C. J.; Barton J. K.; *Meth. Enzymol..*, **1993**, 226, 576.

30. Rehmann, J. P.; Barton J. K.; *Biochemistry*, **1990**, 29, 1710.

31. Ohalloran,T. V.; Lippard, S. J.; Richmond,T. J.; Klug, A.; *J. Mol. Biol.* , **1987**, 194, 705.

32. Jack, A.; Ladner, J. E.; Rhodes, D.; Brown, R. S.; Klug, A.; *J. Mol. Biol.* , **1977**, 111, 315.

33. Hertzberg, R. P.; Dervan, P.B.; *Biochemistry* , **1984**, 23, 3934.

34. Price, M. A.; Tullius, T. D.; *Meth. Enzym.*, **1992**, 212, 194.

35. Dervan, P. B.; *Science* , **1986**, 232, 464.

36. Sigman, D. S.; Mazumder, A.; Perrin, D. M.; *Chem. Rev.* , **1993**, 93, 2295.

37. Burrows, C. J.; Rokita, S. E.; *Acc. Chem. Res.*, **1994**, 27, 295.

38. Magda, D.; Wright, M.; Miller, R. A.; Sessler, J. L.; Sansom, P. I.; *J. Am. Chem. Soc.* , **1995**, 117, 3629.

39. Mastruzzo, L.; Woisard, A.; Ma, D. D. F.; Rizzarelli, E.; Favre, A.; Le Doan, T.; *Photochem. Photobiol.* , **1994**, 60, 316.

40. Hecht, S. M.; Bleomycin: Chemical, biochemical, and biological aspects, **1979**, Springer-Verlag.

41. Wu, A.; Vanderwall, D. E.; Stubbe, J.; Kozarich, J. W.; Turner, C. J.; *J. Am. Chem. Soc.* , **1994**, 116, 10843.

42. Manderville, R. A.; Ellena, J. F.; Hecht, S. M.; *J. Am. Chem. Soc.*, **1994**, 116, 10851.

43. Absalon, M. J.; Wu, W.; Kozarich, J. W.; Stubbe, J.; *Biochemistry* , **1995**, 34, 2076.

44. Pyle, A. M.; Barton, J. K.; *Progress in inorganic chemistry*, **1990**, 38 , 413.

45. Barton, J. K.; *Science*, **1986**, 233, 727.

46. Barton, J. K.; Goldberg J. M.; Kumar C. V.; Turro, N. J.; *J. Am. Chem. Soc.*, **1986**, 108, 2081.

47. Pyle, A. M.; Morii, T.; Barton, J. K.; *J. Am. Chem. Soc.* , **1990**, 112, 9432.

48. Hiort, C.; Lincoln, P.; Norden, B.; *J. Am. Chem. Soc.*, **1993**, 115, 3448.

49. Sitlani, A.; Dupureur, C. M.; Barton, J. K.; *J. Am. Chem. Soc..*, **1993**, 115, 12589.

50. Sitlani, A.; Barton, J. K.; *Biochemistry* , **1994**, 33, 12100.

51. Mei, H. Y.; Barton, J. K.; *Proc. Nat. Acad. Sci.* , **1988**, 85, 1339.

52. Campisi, D.; Morii, T.; Barton, J. K.; *Biochemistry* , **1994**, 33, 4130.

53. Chow, C. S.; Behlen, L. S.; Uhlenbeck, O. C.; Barton, J. K.; *Biochemistry* , **1992**, 31, 972.

54. Lim, A. C.; Barton, J. K.; *Biochemistry* , **1993**, 32, 11029.

55. Pyle, A. M.; Long, E. C.; Barton, J. K.; *J. Am. Chem. Soc.*, **1989**, 114, 2303.

56. Collins, J. G.; Shields, T. P.; Barton, J. K.; *J. Am. Chem. Soc.*, **1994**, 116, 9840.

57. Krotz, A. H.; Barton, J. K.; *Inorg. Chem.* , **1994**, 33, 1940.

58. Hudson, B. P.; Dupureur, C. M.; Barton, J. K.; *J. Am. Chem. Soc.*, **1995**, 117, 9379.

59. Terbrueggen, R. H.; Barton, J. K.; *Biochemistry* , **1995**, 34, 8227.

60. Wu, H. M.; Crothers, D. M.; *Nature* , **1984**, 308, 509.

61. Kim, Y.; Geiger, J. H.; Hahn, S.; Sigler, P.B.; *Nature*, **1993**, 365, 512.

62. Kim, J. L.; Nikolov, D. B.; Burley, S. K.; *Nature*, **1993**, 365, 520.

63. Sardesai, N. Y.; Zimmermann, K.; Barton, J. K.; *J. Am. Chem. Soc.* , **1994**, 116, 7502.

64. Chapnick, L. B.; Chasin, L. A.; Raphael, A. L.; Barton, J. K.; *Mutation Research* , **1988**, 201, 17.

Blank Page

Blank Page

Chapter 2: Investigations into the binding properties of the enantiomers of 1-Rh(MGP)$_2$phi^{5+}.

2.1 Introduction

With their specific and high affinity binding to DNA, the phi complexes of rhodium could potentially inhibit functional interactions between proteins and DNA. In order to fully understand any inhibition which is observed, the binding characteristics of these complexes with DNA must be detailed. As described in Chapter 1, information is available on the binding properties of the enantiomers of 1-Rh(MGP)$_2$phi^{5+}. For both complexes, the highest affinity six base pair sequences are known, as are the effects of mutations in these sequences.[1] 1-Λ-Rh(MGP)$_2$phi^{5+} shows the highest affinity for the sequence 5'-CATATG-3' while 1-Δ-Rh(MGP)$_2$phi^{5+} shows the highest affinity for the similar sequence 5'-CATCTG-3'. Table 2.1 lists the relative affinities, as measured by photocleavage intensity, of these two enantiomers for DNA sites which deviate from these two sequences.

Site	1-Λ-Rh(MGP)$_2$phi^{5+} $I_{site}/I_{5'\text{-CATATG-}3'}$	Site	1-Δ-Rh(MGP)$_2$phi^{5+} $I_{site}/I_{5'\text{-CATCTG-}3'}$
5'-CATATG-3'	1.00	5'-CATCTG-3'	1.00
5'-CA<u>CG</u>TG-3'	0	5'-CA<u>G</u>CTG-3'	0.1
5'-<u>T</u>ATATA-3'	0.73	5'-<u>T</u>ATCTA-3'	0.75
5'-<u>G</u>ATAT<u>C</u>-3'	0.67	5'-<u>G</u>ATCT<u>C</u>-3'	0.68
5'-C<u>T</u>TA<u>A</u>G-3	0.16	5'-C<u>T</u>TC<u>A</u>G-3'	0.48

Table 2.1: Relative photocleavage intensities for Δ and Λ 1-Rh(MGP)$_2$phi^{5+} at various DNA sequences.[1] $I_{site}/I_{5'\text{-CATXTG-}3'}$ is the intensity of photocleavage at the site listed to the immediate left of the number divided by the intensity of photocleavage at 5'-CATXTG-3' for the metal complex listed at the top of the column. Bases which are changed relative to the highest affinity sequence for each complex are underlined.

Previous experiments have yielded information about binding contacts and DNA distortion upon the association of 1-Λ-Rh(MGP)$_2$phi^{5+} with its recognition sequence. Experiments support hydrogen bonding contacts between the guanidinium functionalities on this complex and the N7s of guanine in its recognition sequence. When deazaguanine, which lacks the N7 for hydrogen bonding, is substituted for guanines in the recognition sequence for the Λ enantiomer, lower affinity is observed in binding. This is consistent with the N7 acting as a hydrogen bonding acceptor with a guanidinium functional group from this complex. The Λ enantiomer has also been shown to cause a substantial amount of distortion in the DNA to which it binds. The unwinding angle of DNA upon 1-Λ-Rh(MGP)$_2$phi^{5+} binding has been shown to be 70 degrees which is remarkable for such a small molecule.[2] While the above are important data, more quantitative information is needed for a complete understanding of the binding of these complexes to DNA. In this chapter, investigations of the quantitative affinity constants of the enantiomers of 1-Rh(MGP)$_2$phi^{5+} to specific DNA sites are presented. The rate constants of association and dissociation from these sites and observations of the effects of solution conditions on the photocleavage properties of these complexes will also be described.

One of the most fundamental pieces of information for the understanding of metal complex associations with DNA is affinity constants for individual DNA sites. These data give a quantitative measure of the affinity of DNA/ligand interactions. What is required for the determination of binding constants is some measurable property which is related to the fraction of ligand bound to a specific site. Commonly used methods for the determination of binding constants to DNA such as equilibrium dialysis,

absorbance spectroscopy, and fluorescence spectroscopy are inappropriate for determining site-specific affinity constants.[3,4,5] These methods do not allow the differentiation between ligand binding at different sites and thus their use results in average affinity constants for DNA. The phi complexes of rhodium demonstrate direct strand scission of DNA at the site to which they are bound upon irradiation with UV light.[6] This property can be exploited to determine binding constants at specific DNA sites. At constant ratios of ligand to DNA, increasing levels of DNA photocleavage are observed with increasing concentrations of DNA and rhodium. The fraction of ligand bound to DNA can be estimated at given site by the intensity of photocleavage observed at that site. By plotting photocleavage versus absolute concentration of DNA and rhodium complex, isotherms such as the one shown in Figure 2.1 can be generated. These data can be modeled by the reaction scheme shown in Figure 2.2. An equation to fit binding photocleavage data such as that shown in Figure 2.1 has been previously derived and is presented here.[7] The following three equations describe the concentrations of reactants in a photocleavage sample.

$$K_d = [Rh][DNA]/[Rh{\cdot}DNA] \qquad \text{Equation 2.1}$$

$$[Rh]_t = [Rh] + [Rh{\cdot}DNA] \qquad \text{Equation 2.2}$$

$$[DNA]_t = [DNA] + [Rh{\cdot}DNA] \qquad \text{Equation 2.3}$$

where K_d is the dissociation constant for metal complex binding to a specific DNA site, [DNA] is the concentration of specific DNA sites which are free, [Rh] is the concentration of free metal complex, [Rh·DNA] is the concentration of metal complex bound to specific DNA sites, $[Rh]_t$ is the total

concentration of metal complex, and $[DNA]_t$ is the total concentration of DNA sites. Equations 2.2 and 2.3 can be substituted into Equation 2.1 to yield:

$$K_d = (([Rh]_t - [Rh{\cdot}DNA])([DNA]_t - [Rh{\cdot}DNA]))/[Rh{\cdot}DNA] \qquad \text{Equation 2.4}$$

Equation 2.4 can then be solved for [Rh·DNA] to yield Equation 2.5.

$$[Rh{\cdot}DNA] = (([DNA]_t+[Rh]_t+K_d-(([DNA]_t+[Rh]_t+K_d)^2-4*[DNA]_t*[Rh]_t)^{0.5})/2$$

Equation 2.5

The fraction of DNA cleaved can be modeled with the following equation:

$$FC = PE[Rh{\cdot}DNA]/[DNA]_t \qquad \text{Equation 2.6}$$

where FC is the fraction of DNA cleaved, PE is the photoefficiency of cleavage which is the fraction of bound DNA which is cleaved. Thus PE will vary with irradiation time. Finally, Equation 2.5 can be substituted into Equation 2.6 to yield:

$$FC = \frac{(PE(([DNA]_t+[Rh]_t+K_d-(([DNA]_t+[Rh]_t+K_d)^2-4*[DNA]_t*[Rh]_t)^{0.5})}{(2*[DNA]_t)}$$

Equation 2.7

Fraction cleaved versus DNA and Rh concentration data can then be fit to Equation 2.7 to determine dissociation constants. The inverse of these dissociation constants are then taken to calculate the affinity constant.

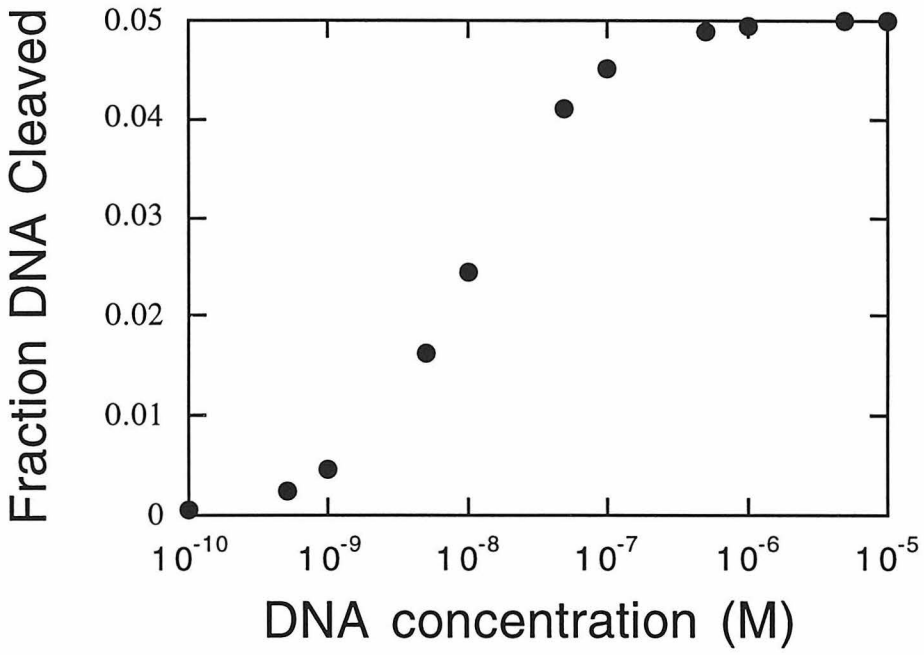

Figure 2.1: Theoretical binding isotherm for a metal complex with a binding constant of $1x10^8$ M^{-1}. The DNA/Rh ratio was held constant at 10:1 for the calculation of this curve.

Another important parameter in the binding of a metal complex to DNA is the exchange rate. The exchange rate is the number of times a metal complex dissociates from a given DNA site and reassociates with a different DNA site per second. This exchange is illustrated in Figure 2.3. The exchange rate for this process is the time it takes for the complex to dissociate from the DNA to which it is bound and reassociate with an unbound DNA. If diffusion between DNA's is neglected, this rate can be described by the following equation:

$$rate_{ex} = rate_a + rate_d \qquad \text{Equation 2.8}$$

where $rate_{ex}$ is the rate of exchange, $rate_a$ is the rate of association with the DNA site, and $rate_d$ is the rate of dissociation from the DNA site. If the exchange rate is measured when the concentrations of bound and free metal complex have reached equilibrium, then the rate of association and the rate of dissociation are equal. Thus equation 2.8 can be rewritten as follows:

$$rate_{ex} = 2rate_d \qquad \text{Equation 2.9}$$

The binding constants of the phi complexes of rhodium are > $1x10^5$ M^{-1}.[8,9,10] Therefore, when rhodium is limiting compared to DNA sites, the concentration of DNA bound rhodium can be assumed to be equal to the concentration of total rhodium. The exchange equation can be rewritten again as follows:

$$rate_{ex} = 2k_d[DNA \bullet Rh] \qquad \text{Equation 2.10}$$

where k_d is the rate constant of dissociation and [DNA•Rh] is the concentration of rhodium bound to DNA. Thus, from the exchange rate and the concentration of bound rhodium, the rate constant for the dissociation of metal complex from DNA can be determined. Furthermore, if the affinity constant for metal complex binding to DNA is known, then the rate constant for the association of metal complex with DNA can be determined by Equation 2.11.

$$K_b = k_a/k_d \qquad \text{Equation 2.11}$$

Thus, if the rate of exchange of metal complex between two DNA sites is known at a given metal and DNA concentrations, the rate constants of metal association and dissociation from the DNA sites can be determined.

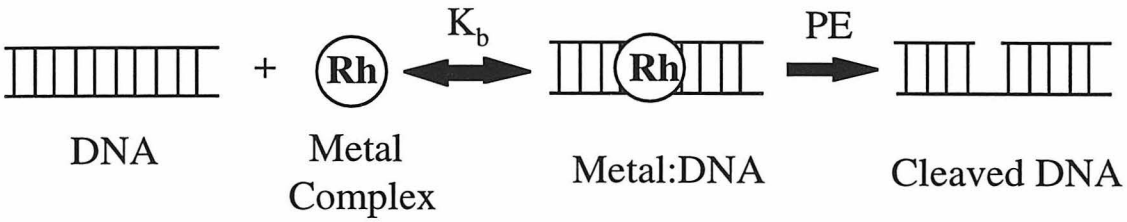

Figure 2.2: Reaction scheme for the photocleavage of DNA. Metal complex binds to the site of interest in an initial equilibrium determined by the binding constant K_b. A fraction of the bound DNA will then become cleaved upon the irradiation of the sample with UV light. The fraction of bound DNA which is cleaved will be referred to as the photoefficiency (PE) of the reaction and depends on many factors such as sample volume, irradiation time, lamp power, and the quantum yield of the complex.

The rate of exchange of molecules moving between two DNA sites can be measured using NMR. In this experiment, metal and metal-specific DNA sites are present at a 1:2 ratio. Thus at any instant, half the DNA molecules are bound and half the molecules are unbound by metal complex. Molecules binding to DNA can be in slow, intermediate, or fast exchange relative to the NMR time scale. Depending on the rate of exchange, different NMR spectra result (see Figure 2.4).[11] When exchange is slow relative to the NMR timescale, distinct peaks will be observed for free and bound DNA. As the rate of exchange increases relative to the NMR time scale, these peaks broaden and move closer together. When the relative exchange rate becomes fast, the signals from free and bound DNA are observed as one sharp peak which is the average of the actual chemical shifts of the two DNA environments.

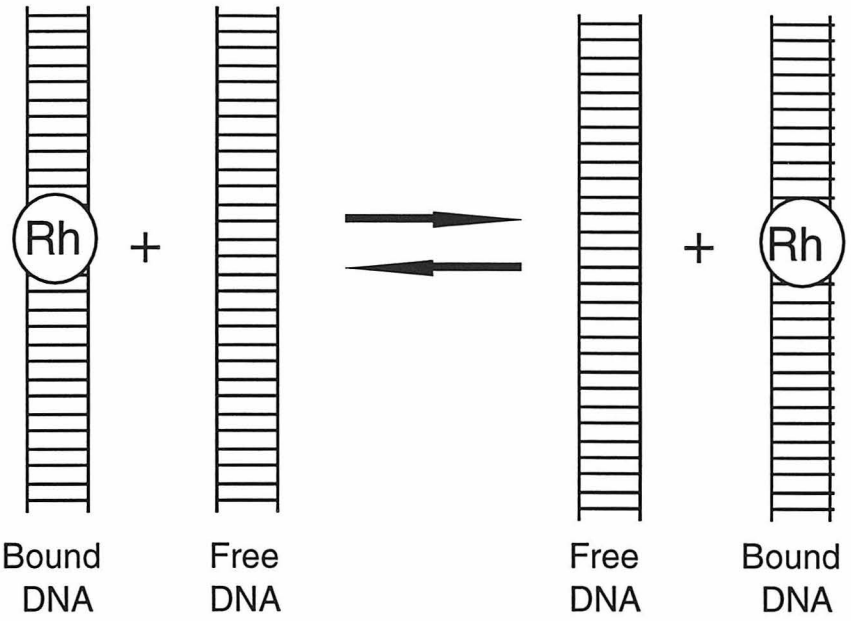

Figure 2.3: Illustration of a metal complex exchanging between two DNA molecules. The exchange illustrated occurs between identical sites on each DNA molecule.

The point at which the two peaks merge is labeled coalescence. At the temperature at which the peaks coalesce, the exchange rate can be determined by the following formula:

$$rate_{ex} = 2.22(\Delta v) \qquad \text{Equation 2.12}$$

where Δv is the difference in the chemical shifts of the peaks (in Hertz) at the coalescence temperature.[8] Different bound and free peak pairs will have non-identical separations in chemical shift and different temperatures at which they coalesce. The exchange rate, and thus the dissociation constant, can be determined at several different temperatures using several different protons to yield a set of temperature versus dissociation constant data. These data can then be plotted using the following form of the Arrhenius equation to determine the activation energy for dissociation:

$\log k_d = \log A - E_a/RT$ Equation 2.13

where A is the Arrhenius constant, E_a is the activation energy of dissociation, R is the gas constant, and T is the temperature.

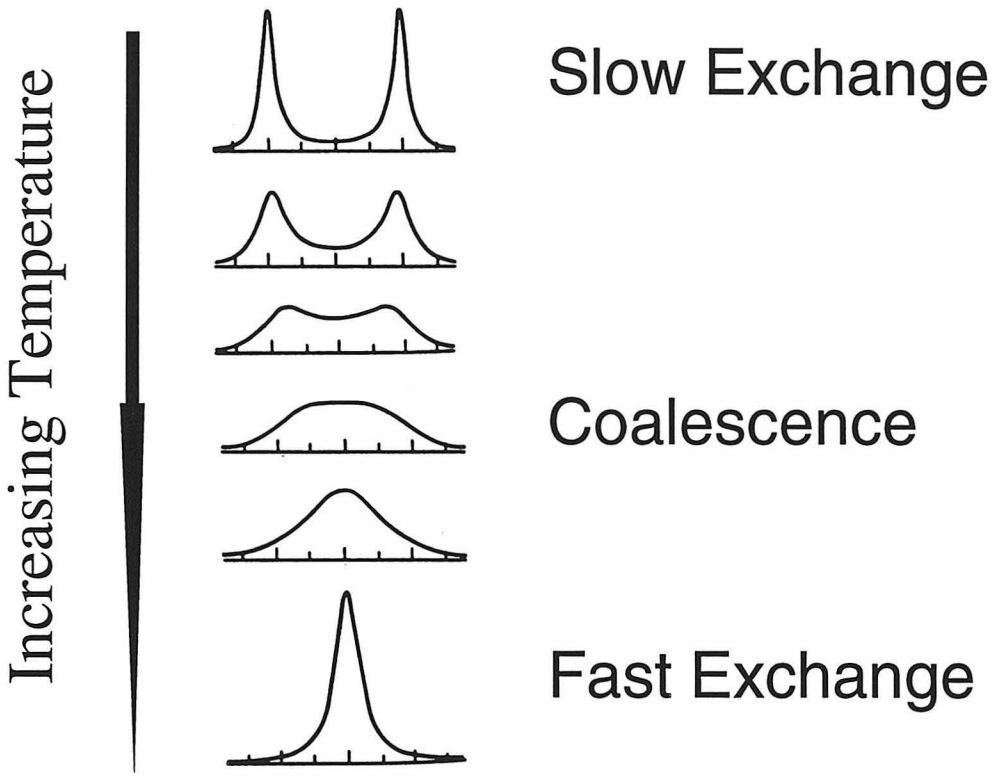

Figure 2.4: Behavior of hypothetical bound and free DNA peaks caused by rhodium exchanging between DNAs at different rates relative to the NMR time scale. At slow exchange, signals from both bound and free forms of DNA can be clearly resolved. As the exchange rate increases, as it does with increasing temperature, bound and free peaks broaden, coalesce, and finally sharpen into one peak which is at the average chemical shift of the bound and free forms. At the coalescence temperature, the exchange rate can be calculated using equation 2.5. Figure was adapted from reference 8.

Thus a plot of the $\log k_{ex}$ versus 1/T will yield a straight line where the slope = -Ea/R. If the activation energy of dissociation is known as well as the

binding constant, the entire reaction profile of the metal complex binding and dissociating from DNA can be constructed.

Investigations into the affinity constants of Δ and Λ -1-Rh(MGP)$_2$phi^{5+} to specific DNA sites as well as rate constants of association and dissociation at those sites are described below. The results of these studies provide a more quantitative understanding of the interactions of these complexes with DNA than previously existed.

2.2 Experimental

2.2.1 Materials

Synthesis and Purification of Oligonucleotides: All oligonucleotides were synthesized and purified in the same manner. A description of the 64mer duplex DNA used for photocleavage experiments is described here. A 64mer double stranded oligonucleotide containing recognition sites for Λ and Δ 1-Rh(MGP)$_2$phi^{5+} is shown in Figure 2.5. Both strands of this duplex were synthesized on an Applied Biosystems 392 DNA/RNA automated synthesizer using phosphoramidite chemistry.[12]

5'-CTCCATATGGAGACTC**CATCTG**GAGACTCTCTAGAGAGACTCTTGCAAGAGACTCCCATGGGAG-3'A

3'-GAGGTATACCTCTGAG**GTAGAC**CTCTGAGAGATCTCTCTGAGAACGTTCTCTGAGGGTACCCTC-5'B

Figure 2.5: The 64mer duplex DNA synthesized for binding constant determinations. The underlined and bolded sequences are the recognition sites for Λ and Δ 1-Rh(MGP)$_2$phi^{5+} respectively. A and B are labels to identify individual strands.

These oligonucleotides were synthesized with trityl groups attached to the 5' end of each. The oligonucleotides were deprotected by 65°C incubation overnight followed by lyophilization to dryness. They were then HPLC purified on a Waters 600E HPLC using a Dynamax C-18 reverse phase column

with the attached trityl group followed by lyophilization. The trityl group was removed by incubation in 80% acetic acid for 20 minutes followed by lyophilization. This was followed by a final HPLC purification and lyophilization to produce pure oligonucleotide. Oligonucleotides for photocleavage were dissolved in 10 mM TrisCl, pH 7.4. NMR oligonucleotides were dissolved in 10 mM PO_4^{3-}, 20 mM NaCl. DNA concentrations were quantitated by ultraviolet-visible spectroscopy (ε_{260} = 10000 M^{-1} nucleotides).

Preparation of Labeled Duplex DNA: 10 picomoles of DNA strand A (Figure 2.5) was radioactively labeled on its 5' hydroxyl with T4 polynucleotide kinase and γ-^{32}P-ATP. This strand was then mixed with 100 picomoles of cold DNA strand B, heated to 90°C, and allowed to slowly return to ambient temperature to anneal the strands. Radioactive duplex was purified by electrophoresis on a 20% non-denaturing polyacrylamide gel followed by excision of a gel slice containing the 64mer duplex. The gel slice was crushed and incubated in 1 ml of TE (10mM TrisCl, 1mM EDTA, pH 7.4) at 37°C for 4 hours. This incubation was followed by filtration of the solution by microcentrifugation with a 0.45mm Nylon-66 microfilterfuge tube (Rainin) to remove gel pieces. The labeled DNA was then desalted by ion exchange chromatography (Nensorb, Dupont). The resulting DNA was lyophilized and redissolved in buffer (10mM sodium cacodylate, 40mM NaCl, pH 7.0). Typical yield for a 10 picomole labeling using this procedure and duplex is 5 to 10 million counts as measured by Cerenkov counting.

Enantiomers of 1-Bis(4-guanidylmethyl-1,10-phenanthroline) (phenanthrenequinonediimine)rhodium(III), 1-Rh(MGP)$_2$phi^{5+}: The enantiomers of 1-Rh(MGP)$_2$phi^{5+} were synthesized and purified as previously described with the exception of the coupling of ligand to

rhodium.[1] 4-guanidylmethyl-1,10-phenanthrene (175mg, 0.7mmole), prepared as previously described,[1] and $Rh(NO_3)_3.xH_2O$ (75mg, 0.25mmole) were dissolved in 20 mL water and the pH of the solution adjusted to 7.0 with a saturated sodium carbonate solution. The solution was degassed, placed under a nitrogen atmosphere and refluxed for 8 hours. 9,10-diaminophenanthroline (63mg, 0.3mmole) was added to the reaction as a solid against a strong flow of nitrogen. The reaction was refluxed for an additional two hours, the pH adjusted to 2.0 with HCl, and 50 mL of water added followed by vigorous stirring in air for 24 hours. This yielded a solution containing the enantiomers of 1-$Rh(MGP)_2phi^{5+}$ which were purified as previously described.[2] The structural isomers of $Rh(MGP)_2phi^{5+}$ were separated by reverse phase HPLC. With a flow rate of 4.5 ml/min and a linear solvent gradient from 100% water to 80/20 water/acetonitrile over 30 minutes, 1-$Rh(MGP)_2phi^{5+}$ elutes at 24 minutes as measured at 270 nm. This isomer was collected and lyophilized to dryness. The Δ and Λ enantiomers of 1-$Rh(MGP)_2phi^{5+}$ were resolved by cation exchange chromatography using potassium antimonyl tartrate as a chiral eluant. The enantiomers were loaded in water onto a column containing Sephadex SP C-25 cation exchange resin. The resin was washed with several volumes of water, followed by elution of the enantiomers with 0.15 M potassium antimonyl tartrate. Clean separation of the enantiomers was obtained with the Λ eluting first. Both enantiomers gave identical ellipticities ($\Delta\varepsilon_{280}$ = 210 cm^{-1} M^{-1}) as measured by circular dicroism indicating 100% purity.

Enantiomers were stored as solid chloride salt at -20°C and redissolved in water buffered to pH 2.0 with trifluoroacetic acid fumes before use. Concentrations were determined by ultraviolet-visible spectroscopy (ε_{362} = 19500 M^{-1}). Purity of solutions older than one week was assayed by HPLC.

With a flow rate of 4.5 ml/min and a linear solvent gradient from 100% water to 80/20 water/acetonitrile over 30 minutes, 1-Rh(MGP)$_2$phi^{5+} elutes at 24 minutes as measured at 270 nm. Any solutions less than 95% pure as measured by absorption at 270 nm were discarded.

Reagents: Water used in all experiments was deionized with a Milli-Q plus PF water purification system. TrisCl, $MgCl_2$, NaCl, and Na_2CO_3 were purchased in electrophoresis grade from Sigma Chemical Company. Sodium cacodylate and 9,10-diaminophenanthroline were purchased from Aldrich Chemical Company. T4 polynucleotide kinase was purchased from New England Biolabs and α-P^{32}-dCTP with a specific activity of 3000 Ci/mmole was purchased from New England Nuclear Research Products. $Rh(NO_3)_3.xH_2O$ was purchased from Alfa-Aesar Johnson-Matthey. 9,10-diaminophenanthroline was purchased from Aldrich. All DNA synthesis reagents were purchased from Glen Research. All materials for electrophoresis were purchased from National Diagnostics.

2.2.2 Instrumentation

DNA concentrations were measured on either a Hewlett-Packard 8452A diode array or a Beckman DU 7400 UV-vis spectrophotometer. Oligonucleotides were synthesized on a ABI 391 DNA synthesizer and purified with a Waters 600E HPLC using a Dynamax C-18 reverse phase column. The purity of 1-Rh(MGP)$_2$phi^{5+} solutions was assayed using a Waters 600E HPLC using a Dynamax C-18 reverse phase column. Irradiations were carried out with a 1000W Oriel Model He/Xe 6140 lamp fitted with a monochometer, infrared filter, and 305 nm cutoff filter. Electrophoretic gels were scanned with a Molecular Dynamics phosphorimager and data quantitated using ImageQuant software. DNA samples were annealed on a

Perkin Elmer Cetus DNA thermal cycler. NMR spectra were obtained using a Bruker AMX500 500 MHz NMR spectrometer.

2.2.3 Effect of Irradiation Volume on Photocleavage Efficiency: A solution containing 1 μM duplex DNA (64mer), 50,000 cts/min 5' radiolabeled duplex DNA (64mer, approximately 1 nM), 1 μM 1-Λ-Rh(MGP)$_2$phi^{5+}, 10 mM sodium cacodylate, and 40 mM NaCl, pH 7.5 was made. 10, 20, 30, 40, 50, 60, 70, and 80 μL aliquots of this solution were placed in separate 1.7 mL eppendorf tubes. Samples were irradiated for 10 minutes at 313 nM on a 1000W Oriel Model He/Xe 6140 lamp. Lamp power, measured at 325 nm with a Liconix 45 pm laser power meter, was approximately 0.5 mW. After irradiation, samples were lyophilized and resuspended in denaturing gel loading dye (0.025% xylene cyanol, 0.025% bromophenyl blue, 10 mM NaOH, 90 mM TrisBorate, 1 mM EDTA, pH 8.3, 80% formamide) followed by loading and electrophoresis on a 20% denaturing polyacrylamide gel. This gel was then covered with Saran Wrap and exposed to a phophorimager screen overnight. The screen was then scanned on a Molecular Dynamics Phosphorimager and the amount of photocleavage at DNA site of interest quantitated. The fraction of the DNA cleaved at specific sites was determined by quantitating the amount of photocleavage at the specific site, subtracting the amount of signal in an equal gel area for a DNA site for which the complex shows no affinity at micromolar concentrations, and dividing by the signal in the parent band.

2.2.4 Effect of Irradiation Time on Photocleavage Efficiency: 20 μL of a solution containing 1 μM duplex DNA (64mer), 50,000 cts/min 5' radiolabeled duplex DNA (64mer, approximately 1 nM), 1 μM 1-Λ-Rh(MGP)$_2$phi^{5+}, 10 mM sodium cacodylate, and 40mM NaCl, pH 7.5 was aliquoted into four 1.7 mL

eppendorf tubes. These samples were then irradiated as described above for 5, 10, 20, or 30 minutes. The fraction DNA cleaved was then determined as described above.

2.2.5 Effect of Buffer on Photocleavage Efficiency: The DNA templates used in this experiment are described in the Results section when this experiment is discussed. 20 μL of a solution containing 1 μM DNA template, 50,000 cts/min 5' radiolabeled DNA template (approximately 1 nM), 1 μM 1-Λ-$Rh(MGP)_2phi^{5+}$ was irradiated for 10 minutes as described above in one of the following buffers: 10 mM sodium cacodylate, and 40 mM NaCl, pH 7.5; 10 mM sodium cacodylate, and 25 mM NaCl, pH 7.5; 10 mM sodium cacodylate, 40 mM NaCl, 1 mM dithiothreitol, pH 7.5; 10 mM sodium cacodylate, 40 mM NaCl, 10 mM $MgCl_2$, pH 7.5; or 10 mM sodium cacodylate, 40 mM NaCl, 40 mM TrisCl, pH 7.5. The fraction DNA cleaved was then determined as described above.

2.2.6 Determination of Binding Constants: A series of photocleavage reactions was carried out at constant ratios of 1-$Rh(MGP)_2phi^{5+}$ to DNA duplex. The ratios used for each enantiomer were 1:10 rhodium:duplex for the Δ enantiomer, and 1:2 rhodium:duplex for the Λ enantiomer. Radiolabeled DNA was present at a concentration 1 nM duplex in each experiment. Triplicate photocleavage experiments were run at total DNA concentrations of 1, 5, 10, 50, 100, 500, and 1000 nM DNA duplex. Buffer conditions were 10mM sodium cacodylate, 40mM NaCl, pH 7.0. Following a 4 minute preincubation upon mixing, samples were irradiated for 5 minutes at 313 nM on a 1000W Oriel Model 6140 He/Xe lamp. Sample volume was 20 μL and samples were contained in a 1.7 mL microcentrifuge tubes. Lamp power,

measured at 325 nm with a Liconix 45 pm laser power meter, was approximately 0.5mW. The fraction DNA cleaved at a specific site was determined as described above. This fraction cleaved was then plotted against DNA or rhodium concentration to generate a binding isotherm. The data used to generate this isotherm was fit to Equation 2.1 using Sigma Plot to determine the binding constant.

2.2.7 Determination of Exchange Rate of Λ–1-Rh(MGP)2phi^{5+}: Exchange rates were determined by variable temperature ^{1}H-NMR on a Bruker AMX500 spectrometer. The 10mer self-complementary oligonucleotide 5'-GACATATGTC-3' was synthesized and purified as described above. This oligonucleotide was resuspended in sodium phosphate buffer, pH 7.0. DNA samples were lyophilized and resuspended in D_2O three times to give a final solution approximately 0.5 mM in double stranded template, 10mM $NaPO_4^{-3}$, 20 mM NaCl. One dimensional ^{1}H-NMR spectra were taken of this solution at 21°C with solvent suppression by presaturation of the water peak.[13] One dimensional NMR spectra were taken at metal to DNA ratios of 0:4, 1:4, and 2:3. Spectra were then taken of this solution at the following temperatures: 5, 10 ,15 , 20, 25, 30, 35, 40, 45°C. Two dimensional NOESY spectra of the half titrated DNA were used to determine bound and free peak pairs in the spectra. Peak pairs which were well resolved at low temperature and coalesced over the temperature range studied were chosen to determine the exchange rate. The separation between these peaks was measured in hertz and used in Equation 2.5 to determine the rate of metal exchange between DNA sites at the coalescence temperature for each peak. Several rate constants of dissociation were determined for different temperatures and

plotted to determine the activation energy as described in the Introduction. The exchange rate at 10°C was also extrapolated from the linear fit of the plot.

2.3 RESULTS

2.3.1 Effects of Conditions on Photocleavage: As can be seen from the hypothetical data plotted in Figure 2.1, photocleavage at DNA concentrations two orders of magnitude higher and lower than the dissociation constant of the metal complex must be studied in order to observe fully bound and fully free metal complex respectively. Photocleavage data for fully bound metal are easily obtained as quantities of DNA and rhodium complex needed for these data can be synthesized. The high affinity of the phi complexes of rhodium makes photocleavage data for fully free metal difficult to obtain. The concentration of radiolabelled DNA which can be detected sets a lower limit on how dilute reactions conditions can become. The concentration of radiolabelled DNA cannot be reduced below a level where reaction products cannot be detected. Thus, the effects of maximizing signal and minimizing radioactive DNA concentration compete in the determination of binding constants. The effects of irradiation time, sample volume, and buffer on photocleavage signal are discussed below in order to address the issue of maximizing signal while minimizing DNA concentration.

2.3.1.1 Effect of Sample Volume on Photoefficiency: One way to decrease the concentration of radioactively labeled DNA is to increase sample volume. However, the effects of sample volume on photocleavage efficiency have not been previously evaluated for 1-Rh(MGP)$_2$phi^{5+} with the lamp system described above. It is possible that the UV radiation is absorbed by the solvent in samples with volumes greater than 20 μL. Thus increasing sample

volume could result in a substantial decrease in photoefficiency. The results of a study of fraction DNA cleaved versus sample volume are shown in Figure 2.6. Greater sample volumes do demonstrate a lower photoefficiency; however, the reduction in fraction cleaved is not as substantial as might be expected. An eightfold increase in volume results in only a twofold decrease in fraction of products produced. Thus, DNA concentrations can be reduced by an increase in volume without a greater than or equal reduction in photoefficiency of cleavage being observed.

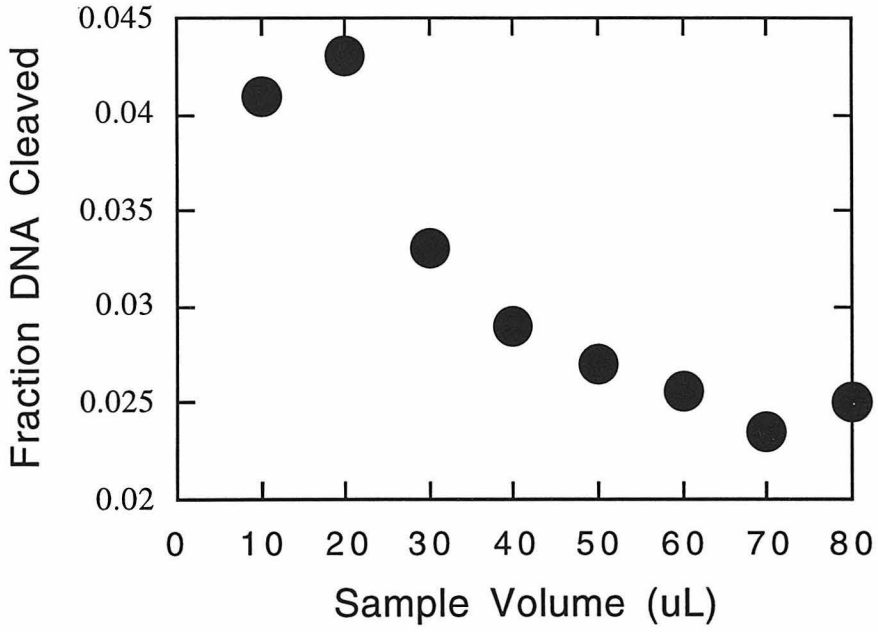

Figure 2.6: Plot of fraction DNA cleaved versus sample volume. The conditions of the experiment are described in the Experimental section. Note that an eightfold increase in sample volume results in only a twofold decrease in fraction DNA photocleaved.

2.3.1.2 Effect of Irradiation Time on Fraction DNA Cleaved: The amount of product observed from a photocleavage experiment can be increased with an increase in irradiation time. However, the relationship between increase in

irradiation time and increased photocleavage has not been previously determined with 1-Rh(MGP)$_2$phi^{5+}. The rate of appearance of photocleavage products can be described by the following equation:

$$rate_P = k_P[DNA \bullet Rh] \qquad \text{Equation 2.13}$$

where $rate_P$ is the rate of appearance of photocleavage products, k_P is a rate constant specific for sample volume and lamp intensity, and [DNA•Rh] is the concentration of 1-Rh(MGP)$_2$phi^{5+} bound to DNA. It is apparent from equation 2.13 that the rate of photocleavage will be linear with irradiation time if the concentration of bound metal complex is constant over the course of the reaction.

Difficulties in the analysis of data will arise if the relationship between irradiation time and photocleavage is not linear. For example, it is assumed that the fraction of the DNA substrate cleaved will be directly proportional to the fraction of DNA which is bound by metal complex. This would not be the case if all bound metal complex was to react rapidly with DNA on the time scale of a photocleavage experiment. The calculated result of this situation is shown in Figure 2.7. Here, all the metal complex in a fully bound sample reacts in the first few minutes of an irradiation while a 10% bound sample damages DNA over the entire length of the irradiation. As can be seen from the plot, these conditions result in an apparently higher than actual fraction bound for samples at low concentrations and thus the determination of a higher than actual affinity for the complex binding to DNA.

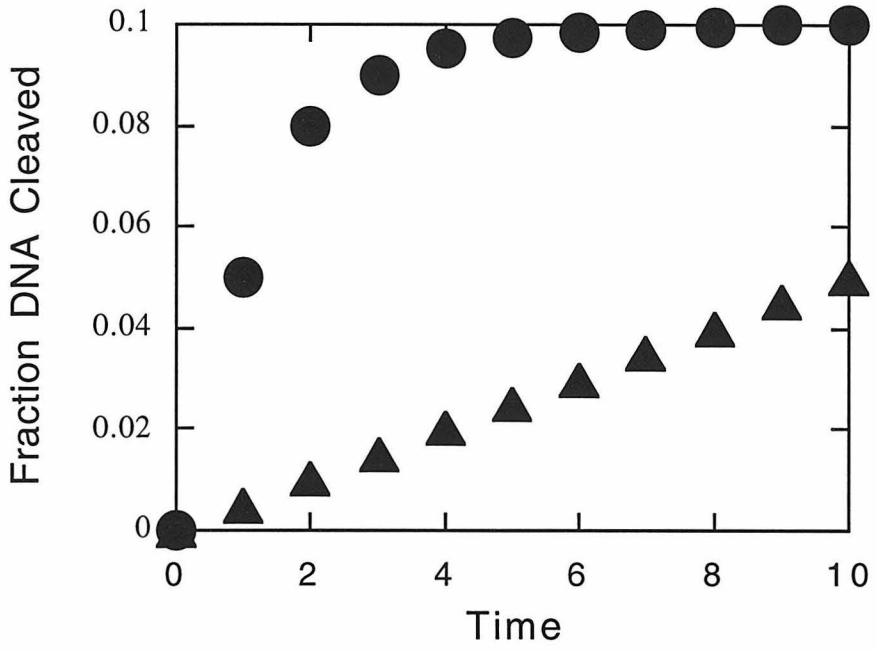

Figure 2.7: Plot of hypothetical data for samples where 100% (closed circles) and 10% (closed triangles) of the metal complex is bound to DNA where bound complex reacts rapidly compared to the time of irradiation. Note that in this case, the amount of cleaved DNA is not directly proportional to the amount of bound complex.

If DNA damage is linearly related to irradiation time for a fully metal complex, then the fraction of DNA cleaved will be directly related to the fraction of DNA bound. An experiment was conducted where fraction DNA cleaved was compared to time of irradiation to determine if this linear relationship between DNA damage and irradiation time exists. The results are plotted in Figure 2.8. In this experiment, the concentrations of DNA duplex and 1-Λ-Rh(MGP)2phi^{5+} are each 1 μM. These concentrations are two orders of magnitude higher than the affinity constant of this complex for its DNA recognition sequence (*vide infra*) and thus all metal and DNA can be considered to be in the bound form. As can be seen from Figure 2.8, the

fraction of DNA cleaved is linear with time of irradiation. Therefore, the concentration of bound metal complex must be constant over irradiation times of 5 to 30 minutes.

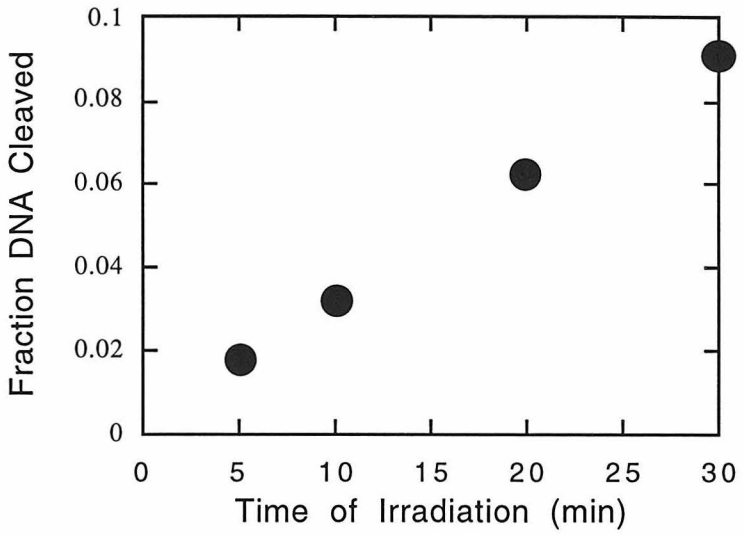

Figure 2.8: Plot of fraction cleaved versus irradiation time. Reaction conditions are described in the Experimental Section. Note that the amount of DNA damage is directly proportional to irradiation time for at least 30 minutes.

Since the greatest decrease in the concentration of uncleaved DNA will occur in fully bound samples, it can be assumed that the amount of uncleaved DNA will remain unchanged at all concentrations of metal complex and DNA at a 1:1 ratio. Thus, from equation 2.7, DNA damage will be directly proportional to the fraction of DNA bound at all concentrations with a DNA/rhodium ratio of 1:1. Moreover, at lower rhodium:DNA ratios than 1:1, less DNA damage can be expected and photocleavage can be assumed to be proportional to bound metal at these ratios as well. At ratios higher than 1:1, more DNA damage can be expected and thus photocleavage proportional to binding cannot be assumed. Finally, these experiments demonstrate that the

amount of signal can be increased by an increase in irradiation time. As can be seen from Figure 2.8, a twofold increase in irradiation time results in a twofold increase in products observed.

2.3.1.3 Effect of Buffer Conditions on Photocleavage Efficiency: The amount of photocleavage products yielded from a given reaction can be increased by the judicious choice of buffer conditions. DNA and 1-Λ-Rh(MGP)$_2$phi^{5+} were irradiated in the presence of sodium cacodylate at various salt and buffer concentrations. The DNA templates used in this experiment are shown in Figure 2.9. The results of these irradiations are shown in Figure 2.10. Note that photocleavage occurs on the radiolabelled template at the bolded bases in the recognition sequence for 1-Λ-Rh(MGP)$_2$phi^{5+}, 5'-CA**TAT**G-3'. This is the expected pattern of photocleavage except for the 3' most thymine. However, this pattern has been observed reproducibly with this set of templates. As can be seen from the figure, the greatest photocleavage was observed in 10 mM sodium cacodylate, 40 mM NaCl (lane 2). Decreasing the NaCl concentration to 25 mM resulted in slightly less photocleavage (lane 5). The addition of dithiothreitol, $MgCl_2$, or Tris resulted in a drastic decrease in photocleavage. This decrease in photocleavage shows that 1-Λ-Rh(MGP)$_2$phi^{5+} is very sensitive to salt concentrations. It is not clear whether the decrease in photocleavage reflects a decrease in binding affinity or a decrease in the efficiency of cleavage by bound metal complex. It is clear that, if adequate photocleavage is to be obtained to determine the affinity constant of this complex for a given DNA site, buffers containing sodium cacodylate and NaCl should be used.

Figure 2.9 DNA templates used for studies of the effects of buffer conditions on the intensity of photocleavage. The 1-Λ-Rh(MGP)2phi^{5+} recognition sequence on template B is shown in bold.

Template A:

5'ATGCAGCTGGCACGACAGCGCTCTAGAGCG3'
3'GCGAGATCTCGCGCGACAGCACGGTCGACGTA5'

Template B:

5'ATGCTAGGCTATGCAGCTGGCACGACAGCGC**CATATG**GCG3'
3'GCG**GTATAC**CGCGACAGCACGGTCGACGTATCGGATCGTA5'

Figure 2.10 Effect of buffer conditions on photocleavage by 1-Λ-Rh(MGP)$_2$phi^{5+}. Photocleavage was carried out as described in the Experimental section. DNA templates are shown in Figure 2.10. Lane 1: DNA and 10 mM sodium cacodylate. Lanes 2-6: 0.5 μM 1-Λ-Rh(MGP)$_2$phi^{5+}, 0.05 μM template A, 0.05 μM template B, 10 mM sodium cacodylate. Other buffer conditions were varied between different lanes. Lanes 1 and 2: 40 mM NaCl. Lane 3: 40 mM NaCl, 1 mM dithiothreitol. Lane 4: 40 mM NaCl, 10 mM $MgCl_2$. Lane 5: 25 mM NaCl. Lane 6: 40 mM NaCl, 40 mM TrisCl. Note that substantial decreases are observed in photocleavage with any buffer reagents besides sodium cacodylate and NaCl.

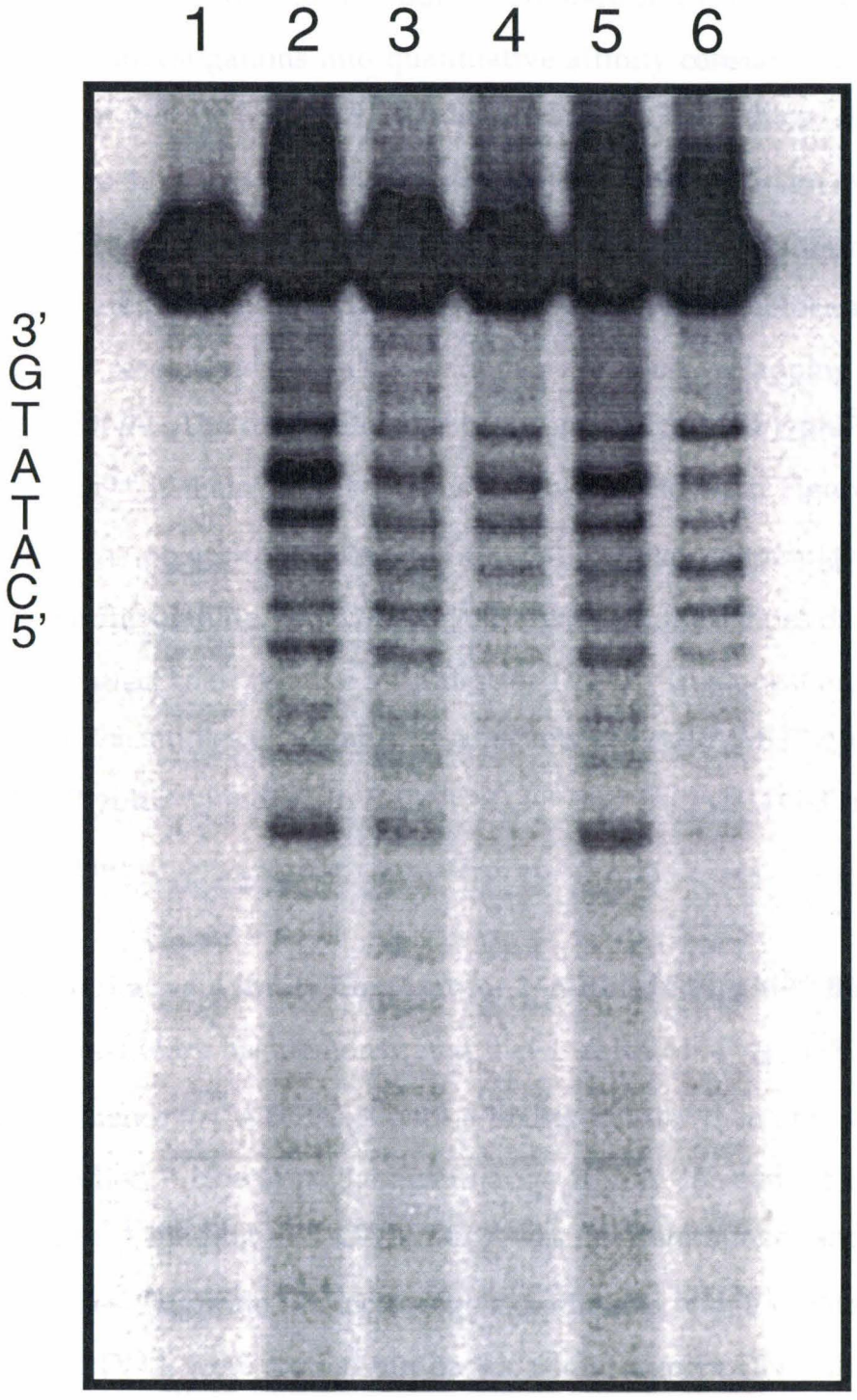
1 2 3 4 5 6
3'GTATAC5'

2.3.2 Quantitative Affinity Constants: As described above, several factors affecting the amount of 1-Rh(MGP)2phi^{5+}-directed photocleavage were investigated. Results from these studies were used in the choosing of conditions for investigations into quantitative affinity constants for the enantiomers of 1-Rh(MGP)2phi^{5+} binding to specific DNA sites. As shown in Table 2.1, each of these enantiomers recognizes a non-overlapping set of sequences. The uniqueness of the site recognized by these enantiomers is further illustrated in Figure 2.11. Note that even the low photocleavage intensity sites recognized by each enantiomer are non-overlapping on this fragment of DNA. The only difference between 1-Λ-Rh(MGP)2phi^{5+} and 1-Δ-Rh(MGP)2phi^{5+} is their chirality. Thus the results shown in Figure 2.11 demonstrate the powerful influence that metal complex shape plays in sequence-specific binding. How do the differences in the shapes of these enantiomers affect their relative affinities for DNA? This question is addressed in the studies of the affinity constants of 1-Λ-Rh(MGP)2phi^{5+} and 1-Δ-Rh(MGP)2phi^{5+} binding to 5'-CATATG-3' and 5'-CATCTG-3' are described below.

2.3.2.1 Quantitative Affinity Constant for 1–Δ-Rh(MGP)2phi^{5+} Binding to DNA: Previous work has demonstrated that 1–Δ-Rh(MGP)2phi^{5+} binds to the DNA sequence 5'-CATCTG-3' with a higher affinity than any other sequence studied.[1] However, the quantitative affinity constant of 1–Δ-Rh(MGP)2phi^{5+} binding to 5'-CATCTG-3' was not determined and is described here. Triplicate photocleavage experiments with a constant ratio of 1:10 rhodium:DNA were carried out on the 64mer duplex DNA shown in Figure 2.5. One of the three photocleavage experiments is shown in Figure 2.12. Positions of photocleavage are delineated by arrows at the right of the

Figure 2.11 Photocleavage by the enantiomers of 1-Rh(MGP)$_2$phi^{5+} on a DNA fragment. All lanes contain 1 μM DNA base pairs in 10 mM sodium cacodylate and 40 mM sodium chloride. The sample from lane 1 was not irradiated while the samples from lanes 2-4 were irradiated for 4 minutes at 313 nm. Lane 2: no rhodium. Lane 3: 0.1 μM 1-Λ-Rh(MGP)$_2$phi^{5+}. Lane 4: 0.1 μM 1-Δ-Rh(MGP)$_2$phi^{5+}. Note that the families of sequences recognized by each enantiomer are non-overlapping. Figure adapted from reference 1.

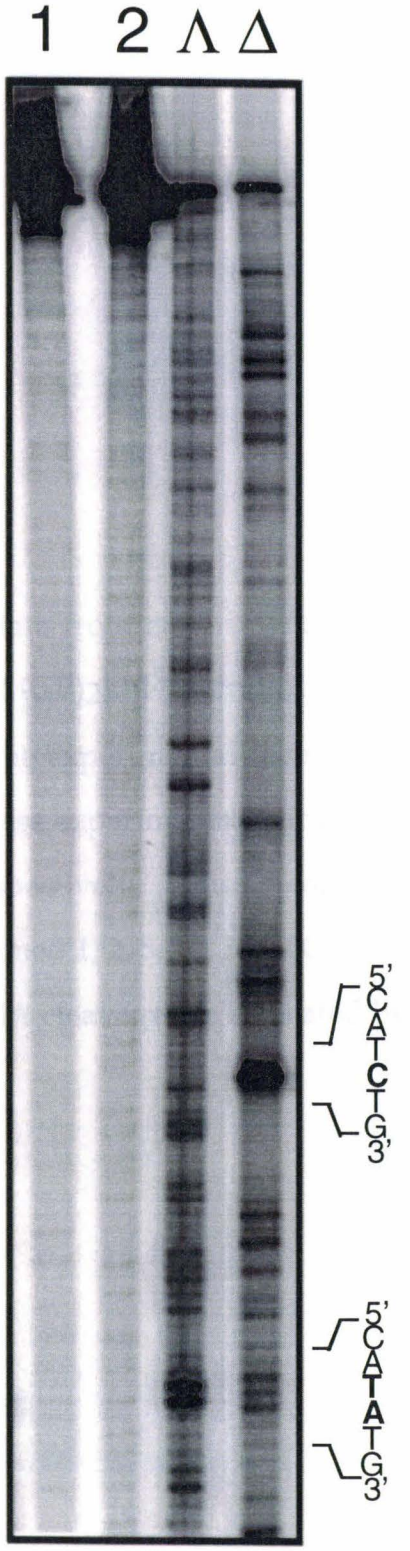
1
2
Λ
Δ
5'
CATCTG,
3'
5'
CATATG,
3'

Figure 2.12 Photocleavage data from experiments determining quantitative affinity constants for 1-Δ-Rh(MGP)$_2$phi^{5+} binding to 5'-CATCTG-3'. Conditions are described in the experimental section. A 1:10 rhodium:DNA template ratio was used in these experiments. Lanes 1 and 2 are A+G and C+T sequencing reactions respectively. Lanes 3 contained no rhodium. Lanes 4, 5, 6, 7, 8, 9, 10, and 11 contained 1, 2, 5, 10, 50, 100, 500, and 1000 nM DNA respectively. Positions of DNA cleavage are indicated by arrows.

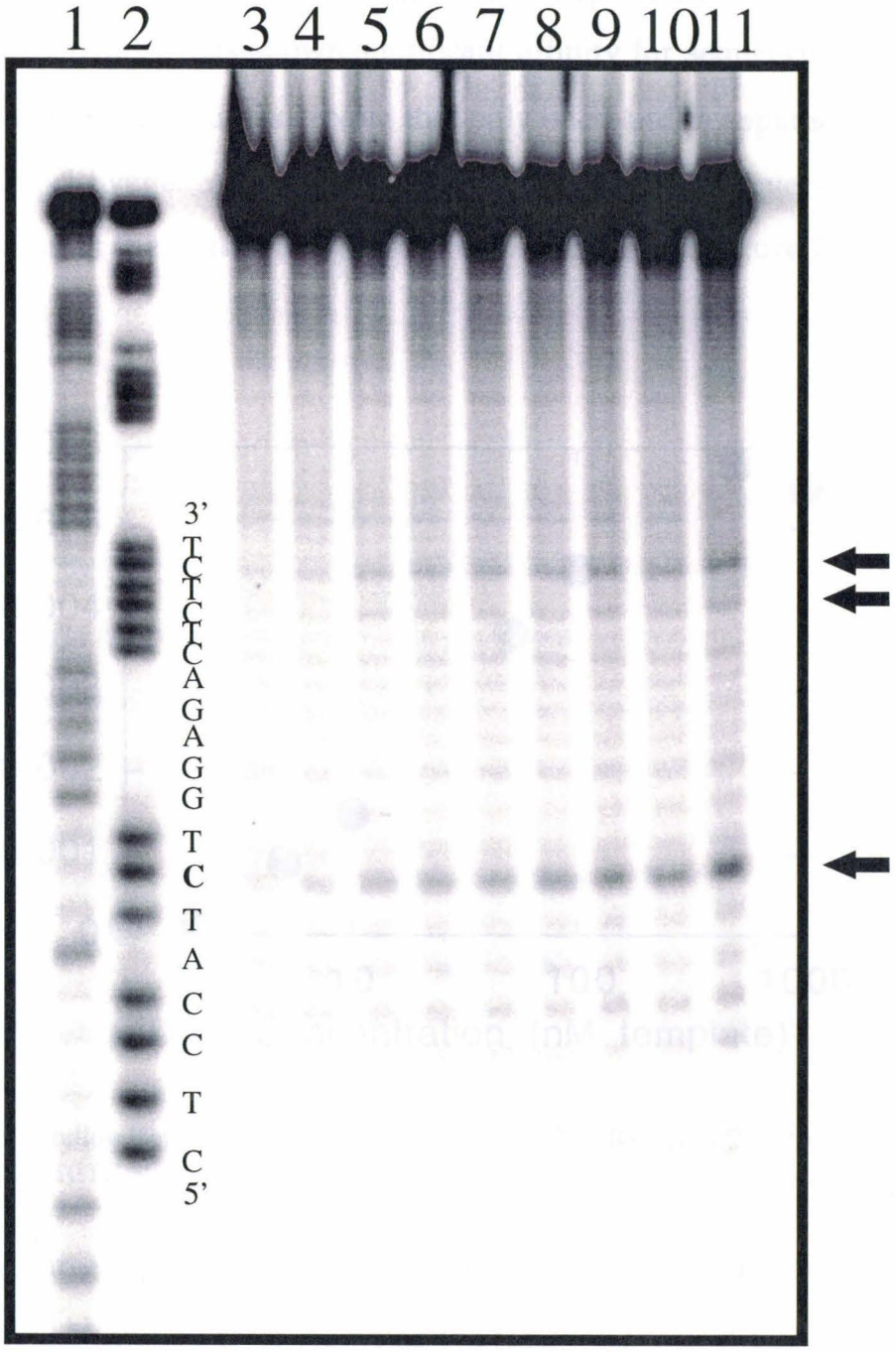
1 2 3 4 5 6 7 8 9 10 11
3' TCTCTCAGAGGTCTACCCTC 5'

figure. The specificity of this complex for its recognition sequence 5'-CATCTG-3' is apparent. The complex also shows affinity for the sequences 5'-CTCTCT-3' and 5'-CTCTAG-3'. The affinity for these two sites is not unexpected as both sequences contain 5'-CT-3' steps. As shown in Table 2.1, 1–Δ-Rh(MGP)$_2$phi^{5+} has shown significant affinity for sequences containing 5'-CT-3' steps in past studies.[2] Note that only one band is apparent for each site of photocleavage. A plot of the fraction of DNA cleaved versus DNA concentration at the sequence 5'-CATCTG-3' is shown in Figure 2.13.

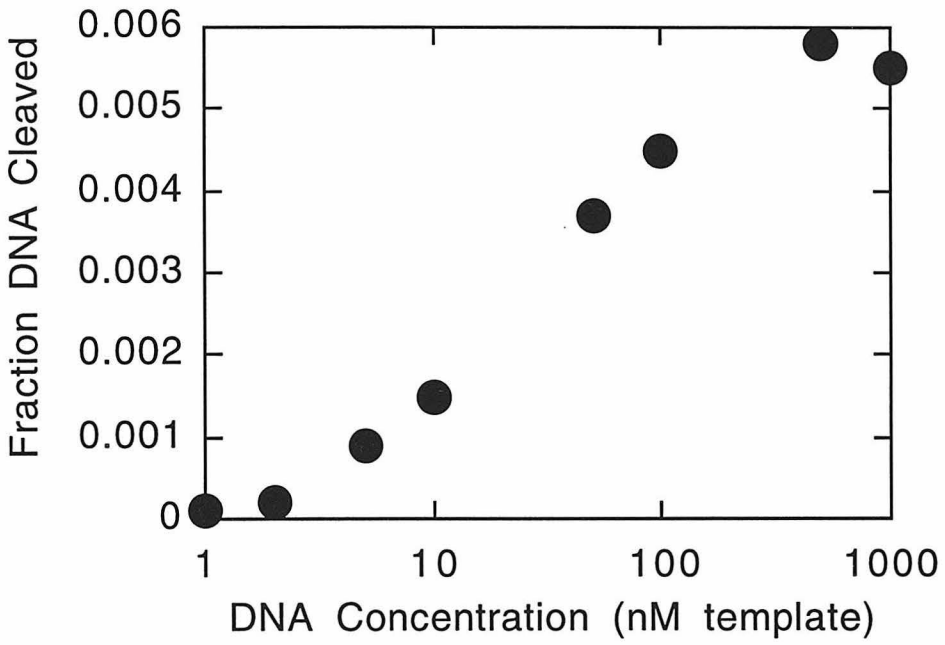

Figure 2.13: Binding isotherm for the interaction of Δ-1-Rh(MGP)$_2$phi^{5+} with the DNA sequence 5'-CATCTG-3'.

Data from three replicate experiments were fit as described in the experimental section to generate a binding constant of $5x10^7 \pm 1x10^7 M^{-1}$ for the complex binding to the sequence 5'-CATCTG-3'. This corresponds to an approximate binding energy of 12 kcal for the complex interacting with DNA

at this site. Attempts were made to calculate an affinity constant for 1–Δ-Rh(MGP)$_2$phi^{5+} binding to 5′-CTCTCT-3′ and 5'-CTCTAG-3'; however, a combination of low signal and high background prevented the accurate quantitation of photocleavage at this site.

2.3.2.2 Quantitative Affinity Constant for 1–Λ-Rh(MGP)$_2$phi^{5+} Binding to DNA: Previous work has demonstrated that 1-Λ-Rh(MGP)$_2$phi^{5+} binds to the DNA sequence 5'-CATATG-3' with a higher affinity than any other sequence studied.[1] However, the quantitative affinity constant of 1-Λ-Rh(MGP)$_2$phi^{5+} binding to 5'-CATATG-3' was not determined and is described here. Triplicate photocleavage experiments with a constant ratio of 1:2 rhodium:DNA were carried out on the 64mer duplex DNA shown in Figure 2.5. One of the three photocleavage experiments is shown in Figure 2.14. DNA damage at the bolded T and A, also indicated by arrows, was used to generate binding isotherms. Note that DNA damage occurs to an equal extent to the bases directly 5' and 3' to the intercalation site. A plot of the fraction of DNA cleaved versus DNA concentration for this site is shown in Figures 2.15. This curve was fit as described in the experimental section to generate binding constants of $1x10^8 \pm 0.2x10^8$ M^{-1}. This is the equivalent of a 12 kcal difference in the energies of the bound and free forms of the metal complex.

2.3.2.3 Photocleavage Efficiency of the Enantiomers of 1-Rh(MGP)$_2$phi^{5+}: Quantitation of the fraction cleaved from the affinity constant data described allows the estimation of the photocleavage efficiency of each enantiomer. To make an estimate, it is important to know what fraction of the DNA is bound

Figure 2.14 Photocleavage data from experiments determining quantitative affinity constants for 1-Λ-Rh(MGP)$_2$phi^{5+} binding to 5'-CATATG-3'. Conditions are described in the experimental section. A 1:2 rhodium:DNA template ratio was used in these experiments. Lane 1 is an A+G sequencing reaction. Lane 2 contained no rhodium. Lanes 3, 4, 5, 6, 7, 8, 9, 10, and 11 contained 1, 5, 10, 50, 100, 500, 1000, 5000, and 10000 nM DNA respectively. The position of photocleavage is indicated by the bold 5'-TA-3' step and the arrows at the bottom of the gel.

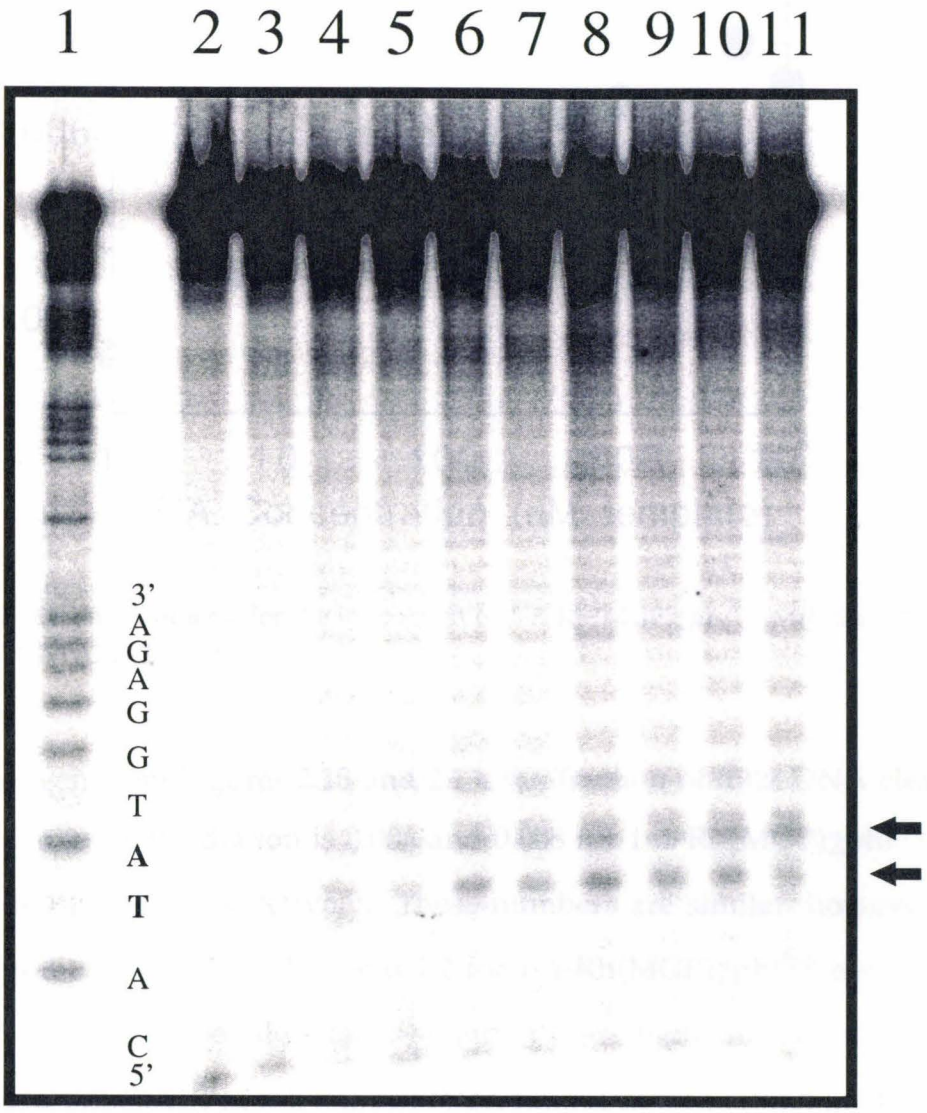
1 2 3 4 5 6 7 8 9 10 11
3'
A
G
A
G
G
T
A
T
A
C
5'

by metal complex. All the metal complex is bound to DNA at the highest concentration of DNA and rhodium in each of the isotherms shown above.

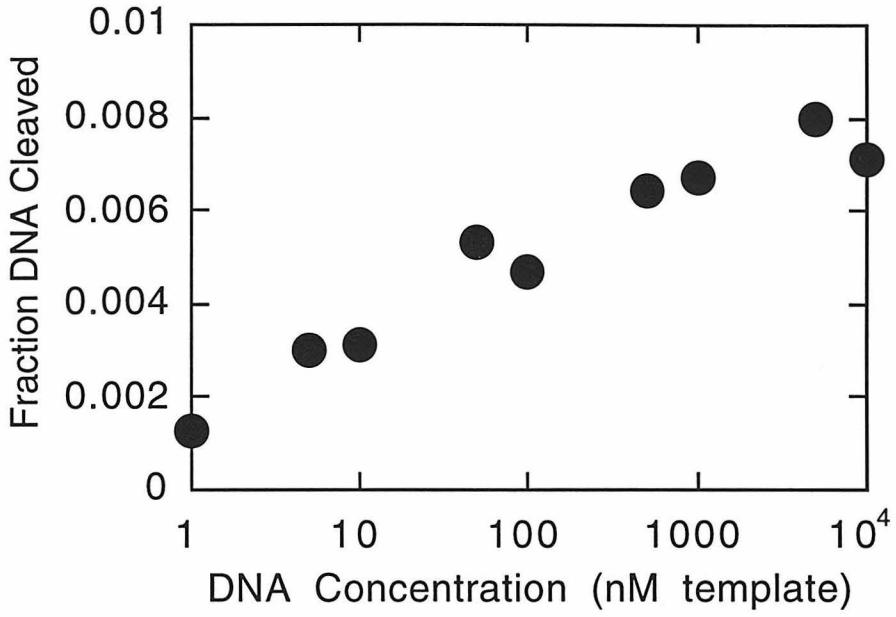

Figure 2.15: Binding isotherm for the interaction of 1-Λ-Rh(MGP)$_2$phi^{5+} with the DNA sequence 5'-CATATG-3'.

As can be seen from Figures 2.13 and 2.15, the fraction of total DNA cleaved during a 5 minute irradiation is 0.006 and 0.008 for 1-Δ-Rh(MGP)$_2$phi^{5+} and 1-Λ-Rh(MGP)$_2$phi^{5+} respectively. These numbers are similar; however, the ratio of rhodium to DNA is 1:10 and 1:2 for 1-Δ-Rh(MGP)$_2$phi^{5+} and 1-Λ-Rh(MGP)$_2$phi^{5+}. Since all metal is bound at these high concentrations, the ratios can be converted to fractions of DNA bound of 0.1 and 0.5 for 1-Δ-Rh(MGP)$_2$phi^{5+} and 1-Λ-Rh(MGP)$_2$phi^{5+}. The fraction cleaved can then be divided by the fraction bound for the comparison of the relative photocleavage efficiencies of the two enantiomers. This relative fraction cleaved is 0.06 and 0.016 for 1-Δ-Rh(MGP)$_2$phi^{5+} and 1-Λ-Rh(MGP)$_2$phi^{5+}.

Thus, the photocleavage efficiency of 1-Δ-Rh(MGP)$_2$phi^{5+} is roughly four times that of 1-Λ-Rh(MGP)$_2$phi^{5+}. Photocleavage of DNA by the phi complexes of rhodium has been proposed to occur through a free radical abstraction of a C3' hydrogen from a ribose in the phosphate backbone. The free radical which participates in this abstraction results from a ligand to metal charge transfer from the phi ligand. Since the free radical is present on the phi ligand, it could be expected that the positioning of this ligand in the intercalation site would have a substantial effect on the efficiency of hydrogen atom abstraction. The fact that 1-Δ-Rh(MGP)$_2$phi^{5+} shows more efficient photocleavage than 1-Λ-Rh(MGP)$_2$phi^{5+} indicates that these two complexes are positioned differently in their intercalation sites with 1-Δ-Rh(MGP)$_2$phi^{5+} better poised for hydrogen atom abstraction. The more efficient positioning of the Δ enantiomer may consist of the intercalating phi being physically closer to the C3' hydrogen. The phi ligand could achieve this proximity to the C3' hydrogen if the Δ enantiomer was canted to one side in its intercalation site.

2.3.3 Determining Binding Constants With Constant DNA: One of the commonly used methods for determining the binding constants of ligands interacting with DNA is to keep the DNA concentration constant and to vary the ligand concentration over several orders of magnitude.[14] The resulting data can then be fit to the following equation:

$$FB = K_b[L]/(1 + K_b[L]) \qquad \text{Equation 2.14}$$

where FB is the fraction DNA bound, K_b is the binding constant, and [L] is the total concentration of ligand. As can bee seen from Equation 2.14, the DNA

concentration need not be known for determination of the binding constant. This is convenient as it is difficult to accurately determine the concentration of radioactive DNA after labeling.

This method is not appropriate for the determination of binding constants for our complexes. First, an assumption that is made in Equation 2.14 is that the concentration of total ligand is essentially the same as that of free ligand. To make this assumption, the DNA concentration must be 20 fold lower than the lowest ligand concentration studied. As photocleavage experiments must be run in volumes on the order of 40 μL, this places restraints on the high affinity limit of binding constants that can be measured. Depending on labeling efficiency for the DNA of interest, this sets a limit of $1x10^7$ to $1x10^8$ M^{-1}. The 64mer used in these studies demonstrated poor labeling and thus would have had an upper limit of $1x10^7$ M^{-1}.

The second reason that this method is inappropriate for our determination of binding constants is that the phi complexes of rhodium complexes demonstrate unusual photophysical effects which are described below. The intensity of photocleavage at a given site should increase with an increasing fraction of that site bound. Once concentrations of metal complex reach a point where the DNA site of interest is fully bound, maximal photocleavage at this site should be observed. In other words, the addition of increasing concentrations of metal complex, once a site is fully occupied, should not result in any increased photocleavage. This is <u>not</u> the behavior which has been observed in experiments where the ligand/DNA ratio is varied. An example of what is observed is shown in Figure 2.16. In this experiment, increasing amounts of 1-Δ-$Rh(MGP)_2phi^{5+}$ result in ever increasing levels of photocleavage at 5'-CATCTG-3'. The binding constant of this complex is $5x10^7$ M^{-1} (*vida infra*), and thus at concentrations of free

metal of 1000 nM, 98% of the DNA sites are bound. Yet as can be seen from Figure 2.16, the intensity of photocleavage increases twofold over the next order of magnitude increase in ligand concentration. This effect makes it impossible to determine when the complex is maximally bound which is essential for determination of fraction bound and thus finding the binding constant. The cause of this effect is yet undetermined. It is possible that there is some energy transfer mechanism at work where a complex, either unbound or bound to a non-specific site, is excited by UV light and transfers this excited state to a complex bound at the specific site of interest, thus increasing the photoefficiency of cleavage at that site.

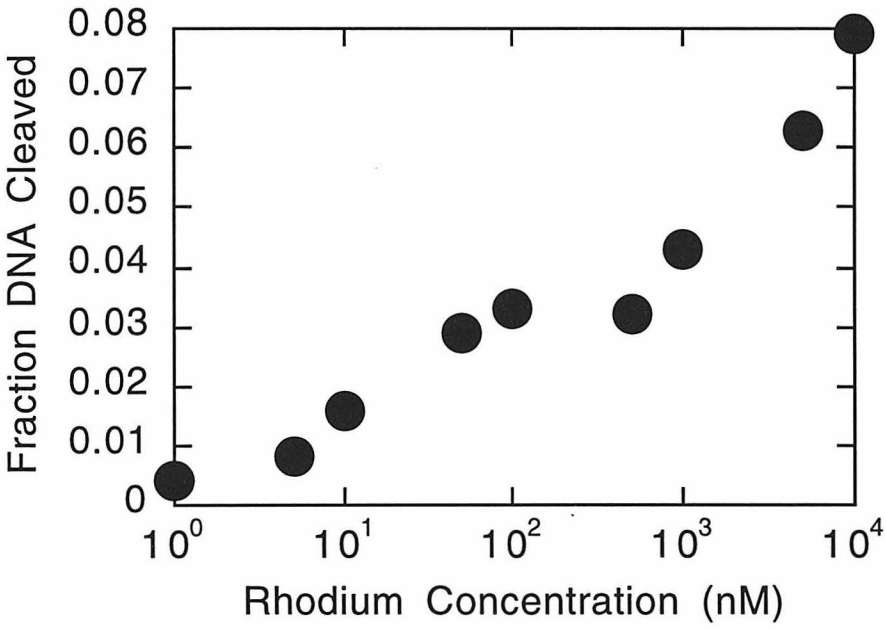

Figure 2.16: Plot of fraction cleaved vs. rhodium concentration where the DNA concentration is held constant. Note that fraction cleaved does not level off at high concentrations. In fact, the rate of change in cleavage actually appear to accelerate.

2.3.4 Determination of Exchange Rate of 1-Λ-Rh(MGP)$_2$phi^{5+}: As described in the Introduction, the exchange rate is the number of times a

metal complex dissociates from a given DNA site and reassociates with a different DNA site per second. If the binding constant and exchange rate of a complex is known for a given site, then the rate constants of association and dissociation from that site can be determined using Equations 2.9 and 2.11. The exchange rate for 1-Λ-Rh(MGP)$_2$phi^{5+} binding its recognition sequence 5'-CATATG-3' was determined through the use of variable temperature NMR. The double-stranded oligonucleotide used in these studies is shown in Figure 2.17. Metal complex was titrated into a solution containing this oligonucleotide until a final ratio of 2:3 metal:DNA sites was achieved. Thus, two-thirds of the 1-Λ-Rh(MGP)$_2$phi^{5+}-specific sites in this sample should be bound by the complex and half the sites should be free. As described in the Introduction, the exchange rate can be calculated at the temperature at which the signals for bound and free DNA coalesce using Equation 2.12. NMR spectra of the 2:3 metal:oligonucleotide sample from 5 to 45^{o}C are shown in Figures 2.18 and 2.19. Peaks from 0 to 3.0 ppm are shown in Figure 2.18 and peaks from 6.0 to 9.0 are shown in Figure 2.19. Peaks for six DNA protons were identified for which estimates of coalescence temperature and chemical shift could be made. The assignments of these peaks were based on previously assigned 2D NOESY spectra of fully bound and free DNA.[15] Spectra for the free and bound DNA are shown in Figures 2.20 and 2.21 respectively. These protons are listed with their chemical shifts and coalescence temperatures in Table 2.2.

$$\begin{array}{l} 5'\text{-}G_1\ A_2C_3A_4T_5A_6T_7G_8T_9C_{10}\text{-}3' \\ 3'\text{-}C_{10}T_9G_8T_7A_6T_5A_4C_3A_2G_1\text{-}5' \end{array}$$

Figure 2.17: Double-stranded oligonucleotide used in the determination of exchange rate for 1-Λ-Rh(MGP)$_2$phi^{5+}.

Several observations can be made from the Figures 2.18 and 2.19. The first observation is that the bound and free peaks associated with each proton are not equal in intensity. The free peaks are approximately one-third the intensity of the bound peaks. This difference in intensity is consistent with a metal:DNA ratio of 2:3.

Proton	Coalescence Temp.	Diff. Chem. Shift	Exchange Rate
Methyl-T5	45°C	79 Hz	175 s^{-1}
Methyl-T7	50°C	98 Hz	218 s^{-1}
Methyl-T9	45°C	46 Hz	102 s^{-1}
Aromatic-T7	40°C	60 Hz	133 s^{-1}
Aromatic-T5	35°C	19 Hz	42 s^{-1}
Aromatic-A6	47°C	41 Hz	91 s^{-1}

Table 2.2: Exchange rate information determined from the data shown in Figures 2.18 and 2.19. Coalescence temperatures have an error of ± 5°C. The difference in chemical shift is between metal bound and free forms of the DNA. The exchange rates were calculated using equation 2.12.

The second observation is that many overlapping proton signals are present in these spectra. The large number of protons in this system has the advantage that there is a large amount of potential information to be drawn from the spectra. However, the overlapping signals make the accurate determination of chemical shift and coalescence temperature difficult. Based on the spectra observed, coalescence temperatures determined have an error or ± 5°C.

The difference in chemical shifts between bound and free peaks used to determine exchange rates with Equation 2.12 is the difference in chemical

Figure 2.18 ^{1}H-NMR spectra of 1-Λ-Rh(MGP)$_2$phi^{5+} and DNA used to determine exchange rates. Conditions are described in the Experimental Section. Metal to oligonucleotide ratio is 1:2. Oligonucleotide is shown in Figure 2.17. Metal bound and free DNA peaks pairs for the methyl groups of thymines 5, 7, and 9 are labeled in the figure.

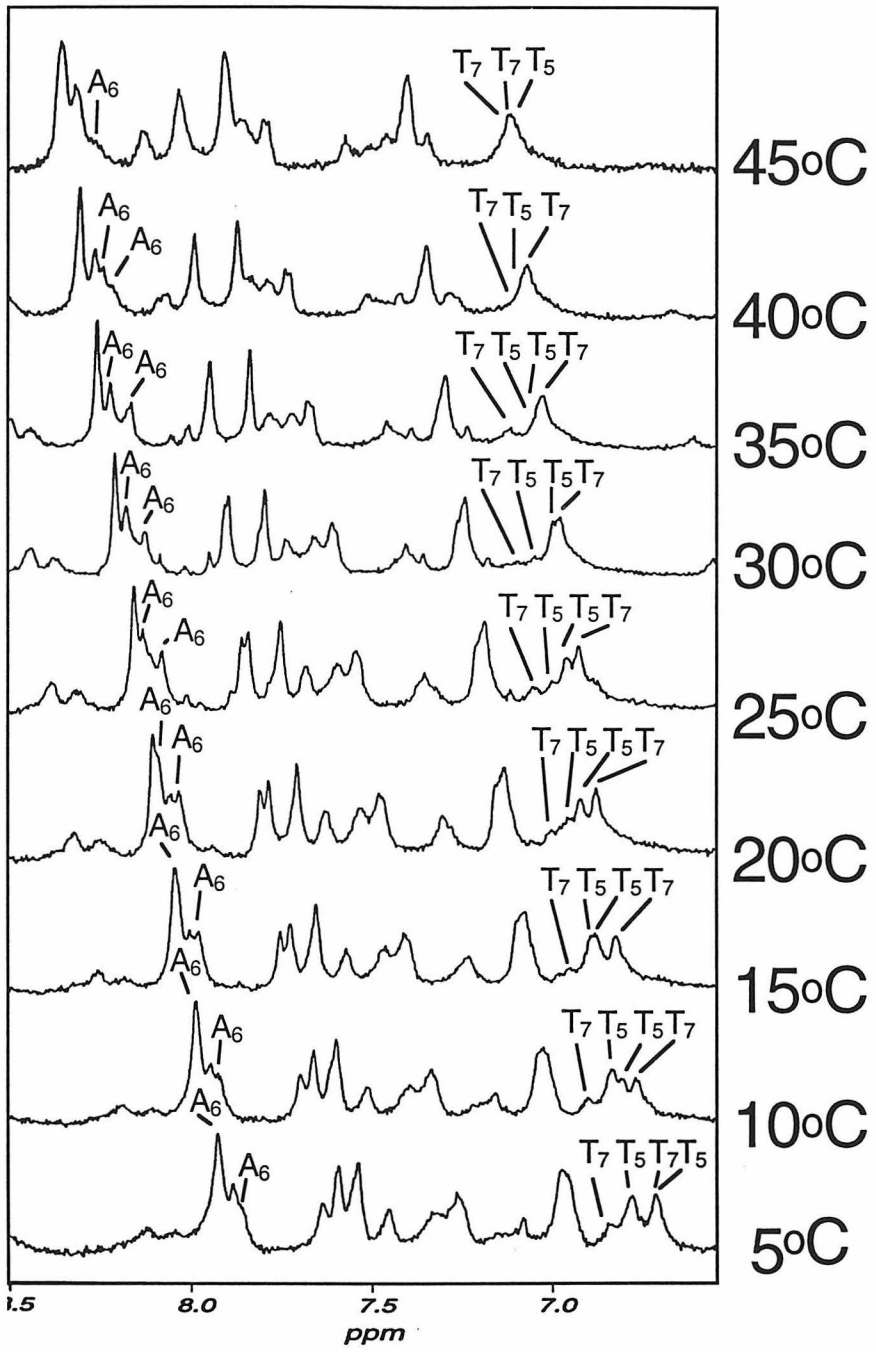
A6
T7 T7 T5
45oC
A6
A6
T7 T5 T7
40oC
A6
A6
T7 T5 T5 T7
35oC
A6
A6
T7 T5 T5 T7
30oC
A6
A6
T7 T5 T5 T7
25oC
A6
A6
A6
T7 T5 T5 T7
20oC
A6
A6
T7 T5 T5 T7
15oC
A6
A6
T7 T5 T5 T7
10oC
A6
T7 T5 T7 T5
5oC
8.0
7.5
7.0
ppm

Figure 2.19 NMR spectra of 1-Λ-Rh(MGP)$_2$phi^{5+} and DNA used to determine exchange rates. Conditions are described in the Experimental Section. Metal to oligonucleotide ratio is 1:2. Oligonucleotide is shown in Figure 2.17. Metal bound and free DNA peaks pairs for the aromatic protons of thymines 5, 7, and for adenine 8 are labeled in the figure.

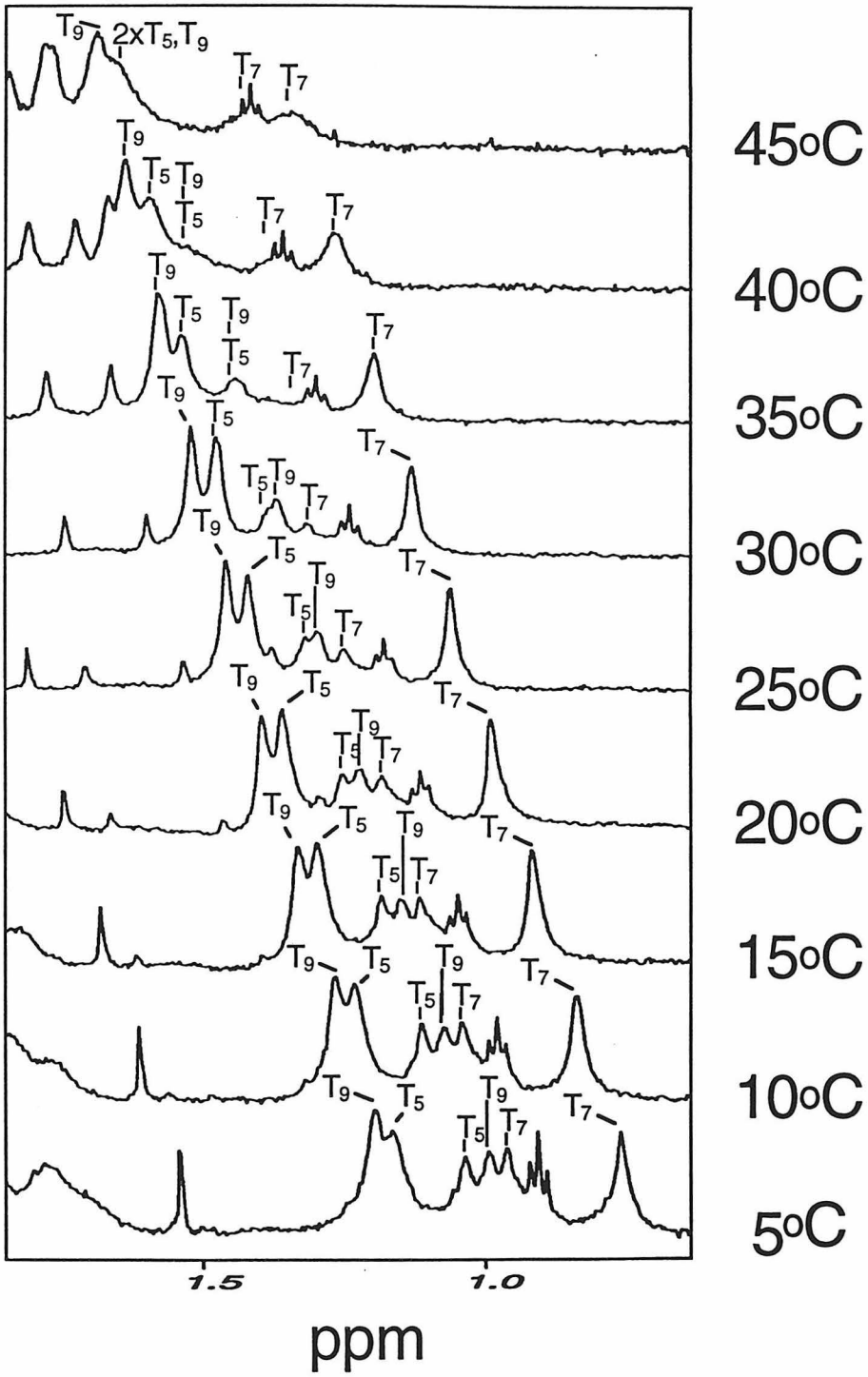
T9
2xT5,T9
T7
T7
45oC
T9
T5
T9
T5
T7
T7
40oC
T9
T5
T9
T5
T7
T7
35oC
T9
T5
T7
T5
T9
T7
30oC
T9
T5
T9
T5
T7
T7
25oC
T9
T5
T9
T5
T7
T7
20oC
T9
T5
T9
T5
T7
T7
15oC
T9
T5
T9
T5
T7
T7
10oC
T9
T5
T9
T5
T7
T7
5oC
1.5
1.0
ppm

Figure 2.20 Previously determined 2D ^{1}H-NOESY spectra of the oligonucleotide shown in Figure 2.17.[15] Shown is a NOE walk (blue and red lines) through the aromatic versus aliphatic region. Note that the connectivities for this walk can be followed from through the entire oligonucleotide starting at G_1. Note also the connectivities between the T_5 and A_6 bases (shown in red). Free DNA peaks are identified in the one-dimensional spectra at the top and left of the figure. 2D ^{1}H-NOESY spectra were taken with a 300 ms mixing time and presaturation of the water peak during recycle delay and mixing time.[13] Solution conditions were 0.5 mM duplex, 10 mM sodium phosphate and 20 mM sodium chloride in D_2O at pH 7.0. Spectra were taken at 300 K.

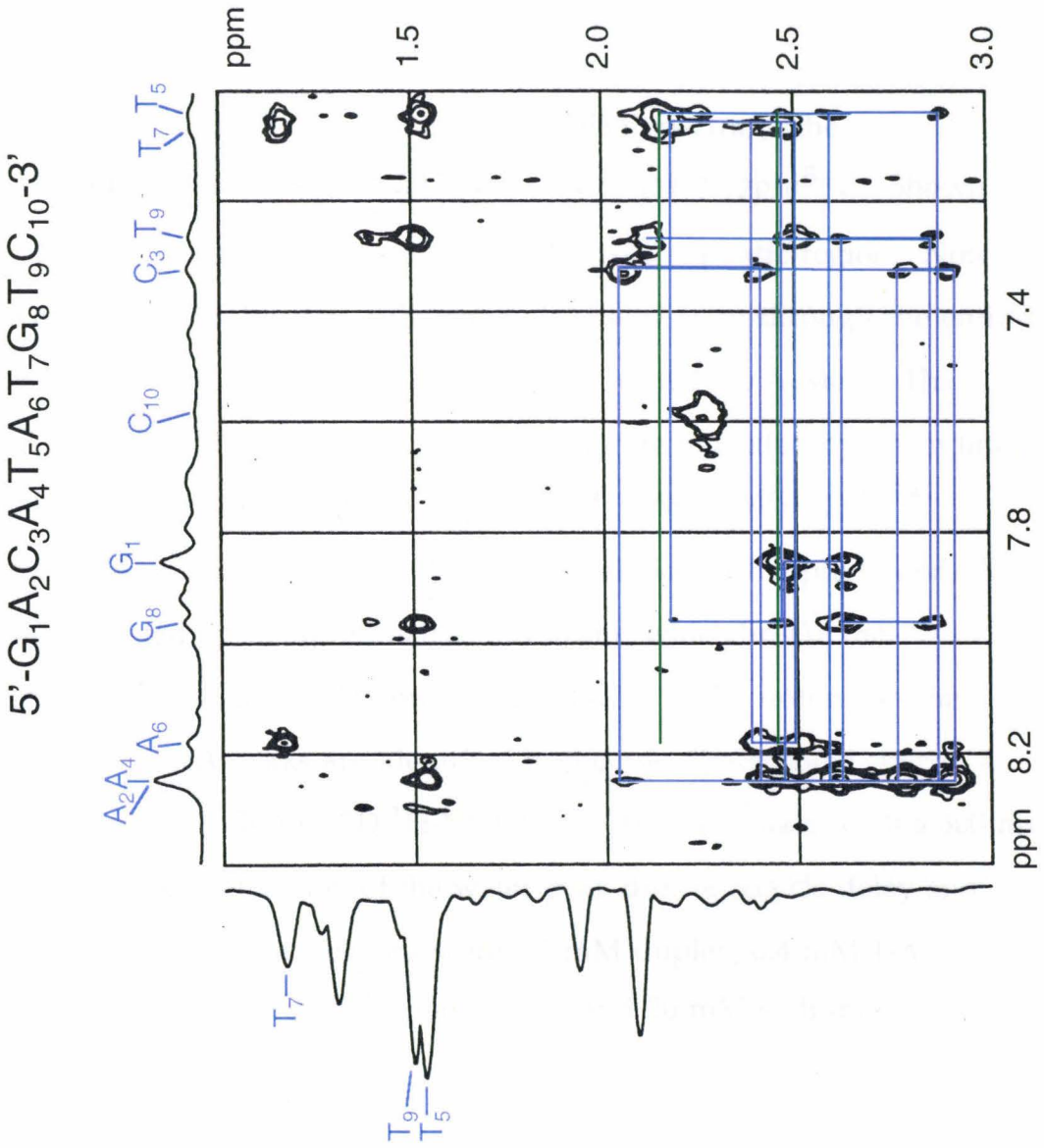
5'-G1A2C3A4T5A6T7G8T9C10-3'
A2
A4
A6
G8
G1
C10
C3
T9
T7
T5
ppm
1.5
2.0
2.5
3.0
7.4
7.8
8.2
ppm
T7
T9
T5

Figure 2.21 Previously determined 2D ^{1}H-NOESY spectra of the oligonucleotide shown in Figure 2.17 with 1-Λ-Rh(MGP)$_2$phi^{5+}.[15] Shown is a NOE walk (blue lines) through the aromatic versus aliphatic region. Note that the connectivities for this walk can be followed from through the entire oligonucleotide starting at G_1 with the exception of the T_5/A_6 step. The expected position of these missing connectivities are indicated by green lines. These missing connectivities are consistent with 1-Λ-Rh(MGP)$_2$phi^{5+} intercalating between T_5 and A_6.[18] Upon intercalation of the phi ligand, these bases are separated by an additional 3.4 angstroms which breaks the connectivity between the A_6-H8 proton and the H2', H2" protons on the T_5 ribose. Bound DNA peaks are identified in the one-dimensional spectra at the top and left of the figure. 2D ^{1}H-NOESY spectra were taken with a 300 ms mixing time and presaturation of the water peak during recycle delay and mixing time.[13] Solution conditions were 0.5 mM duplex, 0.4 mM 1-Λ-Rh(MGP)$_2$phi^{5+}, 10 mM sodium phosphate, and 20 mM sodium chloride in D_2O at pH 7.0. Spectra were taken at 300 K.

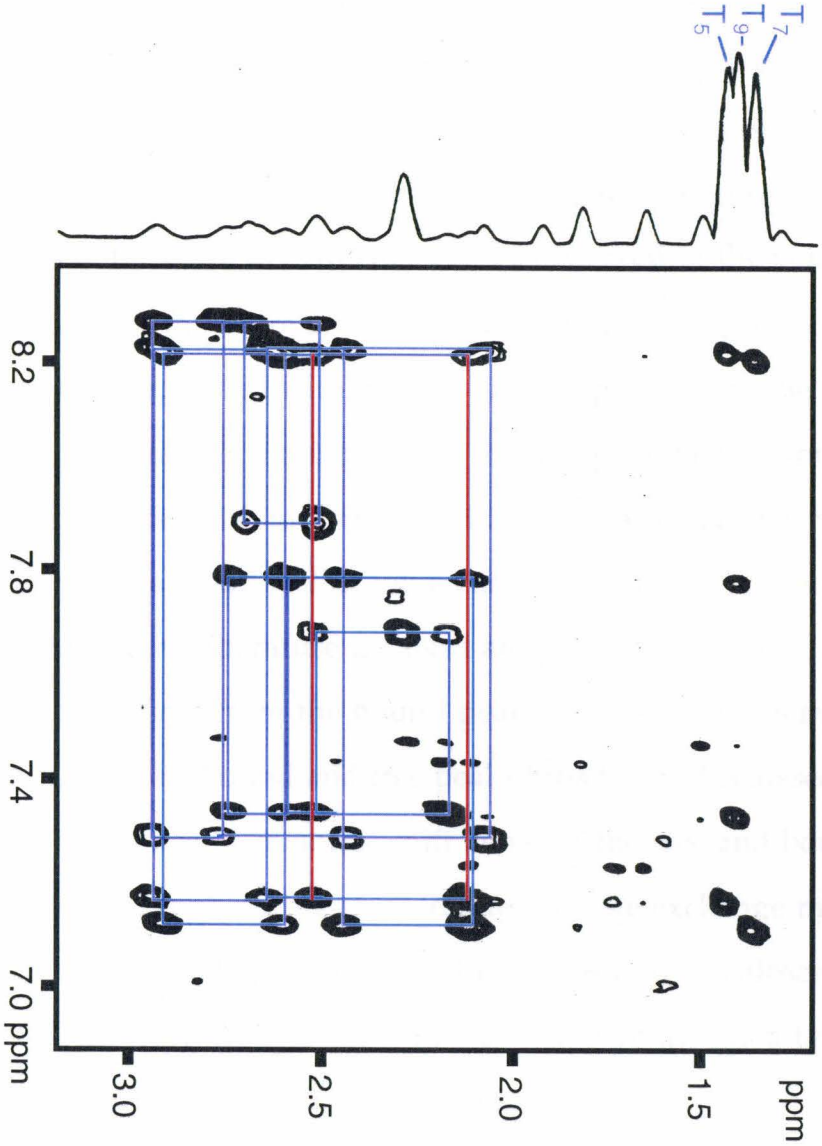

5'-$G_1A_2C_3A_4T_5A_6T_7G_8T_9C_{10}$-3'

shifts at the coalescence temperature. Since the bound and free DNA peaks are coalesced at this temperature, the actual difference in chemical shifts cannot be observed. This value is therefore estimated by using the difference in chemical shifts of bound and free DNA peaks in fast exchange. This estimate is prone to errors as the chemical shifts of protons will change with temperature independent of exchange phenomena. This temperature dependence can be seen in Figures 2.18 and 2.19 in the general movement of peaks to lower field with increasing temperature. More importantly, this temperature dependence can be observed in the behavior of the aromatic T5 proton in Figure 2.19. The bound and free signals for this proton at 5°C are well separated with the free signal upfield from the bound signal. As the temperature is raised 10°C, the free peak moves until it has a nearly identical chemical shift to that of the bound. Coalescence is not occurring because the peaks are still well resolved and peak broadening must occur for coalescence. As the temperature is raised another 10°C, to 25°C, the free peak moves downfield from the bound peak. Finally, as the temperature is raised another 10°C, the bound and free peaks broaden and coalesce. The fact that the difference in chemical shift between the free and bound peaks varies over a wide range during slow to intermediate exchange makes it difficult to estimate what the actual difference is at the coalescence temperature. Therefore, an error of ± 10 Hz should be assigned to the chemical shifts determined in this experiment.

The rate of dissociation of metal from a DNA site can be calculated using Equation 2.9. Rhodium complex was >99% bound in these experiments and thus the concentration of DNA:rhodium complex can be assumed to be identical to the total concentration of added rhodium. The calculated rate constants for dissociation of the complex based on the

coalescence of the signals from the six protons in Table 2.2 are shown in Table 2.3.

Proton	Coalescence Temperature	Dissociation Constant
Methyl-T5	318°K	88 s^{-1}
Methyl-T7	323°K	109 s^{-1}
Methyl-T9	318°K	51 s^{-1}
Aromatic-T7	313°K	67 s^{-1}
Aromatic-T5	308°K	21 s^{-1}
Aromatic-A6	320°K	45 s^{-1}

Table 2.2: Rate constants of dissociation for 1-Λ-Rh(MGP)$_2$phi^{5+} binding to 5'-CATATG-3' at different temperatures. Dissociation constants were calculated using equation 2.3.

These constants can be plotted using Equation 2.13 to yield a straight line plot from which the rate constant of dissociation can be calculated at any concentration. This plot is shown in Figure 2.22 along with a least squares fit of the data. Note that there are only six points and considerable scatter in the plot and thus conclusions drawn from it should be treated as estimates. Using the fit, the rate constant for dissociation was calculated to be 3 s^{-1} and 8 s^{-1} at 10°C and 21°C respectively. The dissociation constant at 10°C will be important in the discussion of results in Chapter 3.

2.3.5 Determination of Exchange Rate of 1-Δ-Rh(MGP)$_2$phi^{5+}:

Experiments have been carried out which allow an estimation of the exchange rate of 1-Δ-Rh(MGP)$_2$phi^{5+} with its highest affinity site 5'-CATCTG-3'. The oligonucleotide used in these experiments is shown in Figure 2.23.

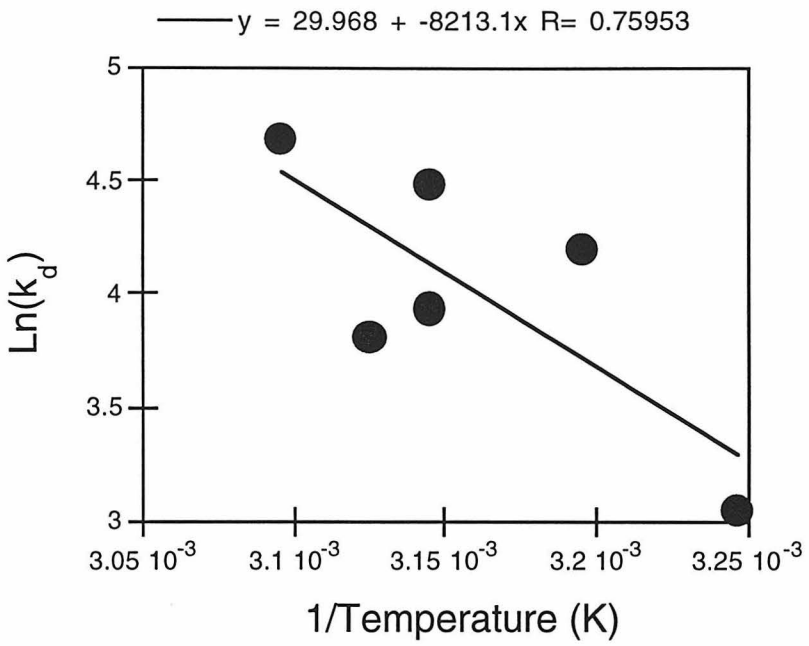

Figure 2.22: Plot of data from Table 2.2 using Equation 2.13. A least squares fit of the data is shown above the plot.

Note that this oligonucleotide is not self complementary. That this duplex is made up of two distinct oligonucleotides makes NMR spectra significantly more complicated. Twice the number of DNA peaks as were observed for the oligonucleotide shown in Figure 2.17 can be expected from this duplex as there are twice the number of unique bases present. 2D H^1-NOESY spectra of the duplex pictured in Figure 2.23 are shown in Figures 2.24 and 2.25. Both figures contain the same spectra with Figure 2.24 showing the NOE walk for nucleotides 1 through 10 and Figure 2.25 showing the NOE walk for nucleotides 11 through 20. As can be seen from both figures, a complete NOE walk cannot be determined for either DNA strand. However, enough of a walk is present to assign all of the aromatic DNA peaks which are labeled in the 1D spectra at the top of these figures. 1-Δ-Rh(MGP)2phi^{5+} was titrated

into this DNA sample to a ratio of 1:1 duplex to rhodium. A 2D H^1-NOESY spectra of this new solution was taken and is shown in Figure 2.26. The metal peaks in this spectra were assigned based on the free DNA spectra and the conductivities of intermolecular NOEs on the metal complex. Metal peaks are labeled in the Figure 2.26. As the complete NOE walk could not be made for the free DNA, arguments cannot be made about breaks in conductivities in this walk and the site of intercalation. Crosspeaks are evident between the intercalating phi ligand and DNA protons (*vide infra*). This spectra and the free DNA spectra were used to assign the 1D spectra shown in Figure 2.27.

$$\begin{array}{l} 5'\text{-}C_1\ G_2\ C_3\ A_4\ T_5\ C_6\ T_7\ G_8\ A_9\ C_{10}\text{-}3' \\ 3'\text{-}G_{20}C_{19}G_{18}T_{17}A_{16}G_{15}A_{14}C_{13}T_{12}G_{11}\text{-}5' \end{array}$$

Figure 2.23: Double-stranded oligonucleotide used in investigations of the exchange rate of 1-Δ-Rh(MGP)$_2$phi^{5+}.

Several conclusions can be made from the spectrum shown in Figure 2.27. First, two DNA peaks are evident for nearly all aromatic DNA protons. This indicates that these protons are experiencing two different environments. 1-Δ-Rh(MGP)$_2$phi^{5+} is present in a 1:1 ratio with the duplex DNA in this solution. If the complex was binding the DNA at one site and in one orientation, only one DNA environment would be present and only one peak for each DNA proton would be observed. The two peaks which are observed indicate that the complex is binding at either two sites or in two orientations. As shown in Table 2.1 and in Figure 2.12, 1-Δ-Rh(MGP)$_2$phi^{5+} binds with a relatively high affinity to sequences containing 5'-TC-3' steps. Two such steps are evident in the duplex shown in Figure 2.23, 5'-T_5C_6-3' and 5'-$T_{12}C_{13}$-3'. Thus it is possible that the complex is binding to both of these sites. This means that while the ratio of DNA duplex to rhodium in this

Figure 2.24 2D 1H-NMR NOESY spectra of the duplex DNA shown in Figure 2.23. An NOE walk for the aromatic versus H2'/H2" region is shown for nucleotides 1 through 10. Note that the NOE walk is not continuous down the entire oligonucleotide. However, enough connectivities were present to assign all the aromatic protons on this oligonucleotide. Assignments are listed in the 1D spectrum at the top of the figure. 2D ^{1}H-NOESY spectra were taken with a 300 ms mixing time and presaturation of the water peak during recycle delay and mixing time.[13] Solution conditions were 0.5 mM duplex, 10 mM sodium phosphate, and 20 mM sodium chloride in D_2O. Spectra were taken at 300 K.

5'-C_1 G_2 C_3 A_4 T_5 C_6 T_7 G_8 A_9 C_{10}-3'
3'-$G_{20}C_{19}G_{18}T_{17}A_{16}G_{15}A_{14}C_{13}T_{12}G_{11}$-5'

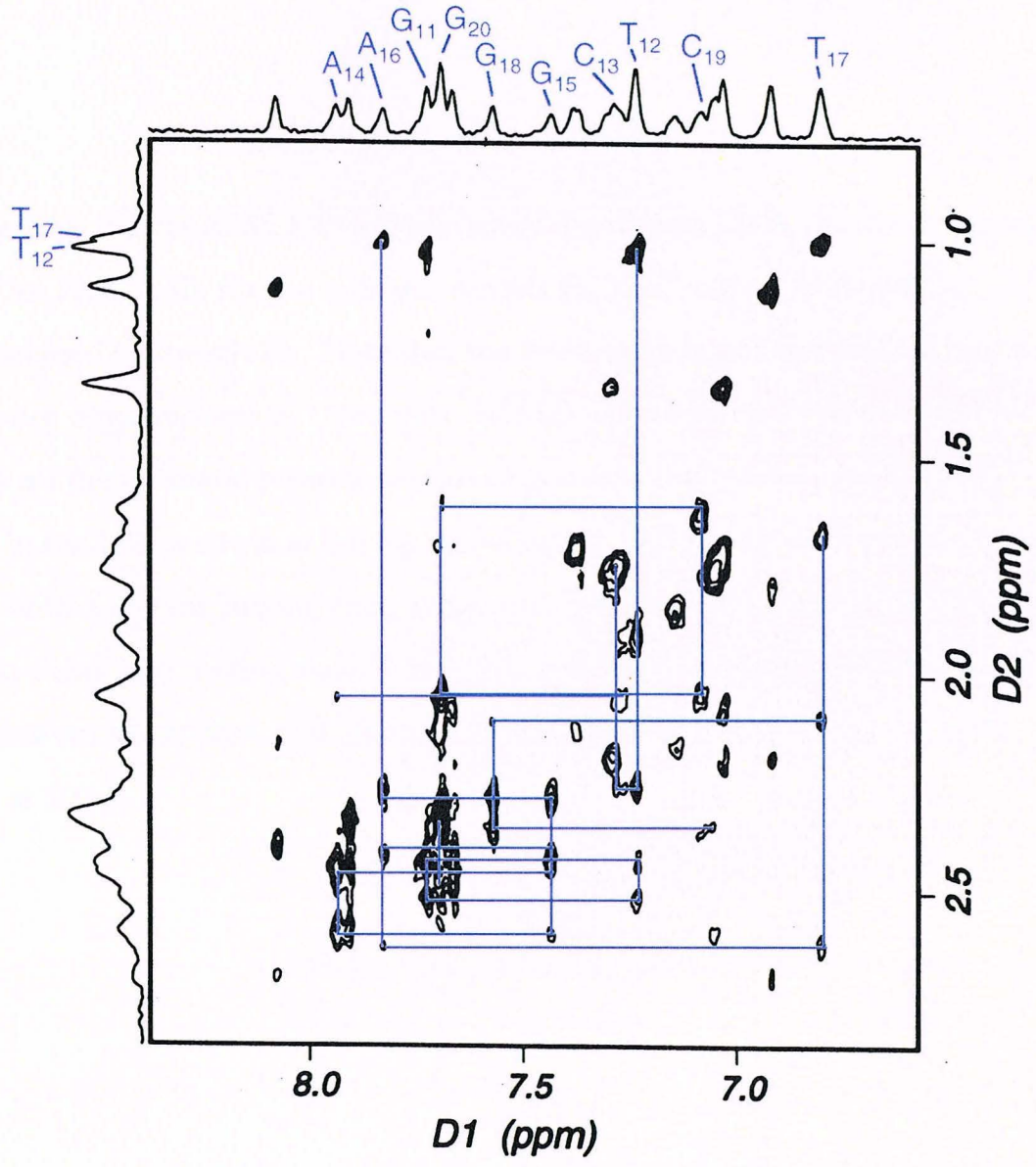

Figure 2.25 2D 1H-NMR NOESY spectra of the duplex DNA shown in Figure 2.23. An NOE walk for the aromatic versus H2'/H2" region is shown for nucleotides 11 through 20. Note that the NOE walk is not continuous down the entire oligonucleotide. However, enough connectivities were present to assign all the aromatic protons on this oligonucleotide. Assignments are listed in the 1D spectrum at the top of the figure. 2D ^{1}H-NOESY spectra were taken with a 300 ms mixing time and presaturation of the water peak during recycle delay and mixing time.[13] Solution conditions were 0.5 mM duplex, 10 mM sodium phosphate, and 20 mM sodium chloride in D_2O. Spectra were taken at 300 K.

5'-C_1 G_2 C_3 A_4 T_5 C_6 T_7 G_8 A_9 C_{10}-3'
3'-$G_{20}C_{19}G_{18}T_{17}A_{16}G_{15}A_{14}C_{13}T_{12}G_{11}$-5'

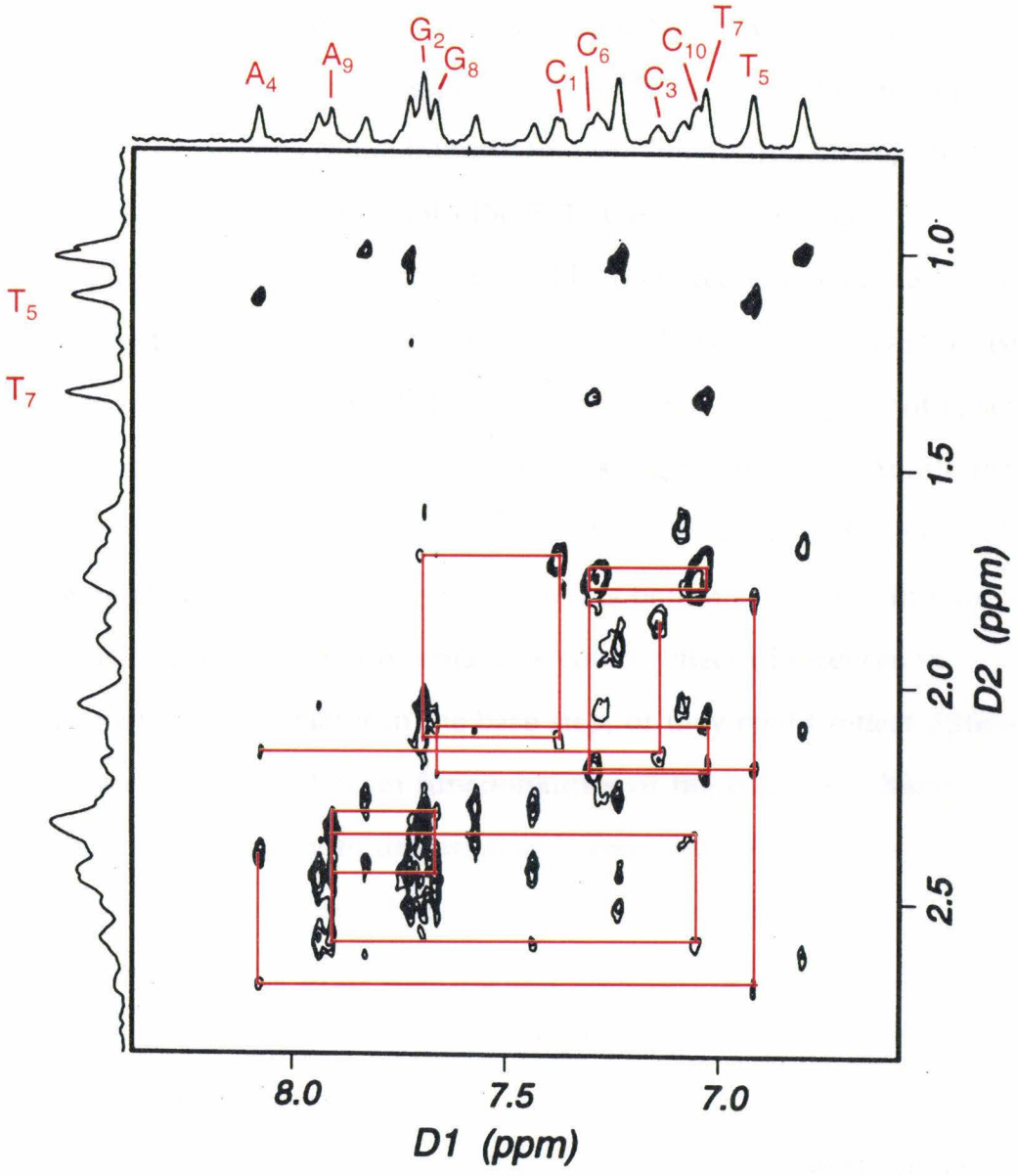

sample is 1:1, the ratio of DNA sites to rhodium is 2:1. This hypothesis proposes that the two peaks observed for each proton are for free and bound DNA sites and is supported by the fact that for each pair of peaks present, one has an identical chemical shift to that of the free DNA.

The hypothesis that 1-Δ-Rh(MGP)$_2$phi^{5+} intercalates into two different 5'-TC-3' steps, however, has one major flaw. As can be seen in Figure 2.26, there is a strong crosspeak between protons on the methyl group of T_5 and the 2,7 protons of the intercalating phi ligand (red circle). If the complex was also intercalating into the 5'-$T_{12}C_{13}$-3' step of this oligonucleotide, a similar crosspeak would be expected between the 2,7 proton of the phi ligand and the methyl protons of T_{12} (blue circle). As can be seen from the figure, this crosspeak between the phi ligand and T_{12} is not observed which argues that the complex is not intercalating at this step. An alternate hypothesis for the double DNA environments observed is that the complex is only intercalated into the 5'-T_5C_6-3' step, but is bound at this site in two orientations. These different orientations could reflect differences in positioning of the intercalator in the base step, or they could reflect different positioning of the guanidinium functionalities of the complex. More experiments are necessary to differentiate between the hypothesis explaining the two site exchange observed for DNA protons. An experiment to test the hypothesis that half the DNA sites are free would be to titrate twice as much metal complex into the existing NMR sample and observe whether or not the "free" DNA peaks disappear.

The second observation which can be made from the spectrum shown in Figure 2.27 is that the signals for phi protons are broad and being averaged. For example, the 1 and 8 protons on the phi ligand are in chemically equivalent positions and thus would give identical signals for

Figure 2.26 2D 1H-NMR NOESY spectra of 1-Δ-Rh(MGP)$_2$phi^{5+} with the DNA duplex shown in Figure 2.23. Metal complex and duplex are at a 1:1 ratio. Metal complex peaks are labeled in blue (MGP) and red (phi). Aromatic thymine peaks are labeled in green. Circled in red is a crosspeak between the 2,7 protons on the phi ligand and T_5 of the duplex DNA. The blue circle indicates the position of a hypothetical crosspeak between the 2,7 protons on the phi ligand and T_{12} of the duplex DNA. 2D ^{1}H-NOESY spectra were taken with a 300 ms mixing time and presaturation of the water peak during recycle delay and mixing time.[13] Solution conditions were 0.5 mM duplex, 0.5 mM 1-Δ-Rh(MGP)$_2$phi^{5+}, 10 mM sodium phosphate, and 20 mM sodium chloride in D_2O. Spectra were taken at 300 K.

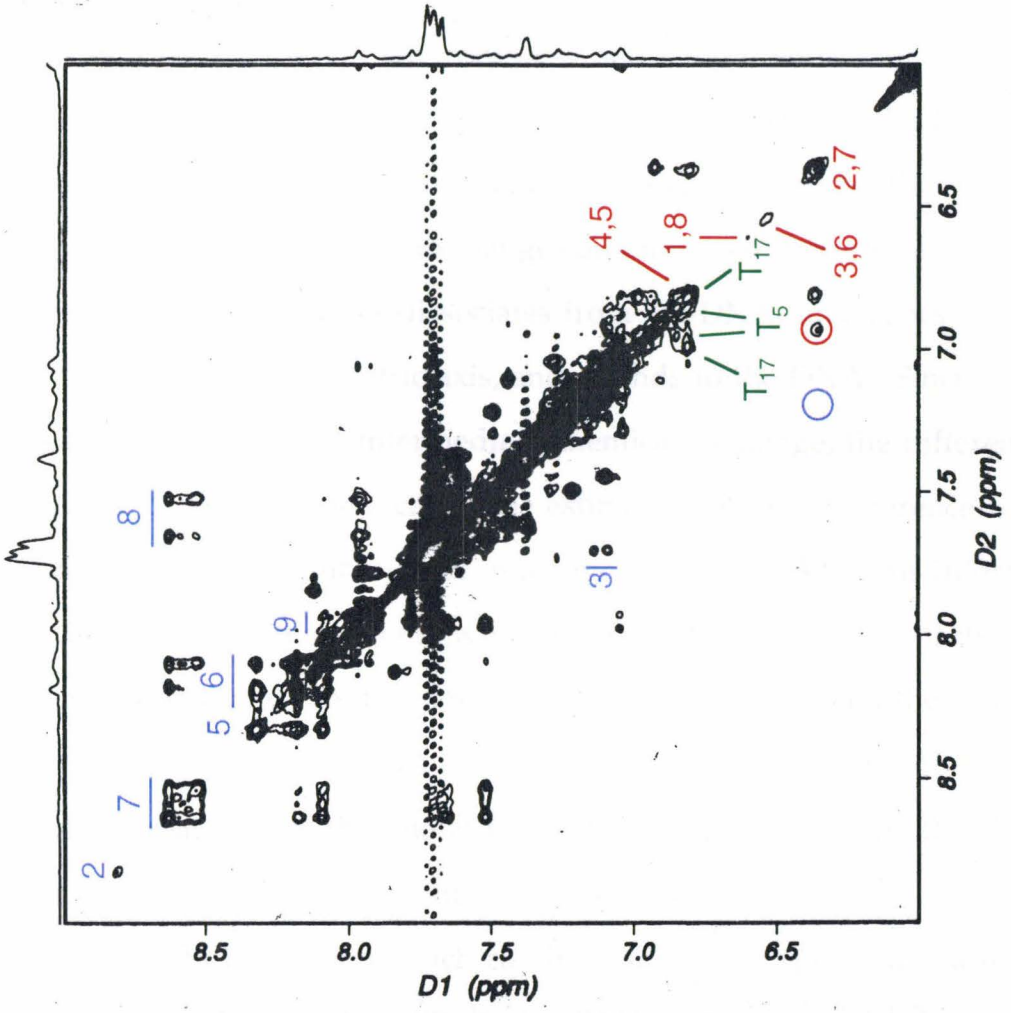
D1 (ppm)
D2 (ppm)
8.5
8.0
7.5
7.0
6.5
2
7
5
6
9
8
3
4,5
1,8
2,7
3,6
T17
T5

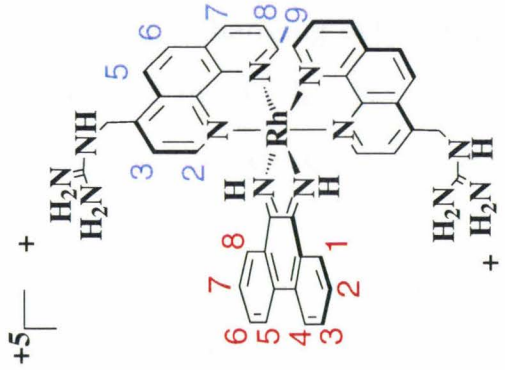
+5
Rh
N
H
H2N
NH

metal complex in solution. However, when the phi ligand is placed in an asymmetric environment such as intercalation into a 5'-TC-3' base step, these protons will be in different environments and should show different chemical shifts. That the same chemical shift is seen for both the 1 and 8 protons indicates that protons are in fast exchange with each other on the time scale of this experiment. Exchange can only occur between these two protons if the metal complex dissociates from the DNA, undergoes a 180 rotation along its C2 symmetric axis, and rebinds to the DNA. Since all the phi peaks observed are in intermediate chemical exchange, the difference in chemical shift between them cannot be estimated. As this difference is necessary for the determination of exchange rate, the lack of this information precludes any estimate of rate at which the complex is undergoing this rotation. However, if the difference in chemical shift between the different environments for the phi peaks is assumed to be similar to that of the DNA protons or greater, then the rate at which the complex "flips" on the DNA is greater than the rate of the two site exchange described above.

A third observation which can be made in the spectrum shown in Figure 2.27 is that the protons on the ancillary ligands of 1-Δ-$Rh(MGP)_2phi^{5+}$ experience two different environments as indicated by two peaks. This is consistent with the complex exchanging between the two different sites or two different orientations on the duplex shown in Figure 2.23. Since these peaks are observed due to the same exchange which causes two DNA peaks, the ancillary protons and the DNA protons can be used to determine the exchange rate between the two sites or orientations on this duplex DNA.

The exchange rate between the two sites or orientations on the duplex shown in Figure 2.23 was determined using variable temperature NMR. 1D ^{1}H-NMR spectra of the 1:1 1-Δ-$Rh(MGP)_2phi^{5+}$ to duplex solution

Figure 2.27 1D ^{1}H-NMR spectrum from the data used to construct Figure 2.26. Peak assignment were made based on spectra presented in Figures 2.24 through 2.26.

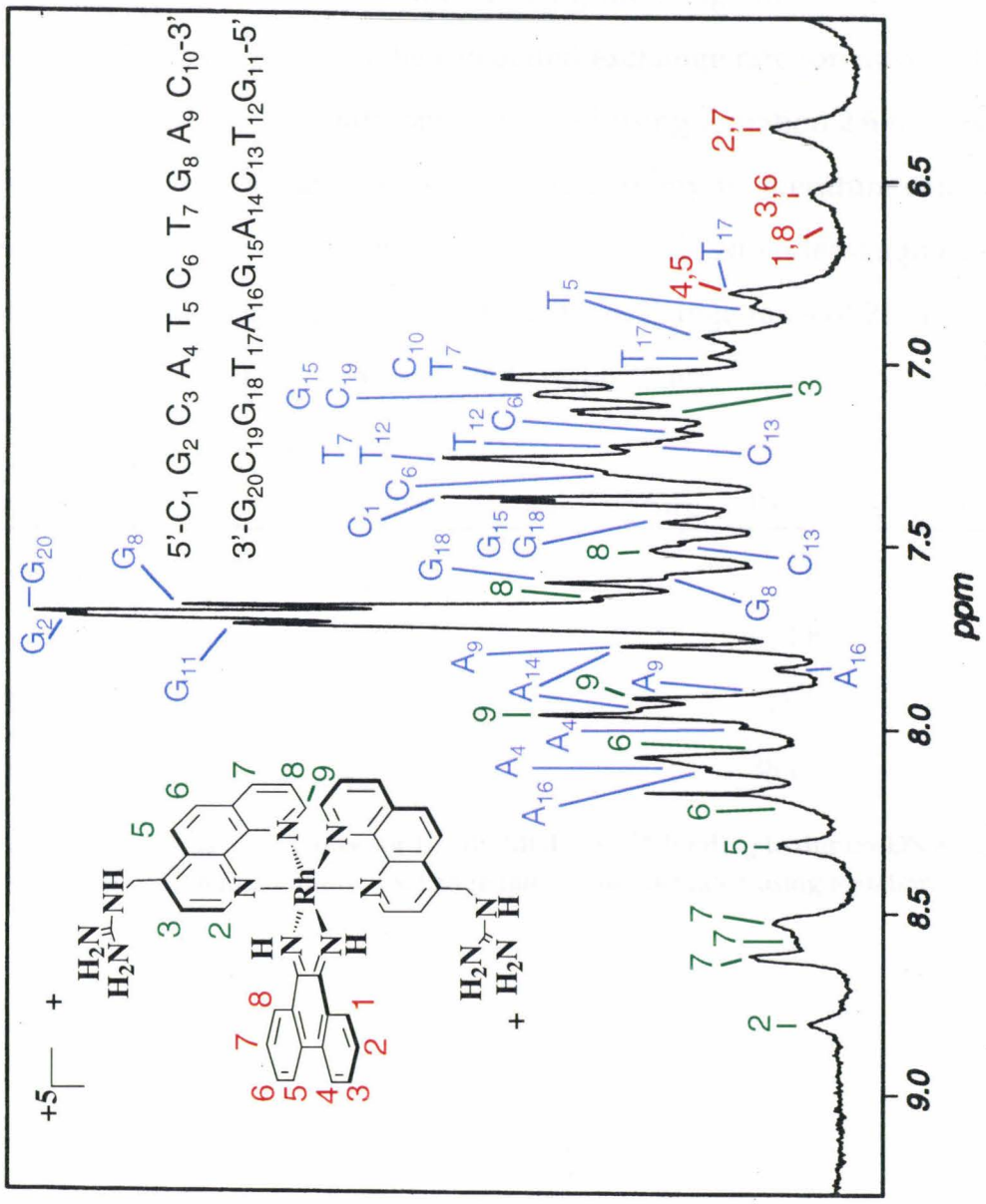
5'-C1 G2 C3 A4 T5 C6 T7 G8 A9 C10-3'
3'-G20C19G18T17A16G15A14C13T12G11-5'
+5
Rh
ppm
9.0
8.5
8.0
7.5
7.0
6.5

described above were acquired at 5, 10, 15, 20, 25, 30, 35, 40, and 45°C. These spectra are shown in Figure 2.28. Signals for two DNA and two metal complex protons were observed to coalesce over the temperature range studied. These protons were identified using the assignments shown in Figure 2.27. Table 2.3 contains the calculated exchange rate for each of these protons. The exchange rate data can be plotted using Equation 2.6 to yield a straight line plot from which the exchange rate at any temperature can be extrapolated. This plot is shown in Figure 2.29 along with a least squares fit of the data. Using the straight line fit of the data, exchange rates of 21 and 8 per second were calculated for 21°C and 10°C respectively.

Proton	Coalescence temperature	Exchange rate
Aromatic T_{17}	42°C	135 Hz
Aromatic T_5	35°C	66 Hz
MGP 8	42°C	115 Hz
MGP 9	27°C	38 Hz

Table 2.3: Rate constants of exchange for 1-Δ-Rh(MGP)$_2$phi^{5+} binding to duplex DNA shown in Figure 2.23 at different temperatures. Exchange rates were calculated using equation 2.12.

Figure 2.28 ^{1}H-NMR spectra of 1-Δ-Rh(MGP)$_2$phi^{5+} and DNA used to determine exchange rates. Metal to oligonucleotide ratio is 1:1. Oligonucleotide is shown in Figure 2.23. Peak assignments were made based on spectra shown in Figure 2.27. Temperatures at which spectra were taken at are listed at the right of the figure. 1D ^{1}H-NMR spectra were taken with presaturation of the water peak.[13] Solution conditions were 0.5 mM duplex, 0.5 mM 1-Δ-Rh(MGP)$_2$phi^{5+}, 10 mM sodium phosphate, and 20 mM sodium chloride in D_2O.

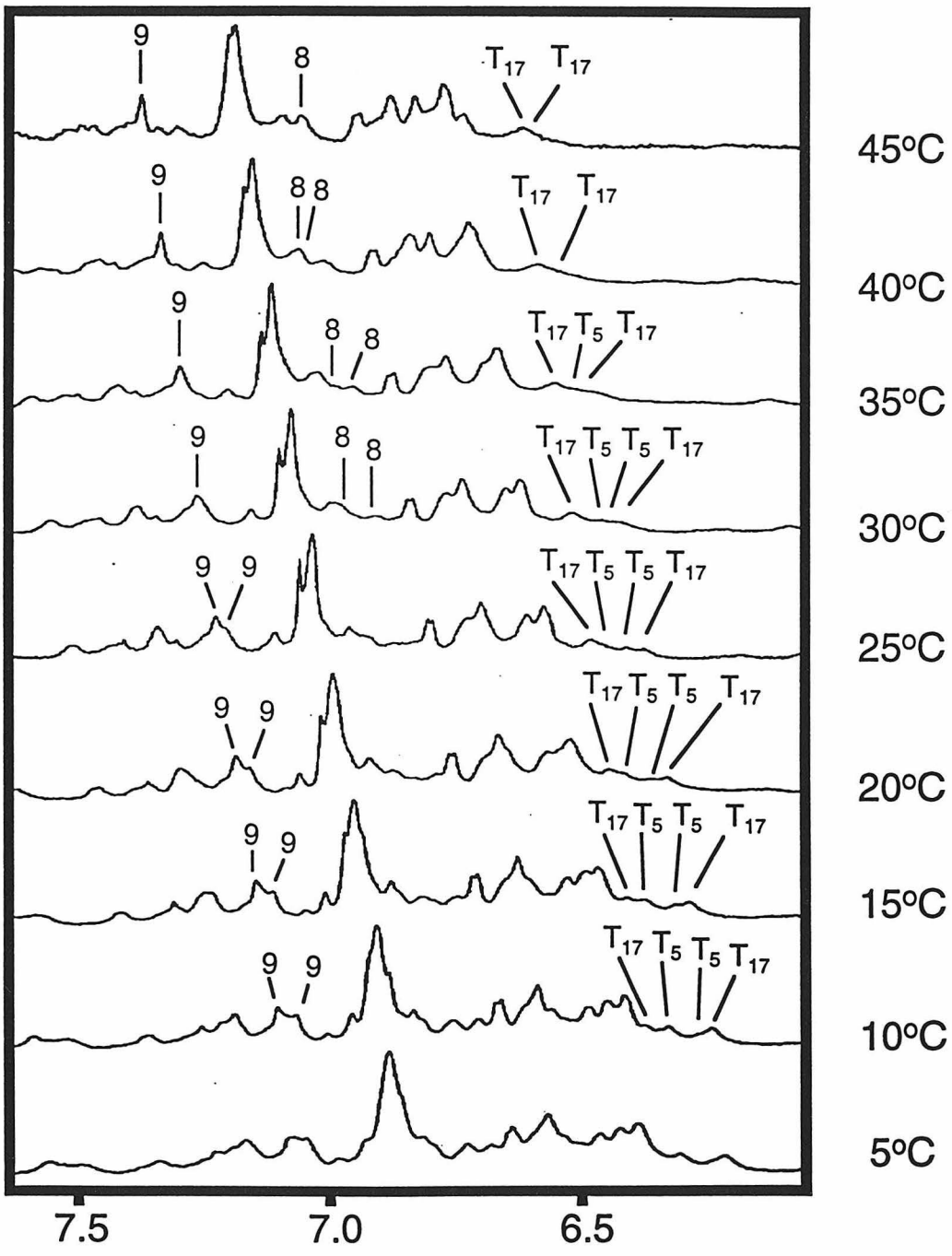
9
8
T17 T17
45°C
9
8 8
T17 T17
40°C
9
8 8
T17 T5 T17
35°C
9
8 8
T17 T5 T5 T17
30°C
9 9
T17 T5 T5 T17
25°C
9 9
T17 T5 T5 T17
20°C
9 9
T17 T5 T5 T17
15°C
9 9
T17 T5 T5 T17
10°C
5°C
7.5
7.0
6.5

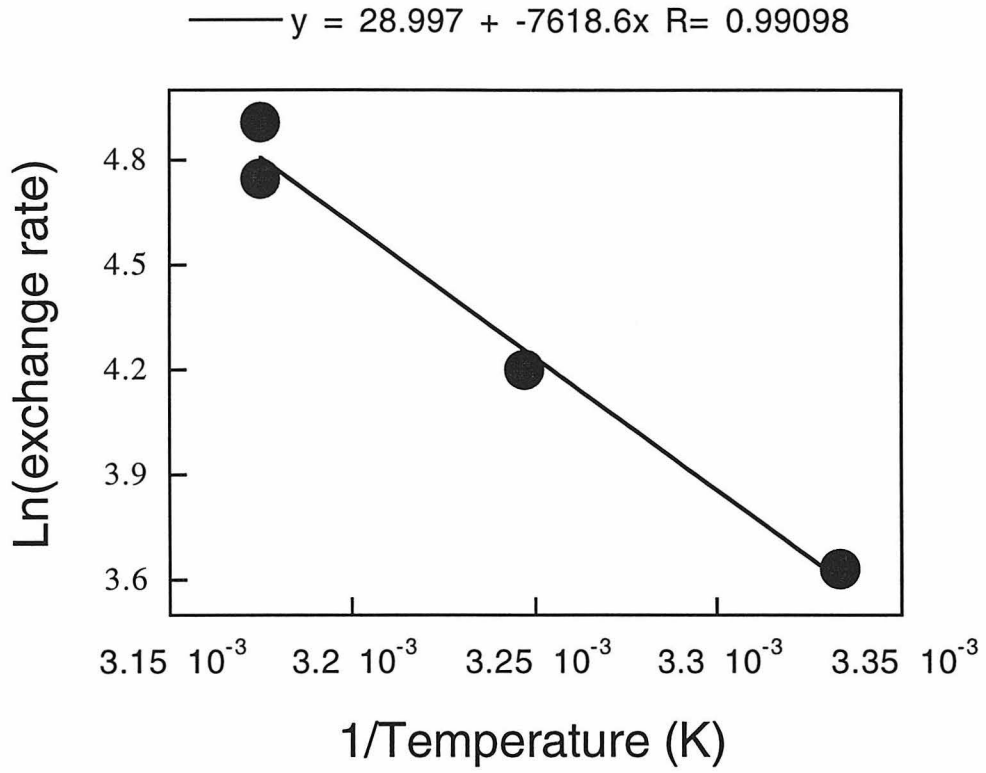

Figure 2.29: Plot of data from Table 2.3 using Equation 2.13. A least squares fit of the data is shown above the plot.

2.4 Discussion

In the Results section above, investigations into the effects of experimental conditions on DNA photocleavage by the enantiomers of 1-Rh(MGP)$_2$phi^{5+} were described. The results from these experiments were then applied in the design of experiments which used the DNA photocleavage properties of 1-Rh(MGP)$_2$phi^{5+} to determine quantitative affinity constants for the complex binding to specific DNA sites. The rate constant for the dissociation of 1-Λ-Rh(MGP)$_2$phi^{5+} from its recognition sequence, 5'-CATATG-3', was determined by variable temperature ^{1}H-NMR. Finally, the exchange rate of 1-Δ-Rh(MGP)$_2$phi^{5+} between two sites or two orientations was determined at 10 and 21°C. The affinity, exchange rate, and dissociation constant data enhance the understanding of the binding characteristics of the enantiomers of 1-Rh(MGP)$_2$phi^{5+}. Conclusions drawn from these experiments are presented below.

2.4.1 Quantitative Affinity Constants for the Binding of Δ and Λ 1-Rh(MGP)$_2$phi^{5+}: The quantitative affinity constant for 1-Λ-Rh(MGP)$_2$phi^{5+} binding to 5'-CATATG-3'was determined to be $1\times10^8 \pm 0.2\times10^8$ M^{-1}. 1-Δ-Rh(MGP)$_2$phi^{5+} was found to have an affinity constant of $5\times10^7 \pm 1\times10^7$ M^{-1} for 5'-CATCTG-3'. The affinity constants for the two complexes are nearly identical. Both correspond to an approximate 12 kilocalorie stabilization upon binding of the metal complex to its specific DNA site. Both complexes are shown in Figure 2.30. These enantiomers are capable of making the same bonding contacts to DNA. Both contain the same intercalator and both have a 5+ charge. Both complexes also contain two guanidinium functionalities capable of making direct hydrogen bonding contacts to guanines in the major groove of DNA. Since the DNA contacts possible for these two enantiomers

are identical, it is not surprising that their binding constants to their recognition sequences would be similar.

Direct hydrogen bonding contacts between the guanidinium functionalities of the Λ enantiomer and guanines in its recognition sequence has been supported by photocleavage experiments using deazaguanines as described in Chapter 1.[2] These hydrogen bonding contacts have not been established for the Δ enantiomer. However, the fact that the DNA sequence for which this complex demonstrates the most affinity, 5'-CATCTG-3', contains guanines at its exterior, is consistent with the Δ enantiomer making direct contacts to these bases. Comparison of the binding sites for the Δ and Λ enantiomers suggests similarities in binding. These sites are 5'-CA**T**C**C**TG-3' and 5'-CA**T**A**A**TG-3' for the Δ and Λ enantiomer respectively. The enantiomers intercalate between the bolded bases in their respective sites. Both sites are nearly identical with the only difference being the base directly 3' to the site of intercalation. This similarity suggests that the complexes are making similar contacts on the outer portions of their recognition sequences. Similarities in binding are further supported by the effects of changes in the recognition sequences for each complex shown in Table 2.1. As can be seen from this data, changes in the exterior portions of these sequences result in relatively small changes in affinity for each complex. However, both complexes show large changes in affinity when changes are made to the internal portions of the recognition sequence.

How is each complex positioned at its site of intercalation? The photocleavage pattern in the binding affinity constant gels shown in Figures 2.11 and 2.13 is instructive in this matter. As can be seen from these gels, photocleavage with 1-Λ-Rh(MGP)$_2$phi^{5+} results in damage at the bases directly 5' and 3' to the intercalation site. Photocleavage with 1-Δ-

Figure 2.30 The structures of Λ and Δ 1-Rh(MGP)$_2$phi^{5+}.

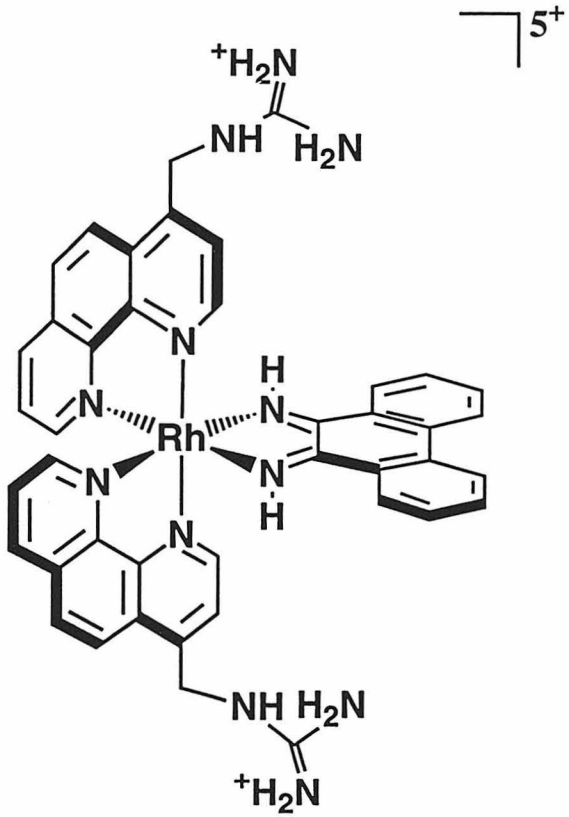

1-Λ-Rh(MGP)$_2$phi^{5+}

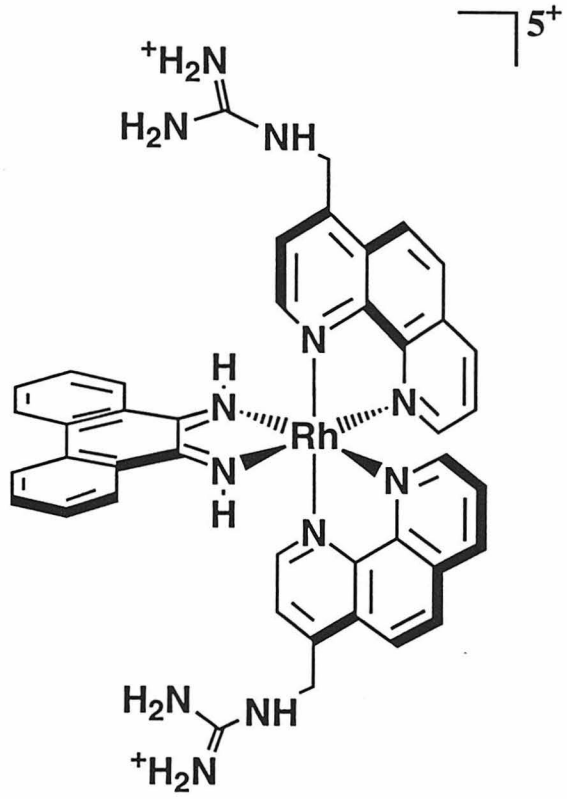

1-Δ-Rh(MGP)$_2$phi^{5+}

$Rh(MGP)_2phi^{5+}$, however, results in DNA damage only to the 3' side of the intercalation site. These differences in DNA damage strongly suggest differences in intercalation. However, that the binding constants of these enantiomers are nearly identical suggests that similar amounts of stacking with the DNA bases occurs with the phi intercalator of each complex. As mentioned in Chapter 1, intercalation affords approximately 7 kilocalories of stabilization upon DNA binding.[16] Δ and Λ 1-$Rh(MGP)_2phi^{5+}$ show 12 kilocalories of stabilization upon binding DNA and therefore the majority of this stabilization results from stacking interactions between the intercalator and the DNA bases. Since intercalation contributes substantially to the affinity of these complexes, large differences in the stacking of the phi intercalator would be expected to result in large differences in the affinity constants measured for these complexes. As the affinities of these complexes are similar, the amount of stacking in the intercalation of each to its DNA site can also be expected to be similar. Differences in photocleavage are likely a result of differences in position of the intercalator in the DNA bases which do not result in differences in the amount of stacking interactions which occur.

The ^{1}H-NMR data described in the Results section are informative with respect to the positioning of 1-Λ-$Rh(MGP)_2phi^{5+}$ in its intercalation site. The spectra of the Λ enantiomer show only one peak for bound protons at the DNA intercalation site. This single bound peak is consistent with symmetric binding. If the Λ enantiomer was canted in its intercalation site, then binding would not be symmetric and two bound peaks for each proton at this site would be observed. Symmetric binding is also expected when a C2 symmetric complex binds to a C2 symmetric DNA structure. A model of the Λ enantiomer bound to DNA is shown in Figure 2.31. This model was produced using InsightII on a Silicon Graphics Indigo XS. Note that in this

Figure 2.31 A model of 1-Λ-Rh(MGP)2phi^{5+} bound to 5'-CATATG-3'. Note that the complex is centered in its intercalation site.

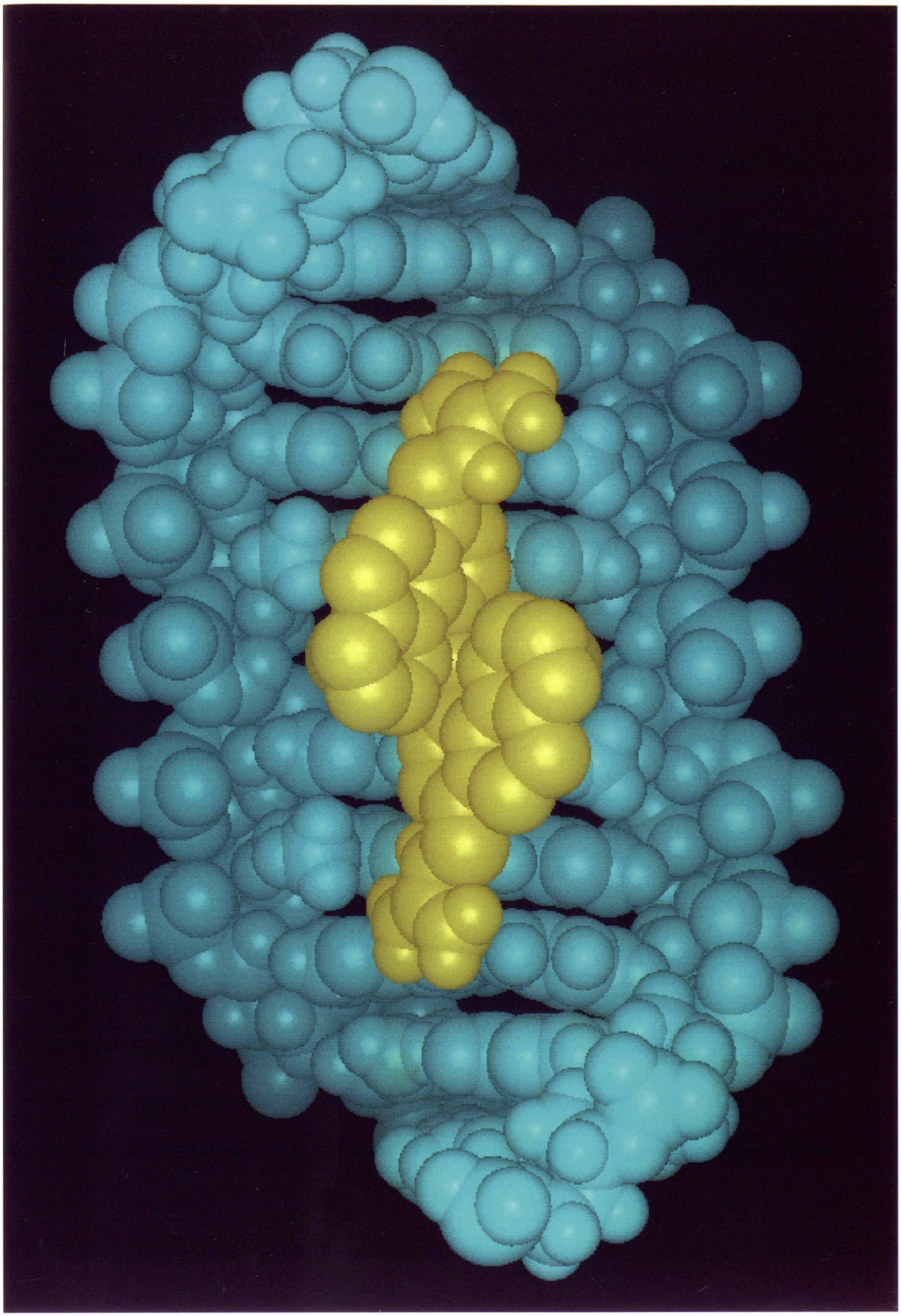

model, the complex is centered in the intercalation site. The 70° unwinding of the DNA, which has been demonstrated (*vide supra*) is necessary for the guanidinium arms of the complex to make direct hydrogen bonding contacts with the guanines of its recognition sequence. This unwinding results in a helical twist of 0° for the base step at the intercalation site in this model. This 0° twist may be responsible for the double band photocleavage observed with 1-Λ-Rh(MGP)$_2$phi^{5+}.

A model for the binding of 1-Δ-Rh(MGP)$_2$phi^{5+} to 5'-CATCTG-3' has not been previously presented. As described above, the data presented in Table 2.1 show the importance of the guanines in the recognition sequence. The removal of these guanines results in decreased affinity for the DNA site. This decreased affinity is similar to that observed for the Λ enantiomer, for which there is evidence of direct hydrogen bonds between the guanines and the metal complex. The data present in Table 2.1 therefore support direct contacts between the guanidinium groups of the Δ enantiomer and the guanines in its recognition sequence.

1-Δ-Rh(MGP)$_2$phi^{5+}-directed cleavage observed at 5'-CATCTG-3' is only at the bolded base on this strand and is observed to a much lesser extent on the opposing strand. Asymmetric photocleavage has been previously suggested to be indicative of canting to one side in the intercalation site.[17] Therefore, the Δ enantiomer may be canted in its DNA site. This hypothesis is further supported by the relative photocleavage efficiency for the Δ and Λ enantiomers present in Section 2.3.2.3. The Δ enantiomer shows four times the photocleavage efficiency of the Λ enantiomer. These complexes are identical except in chirality and have the same electronic characteristics. Thus, the intrinsic reactivity of each complex should be the same. The differences in photocleavage efficiency between these two complexes is

instructive in the positioning of each in its intercalation site. As described above, the Λ enantiomer is positioned symmetrically in its intercalation site. Experiments have supported that photocleavage of DNA is a result of a direct hydrogen abstraction, by a free radical on the phi ligand, from a sugar on the phosphate backbone.[17] The central positioning of the Λ enantiomer places the phi ligand as far as possible from sugars on the backbone. If the Δ enantiomer is canted to the pyrimidine side in its intercalation site, the phi ligand of this enantiomer will be positioned closer to the sugar in this site than the Λ enantiomer phi is in its site. This closer proximity for the Δ enantiomer, due to canting, would explain the differences in photocleavage efficiencies observed for the complexes.

A model of 1-Δ-Rh(MGP)$_2$phi^{5+} bound to 5'-CATCTG-3' was constructed as described above and is shown in Figure 2.32. Note that the complex is canted to one side in this model. Independent of the experimental observations described above, this canting is necessary for a direct contact to be made between a guanidinium functionality of the complex and a guanine in the recognition sequence. Attempts to make both guanidinium/guanine contacts in this model were unsuccessful. The carbon linkers attached to the guanidinium groups are simply not long enough for both contacts to occur whether the complex is centered or canted in the intercalation site. The second guanidinium group therefore was placed in position for a hydrogen bonding or electrostatic interaction with a phosphate oxygen on the DNA backbone.

It is instructive to compare the binding characteristics of 1-Λ-Rh(MGP)$_2$phi^{5+} and Rh(MT)phi^{3+}. As described in Chapter 1, a large amount information is known about the binding of Rh(MT)phi^{3+} to DNA. An ^{1}H-NMR solution structure exists for Rh(MT)phi^{3+} binding to its

Figure 2.32 A model of 1-Δ-Rh(MGP)$_2$phi^{5+} bound to 5'-CATCTG-3'. Note that the complex is canted to one side in its intercalation site. The complex also makes one guanidinium contact with a guanine and one with the phosphate backbone of DNA.

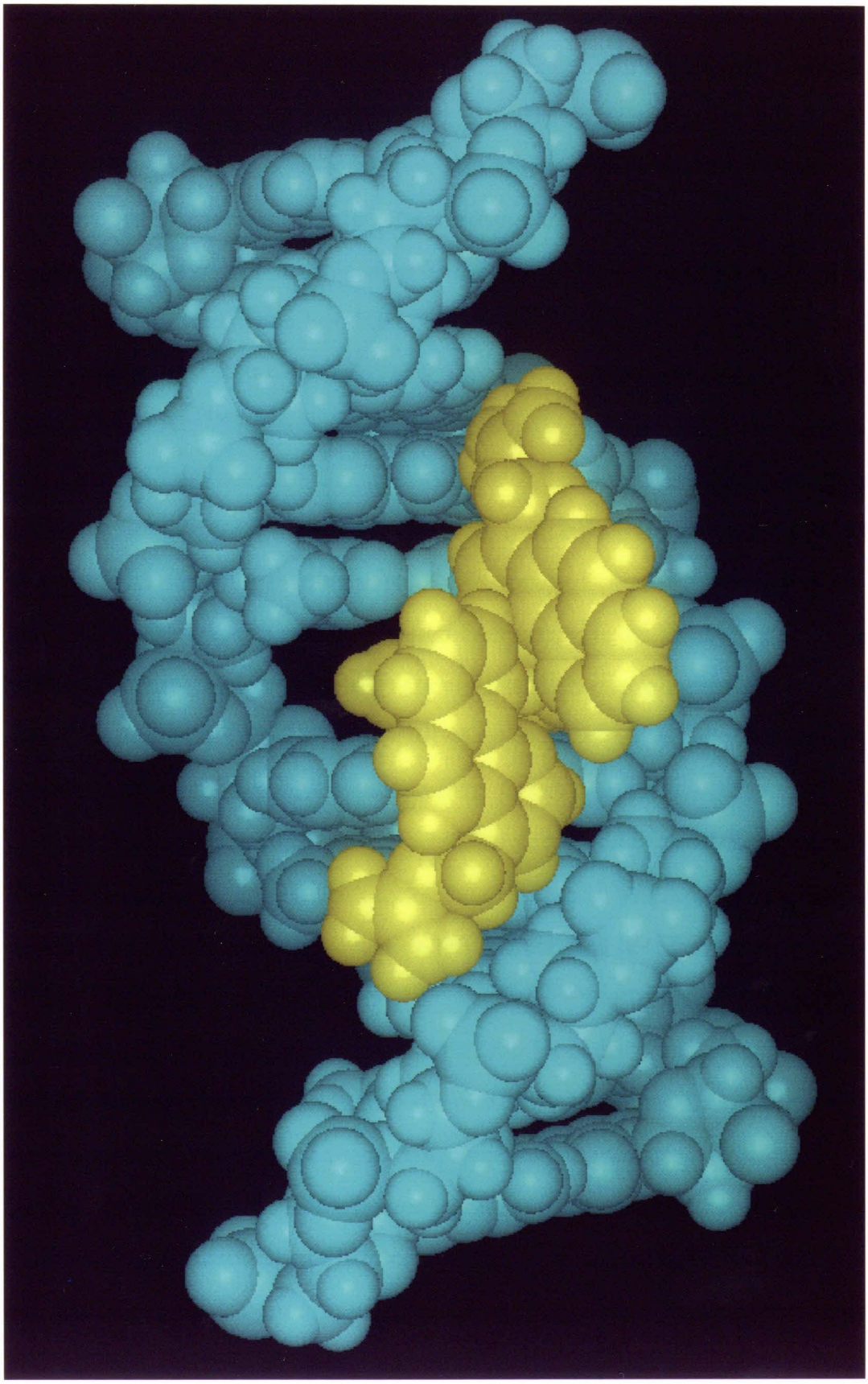

recognition sequence 5'-TGCA-3'.[18] This structure shows that the complex intercalates into the DNA with the axial amines of the complex in position to make direct hydrogen bonding contacts with the guanines directly 5' and 3' to its intercalation site. This structure also shows direct van Der Waals interactions occurring between the methyl groups of $Rh(MT)phi^{3+}$ and the methyl groups of the thymines of 5'-TGCA-3'. Thus, $Rh(MT)phi^{3+}$ binds to DNA via two hydrogen bonding contacts with guanines, two methyl-methyl interactions, and one intercalating phi ligand. $1\text{-}\Lambda\text{-}Rh(MGP)_2phi^{5+}$ binds to DNA via two hydrogen bonding contacts with guanines and one intercalating phi ligand. The electrostatic contributions to binding may also be different between the complexes as $Rh(MT)phi^{3+}$ and $1\text{-}\Lambda\text{-}Rh(MGP)_2phi^{5+}$ have charges of 3+ and 5+ respectively. Differences also exist in the unwinding of the DNA base stack that occurs when these complexes bind to DNA. The NMR structure of $Rh(MT)phi^{3+}$ shows that this complex unwinds the DNA by 20^{o} upon binding. Solution studies have shown that $1\text{-}\Lambda\text{-}Rh(MGP)_2phi^{5+}$ unwinds the DNA by 70^{o} upon binding.

The quantitative affinity constant for $Rh(MT)phi^{3+}$ binding to 5'-TGCA-3' has been determined to be $1x10^8 \pm 0.4x10^8\ M^{-1}$.[10] This value compares to the affinity constant of $1x10^8 \pm 0.2x10^8\ M^{-1}$ for $1\text{-}\Lambda\text{-}Rh(MGP)_2phi^{5+}$ binding to 5'-CATATG-3'. There are significant differences in number and type of contacts made to the DNA by these complexes as well as differences in unwinding caused upon their binding. It is therefore somewhat surprising that these complexes have identical affinities for their recognition sequences. Differences between electrostatic interactions, direct bonding contacts, and intercalator stacking must therefore combine in negative and positive manners to result in the same affinity constant for both complexes. With its increased charge, $1\text{-}\Lambda\text{-}Rh(MGP)_2phi^{5+}$ should have a

greater electrostatic interaction with the DNA than Rh(MT)phi^{3+}. The differences in the electrostatic interactions of the complexes are likely compensated by Rh(MT)phi^{3+} making more direct bonding contacts with the DNA than 1-Λ-Rh(MGP)$_2$phi^{5+}.

2.4.2 Exchange Rate of 1-Λ-Rh(MGP)$_2$phi^{5+} on 5'-CATATG-3': The exchange rate of 1-Λ-Rh(MGP)$_2$phi^{5+} on the sequence 5'-CATATG-3' was described in section 2.3.4. The rate constant of dissociation for 1-Λ-Rh(MGP)$_2$phi^{5+} from 5'-CATATG-3' was determined to be 8 s^{-1} at 21°C using the least squares fit of the data plotted in Figure 2.19. As described above, the affinity constant for 1-Λ-Rh(MGP)$_2$phi^{5+} binding to 5'-CATATG-3' at 21°C is $1x10^8$ M^{-1}. With this data, the rate constant of association of 1-Λ-Rh(MGP)$_2$phi^{5+} binding to 5'-CATATG-3' can be calculated using equation 2.4. The rate constant of association for this binding is $3x10^8$ $M^{-1}s^{-1}$. This association therefore occurs at a rate very close to the limit of diffusion which is estimated to occur with a rate constant of 10^9 to 10^{10} $M^{-1}s^{-1}$.[19]

An estimate of the activation energy necessary for the dissociation of 1-Λ-Rh(MGP)$_2$phi^{5+} from 5'-CATATG-3' can be made using the slope of the line in Figure 2.19. This plot is based on the form of the Arrhenius equation shown in equation 2.6. The slope of the line is equal to $-E_a/R$ where E_a is the activation energy for the dissociation of the complex from its site and R is the ideal gas constant. Using the linear fit of the plot in Figure 2.19, this activation energy was calculated to be 16 kilocalories. This number can be combined with the 12 kilocalorie difference between bound and free metal complex to construct the activation energy diagram shown in Figure 2.33. As can be seen from Figure 2.23, the activation energy of 1-Λ-Rh(MGP)$_2$phi^{5+} binding to its recognition sequence is 4 kilocalories.

Figure 2.33 Free energy diagram of 1-Λ-Rh(MGP)$_2$phi^{5+} binding to 5'-CATATG-3'.

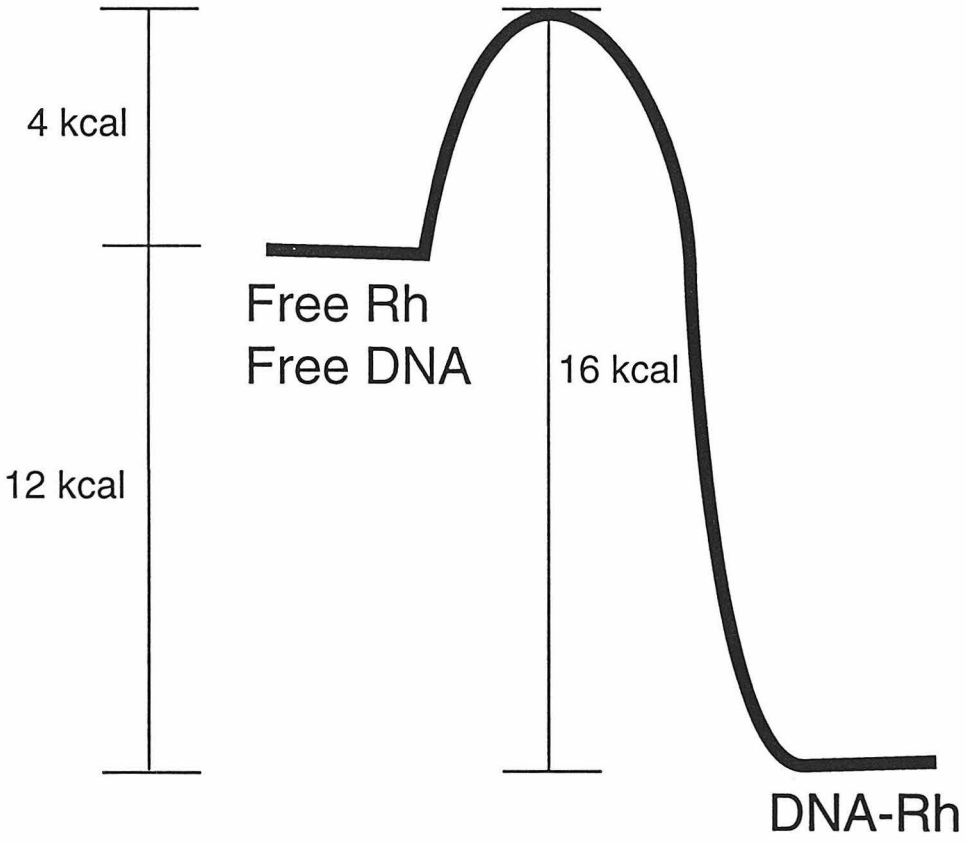
4 kcal
12 kcal
Free Rh
Free DNA
16 kcal
DNA-Rh

When 1-Λ-Rh(MGP)$_2$phi^{5+} is bound to 5'-CATATG-3', this DNA sequence is unwound by approximately 70^o. This degree of unwinding is more than three times that generally observed for other DNA intercalators including all other phi complexes of rhodium which have been studied. This 70^o unwinding of DNA represents a large distortion of the structure of the double helix. It could be expected that this amount of distortion would be associated with a high energetic price. However, as described above, the affinity constant for 1-Λ-Rh(MGP)$_2$phi^{5+} binding to its recognition sequence is equal to that of Rh(MT)phi^{3+} binding to its recognition sequence. If a substantial thermodynamic cost is paid for unwinding when 1-Λ-Rh(MGP)$_2$phi^{5+} binds DNA, it would be expected that the affinity constant of this complex would be less than that of Rh(MT)phi^{3+}. Furthermore, the DNA affinity constants of these complexes are the highest measured for phi complexes to date. These data indicate that there is not a substantial energetic penalty for the unwinding of the recognition sequence for 1-Λ-Rh(MGP)$_2$phi^{5+}. Further support of this conclusion is given by the crystal structure of TBP binding to DNA.[20],[21] In this structure, the TBP protein is bound to a the DNA sequence 5'-TATATA-3' which is similar to 5'-CATATG-3'. The bound DNA in this structure is unwound by 80^o. This unwinding, together with the metal complex data, suggests that there is a small energetic cost for the unwinding of 5'-ATAT-3' sequences.

Further support of a small energetic cost for the unwinding observed for 1-Λ-Rh(MGP)$_2$phi^{5+} could be obtained from the construction of binding energy diagrams, such as the one in Figure 2.23, for other complexes. Work is currently underway attempting to obtain the exchange rate data necessary to construct such a diagram for 1-Δ-Rh(MGP)$_2$phi^{5+}. As mentioned in the Results section, initial attempts to determine exchange rates for the Δ

enantiomer have been unsuccessful since the data is not consistent with one bound form for this enantiomer. Rh(MT)phi^{3+}, however, has demonstrated single site binding in NMR experiments. If enough exchange rate data can be obtained for this complex to determine the activation barrier to its dissociation from DNA, then an energy diagram could be constructed for this process. This diagram would allow the comparison of the relative activation energies of Rh(MT)phi^{3+} and 1-Λ-Rh(MGP)$_2$phi^{5+} binding to DNA which would be instructive in defining what constitutes a low activation energy of binding.

2.4.1 Exchange Rate of 1-Δ-Rh(MGP)$_2$phi^{5+} on 5'-CATATG-3': As described in the results section, ^{1}H-NMR data for 1-Δ-Rh(MGP)$_2$phi^{5+} binding to the duplex shown in Figure 2.23 are consistent with two site exchange on this DNA. Exchange rates between these two environments were calculated from the linear fit of exchange data in Figure 2.29 to be 21 and 8 per second for 21°C and 10°C respectively. Two models have been proposed for the exchange behavior observed. In one model, the complex is binding to two distinct 5'-CT-3' steps of the duplex DNA. These steps are 5'-T_5C_6-3' and 5'-$T_{12}C_{13}$-3' shown in Figure 2.23. If the complex is binding to two sites on this DNA, then the ratio of rhodium to rhodium binding sites in the sample measured is 1:2. Thus, the two site exchange observed for the DNA would be between free and bound forms. This model is supported by the fact that for most of the DNA peak pairs in the exchange observed, one peak is identical in chemical shift to the free DNA. However, there is evidence that indicates that this double binding site model is incorrect. As can be seen from Figure 2.26, a strong NOE crosspeak is seen between protons on the intercalating phi ligand of the metal complex and the methyl group of T_5. If the complex was

binding to the 5'-$T_{12}C_{13}$-3' step as well as the 5'-T_5C_6-3' step, a crosspeak would be expected between the methyl group of T_{12} and the phi ligand. No such crosspeak exists which indicates that the complex is not intercalating at this site. An alternate hypothesis for the double DNA environments observed is that the complex is only intercalated into the 5'-T_5C_6-3' step, but is bound at this site in two orientations. These different orientations could reflect differences in positioning of the intercalator in the base step, or they could reflect different positioning of the guanidinium functionalities of the complex. It seems unlikely, however, that this would lead to two distinct peaks, one of which is identical to that of free DNA, at the intercalated 5'-T_5C_6-3' step. More experiments are necessary to differentiate between these two models. As mentioned above, titrating more metal complex into samples would confirm the first model. Doubling the amount of metal complex would bring the rhodium to rhodium binding sites ratio to 1:1 and result in the disappearance of free DNA peaks if model 1 is correct.

In this chapter, conditions for the optimization of metal complex directed DNA damage in photocleavage experiments have been described. These conditions were then used in the design of experiments to determine the quantitative affinity constants for the enantiomers of 1-Rh(MGP)$_2$phi^{5+} binding to specific sites on DNA. ^{1}H-NMR experiments were conducted to determine the rate of exchange between DNA environments for 1-Δ-Rh(MGP)$_2$phi^{5+}. ^{1}H-NMR experiments were also conducted to determine the rate constant for the dissociation of 1-Λ-Rh(MGP)$_2$phi^{5+} from DNA. Finally, this rate data was combined with the affinity constant data for the Λ enantiomer to generate an energetic profile for this complex binding to and dissociating from DNA. The data described in this chapter have resulted in

an increased understanding of the interactions of the enantiomers of 1-$Rh(MGP)_2phi^{5+}$ with DNA.

2.5 References

1. Terbrueggen, R. H., Ph.D. Thesis.
2. Terbrueggen, R. H.; Barton, J. K.; *Biochemistry*, **1995**, 34, 8227.
3. Pyle, A. M; Rehmann, J. P.; Meshoyrer, R.; Kumar, C. V.; Turro, N. J.; Barton, J. K.; *J. Am. Chem. Soc.*, **1989**, 111, 3051.
4. Gosh, J. K.; Pal, M. K.; *Spect. Acta.*, **1995**, 51A, 489.
5. Oravcova, J.; Bohs, B.; Lindner, W; *J. Chromat. B*, **1996**, 677, 1.
6. Sitlani, A., Long, E., Pyle, A. M., Barton, J. K.; *J. Am. Chem. Soc.*, **1992**, 114, 2303.
7. Jackson, B. A.; unpublished results.
8. Pyle, A. M; Rehmann, J. P.; Meshoyrer, R.; Kumar, C. V.; Turro, N. J.; Barton, J. K.; *J. Am. Chem. Soc.*, **1989**, 111, 3051.
9. Shields, T. P.; Barton, J. K.; *Biochemistry*, **1995**, 34, 15037.
10. Sitlani, A.; Dupureur, C. M.; Barton, J. K.; *J. Am. Chem. Soc.*, **1993**, 115, 12589.
11. Harris, R; Nuclear Magnetic Resonance Spectroscopy, **1983**, John Wiley and Sons, New York.
12. Models 392 and 394 DNA/RNA Synthesizers Users Manual, **1991**, Applied Biosystems.
13. Wuthrich, K.; NMR of Proteins and Nucleic Acids, **1986**, John Wiley and Sons, Inc.
14. Singleton, S. F.; Dervan, P. B.; *J. Am. Chem. Soc.*, **1992**, 114, 6957.
15. Hudson, B. P.; unpublished data.
16. Berman, H. M.; Young, P. R.; *Ann. Rev. Biophys. Bioeng.*, **1981**, 10,87.
17. Sitlani, A.; Long, E.C.; Pyle, A. M.; Barton, J. K.; *J. Am. Chem. Soc.*, **1992**, 114, 2303.

18. Hudson, B. P.; Dupureur, C. M.; Barton, J. K.; *J. Am. Chem. Soc.*, **1995**, 117, 9379.

19. Atkins, P.; Physical Chemistry, 5th ed., **1994**, W. H. Freeman and Company. New York

20. Kim, Y.; Geiger, J. H.; Hahn, S.; Sigler, P. B.; *Nature*, **1993**, 365, 512.

21. Kim, J. L.; Nikolov, D. B.; Burley, S. K.; Nature, **1993**, 365, 520.

Chapter 3. Template-specific inhibition of DNA polymerase by phenanthrene quinone diimine (phi) complexes of rhodium.

3.1 Introduction

The DNA binding characteristics of several RhL_yphi complexes were discussed in detail in Chapters 1 and 2. Four of the complexes described demonstrate sequence-specificity of 4 base pairs or greater in their binding to DNA. These complexes are shown, along with their recognition sequences, in Table 3.1. This level of recognition makes it possible to investigate whether DNA/protein interactions can be inhibited at the distinct DNA sequences to which these complexes bind. In this chapter, studies of the differential inhibition of DNA polymerase based on DNA template sequence will be described. Correlations between metal complex binding and inhibitory properties will then be discussed.

Metal Complex	Recognition Sequence
1-Λ-$Rh(MGP)_2phi^{5+}$	5'-CATATG-3'
1-Δ-$Rh(MGP)_2phi^{5+}$	5'-CATCTG-3'
$Rh(MT)_2phi^{3+}$	5'-TGCA-3'
Δ-$Rh(DPB)_2phi^{3+}$	5'-CTCTAGAG-3'

Table 3.1: Four metal complexes and their recognition sequences.

Molecules which bind to DNA at specific sites are capable of inhibiting the activity of DNA and RNA polymerases at those sites. A few examples of sequence specific inhibition of DNA polymerase have been previously described. Oligonucleotide directed triple helix formation has been demonstrated to halt the initiation and elongation of new DNA

polymers at specific sites.[1,2] Molecules bound covalently to DNA have been shown to inhibit elongation by DNA polymerase. This property has been exploited in the determination of the positions of small molecule binding. The sites of covalent modification by cis-$(NH_3)_2Pt^{2+}$ and cyclopropylpyrroloindole have been elucidated by determining the length of the resulting truncated polymer.[3,4]

RNA polymerase has been the target of several studies of template-directed inhibition. Preferential inhibition of initiation has been observed for chromomycin and tallimustine which bind to GC and AT rich sequences respectively.[5,6] Oligonucleotide-directed triple helix formation has been used to inhibit transcription at specific sites as have triple helix-forming oligonucleotide intercalator conjugates.[7,8,9] Natural and modified DNA binding proteins including *lac* repressor, EcoRI endonuclease mutants, and nucleosomes have also been used to demonstrate sequence specific inhibition.[10,11,12]

From these studies it can be concluded that both covalently and non-covalently bound molecules are capable of inhibiting polymerases in a template-directed manner. It is important that molecules which bind to DNA non-covalently are capable of sequence-specific inhibition for several reasons. First, some of these molecules recognize much larger DNA sites than those which covalently bond to DNA. Second, non-covalent binders are capable of higher levels of sequence-specificity than covalent binders. A molecule associating with DNA via covalent bonds is involved in an irreversible interaction. A covalent binder cannot sample many different sites on the double helix until it finds the thermodynamically most stable binding state. Sampling stops when the molecule encounters the first site to which it can form covalent bonds. The molecule is then irreversibly trapped at that site.

This severly limits the sequence-specificity which is possible for a covalent binder. In contrast, a molecule which associates with DNA via non-covalent interactions can bind to and dissociate from the double helix as many times as is necessary until it finds the most thermodyamically stable site. Finally, the phi complexes of rhodium bind to DNA via non-covalent associations and the demonstration that other non-covalent binders can inhibit DNA polymerase suggests that these metal complexes may have inhibitory potential as well.

Another conclusion which can be drawn from these studies is that it is easier to stop a polymerase from initiating polymerization than it is to stop a polymerase which has begun to elongate a DNA polymer. For example, nucleosomes are efficient inhibitors of the initiation of polymerization by RNA polymerase.[12] When a nucleosome is bound to the polymerase's DNA promoter, no transcription occurs. However, when a nucleosome is bound downstream of the promoter, the RNA polymerase initiates transcription and then proceeds to displace the nucleosome as it transcribes DNA to which the nucleosome is bound.[12] The greater susceptibility of polymerases for inhibition of initiation as compared to inhibition of elongation therefore makes polymerase initiation the preferred target for initial studies of sequence specific inhibition.

The physical properties of the non-covalent inhibitors of polymerase activity are very diverse. These molecules vary in size from 1 kilodalton for chromomycin to over 130 kilodaltons for the nucleosome.[6,13] The charge on these molecules vary from triple helix-forming oligonucleotides with greater than 20 negative charges to the nucleosome which has hundreds of positive charges.[9,13] Dissociation rates span the range from 20 per second for chromomycin to minutes or longer for the EcoRI mutants and triple helix-

forming oligonucleotides.[9,11,14] DNA distortions range from a slight widening of the minor groove upon chromomycin binding to global bending of the DNA by the nucleosome.[13,15] From these studies, it would appear that the physical requirements for an inhibitor of polymerization are not very strict in terms of size, charge, dissociation rate, and distortions of DNA structure. These polymerase inhibitors were not studied under the same conditions and thus it is difficult to make comparisons on their relative potencies. However, the general trend that emerges is that large molecules with slow dissociation rate are more potent inhibitors of polymerization.

The binding characteristics of the phi complexes of rhodium make them promising candidates for the inhibition of polymerases. First, these complexes bind to DNA via intercalation.[16,17] As mentioned in Chapter 1, this causes the DNA base pairs to separate an additional 3.4 Å and unwind 20° or more.[18] Functional groups on opposite sides of the intercalation site are therefore shifted 3.4 Å apart and rotated 20° relative to each other. This results in a substantial distortion of DNA structure. A polymerase must make many precise contacts when binding to a DNA.[19,20] If a phi complex binds the DNA in the middle of a polymerase binding site, this will shift the positions of the functional groups in one half of this site relative to the other half of the site. This could result in the polymerase only being able to make 50% of its normal binding contacts to this site. Thus intercalation, which results in a far greater change in substrate structure than surface binding, should disrupt many of the polymerase/DNA contacts and therefore should be an advantage in inhibition.

Second, the phi complexes of rhodium have high positive charges. This can assist in the inhibition of polymerases as these enzymes are also positively charged.[19] A cocrystal structure of Klenow fragment (the core of E.

coli polymerase I) bound to a DNA template shows positively charged amino acid side chains directed at the phosphate backbone of the DNA substrate.[20] Thus these side chains are positioned to be in close proximity to a positively charged metal complex, resulting in a large electrostatic repulsion.

Previous work has demonstrated sequence specific inhibition of protein/DNA interactions with a phi complex of rhodium. $Rh(DPB)_2phi^{3+}$ has been used to inhibit specific interactions between proteins and DNA.[21] The complex is specific for the sequence 5'-C**TCTAGA**G-3'. The bolded 6 base pairs of this sequence is the recognition site for the restriction enzyme Xba1. The complex was shown to selectively inhibit the site-specific cleavage of DNA by Xba1 while not inhibiting restriction by ScaI which is specific for the sequence 5'-AGTACT-3'. (See Figure 3.1.)

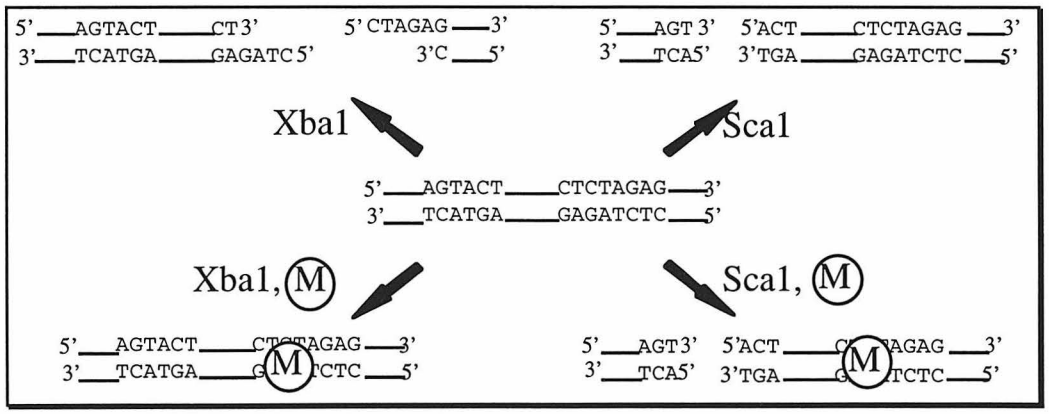

Figure 3.1: Scheme showing sequence specific inhibition of the restriction enzyme XbaI. M = Δ-$Rh(DPB)_2phi^{3+}$. ScaI recognizes the DNA sequence 5'-AGTACT-3'. XbaI and M recognize 5'-CTCTAGAG-'3. The added metal complex binds to the 5'-CTCTAGAG-3' site and blocks its cleavage by XbaI while not affecting the restriction of 5'-AGTACT-3' by ScaI.

While the aforementioned assay is convenient for the demonstration of sequence-specific inhibition of protein/DNA interactions, it is not useful for the comparison of several different complexes. Rarely are two complexes available which demonstrate identical sequence specificities but have

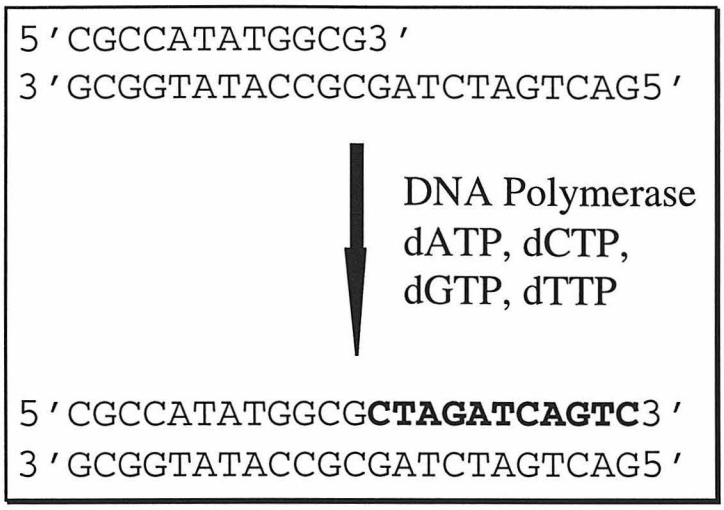

Figure 3.2: Synthesis of DNA complementary to a the single stranded region of a template by DNA polymerase. Newly extended polymer is shown in bold.

different physical properties. It is therefore necessary to use a different restriction enzyme to study each complex. As restriction enzymes demonstrate a wide variety of DNA binding characteristics, the use of several different enzymes does not provide a very controlled study. RNA polymerases suffer from a similar disadvantage. These polymerases bind to specific promoter sequences to initiate transcription.[22] Modifications of these promoter sequences, *i.e.*, to accommodate a metal binding site, often results in abrogation of polymerase activity.[23] It would be desirable to have an assay where the ability of metal complexes to disrupt protein/DNA interactions at a number of different sequences could be studied using the same protein. This would allow the direct comparison of the physical and binding characteristics of metal complexes with the potency of inhibition.

DNA polymerases bind to templates in a relatively sequence neutral manner. The minimal required template for DNA polymerases is a double stranded DNA with an adjacent single-stranded 5' overhang. When all four dNTPs are added in the appropriate buffers, polymerase bound to the double stranded region of the template will synthesize DNA complementary to the overhanging strand (see Figure 3.2).

If instead of all four dNTPs being added to the reaction, only the dNTP complementary to the first nucleotide of the overhang is added and the second nucleotide is non-identical, then the DNA will only be extended by one nucleotide (see Figure 3.3). If the nucleotide added is radioactive, then the products of this reaction can be detected by phosphorimagery of a polyacrylamide gel. If another oligonucleotide of different length is added to the reaction, each will be extended one base and the products resulting from each template can be resolved and quantitated by gel electrophoresis and phosphorimagery. The DNA polymerase assay developed is shown in Figure 3.4. One template contains a specific site for metal complex binding while the other template does not and serves as an internal control. Metal complexes with significant inhibitory activity bind to the specific template and prevent its extension by one nucleotide. The ratio of metal complex specific products to internal control products can be plotted against rhodium concentration as a measure of inhibitory activity.

Below is described the application of this assay for the study of sequence specific inhibition of DNA polymerase by the rhodium complexes listed in Table 3.1. This assay allows the direct comparison of the inhibitory characteristics of these complexes to each other using the same enzyme.

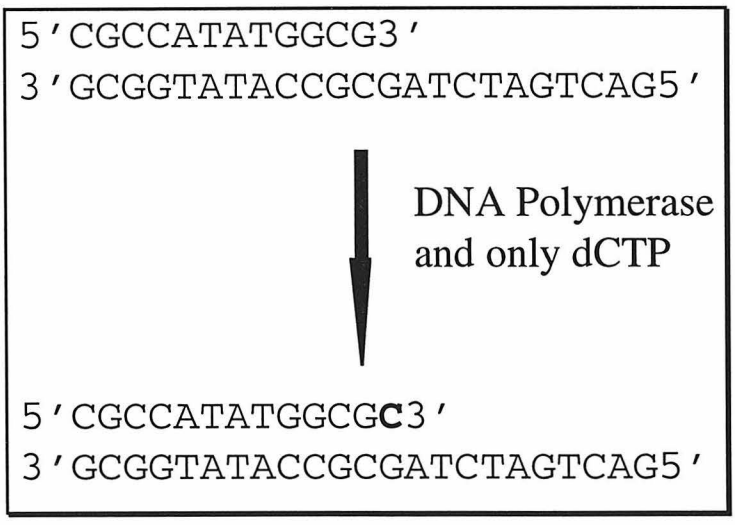

Figure 3.3: Extension of a template by one nucleotide through the use of only one type of dNTP. The added cytosine is shown in bold. Note that another cytosine cannot be added as it is not complementary to the adenosine on the template.

The inhibitory characteristics of each complex can then be compared to physical and binding characteristics such as size, charge, solubility, exchange rate, and DNA unwinding angle in order to determine which of these factors play important roles in template directed inhibition.

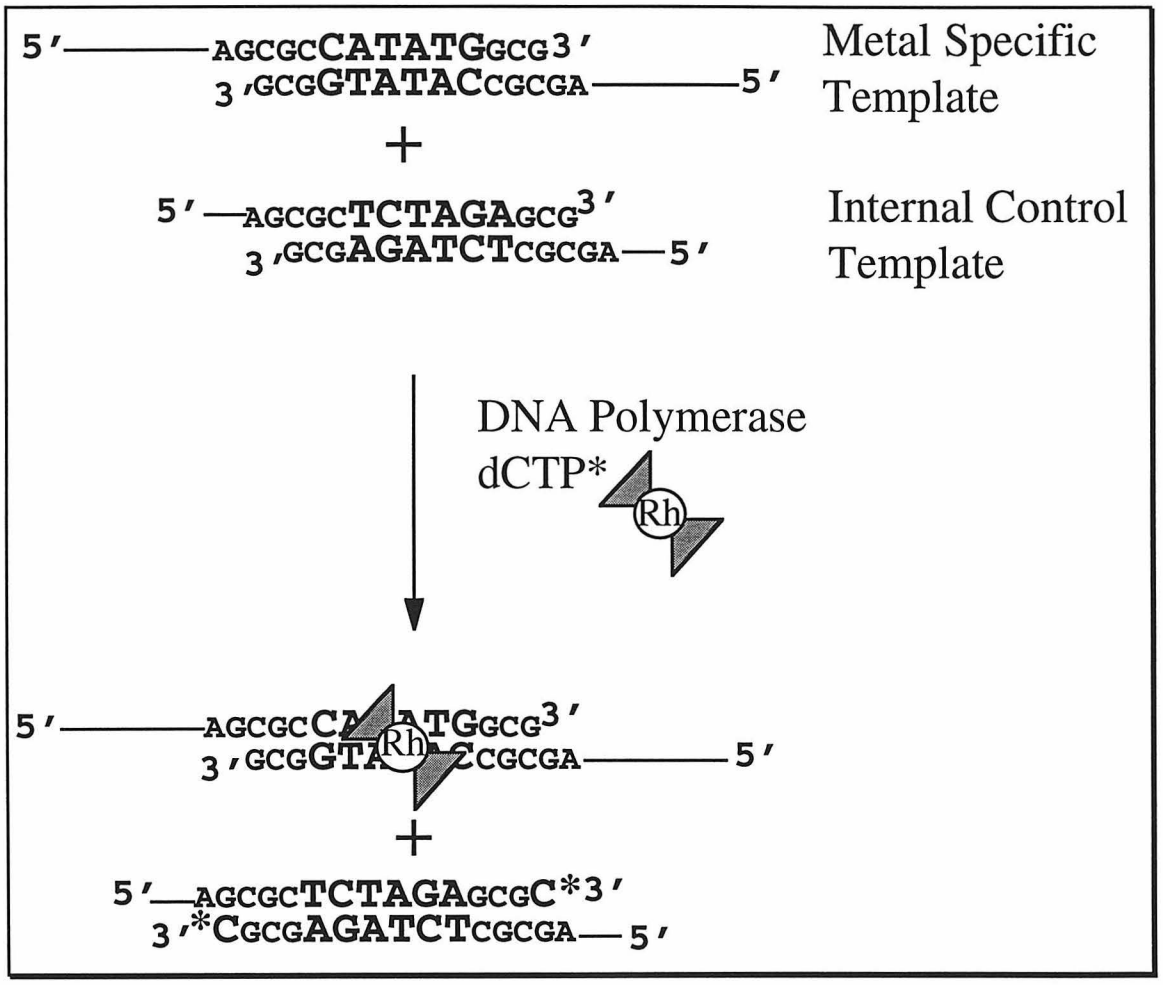

Figure 3.4: Assay used to determine the abilities of rhodium complexes to inhibit DNA polymerase in a sequence-specific manner. Rh designates a metal complex whose recognition sequence is 5'-CATATG-3'. Note that radioactive cytosine is only added to the template which is not bound by rhodium.

3.2 Experimental

3.2.1 Materials

Templates for Comparative Studies: Oligonucleotides were synthesized and purified as described in Chapter 2. DNA concentrations were quantitated by ultraviolet-visible spectroscopy (ε_{260} = 10000 M^{-1} for single stranded oligonucleotides). Templates were annealed at concentrations of 20 micromolar single strands, except for the 1-Δ-Rh(MGP)$_2$phi^{5+} template which was not self complementary. For this template 10 μM of each strand was used. Templates were annealed in 1xDNAP buffer (40 mM TrisCl, 25 mM NaCl, 10 mM $MgCl_2$, pH 7.4). DNA strands were heated to 94°C and linearly cooled to 20°C over 60 minutes. The 10 μM annealed templates were stored at 4°C until use. The sequences of each template are shown, as they are discussed, in the Results section below.

Templates for Head to Head Studies: Hairpin oligonucleotides were synthesized and purified as described in Chapter 2. DNA concentrations were quantitated by ultraviolet-visible spectroscopy (ε_{260} = 10000 M^{-1}). These templates were annealed at concentrations of 10 μM as described above. The sequences of each template are shown, as they are discussed, in the Results section below.

Δ-α-((2R, 9R)-Diamino-4,7-diazadecane)(9,10-phenanthrenequinone diimine)rhodium(III), Rh(MT)phi^{3+} and Δ-Bis(4,4'-diphenyl-2,2'-bipyridyl) (phenanthrenequinonediimine)rhodium(III), Rh(DPB)$_2$phi^{3+}: The complexes Rh(MT)phi^{3+} and Rh(DPB)$_2$phi^{3+} were synthesized and purified as previously described.[24,25,26] Rh(MT)phi^{3+} and Rh(DPB)$_2$phi^{3+} were stored at 4°C as a solid and dissolved in 10 mM TrisCl, pH 7.0, and water respectively before use. Metal complex concentrations were determined by ultraviolet-

visible spectroscopy with extinction coefficients of ε_{362} = 47000 M^{-1} for Rh(DPB)2phi^{3+} and ε_{373} = 13500 M^{-1} for Rh(MT)phi^{3+}.

Enantiomers of 1-Bis(4-guanidylmethyl-1,10-phenanthroline) (phenanthrenequinonediimine)rhodium(III), 1-Rh(MGP)2phi^{5+}: The enantiomers of 1-Rh(MGP)2phi^{5+} were synthesized and purified as described in Chapter 2. They were stored as solid at -20°C and redissolved in water buffered to pH 2.0 with trifluoroacetic acid fumes before use. Concentrations were determined by ultraviolet-visible spectroscopy (ε_{362} = 19500 M^{-1}). Purity of solutions older than one week was assayed by HPLC. With a flow rate of 4.5 ml/min and a linear solvent gradient from 100% water to 80/20 water/acetonitrile over 30 minutes, 1-Rh(MGP)2phi^{5+} elutes at 24 minutes as measured at 270 nm. Any solutions less than 95% pure as measured by UV-vis absorbtion at 270 nm were discarded.

Reagents: Water used in all experiments was deionized with a Milli-Q plus PF water purification system. TrisCl, $MgCl_2$, NaCl, Na_2CO_3, dithiothreitol, and bovine serum albumin were purchased in electrophoresis grade from Sigma Chemical Company. Klenow fragment and Sequenase were purchased from United States Biochemical Corporation. AMV reverse transcriptase was purchased from Pharmacia. α-P^{32}-dCTP with a specific activity of 3000 Ci/mmole was purchased from New England Nuclear Research Products. $Rh(NO_3)_3.xH_2O$ was purchased from Alfa-Aesar Johnson-Matthey. 9,10-diaminophenanthroline was purchased from Aldrich. All DNA synthesis reagents were purchased from Glen Research. All materials for electrophoresis were purchased from National Diagnostics.

3.2.2 Instrumentation

DNA concentrations were measured on either a Hewlett-Packard

8452A diode array or a Beckman DU 7400 UV-vis spectrophotometer. DNA duplex melting temperatures were measured on the Beckman DU 7400 UV-vis spectrophotometer equipped with a 6 cell melting temperature unit. Oligonucleotides were synthesized on a ABI 391 DNA synthesizer and purified with a Waters 600E HPLC using a Dynamax C-18 reverse phase column. The purity of 1-Rh(MGP)$_2$phi^{5+} solutions was assayed using the same HPLC system and column. Electrophoretic gels were scanned with a Molecular Dynamics phosphorimager and data quantitated using ImageQuant software. DNA samples were annealed and inhibition reactions run at a fixed temperature on a Perkin Elmer Cetus DNA thermal cycler.

3.2.3 Melting Temperatures for Comparative Templates: The melting temperatures (T_ms) of the comparative templates were measured under the conditions of the corresponding DNA polymerase inhibition experiments (1 μM DNA template, 40 mM TrisCl, 25 mM NaCl, 10 mM $MgCl_2$). Solutions were heated to 80°C followed by cooling back to 20°C over 1 hour. Solutions were then heated back to 80°C over 1 hour. An absorbance reading at 260 nm was taken every 2°C. Absorbance data were plotted versus temperature and the melting temperatures for the cooling and heating runs on each template were determined by the inflection point of each curve using the Beckman UV-vis software. Results from cooling and heating runs were then averaged to generate the final T_m's for each template.

3.2.4 DNA Polymerase Inhibition Experiments: Concentration as well as type of DNA and metal complex vary from experiment to experiment and are noted with each experiment. The conditions listed below were followed for each experiment except where noted otherwise in Results. A solution (5 μL)

containing 4x the reaction concentration of specific and non-specific template in 80mM TrisCl pH 7.4, 50mM NaCl, and 20mM $MgCl_2$ was mixed with 10 μL of a solution containing 2x the reaction concentration metal complex which recognizes the specific template. This solution was vortexed, spun down in a microcentrifuge for 10 seconds, and incubated at 10°C for at least 10 minutes. To this sample was added 5 μL of a solution of 80mM TrisCl pH 7.4, 50mM NaCl, and 20mM $MgCl_2$ containing 0.1 picomoles/μL sequenase and 0.02 picomoles/μL α-^{32}P-dCTP at 4°C. The solutions were mixed by vigorous pipetting followed by a 3 minute incubation at 10°C. Reactions were quenched with 20 μL of gel loading buffer (0.025% xylene cyanol, 0.025% bromophenyl blue, 10 mM NaOH, 90 mM TrisBorate, 1 mM EDTA, pH 8.3) and placed immediately on dry ice. These reactions were then heated to 90°C and loaded onto a 20% denaturing polyacrylamide gel which had been pre-run to be hot to the touch. Samples were electrophoresed at 75W for 1 to 2 hours followed by a 6 to 8 hours exposure on a phosphorimager screen. The screen was then scanned on a Molecular Dynamics Phosphorimager and the most abundant specific and non-specific product quantitated for each reaction.

3.2.5 Photocleavage Experiments: Photocleavage experiments were carried out as described in Chapter 2 with the exceptions noted in the figure caption.

3.3 Results

3.3.1 Sequence-Specific Inhibition by 1-Λ-Rh(MGP)$_2$phi^{5+}: The ability of 1-Λ-Rh(MGP)$_2$phi^{5+} to inhibit DNA polymerase in a sequence-specific manner was investigated. This complex was chosen for initial investigations because it causes a large amount of distortion to the double helix upon binding, it has a +5 charge, and binds to DNA with a high affinity.[27] The DNA templates

chosen for this inhibition are shown in Figure 3.5. The longer (40mer) template contains the 6 base pair recognition site for 1-Λ-Rh(MGP)$_2$phi^{5+}, 5'-CATATG-3'. Thus the complex is expected to bind tightly to this template and inhibit the interactions of DNA polymerase with it. The duplex portion of the 30mer template contains a repeating 5'-GC-3' sequence for which the complex has shown no affinity.[28] 1-Λ-Rh(MGP)$_2$phi^{5+} is expected not to bind to this template and the activity of DNA polymerase on this DNA should not be affected. Template directed inhibition in a reaction containing both of these templates will result in a significantly larger decrease in products extended from the 40mer template than the 30mer template when 1-Λ-Rh(MGP)$_2$phi^{5+} is added. The products of DNA polymerase activity on each of these templates should be a labeled 41mer and labeled 31mer for the 40mer and 30mer templates respectively. The ratio of the 41mer/31mer products can be plotted versus rhodium concentration as a measure of inhibition. In this case, specific inhibition will result in a decrease in this ratio with increasing rhodium.

The results from a DNA polymerase inhibition experiment are shown in Figure 3.6. The ratio of 41mer/31mer products decreased with added 1-Λ-Rh(MGP)$_2$phi^{5+}. Furthermore, as polymerization on the 40mer template is inhibited, polymerization actually increases slightly on the 30mer template. Note, however, that a substantially larger amount of activity was lost on the specific template than was gained on the control template. The observation that polymerase activity is inhibited on the 40mer template is consistent with the metal complex binding to the 40mer template containing its recognition sequence and blocking polymerase initiation while it does not bind to the non-specific 30mer template and therefore leaves polymerase activity on the 30mer unaffected. The increase in polymerase activity on the

Figure 3.5 Templates used to demonstrate sequence-specific inhibition by 1-Λ-Rh(MGP)$_2$phi^{5+}. Recognition sequence for the complex is shown in bold.

1-Λ-Rh(MGP)$_2$phi^{5+} Specific Template:

5'ATGCTAGGCTATGCAGCTGGCACGACAGCGC**CATATG**GCG3'
3'GCG**GTATAC**CGCGACAGCACGGTCGACGTATCGGATCGTA5'

Control Template:

5'ATGCAGCTGGCACGACAGCGCGCGCGCGCG3'
3'GCGCGCGCGCGCGCGACAGCACGGTCGACGTA5'

30mer template can be explained by the enzymes switching from the metal bound 40mer template to the unoccupied 30mer template. This switching effect will be discussed in more detail below.

It should be noted that more than one product band was observed for each template (see Figure 3.6). The possibility that this might be due to heterogeneity in initial template length was investigated. Both templates were 5' end-labeled with ^{32}P and analyzed for purity by gel electrophoresis. Figure 3.7 shows that both templates produce only one significant band and are >95% pure. Thus the heterogeneity in polymerized products is not due to template impurities. Instead, the polymerase may not have been entirely pure of nuclease activity or the polymerase may have been adding more than one nucleotide to some templates. One or a combination of these possibilities is likely to be the cause of the multiple products observed.

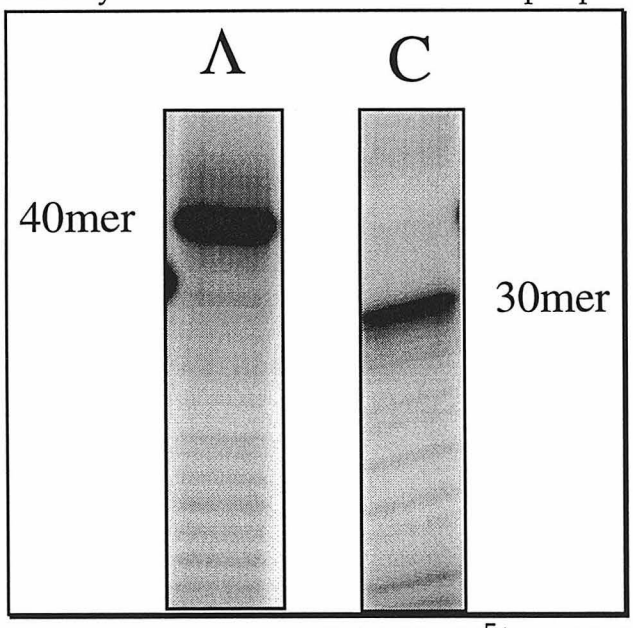

Figure 3.7: Purity of 1-Λ-Rh(MGP)$_2$phi^{5+} specific (Λ) and control (C) templates shown in Figure 3.5. Templates were 5' end-labeled with ^{32}P and electrophoresed through a polyacrylamide gel. Note that only one major band is observed.

3.3.2 Effects of Reaction Conditions on DNA Polymerase Activity and Inhibition: Once template directed inhibition of DNA polymerase activity was demonstrated, the effect of various conditions on the level DNA polymerase activity and inhibition were investigated. This study was carried out in order to better understand the inhibition reaction and to maximize the effects observed. The

Figure 3.6. Sequence-specific inhibition by 1-Λ-Rh(MGP)$_2$phi^{5+}. Templates used for this experiment are shown in Figure 3.5. Gel data are shown at the left. Reactions for lanes 1-5 contained 0, 0.05, 0.1, 0.2, and 0.5 μM 1-Λ-Rh(MGP)$_2$phi^{5+} respectively. The 1-Λ-Rh(MGP)$_2$phi^{5+}-specific template products (41mer) are inhibited with increasing rhodium concentration while the control products increase. Note that multiple products are produced from each template. The ratio of the 41mer to 31mer products is plotted versus concentration of 1-Λ-Rh(MGP)$_2$phi^{5+} (right). Reaction conditions: 0.05 μM 1-Λ-Rh(MGP)$_2$phi^{5+} specific and control templates, 21°C, 10 mM dithiothreitol, 5 minute reaction time, and 0.1 μM α-^{32}P-dCTP. All other conditions are as described in the experimental section.

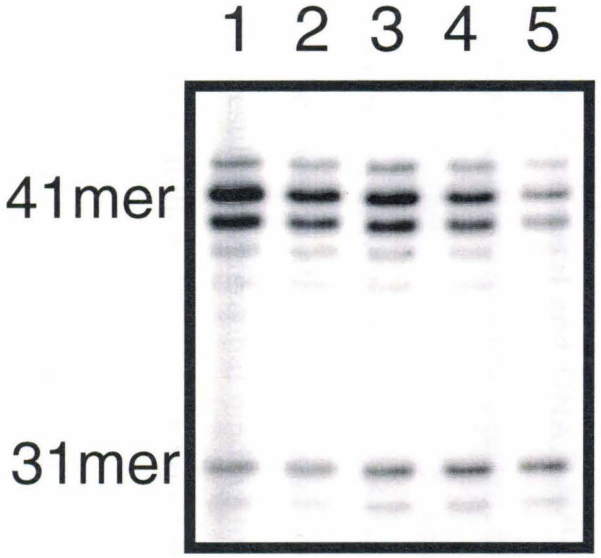
1 2 3 4 5
41mer
31mer

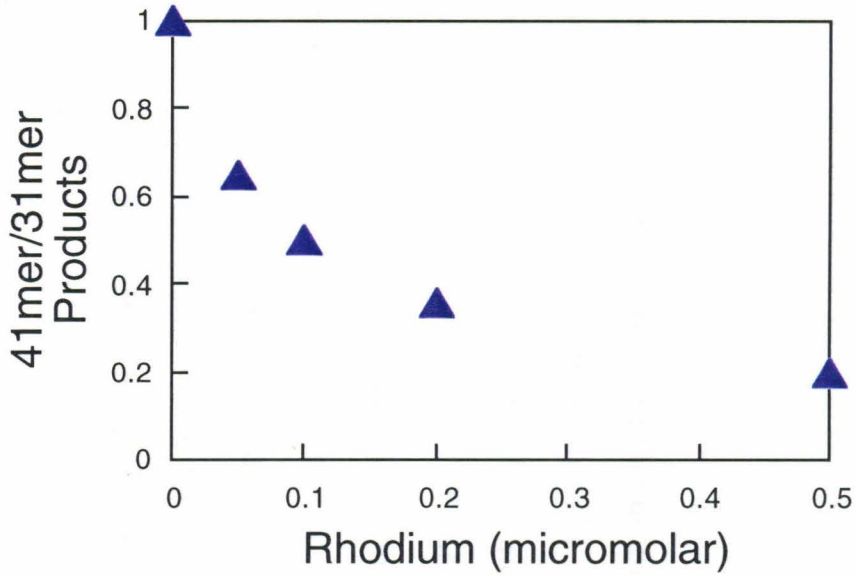
41mer/31mer Products
1
0.8
0.6
0.4
0.2
0
0
0.1
0.2
0.3
0.4
0.5
Rhodium (micromolar)

effects of absolute template concentration, bovine serum albumin, buffer, dCTP concentration, and temperature on the inhibition observed are described below.

3.3.2.1 Effect of Absolute Concentration of Template on Inhibition and DNA Polymerase Activity: DNA template concentration can be expected to have an effect on DNA polymerase inhibition and activity. DNA polymerases bind to templates with approximate affinities of $1x10^{7}$ M^{-1}.[29,30] At concentrations of template less than or equal to $1x10^{-7}$ M, a decrease in polymerization on both templates can be expected as only a fraction of the enzyme will be bound. If concentrations of template become too low, and thus the fraction enzyme bound small, the amount of label incorporated into the templates will be too small to detect. Therefore, there is a certain minimum template concentration necessary in this assay.

Metal complex binding must also be taken into account when choosing template concentration. While the four complexes studied are all specific for the sites described in Table 3.1, all show affinities for other sites at micromolar concentrations of metal and DNA.[21,28,31] If the template concentration is too high, and excess metal present, then the rhodium complexes will bind quantitatively to specific and control templates which could result in the inhibition of both templates. At low template concentrations, the differences in affinities of metal complexes for specific and non-specific sites will result in preferential binding to the specific template. Thus, sequence-specific inhibition should be favored by low concentrations of template.

Since polymerase activity is favored by high concentrations of template and sequence specific inhibition is favored by low concentrations of

template, the effect of DNA template concentration was studied to determine where these factors balance in maximal inhibition. This was first investigated with 1-Λ-Rh(MGP)$_2$phi^{5+}. The templates used in this experiment are shown in Figure 3.8. The template to rhodium ratio was held constant at 1:10 for these experiments. Since equal amounts of 1-Λ-Rh(MGP)$_2$phi^{5+}-specific and control templates were present in these reactions, the 1:10 ratio means that only 5% of the rhodium present could be bound at specific sites. The other 95% of the 1-Λ-Rh(MGP)$_2$phi^{5+} must be either bound to non-specific DNA sites or free in solution. As can be seen from the gel data in Figure 3.9 (top), enough polymerase activity for quantitation is obtained from both templates at concentrations as low as 0.06 uM. A set of reactions without rhodium was run at each template concentration so that the extent of specific inhibition could be determined for rhodium containing lanes. A bar graph of the 41mer/31mer products versus template concentrations is shown in Figure 3.9 (bottom). This ratio is reduced to half its value for all concentrations of template to which 10 equivalents of rhodium is added. Thus for this set of templates and 1-Λ-Rh(MGP)$_2$phi^{5+}, inhibition is independent of template concentration between 0.06 and 1 uM template. Note, however, that relative DNA polymerase activity, in the absence of rhodium, changes with increasing template concentration (blue bars in Figure 3.9 graph). At low concentrations of template, the ratio of 41mer/31mer products is 5:1, while at high concentrations this ratio is reduced to 2:1.

A similar experiment was carried out with Rh(MT)phi^{3+} over three orders of magnitude variation in DNA template concentrations. Templates for this experiment are shown in Figure 3.10. Note that in this experiment, the rhodium specific template is the shorter template. The rhodium to DNA ratio was 5:1 in this set of experiments. However, two recognition sites for

Figure 3.8 Templates used in investigations of the effects of template concentration on sequence specific inhibition by 1-Λ-Rh(MGP)$_2$phi^{5+}. The recognition sequence for 1-Λ-Rh(MGP)$_2$phi^{5+} is shown in bold.

1-Λ-Rh(MGP)$_2$phi^{5+} Specific Template:

5'ATGCTAGGCTATGCAGCTGGCACGACAGCGC**CATATG**GCG3'
3'GCG**GTATAC**CGCGACAGCACGGTCGACGTATCGGATCGTA5'

Control Template:

5'ATGCAGCTGGCACGACAGCGCTCTAGAGCG3'
3'GCGAGATCTCGCGCGACAGCACGGTCGACGTA5'

Figure 3.9 Effect of template concentration on level of inhibition and DNA polymerase activity. 1-Λ-Rh(MGP)$_2$phi^{5+} and template concentrations were held at a constant ratio of 10:1 while their absolute concentrations were varied. Templates are shown in Figure 3.8. A phosphorimage of an electrophoretic gel containing reaction products is shown at the top. Lanes 1-5 contain 0.062, 0.12, 0.25, 0.50, and 1.0 μM each template respectively. Lanes 6-10 contain the same amounts of template but no added rhodium. Note that adequate signal for product determination was obtained at all concentrations of template. The 41mer/31mer ratio of rhodium (red) and non-rhodium (blue) containing reactions are shown in the bar graph at the bottom. The addition of 10 equivalents of rhodium results in approximately 50% sequence specific inhibition at all template concentrations studied. Reaction conditions: 21°C, 10 mM dithiothreitol, 5 minute reactions time and 0.1 μM α-^{32}P-dCTP. All other conditions are as described above in the experimental section.

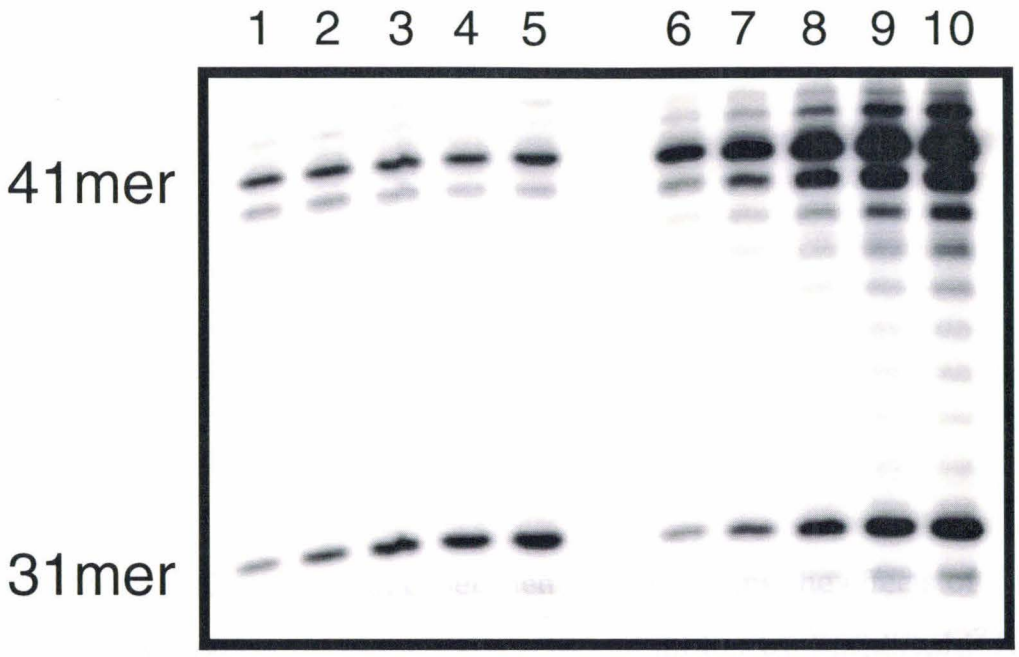
1 2 3 4 5 6 7 8 9 10
41mer
31mer

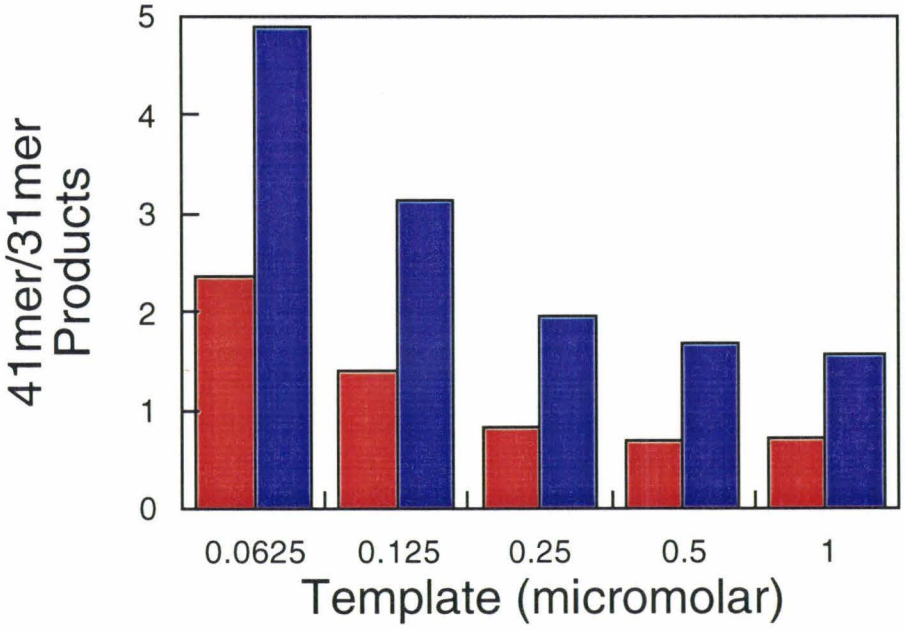
41mer/31mer Products
0
1
2
3
4
5
0.0625
0.125
0.25
0.5
1
Template (micromolar)

Figure 3.10 Templates used in experiments to determine the effects of template concentration on sequence-specific inhibition by Rh(MT)phi^{3+}. Recognition sequences for the complex are shown in bold. Note that the rhodium-specific and control templates contain the same double stranded base composition. Note also that here the specific template is shorter than the control template.

Rh(MT)phi^{3+} Template:

5'ATGGTGCTGGCACGACAGG**TGCA**CG**TGCA**C3'
3'C**ACGT**GC**ACGT**GGACAGCACGGTCGTGGTA5'

Control Template:

5'ATGCTAGGCTATGGTGCTGGCACGACAGGACGTCGACGTC3'
3'CTGCAGCTGCAGGACAGCACGGTCGTGGTATCGGATCGTA5'

Rh(MT)phi^{3+} are present on the specific template. Therefore, 20% of the complex could be bound to specific DNA sites with the other 80% being bound to non-specific sites or free in solution. The gel data for this experiment are shown at the top of Figure 3.11. Note that at template concentrations as low as 0.01 uM, adequate signal is obtained for quantitation. Note also that some smearing and displacement of product bands is observed in lanes 13 and 14. Since Rh(MT)phi^{3+} is not removed from samples before electrophoresis, this smearing is likely a result of the high concentrations of metal complex present in these reactions.

The bar graph of the quantitated data at the bottom of Figure 3.11 shows an unexpected result. Sequence specific inhibition actually increases with increasing template concentration. This is unexpected at concentrations of 1 μM template and 5 μM metal. At these concentrations, Rh(MT)phi^{3+}, which has a specific binding constant of $1x10^8$ M^{-1}, should occupy > 99% of the specific template. Yet greater inhibition is observed as concentrations are raised another order of magnitude. This effect can be explained if the rate at which the complex exchanges on the DNA relative to the rate at which the DNA polymerase binds the DNA is an important factor in inhibition. The rate at which DNA polymerase binds the template is directly related to DNA concentration.[29,30] A tenfold increase in template concentration will result in a tenfold greater rate of DNA polymerase binding. The exchange rate of a metal complex on the DNA template is independent of template concentration (*vide infra*). Thus changes in template concentration result in changes in the rate of DNA polymerase binding relative to metal complex exchange. The possibility of this being the reason for increased inhibition at higher template concentrations will be explored further in the Discussion section below.

Figure 3.11 Effect of template concentration on level of inhibition and DNA polymerase activity. Rh(MT)phi^{3+} and template concentrations were held at a constant ratio of 5:1 while their absolute concetrations were varied over two orders of magnitude. Templates are shown in Figure 3.10. A phosphorimage of an electrophoretic gel containing reaction products is shown at the top. Lanes 1-7 contain 0.01, 0.05, 0.1, 0.5, 1, 5, and 10 μM each template respectively without rhodium. Lanes 8-14 contain the same amounts of template and 5 equivalents of added rhodium. Note that adequate signal for product determination was obtained at all concentrations of template. The 31mer/41mer ratio of rhodium (red) and non-rhodium (blue) containing reactions are shown in the bar graph at the bottom. Increasing the absolute concentrations of template and rhodium results in increased inhibition over all concentrations studied. Reaction conditions: 21°C, 5 minute reactions time and 0.1 μM α-^{32}P-dCTP. All other conditions are as described above in the experimental section.

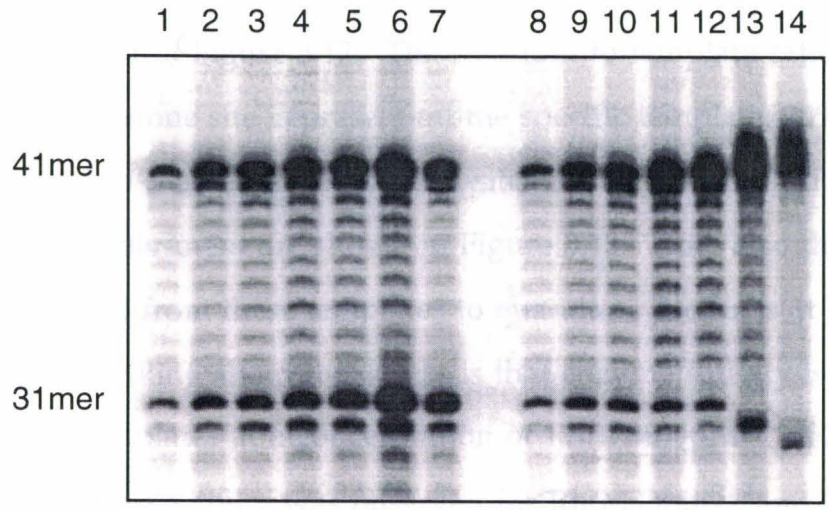
1 2 3 4 5 6 7 8 9 10 11 12 13 14
41mer
31mer

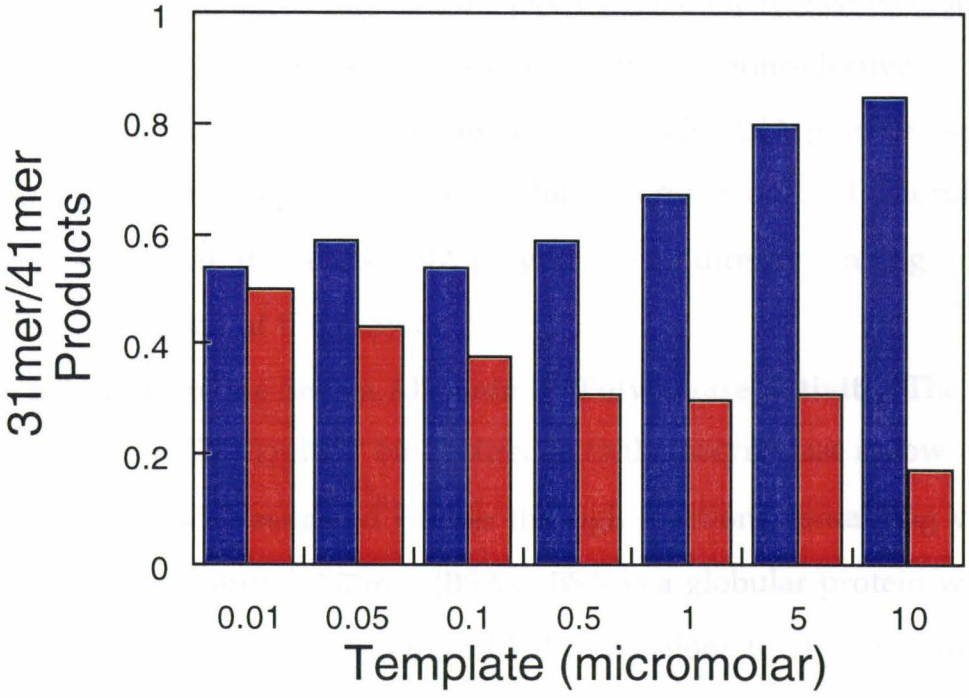
31mer/41mer Products
1
0.8
0.6
0.4
0.2
0
0.01 0.05 0.1 0.5 1 5 10
Template (micromolar)

Finally, the effect of template concentration on polymerase inhibition with racemic Rh(DBP)2phi^{3+} was investigated. The templates used in this experiment are shown in Figure 3.12. The rhodium to template ratio in these studies was 5:1. Since one site is present on the specific template, 90% of the complex must bind to the non-specific DNA sites or be free in solution. The gel data from this experiment are shown in Figure 3.13. Note also that there is not adequate signal from these templates to quantitate products at 0.01 uM template. What is striking about this study is that enzyme activity is inhibited on both templates at a concentration of Rh(DPB)2phi^{3+} of 2.5 μM. Substantial polymerase activity was observed for Rh(MT)phi^{3+} and 1-Λ-Rh(MGP)2phi^{5+} at concentrations of 50 and 10 μM respectively. Rh(DPB)2phi^{3+} was not likely to be binding to both templates as it shows little affinity for sequences other than its recognition sequence or subsequences of its recognition sequence at these concentrations.[21] If the complex was not binding to non-specific DNA sites, then at least 90% of it must be in solution. One possible cause of this potent non-selective inhibition is that free rhodium complex directly binds DNA polymerase. Rh(DPB)2phi^{3+} is hydrophobic, as it is soluble in methanol and chloroform, and it is possible that it inhibits DNA polymerase by directly binding hydrophobic portions of the enzyme.

3.3.2.2 Effect of Bovine Serum Albumin on Polymerase Activity: The possibility that Rh(DPB)2phi^{3+} binds directly to the polymerase at low concentrations was investigated further through reactions containing varied amounts of bovine serum albumin (BSA). BSA is a globular protein with hydrophobic domains which is often added to reactions to improve enzyme activity.[32] If Rh(DPB)2phi^{3+} is binding to DNA polymerase through hydrophobic interactions with the enzyme, the presence of excess BSA should

Figure 3.12 Templates used in experiments to determine the effects of template concentration on sequence-specific inhibition by racemic $Rh(DPB)_2phi^{3+}$. The recognition sequence for Δ-$Rh(DPB)_2phi^{3+}$ is shown in bold.

$Rh(DPB)_2phi^{3+}$ Specific Template:

5'ATGCAGCTGGCACGACAGCG**CTCTAGAG**CG3'
3'GC**GAGATCTC**GCGCGACAGCACGGTCGACGTA5'

Control Template:

5'ATGCTAGGCTATGCAGCTGGCACGACAGCGCCATATGGCG3'
3'GCGGTATACCGCGACAGCACGGTCGACGTATCGGATCGTA5'

Figure 3.13. Effect of template concentration on level of inhibition and DNA polymerase activity. Rh(DPB)phi^{3+} and template concentrations were held at a constant ratio of 5:1 while their absolute concentrations were varied over two orders of magnitude. Templates are shown in Figure 3.12. Lanes 1-5 contain 0.01, 0.05, 0.1, 0.5, and 1 μM each template respectively without rhodium. Lanes 6-10 contain the same amounts of template and 5 equivalents of added rhodium. Note that at 0.01 μM template, adequate signal was not obtained for product determination. Note also that the reaction is completely inhibited on both templates at a rhodium concentration of 2.5 μM. Reaction conditions: 21^{o}C, 5 minute reactions time and 0.1 μM α-^{32}P-dCTP. All other conditions are as described above in the experimental section.

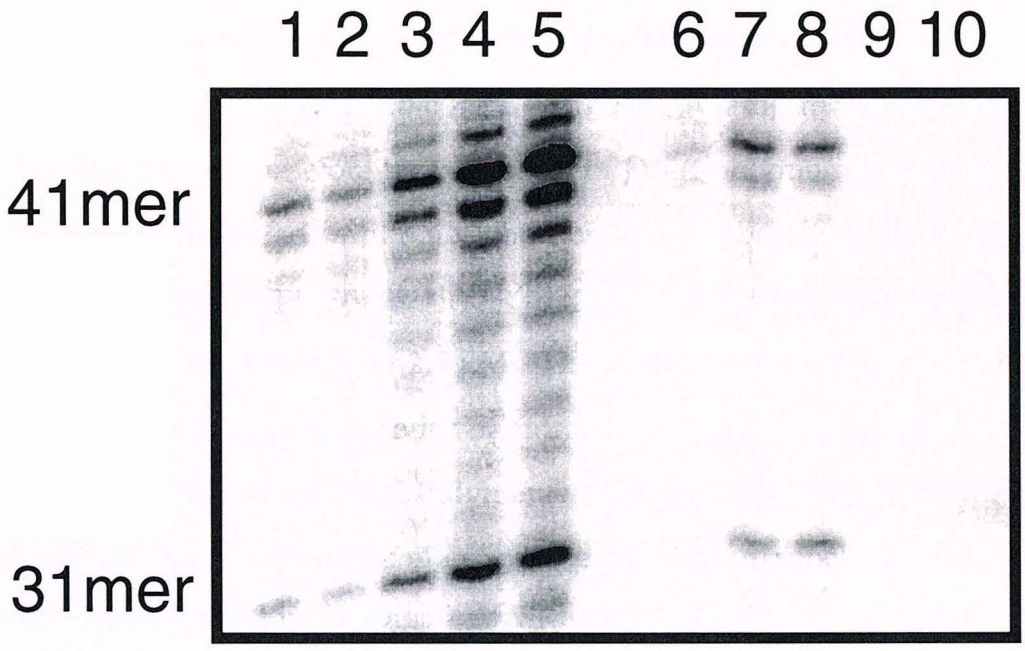
1 2 3 4 5 6 7 8 9 10
41mer
31mer

provide an alternate binding site for metal complex not bound to the DNA. Thus, free metal complex would then competitively bind to BSA and DNA polymerase, resulting in greater DNA polymerase activity.

The templates which were used in this experiment are shown in Figure 3.12. Polymerase reactions were carried out at a constant ratio of 5:1 rhodium: template. As can be seen from Figure 3.14, the addition of increasing amounts of BSA results in increased DNA polymerase activity. The total product produced with 1.6 μM template is plotted versus BSA concentration at the bottom of Figure 3.14. This increase in activity is consistent with excess hydrophobic metal complex binding to the BSA instead of the DNA polymerase. Note that the level of DNA polymerase activity is not substantially inhibited until 8 μM rhodium in the absence of BSA. In the previously described experiment, $Rh(DPB)_2phi^{3+}$ completely inhibited DNA polymerase at a concentration of 2.5 μM. This difference in activity may reflect a variation in specific activity of enzyme between experiments.

3.3.2.3 Effect of Buffer on DNA Polymerase Activity: The identity of the buffer used can have a dramatic effect on the rhodium photocleavage observed. As described in Chapter 2, $1\text{-}\Lambda\text{-}Rh(MGP)_2phi^{5+}$ demonstrates much greater efficiency of photocleavage in sodium cacadylate buffer than in tris buffer. The effect of sodium cacadylate buffer on DNA polymerase activity was therefore investigated. Templates used for this experiment are shown in Figure 3.10. As can be seen in Figure 3.15, the addition of sodium cacodylate to DNA polymerase reactions results in substantial inhibition of DNA polymerase activity. Polymerization products from reactions containing 40 mM TrisCl are shown in lanes 1-6. As can be seen from these lanes, adequate amounts of 41mer and 31mer products are produced for quantitation. In lanes 7-12, the TrisCl has been replaced by 10 mM sodium

Figure 3.14 Effect of BSA on inhibition of DNA polymerase by $Rh(DPB)_2phi^{3+}$. A gel of the data is shown at the top of the figure. Templates used are shown in Figure 3.12. Rhodium to DNA template ratio was held constant at 5:1. Lanes 1-6 contain 0.05, 0.1, 0.2, 0.4, 0.8, and 1.6 μM each template respectively. Lanes 7-12 and 13-18 contain the same pattern of template concentrations. Lanes 1-6 contained no BSA, 7-12 contained 0.1 μM BSA, and 13-18 contained 1 μM BSA. Note that total DNA polymerase activity increases with added BSA. A plot of total products versus BSA concentration for 1.6 μM template is shown at the bottom of the figure.

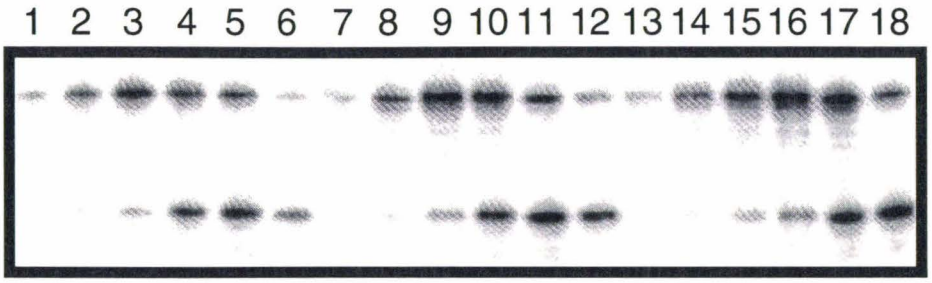
1 2 3 4 5 6 7 8 9 10 11 12 13 14 15 16 17 18

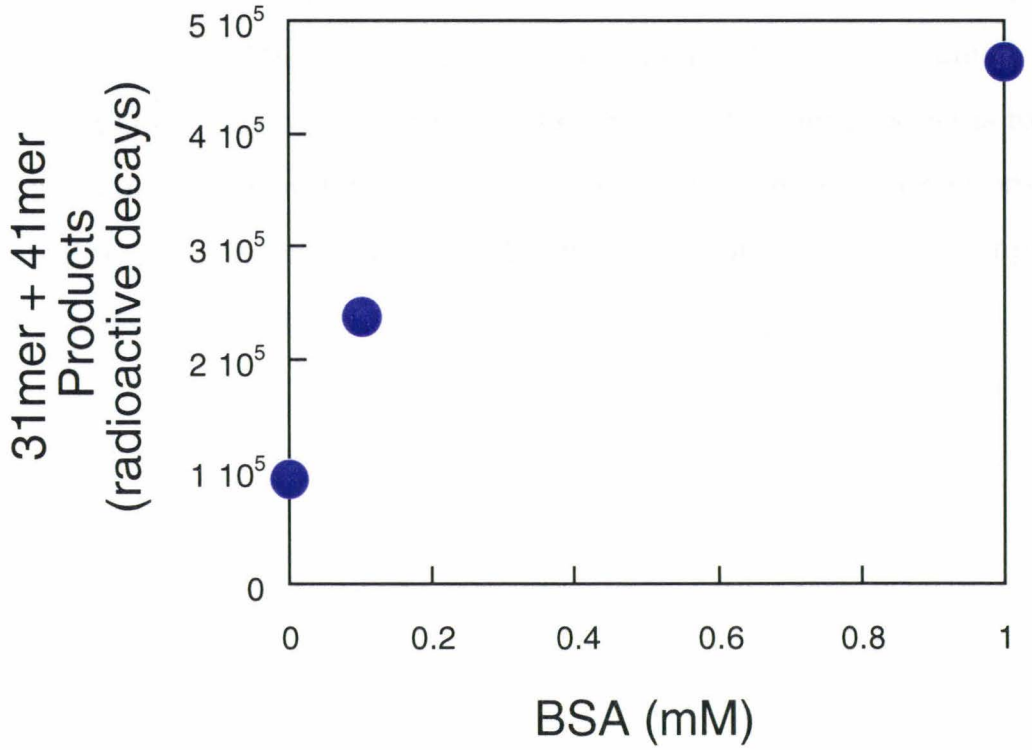
31mer + 41mer
Products
(radioactive decays)
5 10^5
4 10^5
3 10^5
2 10^5
1 10^5
0
0
0.2
0.4
0.6
0.8
1
BSA (mM)

Figure 3.15 Effect of sodium cacadylate (NaCac) on DNA polymerase activity. Templates used are shown in Figure 3.10. Lanes 1-6 contain 40 mM TrisCl, 25 mM NaCl, 10 mM $MgCl_2$, pH 7.5. Lanes 7-12 contain 10 mM NaCac, 25 mM NaCl, 10 mM $MgCl_2$, pH 7.0. Reactions for lanes 1 & 7, 2 & 8, 3 & 9, 4 & 10, 5 & 11, and 6 & 12 were run with $Rh(MT)phi^{3+}$ concentrations of 0, 2.5, 5, 10, and 20 μM respectively. The use of sodium cacadylate results in a substantial decrease in DNA polymerase activity. The amount of 31mer product is too small to accurately quantitate over background. Other reaction conditions are described in experimental with the following exceptions: 1μM each template and 2 min incubation at 21°C.

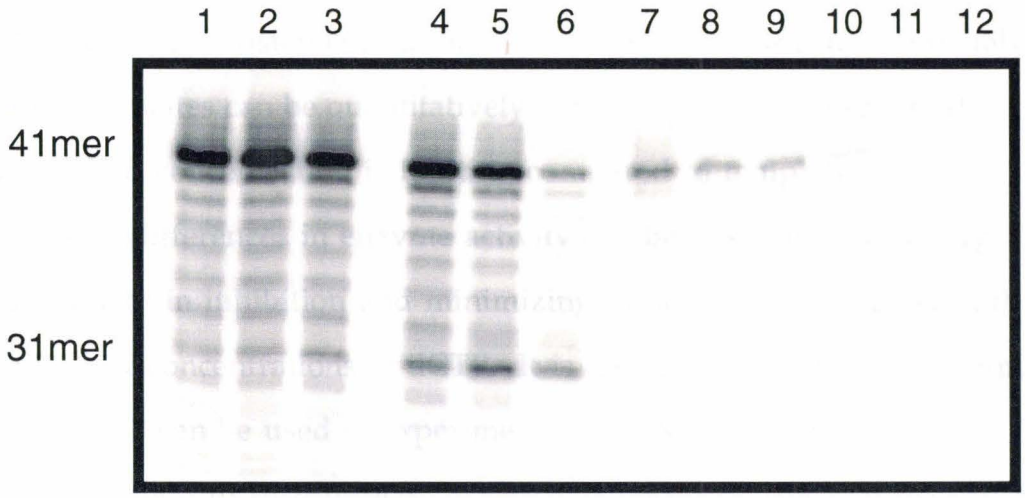
1 2 3 4 5 6 7 8 9 10 11 12
41mer
31mer

cacodylate buffer. The production of 31mer and 41mer products is substantially reduced in these lanes relative to 1-6 indicating that the sodium cacodylate inhibits the polymerase. In fact, 31mer products are too few to accurately quantitate in the presence of sodium cacadylate. Therefore, inhibition reactions could not be carried out in the presence of this buffer.

3.3.2.4 Effect of dCTP Concentration on Inhibition: The effect of dCTP concentration on sequence specific inhibition was investigated. This study was prompted for the purpose of maximizing inhibition while minimizing radioactivity usage. The extent of sequence-specific inhibition observed in experiments can be expected to be reduced when dCTP concentration exceeds template concentration. When there is a larger amount of dCTP than template present in a reaction and there is enough time for it to completely react, both templates can be quantitatively labeled by the polymerase. If, however, dCTP concentration is limiting compared to template concentration, differences in enzyme activity can be observed sensitively. Thus, specificity in inhibition and minimizing radioactivity usage are both favored by low concentrations of dCTP. It is therefore important to determine how little dCTP can be used in experiments while still resulting in quantitatable amounts of products.

Templates used in this study are shown in Figure 3.16. The effect of changing the dCTP concentration is shown in Figure 3.17. Note that adequate amounts of products are produced at both concentrations of dCTP. At the lower concentration, 0.01 uM dCTP, nucleotide is only present at 1% of the template concentration and thus very limiting. This is also a small amount of radioactivity to be used in terms of cost and safety.

Note also that at 0.01 uM, dCTP concentration is limiting compared to polymerase concentration (0.1 uM). At these concentrations, it can be

Figure 3.16 Templates used for experiments investigating the effects of dCTP concentration and temperature on sequence specific inhibition by $Rh(MT)phi^{3+}$. The recognition sequences for the complex are shown in bold.

Rh(MT)phi^{3+} Template:

5′ATGGTGCTGGCACGACAGG**TGCA**CG**TGCA**C3′
3′C**ACGT**GC**ACGT**GGACAGCACGGTCGTGGTA5′

Control Template:

5′ATGCTAGGCTATGCAGCTGGCACGACAGCGCCATATGGCG3′
3′GCGGTATACCGCGACAGCACGGTCGACGTATCGGATCGTA5′

Figure 3.17. Effect of dCTP concentration on DNA polymerase activity. DNA templates used are shown in Figure 3.16. Template concentrations were 0.5 mM each template. Reactions for lanes 1 & 6, 2 & 7, 3 & 8, 4 & 9, and 5 & 10 contained 0, 1, 2, 5, and 7 mM Rh(MT)phi3+ respectively. Reactions for lanes 1-5 contained 0.01 mM dCTP and reactions for lanes 6-10 contained 0.1 mM dCTP. Note that adequate products for quantitation are present in all samples. Other reaction conditions are as listed in experimental except that samples were reacted for one minute at ambient temperature.

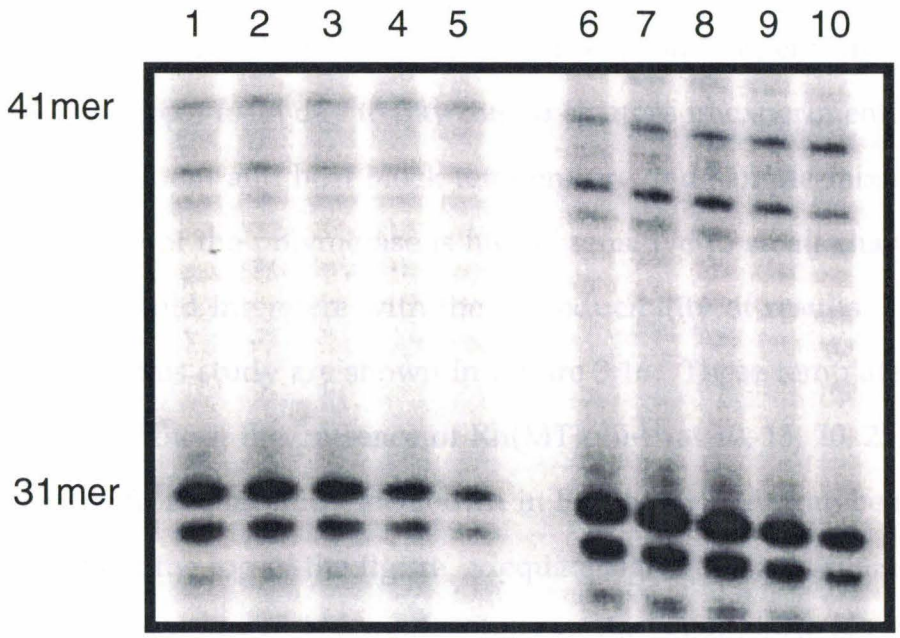
1 2 3 4 5 6 7 8 9 10
41mer
31mer

assumed that all the dCTP will be consumed in the first binding of enzyme to template. In other words, all dCTP is added to template before catalytic turnover can occur. In this case, what is being measured is the inhibition of the initial binding of DNA polymerase to template.

3.3.2.5 Effect of Temperature on Rh(MT)phi^{3+} Inhibition of DNA Polymerase: The effects of reaction temperature were investigated in order to maximize sequence specific-inhibition and to understand their influence on enzyme activity. It is reasonable to assume that reaction temperatures could vary over a few degrees from day to day due to changes in experimental conditions such as room and heat block temperature and sample mixing time. If the activity of the polymerase is highly sensitive to small changes in temperature, this could interefere with the reproducibility of results. Templates used in this study are shown in Figure 3.16. These templates were reacted with and without the presence of Rh(MT)phi^{3+} at 10, 15, 20, 25, and 30°C. The results from this study are shown in Figure 3.18. As can be seen from the gel data at the top of the figure, adequate signal for quantitation was obtained at all temperatures. The total activity of the polymerase is relatively unaffected over 20°C. The level of sequence-specific inhibition, however, is affected by the temperature of the reaction. The level of sequence specificity in inhibition can be determined by comparing the rhodium-containing and non-rhodium containing reactions in the bar graph at the bottom of Figure 3.18. The extent of template-directed inhibition increases at lower temperatures maximizing at 10°C with approximately 50% inhibition being observed. DNA structure does change with changes in temperature. For example, twist between base pairs decreases with decreasing temperature.[33] It is possible that changes in DNA structure result in changes in the relative

Figure 3.18 Effect of temperature on sequence-specific inhibition of DNA polymerase by Rh(MT)phi^{3+}. Templates used in this experiment are shown in Figure 3.16. The rhodium to DNA ratio was held constant at 5:1 for these experiments. The gel data is shown at the top of the figure. Reactions for lanes 1 & 6, 2 & 7, 3 & 8, 4 & 9, and 5 & 10 were run at 10, 15, 20, 25, and 30°C respectively. Reactions for lanes 1-5 and 6-10 were carried out in the absence and presence of rhodium respectively for 1 minute before being quenched. All other conditions are as described in experimental. Note that total DNA polymerase activity does not change substantially over the 20°C temperature range studied. A graph of the 31mer/41mer products vs. temperature is shown at the bottom of the figure. Note that the greatest inhibition is observed at 10°C.

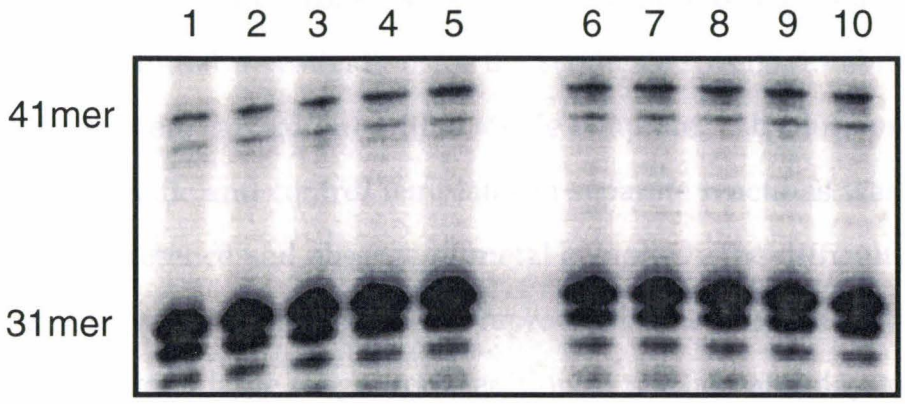
1 2 3 4 5 6 7 8 9 10
41mer
31mer

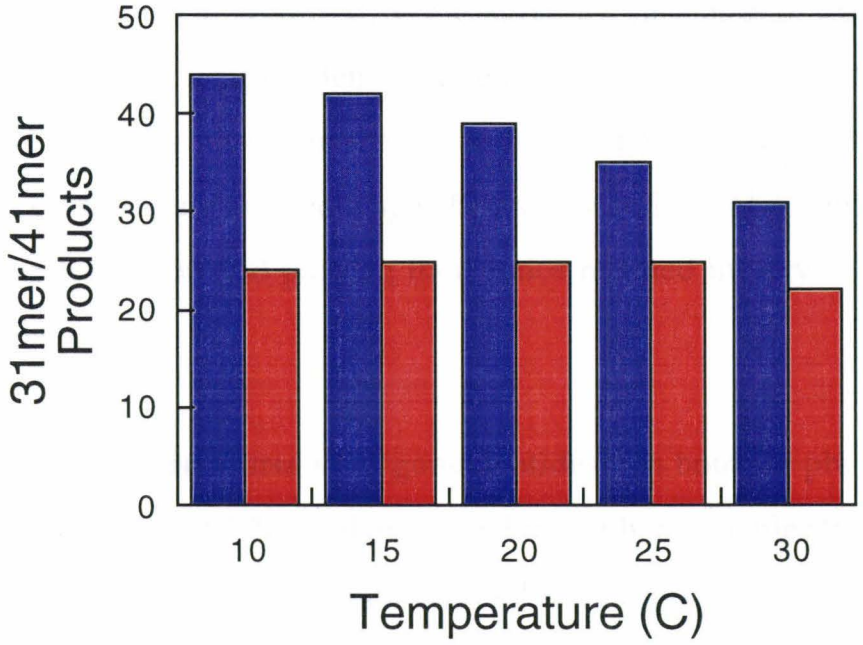
50
40
30
20
10
0
31mer/41mer Products
10 15 20 25 30
Temperature (C)

affinities of DNA polymerase and Rh(MT)phi^{3+} for binding sites and cause the differences in inhibition observed.

3.3.3 Single Template Experiments Demonstrating the Need for an Internal Control: Initial investigations of the sequence specific inhibition of DNA polymerase were carried out with a single template. Absolute product produced from specific and control templates in separate reactions was compared in the presence and absence of metal complex. The difficulty with these experiments was that they were not reproducible. Amounts of products produced varied over a large range from reaction to reaction and day to day. Efforts to determine the cause of this were inconclusive as strict control of temperature, reaction time, and even the use of identical solutions did not result in reproducible data. Figure 3.19 shows the results of two experiments run 5 minutes apart with the same solutions. As can be seen from the figure, the amount of product produced varies greatly between these reactions. Even the rate at which product is produced, as measured by the slopes of the lines, varies by over 50%. If a complex demonstrated modest sequence specific inhibition, this would be missed in the variability of these experiments. Changing to experiments where both specific and control templates were contained in each reaction and plotting their ratios resulted in very reproducible data.

3.3.4 Annealing temperatures of oligonucleotides: As both the phi complexes of rhodium and DNA polymerases bind only to double stranded templates, it is important for the templates used in experiments to be entirely in double stranded form. A significant amount of template in the single stranded form could complicate the results of inhibition. The melting

Figure 3.19 Irreproducibility of single template reactions. Shown are fraction label incorporated into DNA template vs. time for two reactions. Identical solutions and conditions were used for each reaction which were run 5 minutes apart. Note that amounts of products and rate of product production (slope of lines) show a high degree of variation between reactions. The reaction rates are 0.0020 and 0.0034 fraction label incorporated per minute for the circle and square reactions respectively. Reaction conditions, 0.05 μM 1-Λ-$Rh(MGP)_2phi^{5+}$ specific template pictured in Figure 3.22, 0.1 μM dCTP, 10 mM dithiothreitol, 21°C. Aliquots were taken out of each reaction 0.5, 0.75, and 1 minutes, mixed with an equal volume of gel loading buffer (see experimental) and frozen immediately on dry ice. All other conditions are as described in the experimental section.

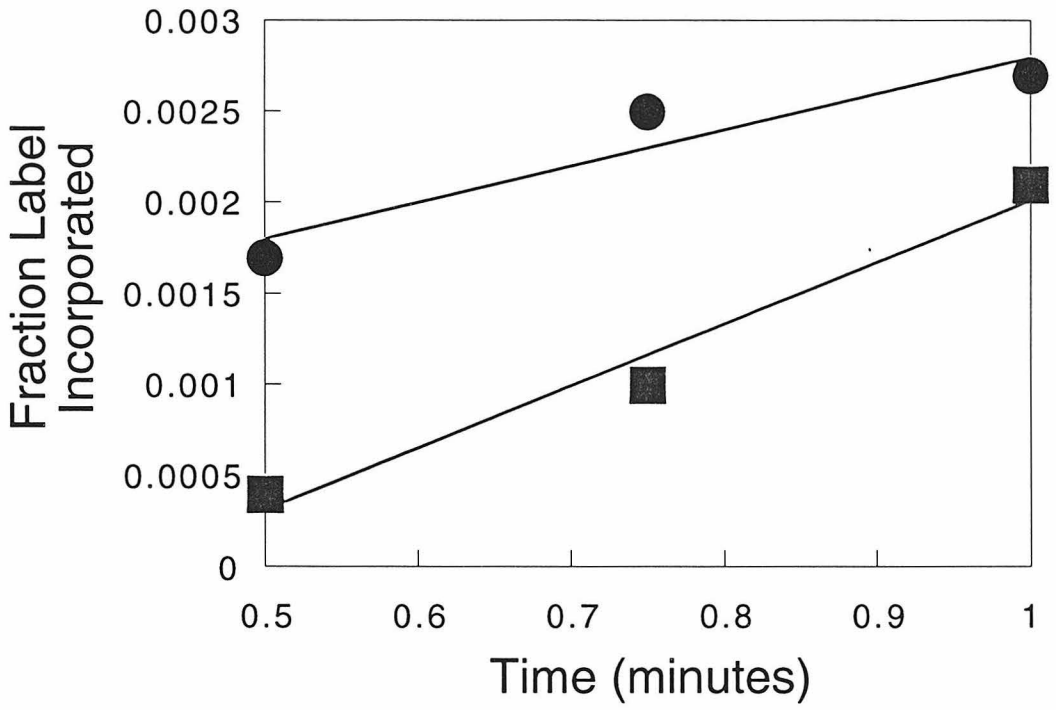
Fraction Label Incorporated
0.003
0.0025
0.002
0.0015
0.001
0.0005
0
0.5
0.6
0.7
0.8
0.9
1
Time (minutes)

temperatures of the oligonucleotides which were used for the comparative studies of DNA polymerase inhibition (templates illustrated in Figure 3.20) were determined through the use of UV-visible spectroscopy. The melting temperatures for these oligonucleotides at 1 μM duplex are shown in Table 3.2. The lowest melting temperature is 52°C for the template containing the recognition sequence for Rh(MT)phi^{3+}. Since inhibition reactions are conducted at 10°C, it can be assumed that essentially all oligonucleotides are present in their double stranded forms under these conditions.[34] Note that the solution conditions under which the melting temperatures were determined are identical to those under which inhibition experiments are carried out except for the absence of metal complex. Note also that a large (10°C) range of melting temperatures is observed for the Λ-1-Rh(MGP)$_2$phi^{5+}, Rh(MT)phi^{3+}, and control templates. These three templates have identical CG:AT ratios. These differences in Tm show the dependence of duplex stability on sequence as well as nucleotide content.

Template	Melting Temp. (C)	Duplex GC Content	Duplex AT Content
Δ-MGP	66	58%	42%
Λ-MGP	63	50%	50%
MT	52	50%	50%
Control	62	50%	50%

Table 3.2: Melting temperatures of the comparative templates pictured in Figure 3.20. Conditions of experiment are described in the experimental section.

3.3.5 Template and DNA Polymerase Effects on Inhibition: As described above, the effects of various reaction conditions such as concentrations, buffers, and temperature were determined to maximize template-directed

Figure 3.20 Templates used in comparative studies of template-directed inhibition of DNA polymerase. The rhodium recognition site in each template is shown in bold.

1-Λ-Rh(MGP)$_2$phi^{5+} specific template (Λ-MGP):

5'ATGCTAGGCTATGGTGCTGGCACGACAGCTC**CATATG**GAG3'
3'GAG**GTATAC**CTCGACAGCACGGTCGTGGTATCGGATCGTA5'

1-Δ-Rh(MGP)$_2$phi^{5+} specific template (Δ-MGP):

5'ATGCTAGGCTATGGTGCTGGCACGACAGCTC**CATCTG**GAG3'
3'GAG**GTAGAC**CTCGACAGCACGGTCGTGGTATCGGATCGTA5'

Rh(MT)phi^{3+} specific template (MT):

5'ATGCTAGGCTATGGTGCTGGCACGACAGCTCT**TGCA**AGAG3'
3'GAGA**ACGT**TCTCGACAGCACGGTCGTGGTATCGGATCGTA5'

Control template (C):

5'ATGGTGCTGGCACGACAGCTCTCTAGAGAG3'
3'GAGAGATCTCTCGACAGCACGGTCGTGGTA5'

inhibition. However, other parameters such as template sequence, length, number of rhodium binding sites and the type of DNA polymerase used could also be expected to affect sequence-specific inhibition. The effects of these variables on polymerase activity and template-directed inhibition are described below.

3.3.5.1 Effect of Template Length on Activity of DNA Polymerase: While any duplex with an adjacent single stranded region can serve as a substrate for DNA polymerase, all templates are not utilized with the same activity. DNA polymerase has been shown to have different substrate affinities based on DNA length and sequence.[25,26,35] The effect of template length on the affinity of DNA polymerase binding to the hairpin templates shown in Figure 3.21 was investigated. Note that these two templates contain the same double stranded regions, but differ in the length of the adjacent single stranded region. The results of the competition of DNA polymerase for these two templates can be seen in Figure 3.22. Lanes 1 and 3 contain 46mer and 67mer templates respectively and demonstrate that both templates can be efficiently extended by DNA polymerase. However, when both templates were combined in lane 5, polymerization occurred almost exclusively on the longer 67mer template. This demonstrates that when these two templates directly compete for extension by DNA polymerase, the 67mer is a more efficient template. As these DNAs differ only in the length of their single stranded regions, it is the template length which is responsible for this difference in activity.

3.3.5.2 Template Sequence and DNA Polymerase Activity: The effect of sequence on DNA polymerase binding can be seen by examining the activity

Figure 3.21 Hairpins used in experiments demonstrating dependence of DNA polymerase activity on template length. Note that the double stranded regions of the 46mer and 67mer templates are identical.

1-Λ-Rh(MGP)$_2$phi^{5+} Specific Template (46mer):

```
 TT
    ACACGTCCACGTCCATATGG3'
T   TGTGCAGGTGCAGGTATACCG5'
 TT
```

1-Δ-Rh(MGP)$_2$phi^{5+} Specific Template (56mer):

```
 TT
    ACGCGTGCACATGCATCTGC3'
T   TGCGCACGTGTACGTAGACGGACAGCACGGT5'
 TT
```

1-Λ-Rh(MGP)$_2$phi^{5+} Specific Template (67mer):

```
 TT
    ACGCGTGCACATGCATATGC3'
T   TGCGCACGTGTACGTATACGGACAGCACGGTGACAGCACGGT5'
 TT
```

Figure 3.22 Effect of template length on DNA polymerase activity. Templates pictured in Figure 3.20 were reacted with DNA polymerase and dCTP in the absence of rhodium. Lane 1: 46mer 1-Λ-Rh(MGP)$_2$phi^{5+} specific template only. Lane 2: 56mer 1-Δ-Rh(MGP)$_2$phi^{5+} specific template only. Lane 3: 67mer 1-Λ-Rh(MGP)$_2$phi^{5+} specific template only. Lane 4: 56mer and 46mer templates. Lane 5: 46mer and 67mer templates. Lane 6: 56mer and 67mer templates. Note that the 46mer is a poor template for DNA polymerase as compared to the 67mer despite both templates having the same double stranded sequence (lane 5). Template concentrations were 1 μM each template. All other conditions were as listed in the experimental section.

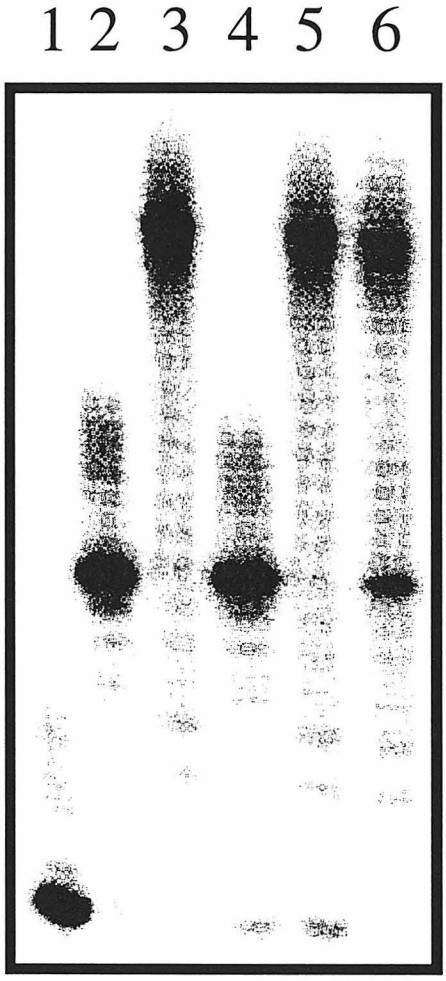
1 2 3 4 5 6

of the comparative templates relative to their control template. The sequences of the 1-Λ-Rh(MGP)$_2$phi^{5+} (Λ-MGP), 1-Δ-Rh(MGP)$_2$phi^{5+} (Δ-MGP), and Rh(MT)phi^{3+}-specific templates (MT) are shown in Figure 3.20. Note that all three templates are the same length. Table 3.3 contains the results of experiments where each template competed with the control template (also shown in Figure 3.20) for polymerization. Note that although each of the non-control templates was the same length, that significant differences in the activity of each template relative to the control template are observed. These differences cannot be attributed to differences in the thermodynamic stability of the duplexes as measured by melting temperature. The 1-Λ-Rh(MGP)$_2$phi^{5+}-specific template has a roughly twofold higher activity with the polymerase than the 1-Δ-Rh(MGP)$_2$phi^{5+}-specific template, yet both templates display similar melting temperatures (Table 3.2). Furthermore, the melting temperatures of the 1-Δ-Rh(MGP)$_2$phi^{5+} and Rh(MT)phi^{3+} templates differ by over 10°C, yet these templates are nearly identical in substrate activity with the DNA polymerase. These results demonstrate that DNA polymerase is not sequence neutral in its activity. It is important to consider what effect this property of the polymerase might have on competitive inhibition data.

Template	Specific/Control Template Product Ratio
Λ-MGP-specific	2.4
Δ-MGP-specific	1.4
MT-specific	1.3

Table 3.3: Activities of comparative templates relative to the control template. Each template was reacted with DNA polymerase, dCTP, and the control template as described in the experimental section. No rhodium complex was present in any of the reactions. All templates are shown in Figure 3.20 and are the same length.

3.3.5.3 Effect of Control Template Sequence on Inhibition of DNA Polymerase: If the inhibition of DNA polymerase is due to an interaction between metal complex and template, the nature of the control template should not affect the extent of inhibition as long as the non-specific template has a poor affinity for the complex of interest. To test the effect of control template sequence, the ability of 1-Λ-Rh(MGP)$_2$phi^{5+} to inhibit DNA in a sequence specific manner was studied using three different control templates. The 1-Λ-Rh(MGP)$_2$phi^{5+} specific and control templates used in this experiment are shown in Figure 3.23. None of the control templates contains a high affinity binding site for 1-Λ-Rh(MGP)$_2$phi^{5+}.[28] The results of this study, plotted in Figure 3.24, show that identical sequence-specific inhibition is observed regardless of which control template is used. This is consistent with the identity of the specific template determining the extent of inhibition as long as high affinity sites are not present on the control template.

This result addresses the concern that the natural affinities of DNA polymerase for a given template might significantly affect the relative extent of inhibition on that template. Table 3.4 contains the specific to non-specific product ratios for all three control templates in the absence of rhodium. As can be seen from the data, there are substantial differences in the relative activities of DNA polymerase on these different templates. Yet the plot shown in Figure 3.23 demonstrates no differences in the sequence specific inhibition of the polymerase by 1-Λ-Rh(MGP)$_2$phi^{5+}. This result indicates that the natural affinity of each template for DNA polymerase is not a significant factor in the extent of inhibition which is observed.

Figure 3.23 Templates used to determine the effect of control sequence on inhibition of DNA polymerase. Recognition sequence for 1-Λ-$Rh(MGP)_2phi^{5+}$ is shown in bold. Note that control templates have identical single stranded regions.

1-Λ-Rh(MGP)$_2$phi^{5+}-specific Template:

5'ATGCTAGGCTATGCAGCTGGCACGACAGCGC**CATATG**GCG3'
3'GCG**GTATAC**CGCGACAGCACGGTCGACGTATCGGATCGTA5'

Control Template A:

5'ATGCAGCTGGCACGACAGCGCGCGCGCGCG3'
3'GCGCGCGCGCGCGCGACAGCACGGTCGACGTA5'

Control Template B:

5'ATGCAGCTGGCACGACAGCGCTCTAGAGCG3'
3'GCGAGATCTCGCGCGACAGCACGGTCGACGTA5'

Control Template C:

5'ATGCAGCTGGCACGACAGCGCACAGATGCG3'
3'GCGTGTCTACGCGCGACAGCACGGTCGACGTA5'

Figure 3.24 Template-directed inhibition of DNA polymerase by 1-Λ-Rh(MGP)$_2$phi^{5+} with three different control templates. Templates are shown in Figure 3.22. Note that inhibition is identical regardless of control template sequence. Reaction conditions: 0.05 μM 1-Λ-Rh(MGP)$_2$phi^{5+} specific template and 0.05 μM control template A (blue squares), B (red triangles), or C (green circles), 0.1 μM dCTP, 21oC, 10 mM dithiothreitol, and 5 minute reaction time. All other conditions are as described in the Experimental Section.

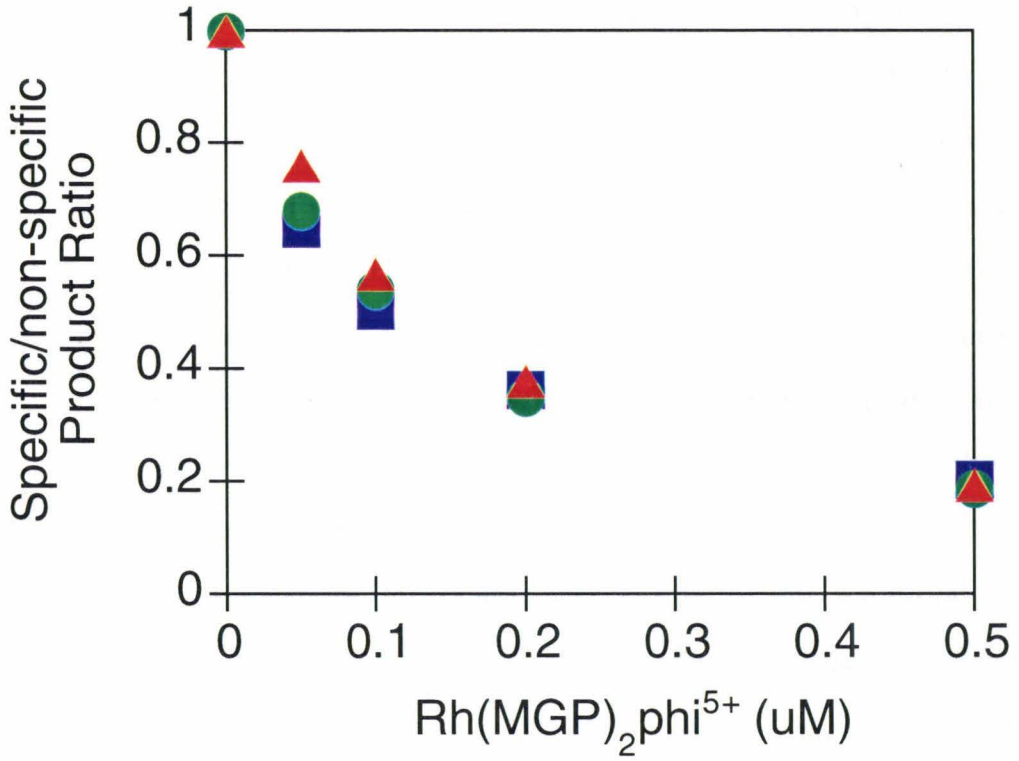
Specific/non-specific
Product Ratio
1
0.8
0.6
0.4
0.2
0
0
0.1
0.2
0.3
0.4
0.5
Rh(MGP)2phi5+ (uM)

Control Template Duplex Sequence	Specific/Control Template Ratio
5'-CGCGCGCGCGCG-3' (A)	3.1
5'-CGCTCTAGAGCG-3' (B)	4.7
5'-CGCATCTGTGCG-3' (C)	4.9

Table 3.4: Activities of the specific template compared to three different control templates in the absence of metal complex. Templates used are shown in Figure 3.23. Reaction conditions are as described in the experimental sections with the following exceptions: 0.05 uM specific and control templates, 21°C, 0.05 uM dCTP, and 5 minute reaction time.

3.3.5.4 Effect of Multiple Metal Binding Sites on Template-Directed Inhibition:

It was of interest to determine whether the binding of more than one metal complex to a template would result in more potent inhibition than the binding of a single metal complex. The binding of two complexes to a template would be expected to result in greater inhibition as this binding will result in twice the positive charge for repulsion of the polymerase. A greater distortion of the double helix will result from two complexes binding, and a greater steric bulk of metal complex will be present to block the polymerase. Furthermore, since the phi complexes of rhodium have binding constants > 10^7, it is statistically improbable that, at any instant, a template will not be bound by at least one complex. All these factors suggest that multiple binding by a metal complex will result in greater inhibition than single binding.

Templates used to investigate the effect of two metal binding sites are shown in Figure 3.25. Rh(MT)phi^{3+} binding sites on these hairpin templates are in bold. Note that the 67mer template contains two metal binding sites while the 56mer template contains one. A competition for polymerization between these two templates will reflect the relative potency of Rh(MT)phi^{3+} inhibition on each of them. Thus, if the 68mer/57mer ratio decreases with

Figure 3.25 Hairpin templates used to determine the effect of multiple Rh(MT)phi^{3+}-recognition sites on a template. Binding sites for the metal complex are shown in bold.

Two-SiteTemplate (67mer):

```
 TT
    ACGCGTGCACATGCATATGC 3'
T   TGCGCACGTGTACGTATACGG ACAGCACGGTGACAGCACGGT5'
 TT
```

One-Site Template (56mer):

```
 TT
    ACACGTCCACGTCCGTGCAG 3'
T   TGTGCAGGTGCAGGCACGTCG ACAGCACGGT5'
 TT
```

added rhodium, this indicates more potent inhibition of the two-site template compared to the one-site template. The results of a competition between these templates is shown in Figure 3.26. The gel at the top of the figure shows that Rh(MT)phi^{3+} was a very potent inhibitor of both templates as no products can be detected at 5 μM metal complex. However, at metal concentrations of 1 and 2 μM substantially greater inhibition was observed on the 67mer template which contains two binding sites. The 68mer/57mer product ratio is plotted at the bottom of Figure 3.26. Both the gel data and the plot suggest that two bound metal complexes are more potent inhibitors than one.

3.3.5.5 Effect of DNA Polymerase on Sequence-Specific Inhibition: Many different DNA polymerases are present in nature. Despite the fact that these enzymes have the same general function, they do not all have the same structure.[36,37] It is of interest to determine whether or not DNA polymerase's structural and functional parameters would have an effect on the extent of inhibition. Three commercially available polymerases were used to explore this question. The results of inhibition studies with 1-Λ-Rh(MGP)$_2$phi^{5+} on these three polymerases are plotted in Figure 3.27. The plotted data show a difference in the extent of polymerization based on which enzyme is used in each experiment. The level of template-directed inhibition observed for three enzymes studied is as follows: Sequenase > AMV reverse transcriptase > Klenow fragment.

Conditions used in these experiments are described in Figure 3.27. Note that conditions are identical for inhibition by each polymerase reaction except that the concentrations of the different polymerases vary. Sequenase, AMV reverse transcriptase, and Klenow fragment are present in each reaction

Figure 3.26 Two site versus one site inhibition by Rh(MT)phi^{3+}. Hairpin templates used in this experiment are shown in Figure 3.29. Gel data is shown at the top of the figure. 1 μM each template was used in this study. Concentrations of Rh(MT)phi^{3+} were 0, 1, 2, 3, 5, 10 and 20 μM in lanes 1, 2, 3, 4, 5, 6, and 7 respectively. Note that polymerization on both templates is inhibited at 3 μM Rh(MT)phi^{3+}. The 68mer product which contains two Rh(MT)phi^{3+} sites is indicated by 2 and the 57mer product which has one Rh(MT)phi^{3+} site is indicated by 1 at the left of the gel. A plot of the 68mer/57mer product ratio versus rhodium concentration is shown at the bottom of the figure. Note that Rh(MT)phi^{3+} is a more potent inhibitor of the two site template than the one site template.


1 2 3 4 5 6 7
2
1

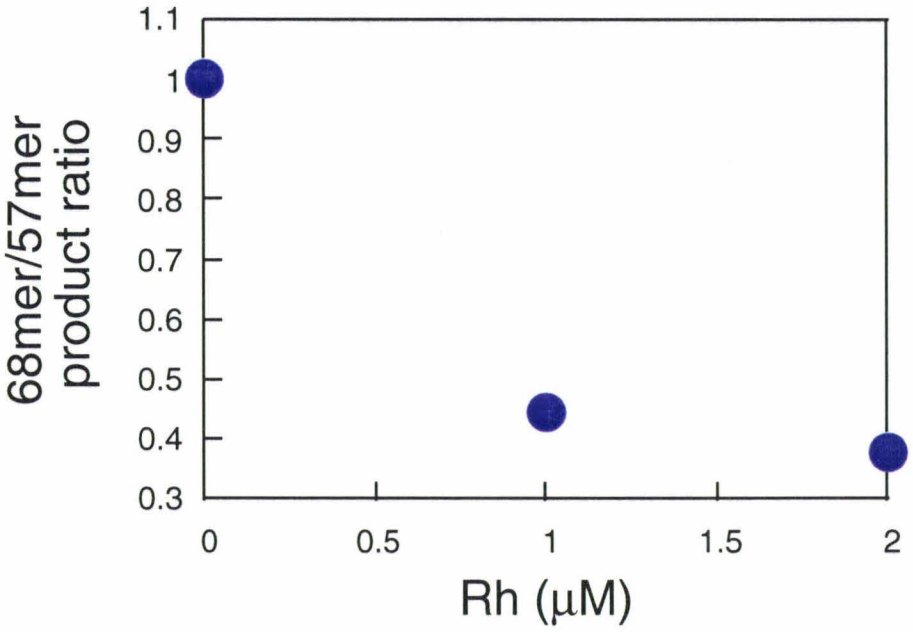
68mer/57mer
product ratio
1.1
1
0.9
0.8
0.7
0.6
0.5
0.4
0.3
0
0.5
1
1.5
2
Rh (μM)

Figure 3.27 Sequence specific inhibition of three different DNA polymerases by 1-Λ-Rh(MGP)$_2$phi^{5+}. Templates used are shown in Figure 3.8. Polymerases used were Klenow fragment (red triangles), AMV reverse transcriptase (green circles), and Sequenase (blue squares). Reaction conditions: 0.05 μM each template, 0.05 μM dCTP, 21°C, and 5 minute reaction time. Polymerase concentrations were 0.025, 0.01, and 0.0025 μM for Sequenase, AMV reverse transcriptase, and Klenow fragment respectively. All other conditions are as described in the experimental section.

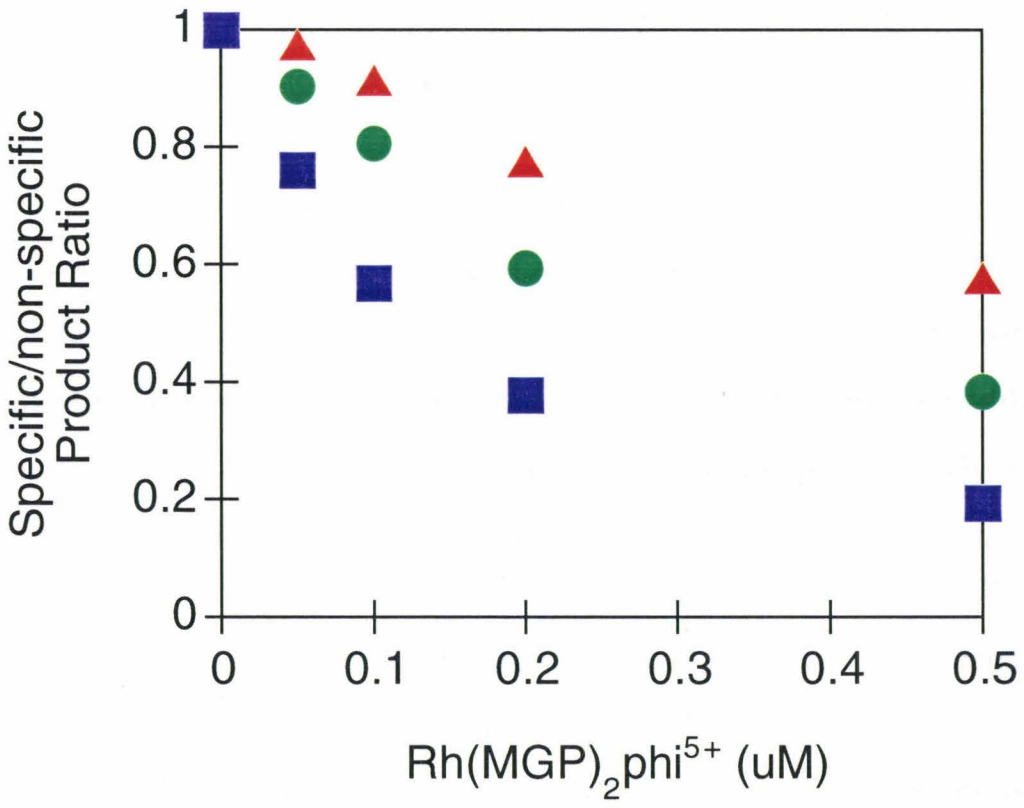
Specific/non-specific
Product Ratio
1
0.8
0.6
0.4
0.2
0
0
0.1
0.2
0.3
0.4
0.5
Rh(MGP)2phi5+ (uM)

at concentrations of 0.025, 0.01, and 0.0025 μM respectively. All polymerase concentrations are limiting when compared to template concentrations and dCTP concentrations. However, the extent to which these polymerases are limiting differs. Sequenase is present at half the concentration of dCTP and Klenow fragment is present at one-twentieth the concentration of dCTP in their respective reactions. Therefore, Sequenase must undergo two catalytic turnovers to incorporate all the dCTP into products while Klenow fragment must undergo 20 catalytic turnovers. It is unclear how extent of catalytic turnover could effect the level of template-directed inhibition observed; however, the differences in catalytic turnover need to be taken into account when analyzing results.

Another factor which must be taken into account in these experiments is the relative activity of each enzyme. dCTP is present in these reactions at the same concentration as the 1-Λ-Rh(MGP)$_2$phi^{5+}-specific and control templates. Thus, if sufficient enzymatic activity is present, either the specific or the control template, but not both, could be quantitatively extended by one nucleotide. As the control template is extended in a reaction, the concentration of unreacted control tempate decreases. If 1-Λ-Rh(MGP)$_2$phi^{5+} is directing polymerization away from the template which contains its recognition sequence, then the concentrations of specific and control templates will change relative to each other. As polymerase binding is concentration dependent, a substantial decrease in unreacted control template relative to specific template will result in a greater fraction of the polymerase binding to the specific template. This shift in binding will result in a decrease in template-directed inhibition. Therefore, if there is a large difference in the amount of templates reacted between the polymerases, this could explain the differences in inhibition observed.

The fraction of templates extended in these reactions was not quantitated. The amount of product measured on the phosphorimager is dependent on exposure time of gels to phosphorimager screens. This exposure time was not rigorously controlled or recorded in these experiments. However, exposure time did not vary by more than ±30% between experiments and thus the amount of products quantitated by the phosphorimager can be used as a rough estimate of products produced by each enzyme. The total amount of product produced (in dimensionless phosphorimager units) for each enzyme in the absence of rhodium is shown in Table 3.5. The relative amount of products produced by each enzyme is as follows: Klenow Fragment>AMV reverse transcriptase>Sequenase. This ordering of activity is consistent with the hypothesis that enzymes with a greater activity consume more template and cause the shifting of polymerase activity described above. These experiments need to be repeated with dCTP concentration limiting as compared to the concentration of the specific template to differentiate whether the differences in polymerization observed are a result of structural and functional differences in the enzymes or an artifact of the experimental procedure. However, it should be noted that regardless of whether or not differences in the extent of template-directed inhibition are present between different polymerases, 1-Λ-Rh(MGP)$_2$phi^{5+} has shown the ability to inhibit all polymerases tested in a sequence-specific manner.

DNA Polymerase	Relative Products Produced
Sequenase	$7(2)x10^6$
AMV Reverse Transcriptase	$13(4)x10^6$
Klenow Fragment	$34(10)x10^6$

Table 3.5: Relative sum of products produced from 1-Λ-Rh(MGP)$_2$phi^{5+}-specific and control templates. No rhodium was present in reactions and conditions are as described in Figure 3.27. Products are reported in dimensionless phosphorimager units.

3.3.6 Sequence Specific Inhibition of DNA Polymerase Using Comparative Templates:

The templates shown in Figure 3.20 were constructed to analyze the inhibition properties between different metal complexes. All rhodium-specific templates are the same length and contain identical sequences except for the one rhodium-specific site (shown in bold). The intercalation site for each complex is positioned at the center of each duplex in order to eliminate differences in inhibition which might arise from differences in the position of complex binding relative to the site of polymerization. In the study of each complex, the control template shown in Figure 3.20 is used. The results of sequence specific inhibition by 1-Λ–Rh(MGP)$_2$phi^{5+}, 1-Δ–Rh(MGP)$_2$phi^{5+}, and Rh(MT)phi^{3+} on these templates are described below.

3.3.6.1 Sequence Specific Inhibition of DNA Polymerase by 1-Λ–Rh(MGP)$_2$phi^{5+}:

The ability of 1-Λ–Rh(MGP)$_2$phi^{5+} to inhibit polymerization on the 1-Λ–Rh(MGP)$_2$phi^{5+}-specific and control templates (shown in Figure 3.20) was investigated. The template containing the recognition site for the complex is a 40mer, thus sequence-specific inhibition is expected to result in a decrease in the 41mer/31mer product ratio with

added 1-Λ–Rh(MGP)$_2$phi^{5+}. The results of this study are shown in Figure 3.28. The gel data show a decrease in intensity of the band corresponding to the 41mer product (indicated by Λ) with added rhodium. Little effect on the intensity of the band corresponding to the 31mer product (C) was observed at rhodium concentrations less than 20 μM. The apparent decrease in products from both templates at 5 μM rhodium was due to less total reaction being loaded on the gel. Thus 1-Λ–Rh(MGP)$_2$phi^{5+} inhibited production of products from the template containing its recognition sequence (41mer) while not affecting production of products from the control template (31mer). The 41mer/31mer product ratio is plotted versus 1-Λ–Rh(MGP)$_2$phi^{5+} concentration at the bottom of Figure 3.28. The reduction in this ratio was consistent with template-directed inhibition by 1-Λ–Rh(MGP)$_2$phi^{5+}. At concentrations greater than 20 μM, polymerization on both templates began to be inhibited and this was the same concentration at which the 41mer/31mer ratio reaches its minimum.

In order to compare the level of template-directed inhibition between metal complexes, it is of interest to determine the concentration of rhodium necessary to reduce the normalized product ratio to 0.5. For 1-Λ–Rh(MGP)$_2$phi^{5+}, this value is approximately 7 uM. Note that both templates are significantly inhibited at 40 uM metal complex. As rhodium is in twentyfold excess over template at this concentration, this inhibition could be a result of either direct inhibition of the DNA polymerase, or it could be due to both templates being loaded with metal complex at this concentration.

3.3.6.2 Sequence Specific Inhibition of DNA Polymerase by 1-Δ–Rh(MGP)$_2$phi^{5+}: The ability of 1-Δ–Rh(MGP)$_2$phi^{5+} to inhibit polymerization on the template containing its recognition site relative to the

Figure 3.28 Sequence-specific inhibition of DNA polymerase by 1-Λ-$Rh(MGP)_2phi^{5+}$. The Λ-MGP and C templates pictured in Figure 3.20 were used in this experiment. Λ-MGP and control template products are 41mers and 31mers respectively and are indicated in the gel at the top of the figure by Λ and control. Template concentrations are 1 μM each template and 1-Λ-$Rh(MGP)_2phi^{5+}$ concentrations (μM) are indicated above the gel lanes and in the graph. All other conditions are as described in the experimental section.

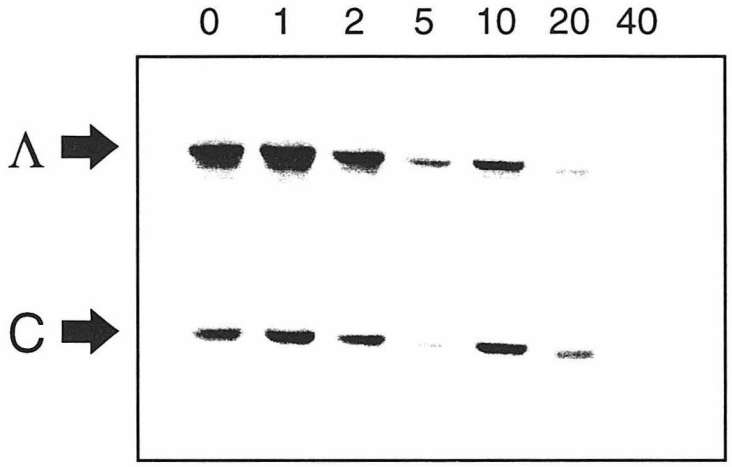
0 1 2 5 10 20 40
Λ
C

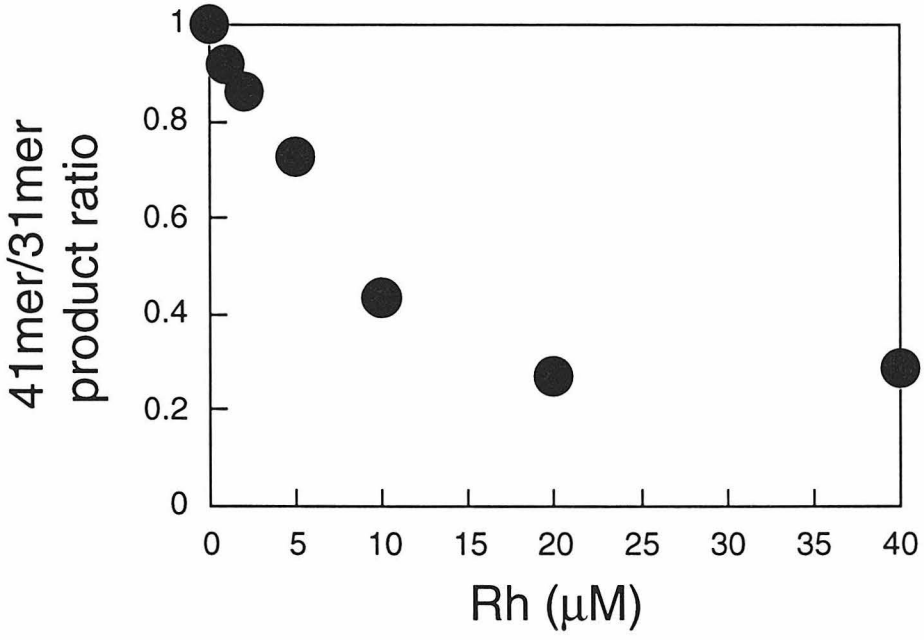
41mer/31mer product ratio
1
0.8
0.6
0.4
0.2
0
0 5 10 15 20 25 30 35 40
Rh (μM)

control template was investigated. The 1-Δ–Rh(MGP)$_2$phi^{5+}-specific and control templates used in this experiment are shown in Figure 3.20. The 1-Δ–Rh(MGP)$_2$phi^{5+}-specific and control templates are 40 and 30 nucleotides long respectively. Thus the 41mer/31mer ratio will decrease with added rhodium if sequence-specific inhibition occurs. The results of this study are shown in Figure 3.29. As indicated by the product bands in the gel, very little inhibition of either template was observed until the concentration of rhodium exceeded 5 μM. The gel shows that at concentrations of 10, 20, and 40 μM, extension of both templates was inhibited with a greater reduction of 41mer products being observed. Thus, the 41mer/31mer ratio did decrease with added rhodium as shown in the plot at the bottom of Figure 3.29. The decrease in this ratio is consistent with 1-Δ–Rh(MGP)$_2$phi^{5+} preferentially inhibiting polymerization on the template containing its recognition sequence.

Note that, in this experiment, differential inhibition does not reach its maximum before both templates are substantially inhibited at 40 μM rhodium. For 1-Λ–Rh(MGP)$_2$phi^{5+} the 41mer/31mer ratio reached its minimum value at 20 μM indicating that the Λ enantiomer is a more potent template directed inhibitor of DNA polymerase than the Δ enantiomer. The concentration of 1-Δ–Rh(MGP)$_2$phi^{5+} necessary to reduce the normalized product ratio to 0.5 is 20 μM. This can be compared to 7 μM for 1-Λ–Rh(MGP)$_2$phi^{5+} which is also consistent with more potent inhibition by the Λ enantiomer.

3.3.6.3 Sequence Specific Inhibition of DNA Polymerase by Rh(MT)phi^{3+}:

The ability of Rh(MT)$_2$phi^{3+} to inhibit polymerization on the template containing its recognition site relative to the control template was investigated. The Rh(MT)$_2$phi^{3+}-specific and control templates used in this

Figure 3.29 Sequence-specific inhibition of DNA polymerase by 1-Δ-$Rh(MGP)_2phi^{5+}$. The Δ-MGP and C templates pictured in Figure 3.20 were used in this experiment. Δ-MGP and C template products are 41mers and 31mers respectively and are indicated in the gel at the top of the figure by Δ and C. Template concentrations are 1 μM each template and 1-Δ-$Rh(MGP)_2phi^{5+}$ concentrations (μM) are indicated above the gel lanes and in the graph. All other conditions are as described in the experimental section.

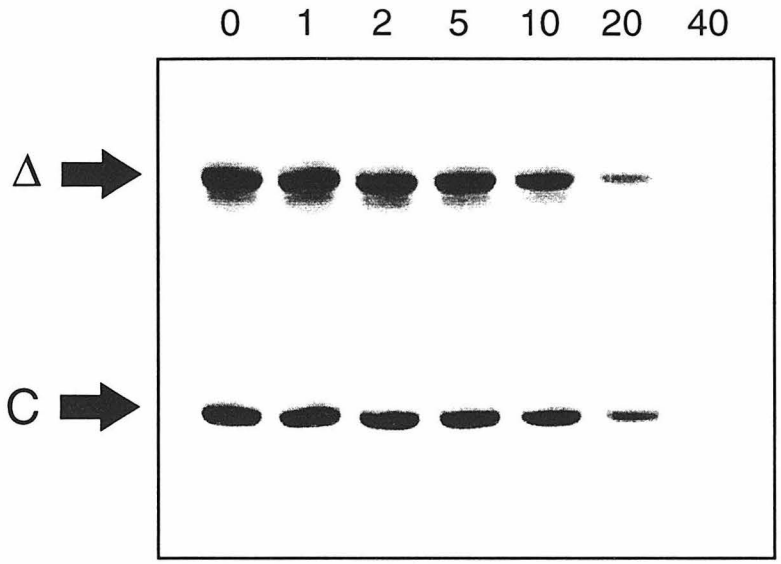
0 1 2 5 10 20 40
Δ
C

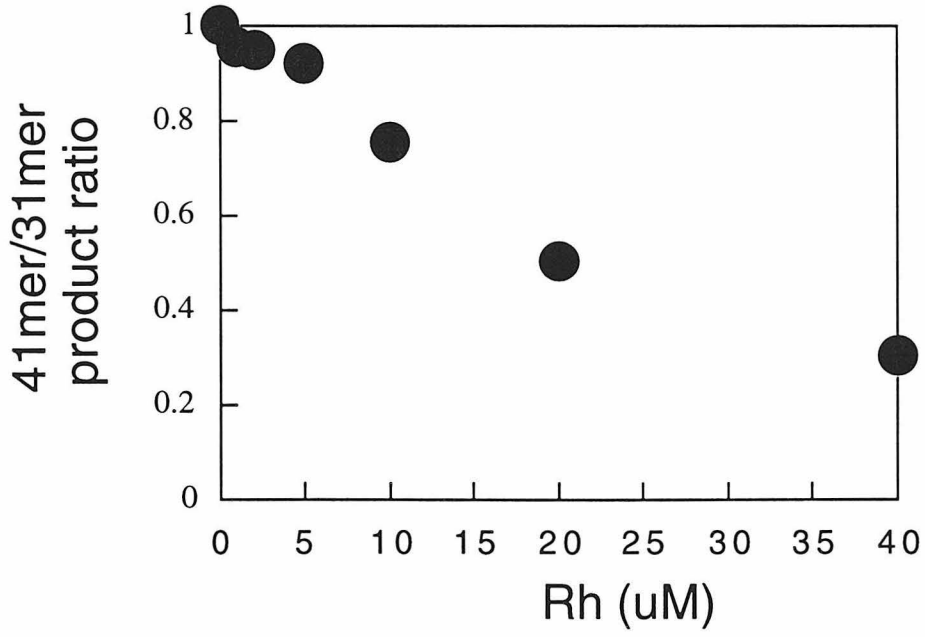
41mer/31mer product ratio
1
0.8
0.6
0.4
0.2
0
0 5 10 15 20 25 30 35 40
Rh (uM)

experiment are shown in Figure 3.20. As the Rh(MT)$_2$phi^{3+}-specific and control templates are 40 and 30 nucleotides long respectively a decrease in the 41mer/31mer product ratio with added rhodium indicates template-directed inhibition by the metal complex. The results of this study are shown in Figure 3.30. As shown by the product bands in the gel at the top of the figure, scant inhibition is observed of products from either template at Rh(MT)phi^{3+} concentrations less than 10 μM. At Rh(MT)phi^{3+} concentrations of 10, 20, and 40 μM, products from both templates are inhibited with greater inhibition observed on the Rh(MT)phi^{3+}-specific template. Thus the 41mer/31mer product ratio decreases with added Rh(MT)phi^{3+} as plotted at the bottom of Figure 3.30 which is consistent with template directed inhibition by this complex. This inhibition is similar to that observed for 1-Δ–Rh(MGP)$_2$phi^{5+} in that the 41mer/31mer product ratio does not reach a minimum before the addition of 40 μM Rh(MT)phi^{3+}. The concentration of rhodium necessary to reduce the normalized product ratio to 0.5 is approximately 25 μM. Thus Rh(MT)phi^{3+} and 1-Δ–Rh(MGP)$_2$phi^{5+} show similar inhibition characteristics which are less potent than those observed for 1-Λ–Rh(MGP)$_2$phi^{5+}.

3.3.7 Head to Head Comparisons of Sequence Specific Inhibition of DNA Polymerase:

Three complexes were available which demonstrated sequence specific inhibition on three different templates. It was of interest to determine whether or not experiments could be conducted in the presence of two templates when each contained a binding site for a different metal complex. In this case, polymerase activity can be inhibited at either template depending on the metal complex added.

Figure 3.30 Sequence-specific inhibition of DNA polymerase by Rh(MT)phi^{3+}. The control template products are 41mers and 31mers respectively and are indicated in the gel at the top of the figure by MT and control. Template concentrations are 1 μM each template and Rh(MT)phi^{3+} concentrations (μM) are indicated above the gel lanes and in the graph. All other conditions are as described in the experimental section.

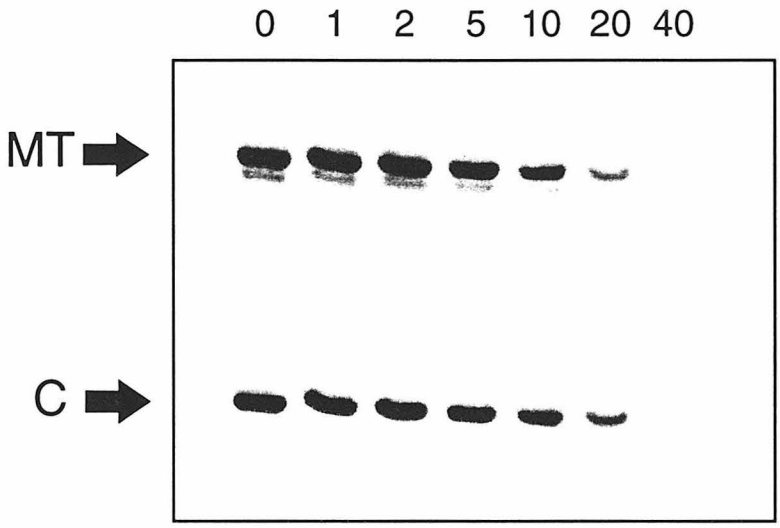
0 1 2 5 10 20 40
MT
C

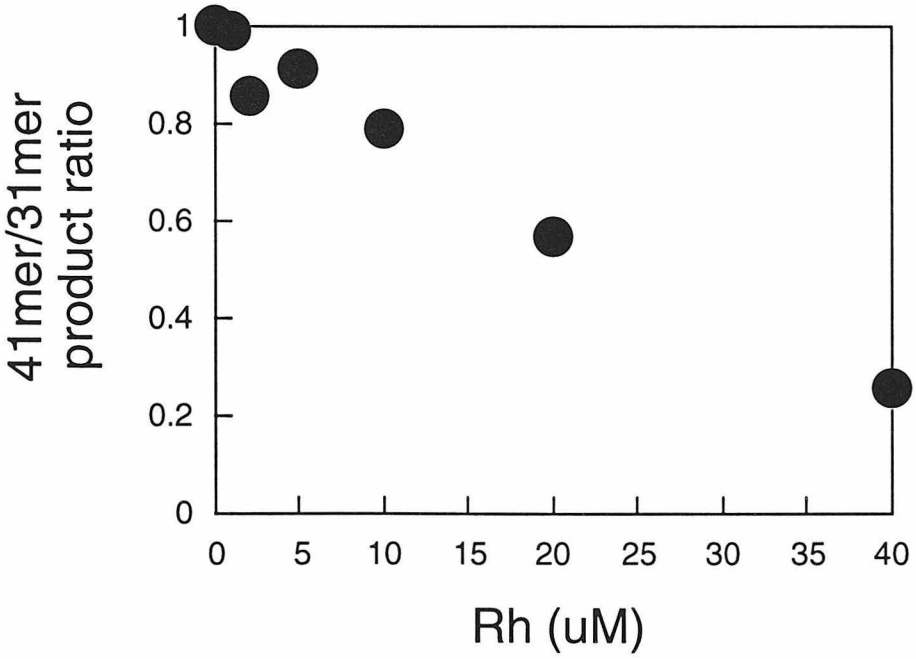
41mer/31mer product ratio
1
0.8
0.6
0.4
0.2
0
0 5 10 15 20 25 30 35 40
Rh (uM)

3.3.7.1 Head to Head Comparisons of Sequence Specific Inhibition of DNA Polymerase by the Enantiomers of 1-Rh(MGP)$_2$phi^{5+}: 67mer 1-Λ–Rh(MGP)$_2$phi^{5+} specific and 56mer 1-Δ–Rh(MGP)$_2$phi^{5+} specific templates (Figure 3.21) were constructed to test the ability of the corresponding metal complexes to inhibit DNA polymerase activity in a sequence-specific manner. Note that these templates differ only by one base pair in their duplex regions. Each enantiomer was titrated into solutions containing each template in a 1:1 ratio. The ratio of 68mer/57mer products was then plotted versus rhodium concentration. A decrease in this ratio indicates preferential inhibition of the template containing the recognition site for the Λ enantiomer. Conversely, an increase in the ratio indicates preferential inhibition of the template containing the recognition site for the Δ enantiomer. The results of this assay are shown in Figure 3.31. As can be seen in the gel at the top of the figure, the addition of 1-Λ–Rh(MGP)$_2$phi^{5+} resulted in a decrease in 68mer products. Furthermore, an increase in 57mer products nearly equal to the decrease observed in 68mer products occurred. The normalized ratio 68mer/57mer product is shown at the bottom of Figure 3.31. This ratio decreases with increasing 1-Λ–Rh(MGP)$_2$phi^{5+} concentration. The data shown in the gel and plot are consistent with 1-Λ–Rh(MGP)$_2$phi^{5+} blocking the action of DNA polymerase on the template containing its recognition sequence and causing the enzyme to switch to the template containing the recognition sequence for the Δ enantiomer. The specificity of this inhibition is remarkable since the two templates in this study differ by only one base pair.

The Δ enantiomer, however, showed different behavior than the Λ enantiomer. The Δ enantiomer displayed little inhibition of DNA synthesis on either template. Very slight inhibition was observed on the template conatining the recognition sequence for the Δ enantiomer and no inhibition

Figure 3.31 Plot of normalized data from a head to head competition between templates specific for each enantiomer of 1-Rh(MGP)$_2$phi^{5+}. The 56mer and 67mer templates used are shown in Figure 3.20. R is the ratio of the Λ specific products divided by the Δ specific products. Blue circles show the effects of titration of 1-Λ-Rh(MGP)$_2$phi^{5+} and red triangles show the effects of titration of 1-Δ-Rh(MGP)$_2$phi^{5+}. Reaction conditions: 1 μM each template. All other conditions are as described in experimental.

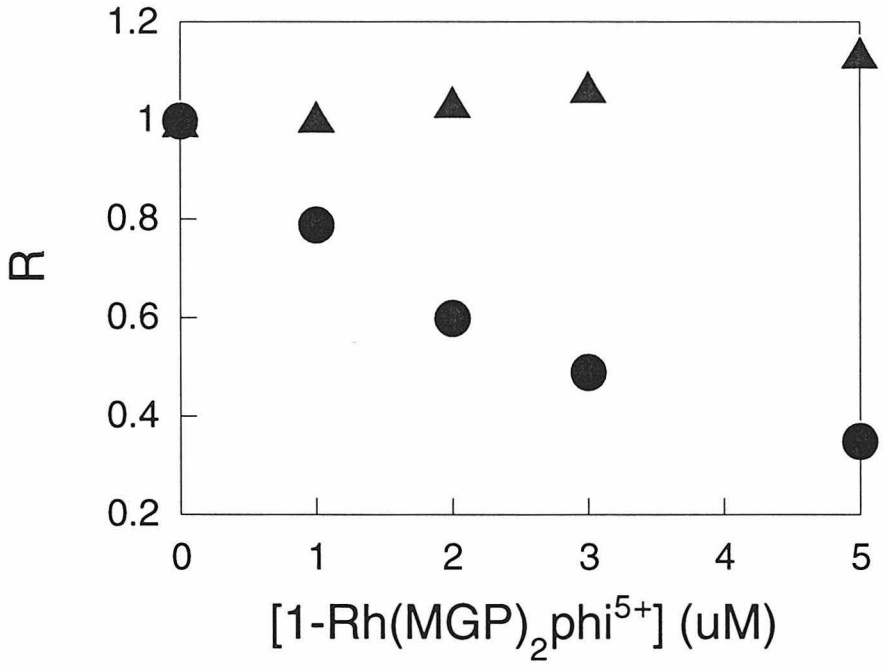
1.2
1
0.8
0.6
0.4
0.2
R
0
1
2
3
4
5
[1-Rh(MGP)2phi5+] (uM)

was observed on the template specific for the Λ enantiomer. This inhibition can be seen in the plot as a slight increase in the 68mer/57mer ratio with added 1-Δ–Rh(MGP)$_2$phi^{5+}. It is unclear why the Δ enantiomer shows such poor inhibition in this system. Outside of the one site on the specific template, there are no other potential binding sites for the complex. Further experiments are necessary to determine why this difference in sequence specific inhibition is observed for the Δ enantiomer.

3.3.7.2 Head to Head Comparisons of Sequence Specific Inhibition of DNA Polymerase by the 1-Λ-Rh(MGP)$_2$phi^{5+} and Rh(MT)phi^{3+}: The ability of 1-Λ-Rh(MGP)$_2$phi^{5+} and Rh(MT)phi^{3+} to inhibit polymerization in head to head experiments was investigated. Templates used in this experiment are shown in Figure 3.32. Note that the Rh(MT)phi^{3+}-specific template contains two recognition sites while the 1-Λ-Rh(MGP)$_2$phi^{5+}-specific template contains only one. The experiments described in Section 3.3.5.4 showed that the presence of two metal binding sites results in greater template directed inhibition than the presence of one metal binding site. Since more sites are present on the Rh(MT)phi^{3+}-specific template than the 1-Λ-Rh(MGP)$_2$phi^{5+}-specific template, the relative inhibition for Rh(MT)phi^{3+} compared to 1-Λ-Rh(MGP)$_2$phi^{5+} will appear to be more potent than it would be if only one metal site was present on each template. The 1-Λ-Rh(MGP)$_2$phi^{5+}-specific template was a 40mer and the Rh(MT)phi^{3+}-specific template was a 30mer. Thus, a decrease in the 41mer/31mer ratio indicates preferential inhibition of the template containing the recognition sequence for 1-Λ-Rh(MGP)$_2$phi^{5+}. An increase in this ratio indicates preferential inhibition of the template containing the recognition sequence for Rh(MT)phi^{3+}.

The results of this study are shown in Figure 3.33. The plot shows

Figure 3.32 Templates used in experiment demonstrating head to head inhibition of DNA polymerase by 1-Λ-Rh(MGP)$_2$phi^{5+} and Rh(MT)phi^{3+}. Recognition sites for the complexes are shown in bold. Note that the Rh(MT)phi^{3+}-specific template has two metal binding sites while the 1-Λ-Rh(MGP)$_2$phi^{5+}-specific template has only one.

Rh(MT)phi^{3+}-Specific Template:

5'ATGGTGCTGGCACGACAGG**TGCA**CG**TGCA**C3'
3'C**ACGT**GC**ACGT**GGACAGCACGGTCGTGGTA5'

Rh(MGP)$_2$phi^{5+}-Specific Template:

5'ATGCTAGGCTATGGTGCTGGCACGACAGCGC**CATATG**GCG3'
3'GCG**GTATAC**CGCGACAGCACGGTCGTGGTATCGGATCGTA5'

Figure 3.33 Head to head inhibition by Rh(MT)phi^{3+} and 1-Λ-Rh(MGP)$_2$phi^{5+}. Templates used in these experiments are shown in Figure 3.32. 1 μM each template was used in this study. The ratio of 41mer to 31mer products is plotted versus Rh(MT)phi^{3+} (circles) and 1-Λ-Rh(MGP)$_2$phi^{5+} concentration (triangles). Conditions of experiments are described in the Experimental section.

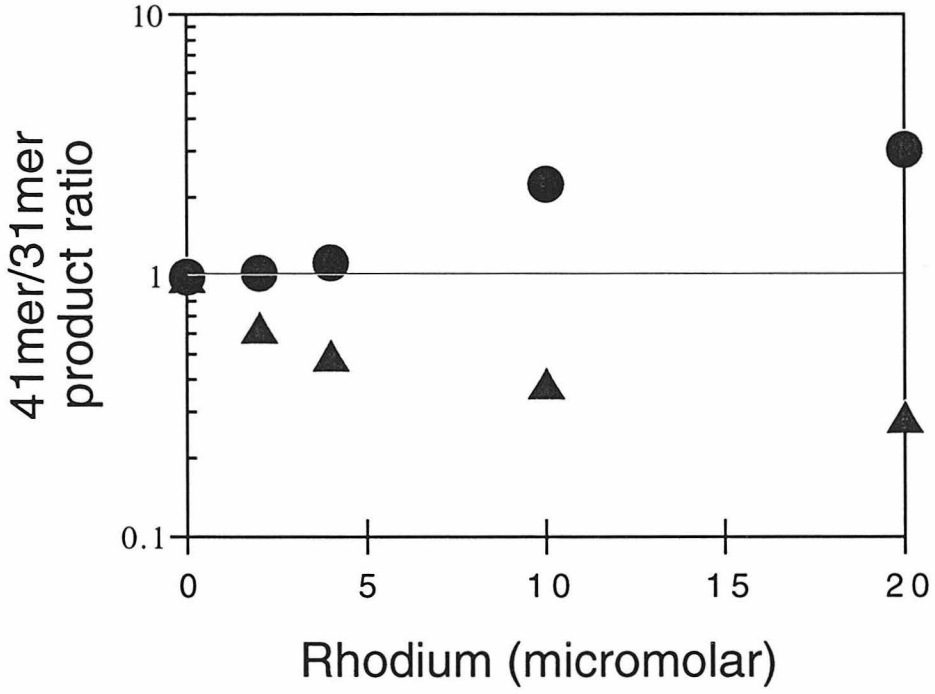
10
1
0.1
41mer/31mer
product ratio
0
5
10
15
20
Rhodium (micromolar)

that the 41mer to 31mer product ratio decreases with increasing 1-Λ-Rh(MGP)$_2$phi^{5+}. This is consistent with preferential inhibition of polymerization by 1-Λ-Rh(MGP)$_2$phi^{5+} on the template containing its recognition sequence. The 41mer to 31mer ratio reaches a minimum value of 0.3 at 20 μM 1-Λ-Rh(MGP)$_2$phi^{5+}. A value of 0.3 represents threefold inhibition of the 1-Λ-Rh(MGP)$_2$phi^{5+}-specific template relative to the Rh(MT)phi^{3+}-specific template by 1-Λ-Rh(MGP)$_2$phi^{5+}. Thus, as in the head to head competition between the Δ and Λ enantiomers of 1-Rh(MGP)$_2$phi^{5+}, significant template-directed inhibition is observed with 1-Λ-Rh(MGP)$_2$phi^{5+}.

Addition of Rh(MT)phi^{3+} to reactions containing the templates shown in Figure 3.32 resulted in an increase in the 41mer to 31mer ratio as shown in the plot in Figure 3.33. As the 30mer template is Rh(MT)phi^{3+}-specific, an increase in this ratio is consistent with preferential inhibition of the Rh(MT)phi^{3+}-specific template relative to the 1-Λ-Rh(MGP)$_2$phi^{5+}-specific template. This ratio reaches its maximum at a value of 3 at 20 μM. This value of three represents threefold inhibition of the Rh(MT)phi^{3+}-specific template relative to the 1-Λ-Rh(MGP)$_2$phi^{5+}-specific template by Rh(MT)phi^{3+}.

Both 1-Λ-Rh(MGP)$_2$phi^{5+} and Rh(MT)phi^{3+} show threefold inhibition of templates containing their recognition sequences suggesting similar potencies for each complex. However, as described above, the Rh(MT)phi^{3+}-specific template contains two recognition sites while the 1-Λ-Rh(MGP)$_2$phi^{5+}-specific template contains only one. Therefore, the relative abilities of each complex to inhibit DNA polymerase cannot be compared in this system.

3.3.8 Sequence Specific Inhibition of DNA Polymerase by the Enantiomers

of Rh(DPB)$_2$phi^{3+}: The ability of the enantiomers of Rh(DPB)$_2$phi^{3+} to inhibit DNA polymerase in a sequence specific manner was investigated. Templates used in this study are shown in Figure 3.34. Δ-Rh(DPB)$_2$phi^{3+} binds tightly and specifically to the eight base pair sequence 5'-CTCTAGAG-3' and could be expected to show significant sequence-specific inhibition.[21] Λ-Rh(DPB)$_2$phi^{3+} has shown no affinity for any DNA sequence at concentrations higher than those used in these studies and would not be expected to promote template directed inhibition. The results of this study are shown in Figure 3.35. The gel data demonstrate that both Λ and Δ-Rh(DBP)$_2$phi^{3+} completely inhibit DNA polymerase at concentrations as low as 2.5 μM. For the Λ enantiomer, it is unlikely that this inhibition is template directed as this complex has shown no affinity for any DNA sequence at concentrations of 10 μM.[17] That the Λ enantiomer is a very potent inhibitor is consistent with the data presented above in Section 3.3.2 which indicates that Rh(DBP)$_2$phi^{3+} inhibits DNA polymerase by directly interacting with the enzyme. Furthermore, as the change in product ratio with added rhodium for the Δ enantiomer is very similar to that of the Λ enantiomer, it is likely that this complex directly inhibits the enzyme as well. A plot of the 31mer/41mer product ratio versus metal complex concentration is shown at the bottom of Figure 3.35. Slight sequence specific inhibition is observed for the Δ enantiomer before polymerization on both templates is inhibited. However, this inhibition is nearly identical to that of the Λ enantiomer. The Λ enantiomer has not shown binding to DNA at these concentrations and therefore should not demonstrate any sequence selectivity in its inhibition. The possibility that the sequence-selectivity in this inhibition is not template directed should be considered.

Figure 3.34 Templates used for the investigation of the inhibition of DNA polymerase by the enantiomers of $Rh(DPB)_2phi^{3+}$. The recognition sequence for the complex is shown in bold.

Control Template:

5'ATGCTAGGCTATGCAGCTGGCACGACAGCGCCATATGGCG3'
3'GCGGTATACCGCGACAGCACGGTCGACGTATCGGATCGTA5'

Δ-Rh(DPB)$_2$phi^{3+} Specific Template:

5'ATGCAGCTGGCACGACAGCG**CTCTAGAG**CG3'
3'GC**GAGATCTC**GCGCGACAGCACGGTCGACGTA5'

Figure 3.35 Inhibition of DNA polymerase by the enantiomers of $Rh(DPB)_2phi^{3+}$. A polyacrylamide gel of reaction products is shown at the top of the figure. Reactions for lanes 1-8 contain the Λ enantiomer and reactions for lanes 9-16 contain the Δ enantiomer. Reactions for lanes 1 & 9, 2 & 10, 3 & 11, 4 & 12, 5 & 13, 6 & 14, 7 & 15, and 8 & 16 contained 0, 0.05, 0.1, 0.25, 0.5, 1, 2.5, and 5 μM $Rh(DPB)_2phi^{3+}$ respectively. DNA concentrations were 0.05 μM each template. Templates are shown in Figure 3.31. Reaction time was eight minutes at 21°C and dCTP concentration was 0.2 μM. All other conditions were as described in experimental. Note that all polymerase activity is abbrogated for both enantiomers at 2.5 μM rhodium. A plot of the 31mer/41mer product ratio vs. Δ enantiomer concentration (red triangles) and Λ enantiomer concentration (blue circles) is shown at the bottom of the figure.

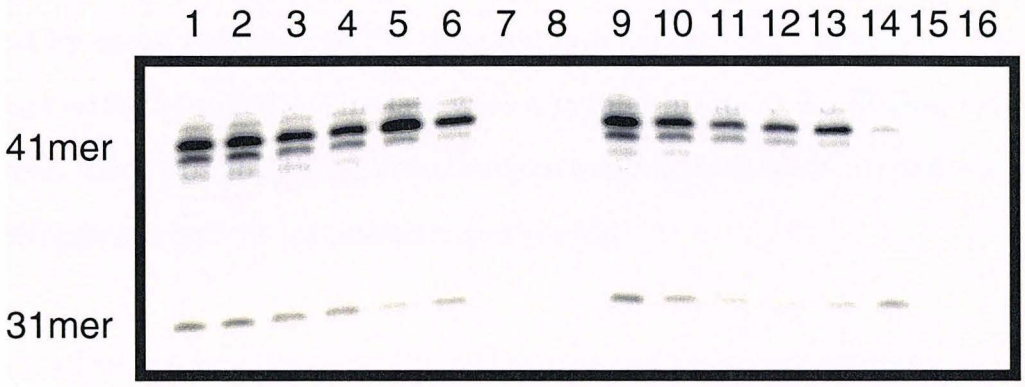
1 2 3 4 5 6 7 8 9 10 11 12 13 14 15 16
41mer
31mer

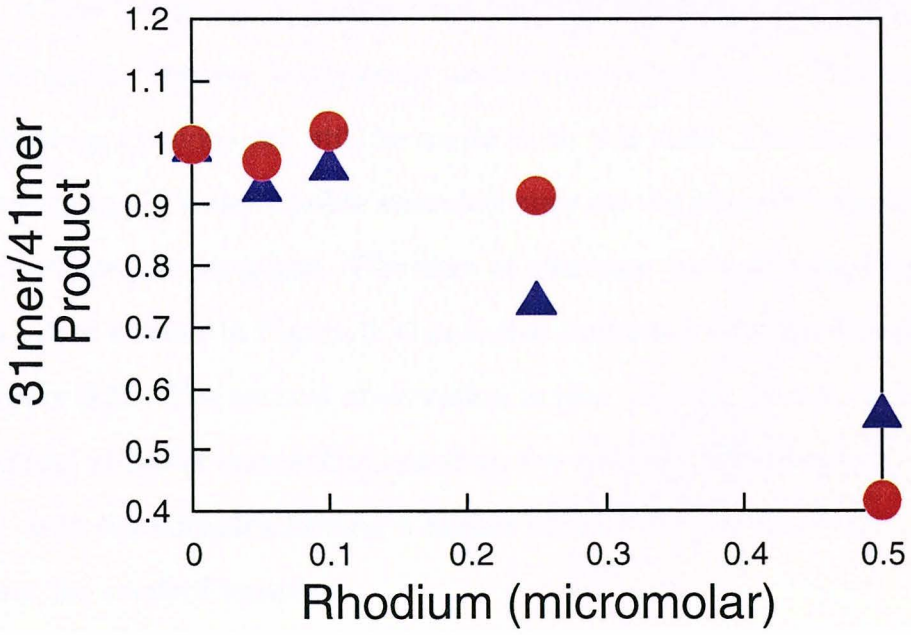
31mer/41mer Product
1.2
1.1
1
0.9
0.8
0.7
0.6
0.5
0.4
0
0.1
0.2
0.3
0.4
0.5
Rhodium (micromolar)

3.3.9 Correlations Between Photocleavage and Sequence-Specific Inhibition:

Sequence-specific inhibition has been demonstrated for three different metal complexes with a variety of different templates. This inhibition may be the result of a greater fraction of specific template being bound by metal complex, or the complex may bind to both templates, but interact with the specific template with a greater affinity. To distinguish between these possibilities, photocleavage experiments were carried out on the templates used in inhibition experiments.

3.3.9.1 Correlations Between Photocleavage and Sequence-Specific Inhibition with Rh(MT)phi^{3+}:

Rh(MT)phi^{3+} has shown effective sequence specific inhibition with the templates pictured in Figure 3.10. These templates were 5' end labeled, irradiated with ultraviolet light in the presence of metal complex, and electrophoresed on a polyacrylamide gel to determine the positions of photocleavage. The results of this experiment are shown in Figure 3.33. A few things are apparent from viewing this data. The first is that very little photocleavage is apparent under these conditions. However, some important conclusions can still be made from this data. One is that the complex binds to many more double stranded sites on the specific template than on the non-specific template. The sites of cleavage on both templates are indicated by green arrows in Figure 3.36 and also indicated with the templates shown in Figure 3.37. The second observation is that binding occurs to the specific template at lower concentrations than the non-specific template. This is consistent with the complex having a higher affinity for the specific template than the control template.

Only two sites of photocleavage per strand were expected for the specific template. Yet the complex demonstrates photocleavage at five sites.

Figure 3.36 Gel of photocleavage by Rh(MT)phi^{3+} on 5' labeled templates shown in Figure 3.10. Sequences of the double stranded regions of each template are listed in red. All samples were treated as described in Chapter 2-experimental with the following exceptions. DNA concentrations were 0.5 μM each template in all lanes. Lanes 1-9 had 50,000 cts/min 30mer template, lanes 12-20 50,000 cts/min 40mer template. All samples were irradiated at 313 nm for 10 minutes except 1 and 12. Lanes 1, 2, 12, and 13 contained no rhodium complex. Lanes 3 &14, 4 &15, 5 & 16, 6 & 17, 7 & 18, 8 & 19, and 9 & 20 contained 0.5, 1 , 2, 5, 10, 20, and 50 μM rhodium complex respectively. Lanes 10 & 21, and 11 & 22 are A+G and C+T Maxam and Gilbert Sequencing reaction respectively.

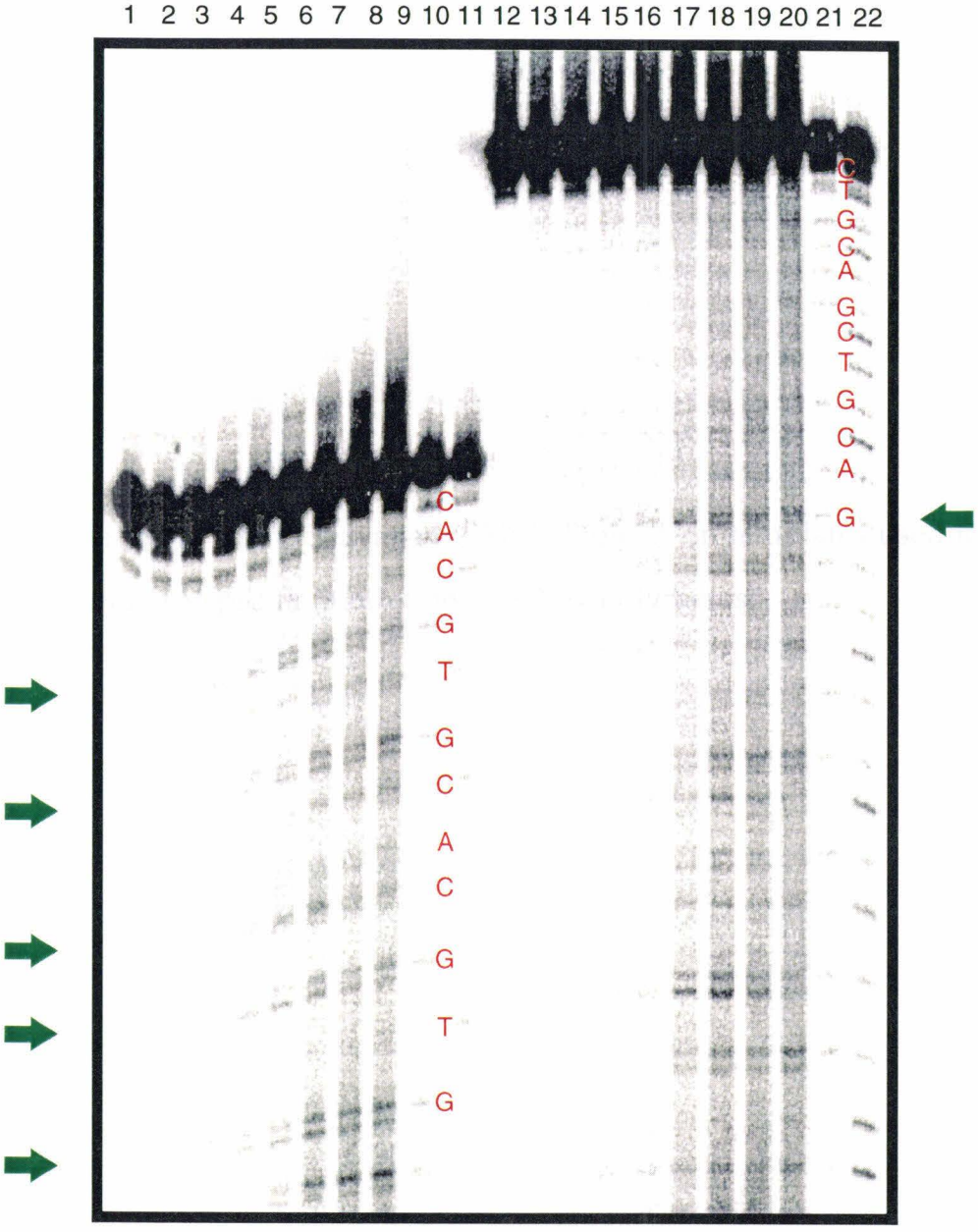
1 2 3 4 5 6 7 8 9 10 11 12 13 14 15 16 17 18 19 20 21 22
C A C G T G C A C G T G
C T G C A G C T G C A G

Figure 3.37 Position of photocleavage by Rh(MT)phi^{3+} on templates used to demonstrate sequence specific inhibition of DNA polymerase.

Rh(MT)phi^{3+} Template:

Control Template:

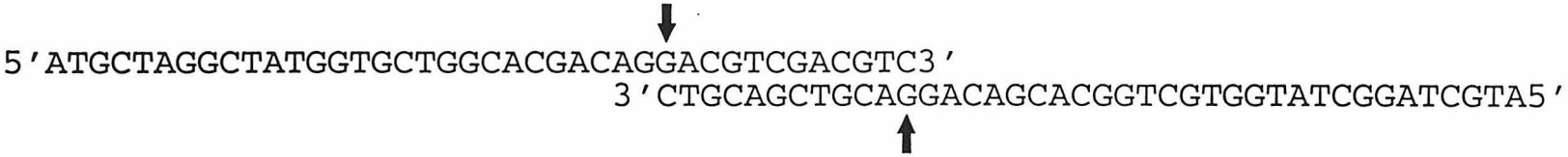

In two of these sites and on the only site cleaved on the control template, the guanine cleaved is at the end of the duplex portion of the template and the cleavage here is likely to be a result of the complex associating with the double/single stranded junction. The third cleavage site on the Rh(MT)phi^{3+}-specific template is at a 5'-CG-3' step for which the complex has not shown substantial affinity. Photocleavage at this site is difficult to explain. However, the photocleavage observed is consistent with more complex binding and with a greater affinity to the specific template than the control template. This supports the hypothesis that inhibition is template directed. Thus more binding to and greater affinity for the specific template is observed for Rh(MT)phi^{3+}. Since both of these effects are present in this system, their relative importance in inhibition cannot be determined.

3.3.9.2 Correlations Between Photocleavage and Sequence Specific Inhibition with Rh(MGP)$_2$phi^{5+}: Correlations of photocleavage and inhibition by 1-Λ-Rh(MGP)$_2$phi^{5+} have been investigated. The DNA templates used in this experiment were the 1-Λ-Rh(MGP)$_2$phi^{5+} specific and control template C shown in Figure 3.32. These templates were 5'labeled, irradiated, and electrophoresed to determine the positions of photocleavage. The results of this experiment are shown in Figures 3.38 and 3.39. Photocleavage is observed on both templates, with an equal number of sites cleaved on both specific and non-specific template by the metal complex. In the context of sequence-specific inhibition, this binding to both templates is not yet understood.

Figure 3.38 Gel of photocleavage by 1-Λ-Rh(MGP)2phi^{5+} on 5' labeled templates shown in Figure 3.22. Sequences of the double stranded regions of each template are listed in red. All samples were treated as described in Chapter 2-experimental with the following exceptions. A 1:1 DNA template to rhodium ratio was maintained for all lanes except 2 & 7. DNA concentrations were 0.01, 0.1, and 1 μM each template in lanes 4 & 9, 5 & 10, and 6 & 11 respectively. Buffer conditions were 10 mM sodium cacadylate, 40 mM NaCl, pH 7.0. Lanes 2-6 had 50,000 cts/min 40mer template and lanes 7-11 50,000 cts/min 30mer template. All samples were irradiated at 313 nm for 4 minutes except 2 and 7. Lanes 2, 3, 7, and 8 contained no rhodium complex. Lanes 1 & 12 are A+G Maxam and Gilbert Sequencing reactions.

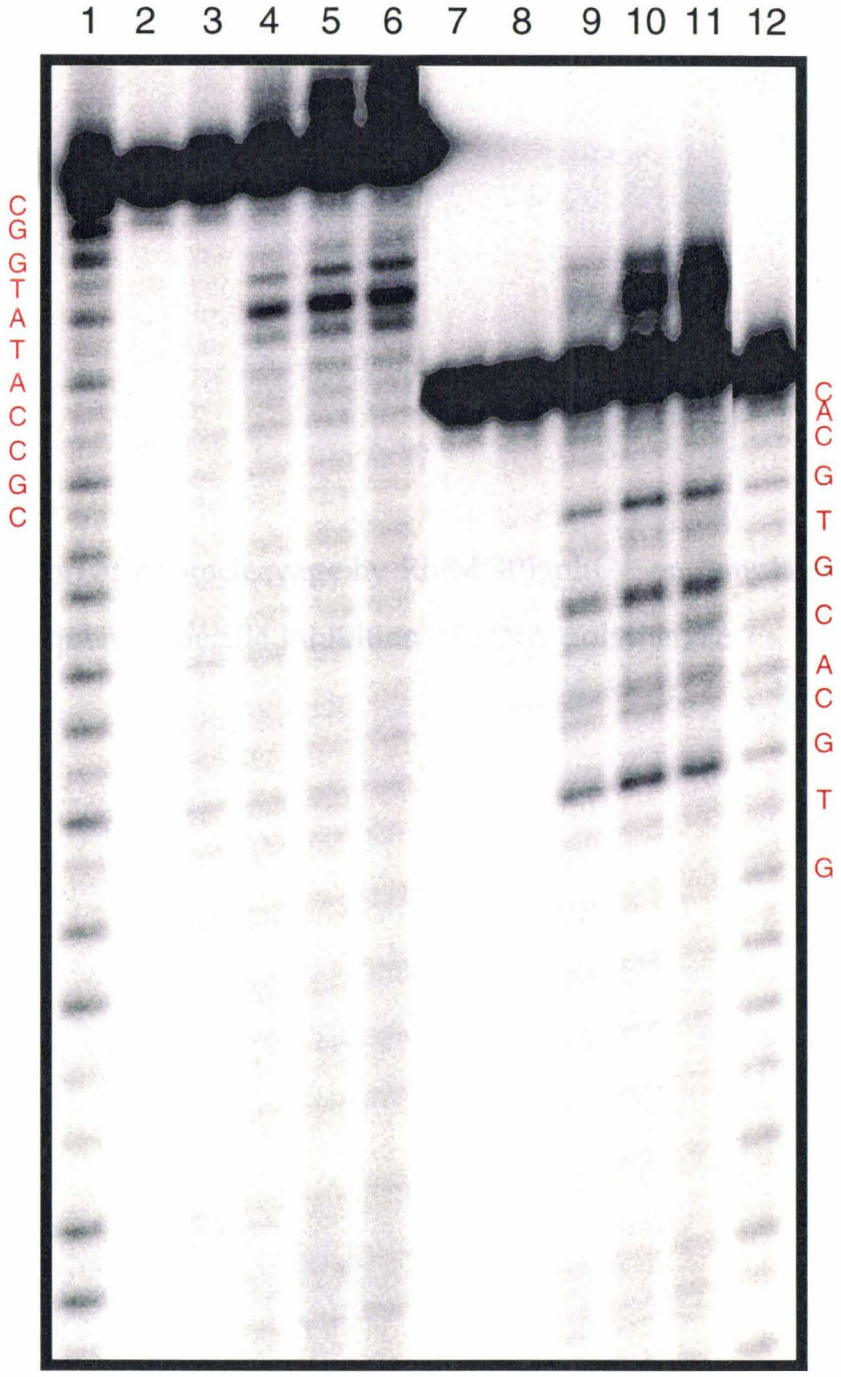
1 2 3 4 5 6 7 8 9 10 11 12
CGGTATACCGC
CACGTGCACGTG

Figure 3.39 Position of photocleavage by $Rh(MGP)_2phi^{5+}$ on templates used to demonstrate sequence specific inhibition of DNA polymerase.

Control Template:

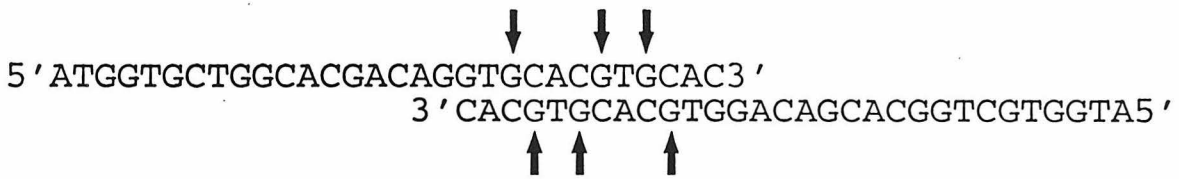

Rh(MGP)$_2$phi^{5+} Template:

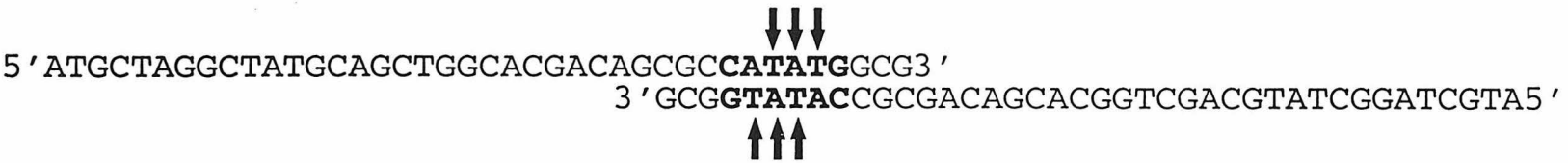

3.4 Discussion

As described in the Results section, many experiments have been described which investigated the effects of various parameters on template-directed inhibition of DNA polymerase. These parameters fall into three general catagories: Solution conditions, template characteristics, and metal complex characteristics. Of primary interest are correlations between rhodium complex characteristics and the potency of template-directed inhibition. These correlations provide clues to the design of more potent inhibitors. The effects of solution conditions and template charateristics are also of importance as they provide a greater understanding of the inhibition assay used in these experiments. Thus, results from solution condition and template characteristic experiments are included in the discussions of metal complex potency to assist in the interpretation of results. Finally, the implications of what we have learned on the design of inhibitors and a discussion of future experiments with these complexes will be presented.

3.4.1 Comparison of Specific Inhibition by 1-Λ–Rh(MGP)$_2$phi^{5+}, 1-Δ–Rh(MGP)$_2$phi^{5+}, and Rh(MT)phi^{3+}: The metal complexes 1-Λ–Rh(MGP)$_2$phi^{5+}, 1-Δ–Rh(MGP)$_2$phi^{5+}, and Rh(MT)phi^{3+} all show significant, sequence-specific inhibition of DNA polymerase. These three complexes are distinct from each other in chemical parameters such as size and charge. These complexes also differ in DNA binding characteristics such as sequences to which they bind, the amount of unwinding of DNA which results from their binding, and dissociation rate from the bound sequences on DNA. That these complexes are not identical allows the comparisons of chemical and binding parameters with the potency of template directed inhbition. These comparisons will facilitate the identification of which metal

complex characteristics are important to DNA polymerase inhibition. Table 3.7 contains a summary of the inhibition data as well as physical information about these three complexes.

Complex	Size (Å)	Binding Affinity (M^{-1})	Exchange Rate at 21°C	Unwind. Angle	Charge	Conc. 0.5 ratio (μM)
1-Λ-Rh(MGP)$_2$phi^{5+}	17	1x10^8	8 sec^{-1}	70°	5+	7
1-Δ-Rh(MGP)$_2$phi^{5+}	17	0.5x10^8	---	---	5+	20
Rh(MT)phi^{3+}	9	1x10^8	5 sec^{-1}	23°	3+	25

Table 3.7: Physical properties of metal complexes and the concentration required for a 0.5 specific to non-specific normalized product ratio.[25,38,41] Size is the span of the ancillary ligands as described in section 3.4.1.2. Exchange rate and DNA unwinding angle for 1-Δ–Rh(MGP)$_2$phi^{5+} have not been determined. The Conc. 0.5 ratio is the concentration of metal complex required to reduce the ratio of specific to control template products to half its value in the absence of metal as described in 3.3.6.

3.4.1.1 Effect of Charge on Sequence Specific Inhibition of DNA Polymerase:

The charge of a metal complex might have a large effect on its ability to inhibit DNA polymerase in a sequence specific manner. DNA polymerases are positively charged proteins and thus an increased charge on a metal complex bound to DNA could result in an increased repulsive force against DNA/polymerase interactions.[20] Comparison of sequence specific inhibition by 1-Λ-Rh(MGP)$_2$phi^{5+}, 1-Δ-Rh(MGP)$_2$phi^{5+}, and Rh(MT)phi^{3+} provides a useful demonstration of the importance of charge in inhibition. As can be seen from Table 3.7, Rh(MT)phi^{3+} and 1-Δ-Rh(MGP)$_2$phi^{5+} demonstrate similar levels of sequence specific inhibition. Yet these complexes differ in charge by 2. Therefore, the charge of the complex does not appear to be a dominant factor in the sequence specific inhibition of DNA polymerase by these complexes. Moreover, 1-Λ-Rh(MGP)$_2$phi^{5+} and 1-Δ-Rh(MGP)$_2$phi^{5+} both have identical charges, yet the Λ enantiomer demonstrates more potent

specific inhibition. This again supports charge not being the primary source of inhibition. Thus it can be concluded that at least for complexes with charges from +3 to +5, that the charge of the complex has little effect on the potency of inhibition.

The lack of a significant correlation between increasing positive charge and increasing inhibition is not too surprising. The phosphate backbone of DNA provides abundant negative charge to neutralize the positive charge of the metal complex. Furthermore, when rhodium complex is not present, the DNA polymerase encounters positively charged magnesium and sodium ions associated with the phosphate backbone of DNA. It is likely that the metal complex displaces these ions and that the total charge-based replusive interactions affecting the polymerase are not significantly different.

3.4.1.2 Effect of Size on Sequence-Specific Inhibition of DNA Polymerase:

Complex size could play a significant role in the sequence specific inhibition of DNA polymerase. The complex must, at least in part, block binding and initiation by DNA polymerase by negative steric interactions. In this type of inhibitory interaction, it can be expected that a larger complex would block more of the DNA and result in greater steric repulsion. Comparison of the inhibition produced by 1-Λ-Rh(MGP)$_2$phi^{5+}, 1-Δ-Rh(MGP)$_2$phi^{5+}, and Rh(MT)phi^{3+} provides some insight into this factor. As the intercalating ligand is identical for all these complexes, there is no difference in its size to compare. However, there are differences in the sizes of the ancillary ligands of these complexes. Rh(MT)phi^{3+} and 1-Λ-Rh(MGP)$_2$phi^{5+} were modeled using InsightII on a Silicon Graphics Indigo xs/24 and the size of the ancillary ligand measured as shown in Figure 3.40. The enantiomers of 1-

Figure 3.40 Sizes of Rh(MT)phi^{3+} (left) and 1-Λ-Rh(MGP)$_2$phi^{5+} (right) as measured by Insight II using a Silicon Graphics Indigo xs/24.

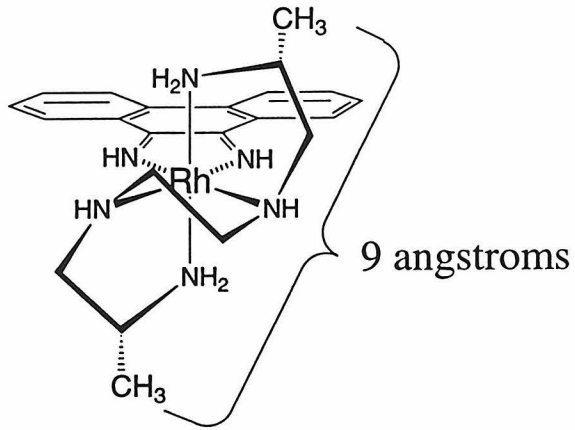

9 angstroms

17 angstroms

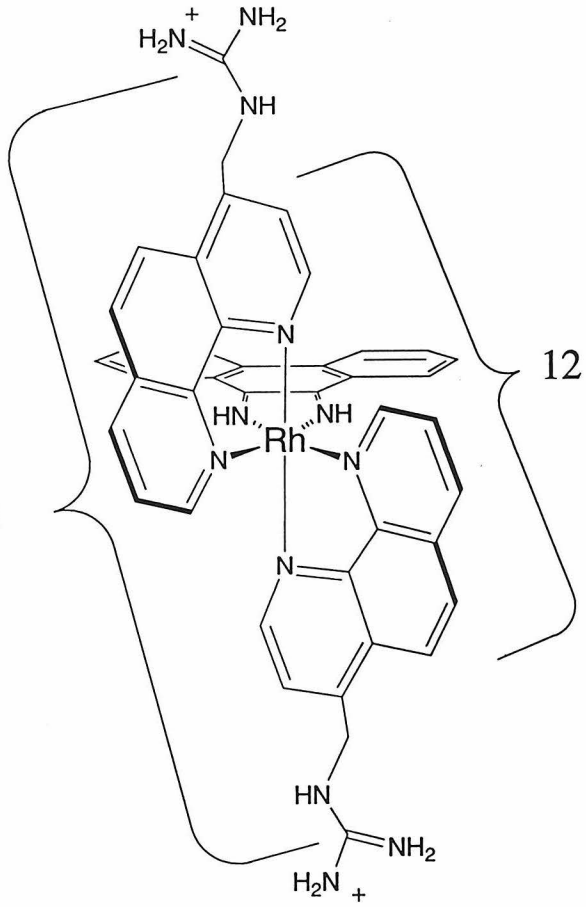

12 angstroms

$Rh(MGP)_2phi^{5+}$ measure 17 Å from the tip of the guanidinium arm to the tip of the guanidinium arm extended. They also measure 12 Å from ancillary phenanthroline ligand to ancillary phenanthroline ligand. $Rh(MT)phi^{3+}$, on the other hand, measures 9 Å from methyl group to methyl group. As can be seen from Table 3.7, $Rh(MT)phi^{3+}$ and 1-Δ-$Rh(MGP)_2phi^{5+}$ show very similar inhibitory properties while 1-Δ-$Rh(MGP)_2phi^{5+}$ is a significantly larger complex. Thus the difference in steric bulk between $Rh(MT)phi^{3+}$ and 1-Δ-$Rh(MGP)_2phi^{5+}$ is not a dominant factor in the sequence-specific inhibition of DNA polymerase. As 1-Λ-$Rh(MGP)_2phi^{5+}$ and 1-Δ-$Rh(MGP)_2phi^{5+}$ are enantiomers of each other, there is no difference in the steric bulk of these complexes. Yet the Λ enantiomer shows substantially more potent inhibition than the Δ enantiomer. If the size of the metal complex was the primary factor in inhibition, then these enantiomers would be expected to show similar properties of inhibition. That there are substantial differences in the inhibition observed with these enantiomers suggests that the steric bulk of a complex is not the primary source of inhibition. Thus it can be concluded that, at least for complexes with ancillary ligands spanning 9 Å to 17 Å, the size of the complex has little effect on the potency of inhibition.

3.4.1.3 Effect of Binding Constant on Sequence Specific Inhibition of DNA Polymerase: Binding affinities of metal complexes for DNA provide information which can be used to determine DNA-site occupancy and the free energy of stabilization upon metal complex association with DNA. The site-specific binding affinities of all complexes studied are all between $0.5x10^8$ to $1x10^8$ M^{-1}. Since DNA polymerase experiments are conducted at micromolar concentrations of specific sites and metal complex, these affinities

indicate that all the specific sites were bound under the conditions of the experiment. When the concentration of rhodium complex is equal to the concentration of specific template, all of the specific template should be bound by metal complex. It would be expected that, when all the specific template is bound, that polymerization on that template would be maximally inhibited. The addition of more complex should not effect the occupancy on that template as it is already fully bound. Moreover, complex beyond the first equivalent could bind to the control template or to the DNA polymerase and reduce the level of sequence-specific inhibition observed. Template-selective inhibition, as measured by the ratio of specific to control products, should be maximized at one equivalent of rhodium. Thus, the specific to control product ratio should reach a minimum value at one equivalent of rhodium. However, in all experiments described in section 3.3.6, increasing metal concentration above one equivalent results in a further decrease in this ratio consistent with greater sequence-specific inhibition. In fact, very little inhibition is observed at one equivalent of rhodium (see Figures 3.28, 3.29, and 3.30.) Maximal inhibition for 1-Λ-Rh(MGP)$_2$phi^{5+}, 1-Δ-Rh(MGP)$_2$phi^{5+}, and Rh(MT)phi^{3+} occurs at concentrations of 20 μM, ≥ 40 μM, and ≥ 40 μM respectively.

The increase in sequence-specific inhibition with increasing rhodium over one equivalent may be related to template structure. Comparison of the inhibition observed by 1-Λ-Rh(MGP)$_2$phi^{5+} on the comparitive templates shown in Figure 3.20 and on the hairpin templates shown in Figure 3.21 is instructive. Inhibition experiments using the comparative and hairpin templates are shown in Figures 3.28 and 3.31 respectively. Note that the specific to control template product ratio reaches a minimum value at 20 μM in Figure 3.28. In Figure 3.31, the ratio is approaching a minimum value at 5

μM. It would appear that the inhibition by 1-Λ-Rh(MGP)$_2$phi^{5+} is more potent on the hairpin template than the comparative template. It should be noted that the sequence of the control template is not the same in each of these experiments. However, 1-Λ-Rh(MGP)$_2$phi^{5+} has shown no affinity for sequences on either control template. Futhermore, the nature of the control template sequence was shown not to be a factor in sequence-specific inhibition in section 3.3.5.3. The difference in control template sequence is therefore not likely to be the cause of the more potent inhibition on the hairpin template.

Three differences are apparent when comparing the structures of the comparitive and hairpin templates. The first difference is that the hairpin templates have a duplex region of 20 base pairs while the comparative templates have a duplex region of only 12 base pairs. This difference in duplex size could result in differences in annealing with a large fraction of the comparitive templates existing in single stranded form relative to the hairpin templates. With their 20 base pair duplex regions and their covalently attached complementary strands, the hairpin templates are certainly fully annealed under the experimental conditions. However, the melting temperatures of the comparative templates were measured to be at least 40°C above the temperature at which the inhibition experiments are conducted and thus these templates should be fully annealed as well.[34] Therefore, differences in annealing are not likely to be the cause of more potent inhibition on the hairpin templates.

The second difference between the comparative and hairpin templates is the distance of the intercalation site for the metal complex from the site of initiation of polymerization (the double-stranded/single-stranded junction). On the comparative templates, the site of binding for 1-Λ-

$Rh(MGP)_2phi^{5+}$ is 6 base pairs away from the initiation of polymerization while on the hairpin templates, this site is 4 base pairs away. The closer proximity of metal binding to the initiation of polymerization may position 1-Λ-$Rh(MGP)_2phi^{5+}$ where it can more effectively inhibit the enzyme.

Examination of the experiments on templates containing multiple metal binding sites (3.3.5.4) is instructive in the effects of metal-binding site position. The templates for these experiments are shown in Figure 3.25 and the results are shown in Figure 3.26. These templates are also hairpins and what should be first noted in Figure 3.26 is that $Rh(MT)phi^{3+}$ is a very potent inhibitor of polymerization on both templates. In fact, polymerization on both templates is almost completely inhibited at a $Rh(MT)phi^{3+}$ concentration of 3 μM which is the concentration where there is a 1:1 ratio of metal to metal-specific sites. Note that on the one-site template, the position of $Rh(MT)phi^{3+}$ binding is 3 base pairs away from the site of initiation of polymerization while the closest site on the two-site template is 7 base pairs away from the site of initiation of polymerization. Thus the one-site template contains a metal binding site 4 base pairs closer to the site of initiation of polymerization, and if this distance is critical in the potency of inhibition, the one-site template should show a greater decrease in products than the two-site template with added rhodium. However, the plot in Figure 3.36 shows that inhibition of the two-site template is more potent, and therefore positioning is not likely to be the cause of the differences in inhibition observed when using comparative and hairpin template.

Large differences are observed in the inhibition of polymerization on the comparative and hairpin template. The reasons for these differences are unclear. Since the binding constant of 1-Λ–$Rh(MGP)_2phi^{5+}$ is $1x10^8$ M^{-1}, it should fully occupy the specific sites on both templates at a concentration of 1

μM, and differential binding should not be the cause of the differences in inhibition. These differences cannot be explained by differences in annealing or metal binding site position between these templates. The combination of these differences and the fact that one equivalent of metal does not produce maximal inhibition suggests that the template-directed inhibition of DNA polymerase is not as simple as a metal complex binding to a template and blocking the polymerase.

It is important to note the relative affinities of 1-Λ–$Rh(MGP)_2phi^{5+}$, 1-Δ–$Rh(MGP)_2phi^{5+}$, and $Rh(MT)phi^{3+}$ for DNA as compared to the affinity of DNA polyermase for DNA. These three complexes have binding constants of $\geq 5x10^7\ M^{-1}$ for their recognition sequences. DNA polymerase shows an affinity of $1x10^7\ M^{-1}$ for DNA. Thus all three complexes have greater affinities for DNA than the enzyme. It would be of interest to compare metal complex affinities for DNA relative to DNA polymerases affinity for DNA with the inhibition properties of those complexes. That comparison is not possible in this study as the affinities of these complexes are too similar for any differences in inhibition to be attributed to them. This similarity in binding affinity, however, does mean that differences in the activities of the three complexes must be due to factors other than binding affinity.

3.4.1.4 Effect of Exchange Rate on Sequence Specific Inhibition of DNA Polymerase: The exchange rate of a complex could be expected to have a significant impact on the ability of a complex to inhibit DNA polymerase in a sequence specific manner. The polymerization inhibition experiments are run with dCTP as a limiting reagent relative to both DNA polymerase and to DNA template. All the dCTP should be consumed in the first binding of DNA polymerase and catalytic turnover will not occur. Under these

conditions, the competition for production of product is essentially a competition for the initial binding of DNA polymerase. Therefore, the rate of DNA polymerase binding to template should be compared to the exchange rate of the complex on the DNA to determine whether exchange rate is important in inhibition.

The rate of DNA polymerase binding to template in these reactions can be estimated. The association rate for the second order binding of DNA polymerase to a DNA template has been determined to be $1x10^7$ s^{-1}.[29,30] The concentration of DNA template used in these experiments is 20-fold higher than the enzyme concentration and thus the amount of free DNA can be considered to be constant. The rate of DNA polymerase binding to the DNA template can therefore be modeled using the following pseudo-first order equation:

$$-d[E]/dt = k[E][D] \qquad \text{Equation 3.1}$$

where [E] is the concentration of enzyme, [D] is the concentration of template, k is the association rate, and dt is change in time. This equation can be solved to determine the time required for a specific fraction of polymerase to bind.

$$\ln[E]_O - \ln[E]_f = k[D]\Delta t \qquad \text{Equation 3.2}$$

where $[E]_O$ is the initial concentration of free enzyme and $[E]_f$ is the final concentration of free enzyme.

At the concentrations of DNA at which these competition experiments are conducted (2 μM), 90% of the polymerase will be bound to DNA in the first 0.2 seconds of reaction. Molecules which have dissociation

rates much slower than this can be expected to be more potent sequence-specific inhibitors than those with rates similar to the binding of DNA polymerase or faster. It can be assumed that the DNA polymerase needs an unoccupied template to which to bind. Metal complexes which are bound to DNA for the first 0.2 seconds of reaction can be expected to effectively block polymerase action on all templates to which they are bound. If, instead, these complexes are dissociating and associating (exchanging) with the DNA several times over the first 0.2 seconds, this could provide the enzyme several chances to bind to an unoccupied template. The more times the complex exchanges on the DNA, the more opportunities the DNA polymerase has to bind and the less potent the inhibition observed.

The rate at which the DNA polymerase binds is directly proportional to the DNA template concentration which provides a context for the results observed in section 3.3.2.1. In these experiments, sequence-specific inhibition was found to increase with increasing template concentration. This effect was observed over concentration ranges where the complex was fully bound and thus was not due to a higher concentration resulting in greater template occupancy by metal complex. If metal complex is fully bound to specific sites, an increase in concentration of metal and template would be expected to result in metal binding to non-specific sites and thus the observation of less potent inhibition.

The increased sequence-specific inhibition can be explained in the rate at which DNA polymerase binds to template is taken into account. A higher concentration of template will result in a faster rate of association of DNA polymerase with the template. As described in Chapter 2, the rate of metal complex dissociation is a first order process and thus its half life is independent of template concentration. Thus, increasing the template

concentration results in an increase in the association rate of the DNA polymerase with DNA while not affecting the dissociation rate of the metal complex. The increase in inhibition with increased template concentration described in section 3.3.2.1 may be a result of the change in the rate of association of DNA polymerase relative to metal complex dissociation.

The dissociation constants are known for the metal complexes $Rh(MT)phi^{3+}$ and $Rh(MGP)_2phi^{5+}$ based on NMR data. The determined constants for these complexes are 5 sec^{-1} and 8 sec^{-1} at 20°C respectively.[41] Both complexes dissociate from their respective DNA sites at a rate significantly faster than the time it takes for the DNA polymerase to bind. The amount of DNA polymerase bound after half of each complex has dissociated from the DNA can be calculated using equation 3.2. Quantitatively 75% and 94% of the DNA polymerase will be bound by the time half the bound $Rh(MGP)_2phi^{5+}$ and $Rh(MT)phi^{3+}$ have dissociated from the DNA once respectively. Thus, if the rate of dissociation played a substantial role in the sequence specific inhibition of DNA polymerase, one would expect to see significantly more potent inhibition by $Rh(MT)phi^{3+}$ as compared to $Rh(MGP)_2phi^{5+}$. As can be seen from Table 3.6, the reverse is actually the case with $Rh(MGP)_2phi^{5+}$ being the more potent inhibitor. It can therefore be concluded that the rate of dissociation does not play a primary role in the sequence-specific inhibition of DNA polymerase over this range. It may play some role, however. It can also be concluded that it is not essential for a metal complex to be bound over the full time the DNA polymerase is initially binding to be an effective inhibitor.

3.4.1.5 Effect of Unwinding Angle on Sequence-Specific Inhibition of DNA Polymerase: DNA polymerase binds to duplex DNA as its substrate. As this

enzyme can initiate synthesis adjacent to many different double stranded sequences, it can be concluded that its substrate is generally B-form DNA in nature.[19] The enzyme does, however, show sequence-specificity in its activity (see 3.3.5.2).[29,30] This sequence-specificity in activity is not that surprising. The polymerase is capable of binding many different DNA templates because it makes non-specific electrostatic interactions with the phosphate backbone of DNA instead of direct contacts to specific bases. Although the contacts made are non-specific, any phosphate can make the electrostatic interactions, the positioning of the phosphates is important. DNA structure varies with DNA sequence. Thus, the relative positions of phosphate groups in the backbone of the double helix will vary with sequence. Shifting in the positions of these phosphate groups would be expected to result in a change in enzymatic activity.

One way to distort the DNA double helix is to bind it with an intercalator. For the metal complexes described herein, the base pairs must separate by an additional 3.4 angstroms and unwind by at least 20° to accommodate the intercalator.[27,39] This distortion could play a substantial role in discouraging the binding of DNA polymerase. Furthermore, the potency of this inhibition could correlate with the level of distortion. Once again, a comparison of the complexes $Rh(MT)phi^{3+}$ and $1\text{-}\Lambda\text{-}Rh(MGP)_2phi^{5+}$ is instructive. Although it has only been demonstrated for $Rh(MT)phi^{3+}$, both complexes can be assumed to cause an additional 3.4 angstrom separation between the two base pairs that are intercalated. However, large differences have been observed in the unwinding of DNA caused by the binding of these complexes. The binding of $Rh(MT)phi^{3+}$ to its recognition sequence has been extensively studied by two dimensional NMR. A solution structure of $Rh(MT)phi^{3+}$ with a 10mer DNA duplex shows that the complex

unwinds DNA by 20° upon intercalation. Importantly, this structure also shows little distortion of the structure of the DNA outside of the intercalation site. The 20° unwinding is localized to the two base pair step between which the intercalator is inserted and the DNA does not show any bending as a result of Rh(MT)phi^{3+} binding. While an NMR solution structure does not exist for 1-Λ-Rh(MGP)$_2$phi^{5+} bound to its recognition site, the unwinding angle which occurs when this complex binds to DNA has been measured.[27] 1-Λ-Rh(MGP)$_2$phi^{5+} has been shown to unwind DNA by 70° upon binding. Although it is not know how this unwinding is distributed, it is unlikely that it occurs over two base pairs as is the case for Rh(MT)phi^{3+}. An unwinding angle of 85° has been observed in the binding of the TATA Box Binding protein (TBP) to the sequence 5'-TATATA-3' which is similar to 5'-CATATG-3', the recognition site for 1-Λ-Rh(MGP)$_2$phi^{5+}.[39,40] In the case of TBP, the unwinding is spread out over 7 base pairs. Thus, 1-Λ-Rh(MGP)$_2$phi^{5+} distorts the DNA to a much greater extent than Rh(MT)phi^{3+}. If DNA distortion is a primary factor in the sequence specific inhibition of DNA polymerase, 1-Λ-Rh(MGP)$_2$phi^{5+} can be expected to be a more potent inhibitor than Rh(MT)phi^{3+}. As can be seen from Table 3.7, 1-Λ-Rh(MGP)$_2$phi^{5+} does show greater inhibition. It can, therefore, be concluded that complexes which cause large distortions in DNA structure will be more potent in the template dependent inhibition of DNA polymerase.

3.4.1.6 Effect of Complex Solubility on Sequence Specific Inhibition: The three complexes which demonstrate significant sequence-specific inhibition are all very soluble in water. This is in comparison to Rh(DPB)$_2$phi^{3+} which is very soluble in methanol and chloroform, but only slightly soluble in water.[41] While Rh(DPB)$_2$phi^{3+} showed substantial inhibition of the activity

of DNA polymerase at low concentrations, the inhibition did not appear to be template directed (see figures 3.13, 3.14, and 3.32). It is possible that the inhibitory activity of Rh(DPB)2phi^{3+} on DNA polymerase results from direct interactions between the complex and the polymerase and not from a DNA bound complex blocking initiation by the polymerase. This hypothesis is supported by the bovine serum albumin (BSA) rescue experiment described in Section3.3.2.2. The addition of BSA, a protein with hydrophobic domains, resulted in increased DNA polymerase activity.[32] The increase in polymerase activity is consistent with complex which is not bound to DNA template directly interacting with excess BSA in solution instead of DNA polymerase.

The possibility of a direct interaction between DNA polymerase and Rh(DPB)2phi^{3+} is further supported by the experiment shown in Figure 3.32. In this experiment, the Λ enantiomer of Rh(DPB)2phi^{3+} fully inhibited DNA polymerase at 2.5 μM metal complex and 1.2 μM DNA base pairs. This enantiomer has shown no affinity for DNA at rhodium and base pair concentrations of 10 and 50 μM respectively.[26] The Λ enantiomer is not bound to the DNA templates and its inhibition of DNA polymerase is not template-directed. As both enantiomers show the same inhibition activity (Figure 3.32), it is likely that both are inhibiting by the same mechanism. Thus, the inhibition of the Δ enantiomer is likely also to be due to a direct interaction between polymerase and metal complex. These results indicate that non-polar metal complexes can inhibit DNA polymerase by direct interaction with the enzyme. Thus, the design of polar complexes for the template directed inhibition of DNA polymerase may result in more specific inhibition.

3.4.2 Significance of Differential DNA Polymerase Activity Based on

Template Sequence: DNA polymerase was chosen as the target for studies of template-directed inhibition because it is capable of interacting with any DNA sequence. This allowed the comparison of template directed inhibition at many different DNA sequences. As can be seen in section 3.3.7, the enzyme does not demonstrate strict sequence neutrality in its activity. This differential activity could play a role in the level of template-directed inhibition observed in experiments. Table 3.4 contains the specific to non-specific product ratio of three different control templates compared to a 1-Λ-$Rh(MGP)_2phi^{5+}$ specific template in the absence of rhodium. DNA polymerase displays substantially greater activity on control templates B and C than it does on A. If this differential activity plays an important role in template directed inhibition, then significant differences should occur in the level of inhibition observed when reactions are carried out with these control templates. As can be seen in Figure 3.23, identical levels of inhibition are observed when any of these templates is used as a control. This indicates that differences in the activity of DNA polymerase due to template sequence does not play a significant role in sequence-specific inhibition.

3.4.3 Shifting of DNA Polymerase Activity with the Addition of Rhodium:

DNA polymerase concentration was limiting compared to DNA template concentration in all experiments described in this chapter. When the polymerase is blocked by metal complex binding to a specific template, free control template should be available for binding. If the inhibition of the polymerase is purely template directed, a decrease of the polymerization on a specific template should result in an equal increase in polymerization on the control template. Increasing polymerization on the control template with added rhodium is observed in a fewer of the experiments (see Figure 3.6)

than constant or decreasing control products are observed with added rhodium (Figures 3.28, 3.29, and 3.30).

That control-template products do not show an increase that is equal to the decrease in specific-template products is difficult to explain. A direct interaction between any of the three complexes and the polymerase is unlikely. Such an inhibitory interaction would result in decreased polymerase activity when metal and template concentrations are increased at a fixed ratio. As described in section 3.3.2.1, polymerization activity actually increases with increasing template and rhodium concentrations. Metal complex may be binding to the control template as well as the specific template in these experiments and causing an overall decrease in activity. It can be concluded, due to the fact that enzyme activity does not quantitatively switch, that inhibition is more complicated than a metal complex binding only to its specific template to block DNA polymerase.

3.4.4 Implications for Metal Complex Design: One of the goals of these studies is to determine what factors are important in template-directed inhibition. Determination of these factors would be useful in the rational design of theraputics for the treatment of genetic disease. Several important conclusions can be drawn from these studies. Changes in metal complex size between 9 and 17 Å has little effect on template-directed inhibition. The charge of a complex also has little effect over the range of +3 to +5. However, the hydrophobicity of the complex can play an important role in sequence-specific inhibition. The hydrophilic metal complexes Rh(MT)phi^{3+}, 1-Λ-Rh(MGP)$_2$phi^{5+}, and 1-Δ-Rh(MGP)$_2$phi^{5+} are potent template directed inhibitors of DNA polymerase. The hydrophobic complex Rh(DPB)$_2$phi^{3+} is also a potent inhibitor of DNA polymerase. However, the inhibition

observed with Rh(DPB)2phi^{3+} is consistent with a direct interaction between the polymerase and the metal complex, not template-directed inhibition. Thus, a template-directed inhibitor should be hydrophilic to avoid direct interactions with the enzyme. The need for hydrophilic inhibitors complicates the design of therapeutics. Hydrophobic molecules are taken up by cells to a much greater extent than hydrophilic molecules.[42] A balance between properties which favor cellular uptake and inhibition may need to be designed in future therapeutics.

The exchange rate of metal complexes on their DNA sites does not appear to be important over the ranges studied. Rh(MT)phi^{3+} and 1-Λ-Rh(MGP)2phi^{5+} differ in their exchange rates with DNA, yet exchange related effects on template-directed inhibition were not observed. Rh(MT)phi^{3+} and 1-Λ-Rh(MGP)2phi^{5+} exchange at a relatively fast rate on DNA, 10 per second and 40 per second respectively. It is important to note that complexes with a rapid exchange rate can inhibit DNA polymerase in a template-directed manner. A rapid exchange rate is important for the sequence specificity of these complexes as it allows the sampling of many different DNA sites in a short period of time.

It should be noted that the exchange rates for Rh(MT)phi^{3+} and 1-Λ-Rh(MGP)2phi^{5+} are very similar. Any subtle effects caused by this difference in exchange rate is likely to be overshadowed by other effects such as differences in DNA distortion (*vide infra*). Furthermore, that increased template directed inhibition is observed with increased template concentration can be explained if the rate of metal exchange relative to the rate of DNA polymerase binding is important. Thus, while the exchange rate did not have a primary effect on inhibition in these studies, it may play some role in template-directed inhibition.

The extent of DNA distortion caused upon metal complex binding has been shown to be most important in template-directed inhibition. 1-Λ-Rh(MGP)$_2$phi^{5+} has been shown to distort the DNA double helix to a much greater extent than Rh(MT)phi^{3+}. Thus, a template bound by 1-Λ-Rh(MGP)$_2$phi^{5+} deviates from the normal DNA polymerase substrate to a greater extent than a template bound by Rh(MT)phi^{3+}. 1-Λ-Rh(MGP)$_2$phi^{5+} demonstrates substantially greater template-directed inhibition than Rh(MT)phi^{3+}. Thus, new metal complexes which cause major distortions in double helix structure should be more potent inhibitors of DNA polymerase than complexes which cause only minor disruptions of the DNA.

DNA distortion was found to be the most important parameter in template directed inhibition in these studies. It is of interest to consider the distortion caused by small molecule therapeutics currently in use. Adriamycin and daunomycin are anthracycline antibiotics which have been widely used in the treatment of leukemias and solid tumors.[43,44] The anti-cancer activity of these compounds is believed to be the result of template-directed inhibition of transcription and replication. These two compounds bind to DNA via intercalation from the minor groove. Crystal structures of both compounds have shown that DNA binding results in the expected 3.4 Å separation of the base pairs.[44,45] Despite the fact that these molecules intercalate, they do not cause substantial unwinding of the DNA upon binding. The unwinding angle per bound molecule is 8^o and spread out over 4 base pairs.

Mithramycin is an antitumor agent which has shown success in the treatment of leukemia.[46,47] The method of action for this therapeutic is proposed to be the template-directed inhibition of transcription by RNA polymerase. NMR solution studies have shown mithramycin to bind non-

covalently to DNA as a dimer in the major groove.[48] Structural perturbations to the DNA are smaller than those observed for adriamycin and daunomycin. As mithramycin does not intercalate, no separation of the base pairs is observed upon binding. Furthermore, no unwinding of the DNA is observed, with binding. The level of DNA distortion observed for adriamycin, daunomycin, and mithramycin is relatively small when compared to our metal complexes and most other intercalators. Yet all three molecules are effective in the treatment of cancer. Although it may play a role in the potency of a therapeutic, severe DNA distortion certainly does not appear to be a prerequisite for anticancer activity.

Anticancer therapeutics exist that bind to DNA and cause large distortions in the structure of the double helix. Cisplatin is widely used in the treatment of genitourinary tumors.[49] This molecule covalently binds to adjacent guanines on a DNA strand. The antitumor activity of cisplatin arises when the molecule is bound by HMG proteins in the cell which prevent repair of the cisplatin-DNA lesion. Solution studies and a recent crystal structure of cisplatin bound to double stranded DNA show that the molecule bends the DNA by 35-55^{o} and unwinds the DNA by 13^{o} upon binding.[50,51] It is this structural perterbation of the DNA which is complementary to HMG protein binding. Thus, both molecules which cause large and small distortions of DNA structure can be effective anticancer agents.

The metal complexes Rh(MT)phi^{3+}, 1-Λ-Rh(MGP)$_2$phi^{5+}, and 1-Δ-Rh(MGP)$_2$phi^{5+} have been demonstrated to be effective template directed inhibitors of DNA polymerase. This makes these complexes promising candidates for the inhibition of other enzymes such as RNA polymerase and other protein factors involved in transcription. The sequence-specific inhibition of RNA polymerase would provide an "off switch" for

transcription. Metal complex binding could also be used to inhibit repressors which discourage the action of RNA polymerase. The inhibition of binding of a repressor would result in an increase in RNA polymerase activity and thus provide an "on switch" for gene expression. Investigations into the abilities of $Rh(MT)phi^{3+}$, 1-Λ-$Rh(MGP)_2phi^{5+}$, and 1-Δ-$Rh(MGP)_2phi^{5+}$ to inhibit and promote transcription by RNA polymerase would help to further demonstrate the potential of these complexes as therapeutics as well as yield more information for the rational design of new molecules.

Further investigations into the effect of different chemical parameters would also be informative for rational design. What would be the effect on sequence-specific inhibition if the metal complex's binding constant was significantly lower than the binding constant for DNA polymerase? This effect could be investigated by making specific templates for the complexes studied above which contain different recognition sequences. For example, $Rh(MT)phi^{3+}$ has demonstrated affinity for 5'-GC-3' steps as well as its recognition sequence, 5'-TGCA-3'. However, the affinity of the complex for 5'-GC-3' steps is lower than for 5'-TGCA-3'. The construction of a specific template containing a 5'-GC-3' step would allow the investigation of inhibition effects caused by changes in metal complex affinity.

More investigations into the effect of exchange rate would also be instructive for rational design. Experiments described above suggested that exchange rate could be important in the potency of inhibition. However, the exchange rates of the metal complexes studied did not show much variation and any effects due to the differences in exchange rates between complexes were likely masked by the effect of DNA distortion. Rhodium-peptide conjugates designed in this laboratory have shown exchange rates on DNA of greater than 5 minutes. Investigations of the inhibitory properties of these

complexes would be instructive in determining the importance of exchange rate in inhibition.

The studies herein have described the development and refinement of an assay for determining the ability of a given metal complex to disrupt protein DNA interactions. This assay was then used with several different rhodium complexes to determine what chemical properties are important for sequence-specific inhibition of these interactions. The results of these studies have provided useful information for the design of new sequence-specific inhibitors of protein DNA interactions.

3.5 References

1. Guieysse, A.; Praseuth, D.; Francois, J.; Helene, C; *Biochem. Biophys. Res. Comm.* **1995**, 217, 186.
2. Hacia, J. G.; Dervan, P. B.; Wold, B. J.; *Biochemistry* **1994**, 33, 6192.
3. Pinto, A. L.; Lippard, S. J.; Proc. *Natl. Acad. Sci. U.S.A.* **1985**, 82, 4616.
4. Weiland, K. L.; Dooley, T. P.; *Biochemistry* **1991**, 30, 7559.
5. Bellorini, M.; Moncollin, V.; D'Incalci, M.; Mongelli, N.; Mantovani, R.; *Nucl. Acids Res.* **1995**, 23, 1657.
6. Biancji, N.; Passadore, M.; Rutigliano, C.; Feriotto, G.; Mischiati, C.; Gambari, R.; *Biochem. Pharm.* **1996**, 52, 1489.
7. Rando, R. F.; DePaolis, L.; Durland, R. H.; Jayaraman, K.; Kessler, D. J.; Hogan, M. E.; *Nucl. Acids Res.* **1994**, 22, 678.
8. Giovannangeli, C.; Perrouault, L.; Escude, C.; Thuong, N.; Helene, C.; *Biochemistry*, **1996**, 35, 10539.
9. Kim, H.; Miller, D. M.; *Biochemistry*, **1995**, 34, 8165.
10. Giordano, T. J.; Deuschle, U.; Bujard, H.; McAllister, W. T.; Gene 1989, 84, 209.
11. Pavco, P. A.; Steege, D. A.; *Nucl. Acids Res.* **1991**, 19, 4639.
12. Lorch, Y.; LaPointe, J. W.; Kornberg, R. D.; *Cell* **1987**, 49, 203.
13. Stryer, L.; Biochemistry 3rd ed., **1988**, W. H. Freeman and Company.
14. Leroy, J. L.; Gao, X.; Gueron, M.; Patel, D. J.; *Biochemistry*, **1991**, 30, 5653.
15. Gao, X.; Patel, D. J.; *Biochemistry*, **1989**, 28, 751.
16. David, S. S.; Barton, J. K.; *J.Am. Chem. Soc.*, **1993**, 115, 2984.
17. Collins, J. G.; Shields, T. P.; Barton J. K.; *J. Am. Chem. Soc.*, **1994**, 116, 9840.
18. Long, E. C.; Barton, J. K.; *Acc. Chem. Res.*, **1990**, 23, 271.
19. Kornberg, A.; Baker, T. A.; DNA Replication, 2nd Ed. **1992**, W. H.

Freeman and Company.

20. Beese, L. S.; Derbyshire, V.; Steitz, T. A.; *Science*, **1993**, 260, 352.
21. Sitlani, A.; Dupureur, C. M.; Barton, J. K.; *J. Am. Chem. Soc.*, **1993**, 115, 12589.
22. Schick, C.; Martin, C. T.; *Biochemistry*, **1993**, 32, 4275.
23. Milligan, J. F.; Groebe, D. R.; Witherell, G. W.; Uhlenbeck, O. C.; *Nuc. Acids Res.*, **1987**, 15, 8783.
24. Krotz, A. H.; Barton, J. K.; *Inorg. Chem.*, **1994**, 33, 1940.
25. Sitlani, A.; Barton, J. K.; *Biochemistry*, **1994**, 33, 12100.
26. Sitlani, A.; Dupureur, C. M.; Barton, J. K.; *J. Am. Chem. Soc.*, **1993**, 115, 12589.
27. Terbrueggen, R. H.; Barton, J. K.; *Biochemistry*, **1995**, 34, 8227.
28. Terbrueggen, R. H.; Ph.D. Thesis.
29. Patel, S. S.; Wong, I.; Johnson, K. A.; *Biochemistry* **1991**, 30, 511.
30. Kuchta, R. D.; Mizrahi, V.; Benkovic, P. A.; Johnson, K. A.; Benkovic, S. J.; *Biochemistry*, **1987**, 26, 8410.
31. Krotz, A. H.; Hudson, B. P.; Barton, J. K.; *.J.Am. Chem. Soc.*, **1993**, 115, 12577.
32. Peters, T.; Taniuchi, H.; Anfinsen, C. B.; *J. Biol. Chem.*, **1973**, 248, 2447.
33. Depew, R. E.; Wang, J. C.; *Proc. Natl. Acad. Sci. U.S.A.*, **1975**, 72, 4275.
34. Sambrook, J.; Fritsch, E. F.; Maniatis, T.; Molecular Cloning 2nd. ed.; **1989**, Cold Spring Harbor Laboratory Press.
35. Kolocheva, T. I.; Nevinsky, G. A.; Levina, A. S.; Khomov, V. V.; Lavrik, O. I.; *J. Biomol. Struct. Dyn.* **1991**, 9, 169.
36. Kornberg, A.; Baker, T. A.; DNA Replication 2nd ed., **1992**, W. H. Freeman and Co., New York.
37. Grandgenett, D. P.; Gerard, G. F.; Green, M.; *Proc. Natl. Acad. Sci.*

U.S.A., **1973**, 70, 230.

38. Hudson, B. P.; Dupureur, C. M.; Barton, J. K.; *J. Am. Chem. Soc.*, **1995**, 117, 9379.
39. Kim, Y.; Geiger, J. H.; Hahn, S.; Sigler, P. B.; *Nature*, **1993**, 365, 512.
40. Kim, J. L.; Nikolov, D. B.; Burley, S. K.; Nature, **1993**, 365, 520.
41. Sitlani, A.; Ph.D. Thesis.
42. Wolff, M. E.; Burger's Medicinal Chemistry and Drug Design, vol 1. 5th ed. **1994**, John Wiley and Sons, New York.
43. Frederick, C. A.; Williams, L. D.; Ughetto, G.; van der Marel, G.; van Boom, J. H.; Rich, A.; Wang, A. H. J.; *Biochemistry*, **1990**, 29, 2538.
44. Henry, D. W.; Can. Treat. Rep., **1979**, 63, 845.
45. Moore, M. H.; Hunter, W. N.; d'Estaintot, B. L.; Kennard, O.; *J. Mol. Biol.*, **1989**, 206, 693.
46. Ray, R.; Snyder, R. C.; Thomas, S.; Koller, C. A.; Miller, D. M.; *J. Clin. Invest.*, **1989**, 83, 2003.
47. Koller, C. A.; Campbell, V. W.; Polansky, D. A.; Mulhern, A.; Miller, D. M.; *J. Clin. Invest.*, **1985**, 76, 365.
48. Sastry, M.; Fiala, R.; Patel, D. J.; *J. Mol. Biol.*, **1995**, 251, 674.
49. Lippard, S. J.; Progress in Inorganic Chemistry, Vol. 38, **1990**, John Wiley and Sons, New York.
50. Poklar, N.; Pilch, D. S.; Lippard, S. J.; Redding. E. A.; Dunham, S. U.; Breslauer, K. J.; *Proc. Natl. Acad. Sci. U.S.A.*, **1996**, 93, 7606.
51. Takahara, P. M.; Rosenzweig, A. C.; Frederick, C. A.; Lippard, S. J.; *Nature*, **1995**, 377, 649.